Corrosion Fatigue Short Crack Growth Behaviour in a High Strength Steel

Ghulam Murtaza
BSc. Eng. (Hons.)

Thesis submitted to the University of Sheffield for the Degree of Doctor of Philosophy in the Faculty of Engineering

Department of Mechanical and Process Engineering

University of Sheffield

March 1992

Preface

This thesis is based on the findings of research carried out in the Department of Mechanical and Process Engineering at the University of Sheffield.

The content of this thesis is original except where specific reference is made to other work. No part of this thesis has been submitted to any other university for a degree.

Acknowledgements

I would like to express my hearty gratitude to my supervisors Dr. R Akid and Professor K J Miller for their invaluable guidance, help and encouragement during my time within the department. My thanks are also due to the Head of the Department of Mechanical and Process Engineering for the use of the departmental facilities.

I am also thankful to Dr. E R de Los Rios and Dr. M W Brown for their sincere advice and help.

I am especially grateful to the Ministry of Science and Technology, Government of Pakistan for a research award and to the Pandrol International UK for providing material and other useful information.

I would like to thank members of the technical staff for their help, notably Mr. J Smith for workshop work, Mr. J Goodliffe for maintaining the electronic and computer systems for expeimental facilities, Mr. D Halford for his photographic skills and Mr. K S Morris for tracing the figures.

Finally I shall also be indebted to my all family members for their continued encouragement and support throughout my studies.

Contents

Summary

A frequent cause of the premature failure of structural components is *Corrosion Fatigue Cracking.* Historically corrosion fatigue studies have shown that this failure process depends strongly on the interactions between loading mode, metallurgical texture and electrochemical parameters. This has become a serious problem for concerns such as the nuclear, automobile, oil, gas, aerospace and marine industries.

This research study was carried out using a quenched and tempered silico-manganese spring steel (BS 250A53). Smooth hour-glass shaped fatigue specimens were tested under fully reversed torsional loading in both laboratory air and aerated 0.6M NaCl solution environments. Crack growth behaviour in both air and corrosion fatigue tests was monitored using a plastic replication technique. Intermittent air fatigue/corrosion fatigue tests were also conducted at sub-fatigue limit stress levels in an attempt to determine an environment-assisted critical (threshold) crack length necessary to cause subsequent air fatigue failure and therefore elucidate the mechanisms operative during the first stages of crack development and growth. To assist in this electrochemical experiments were performed to determine the corrosion characteristics for this metal-environment system.

In air fatigue tests cracks initiated at non-metallic inclusions due to a strain incompatibility between the inclusion and the matrix. Air fatigue modelling was based on the observation that crack growth rate decreases as cracks approach microstructural barriers. In the present study it is suggested that the 4th prior austenite grain boundary was the major barrier to a growing crack. This regime of crack growth is described as the *short crack* regime and may be represented by

the following equation;

$$(\frac{da}{dN})_{sa} = C_{sa}(d_i - a)$$

After overcoming the major microstructural barrier crack growth rate increases with an increase in its length. This regime of crack growth is represented by *long crack* regime and may be quantified by the expression;

$$(\frac{da}{dN})_{la} = C_{la}a - D_t$$

Corrosion fatigue crack initiation was associated with chemical pitting of these inclusions. Failure at stresses close to the 'in-air' fatigue limit was due to the coalescence of a small number of cracks. While at low stresses growth of individual cracks led to failure. Corrosion fatigue crack growth modelling suggested that a chemical driving force arising from chemical reactions was present in addition to the mechanical driving force of the applied stress. The presence of this additional force enabled a crack to continue its propagation at low stresses which would otherwise arrest under air fatigue conditions. Corrosion fatigue crack growth rate was calculated using the following superposition model.

$$(\frac{da}{dN})_{cf} = (\frac{da}{dN})_a + (\frac{da}{dN})_e$$

where $(\frac{da}{dN})_a$ and $(\frac{da}{dN})_e$ represent air fatigue crack growth rate and environmental crack growth rate respectively.

Nomenclature

$A, B, C_{sa}, C_{la}, C_p, \alpha, \beta$: constants

a_0: initial crack length

a: surface crack length

a_{av}: average crack length

a_f: failure crack growth

a_r: surface area

a_{th}: threshold crack length

b: Burgers vector

d: microstructural dimension

d_m: dominant deceleration barrier length

D_t: threshold crack growth rate

$\frac{da}{dN}$: crack growth rate

$(\frac{da}{dN})_{cf}$: corrosion fatigue crack growth rate

$(\frac{da}{dN})_e$: environmental crack growth rate

E: Young's modulus

f: cyclic frequency

F: Faraday's constant

G: shear modulus

K: stress intensity factor

M: molecular weight

N: number of loading cycles

N_{cf}: number of cracks contributing to corrosion fatigue failure

N_f: number of cycles to failure

N_i: number of cracks initiated in corrosion fatigue

N_l: number of cycles for long crack regime

N_p: number of cycles for pit development

N_s: number of cycles for short crack regime

N_t: calculated total number of cycles

R: stress ratio

T: torque

t: time

Y: geometry factor

z: valence charge on cation

τ: shear stress

$\Delta\tau$: shear stress range

σ: stress

$\Delta\sigma$: stress range

σ_y: yield stress

σ_{cy}: cyclic yield stress

σ_T: tensile strength

τ_{fl}: fatigue limit shear stress

ΔK: stress intensity factor range

ΔK_{th}: threshold stress intensity factor range

ΔK_I: mode I stress intensity factor range

r_0: minimum radius of cross-section

r_p: plastic zone size

δ: crack tip opening displacement

ϵ: strain

$\Delta\epsilon_e$: elastic strain range

$\Delta\epsilon_p$: plastic strain range

ϕ: crack tip plastic displacement

θ: angle of twist

$\Delta\theta$: range of angle of twist

γ: shear strain

$\Delta\gamma_p$: plastic shear strain range

$\Delta\gamma_t$: total shear strain range

$\Delta\gamma_{fl}$: fatigue limit shear strain range

Chapter 1

Introduction

Many components fail in service due to the process of fatigue. Failure can take place at very low stress levels, σ_a, as shown in figure 1.1 which is considerably less than both the yield stress σ_y and tensile strength of the material σ_T.

The reason for such failure is that the stress is of a cyclic nature which causes a crack to initiate at stress concentrations on a free surface and to grow across the material.

This thesis explores the initiation and growth behaviour of fatigue cracks in a quenched and tempered silico-manganese spring steel used for railway fastenings. In particular it has been the aim to understand the possible influence of a corrosive environment on the conventional "in-air fatigue limit".

In the present study experimental fatigue crack growth data has been used to develop crack growth models which incorporate Elastic Plastic Fracture Mechanics (EPFM) parameters as opposed to the more conventional Linear Elastic Fracture Mechanics (LEFM) approach. This is due to the fact that an LEFM approach

to the quantification of defects subject to large plastic deformations, or having a length comparable to the microstructural dimension of the material, provides severe limitations as a result of the lack of small scale yielding. Crack growth models developed in this way have been employed to predict fatigue lifetimes and hence produce an S-N type relationship.

This thesis consists of 8 chapters. Chapter 2 presents a literature review on air fatigue, fracture mechanics and existing fatigue carck growth models. Chapter 3 presents a literature review on environment-assisted failures with an emphasis on corrosion fatigue. The experimental work describing material under investigation, specimen design, basic test facilities and test procedure are explained in chapter 4. The results achieved in this study and crack growth modelling and analyses of these results are presented in chapter 5 and chapter 6 respectively. Chapter 7 describes the discussion made on the results. The conclusions drawn from the present work and some suggestions for possible future work are given in chapter 8.

Chapter 2

Literature Review — Air Fatigue

2.1 Introduction

The majority of fatigue studies to date have been conducted in air despite the fact that air is considered as a corrosive environment when compared to that of a vacuum. The reason that air is considered an inert environment is that, for ferrous materials, a fatigue limit exists.

2.2 Historic Survey

Many engineering components and structures which are subject to simple static loading conditions survive for longer periods than those subjected to repeated stresses. Early comments by engineers on such failures gave a reasoning that material keeps on changing its properties in such a way that it seems to be 'tired'. The term "FATIGUE" was introduced to explain failures which arose as a result

of cyclic loading, this in turn led to a crucial debate among scientists and engineers as to the nature of such failures.

Fatigue is considered to be the cause of about 90 percent of the total failures in the world [1,2]. It is more than one and a half century since fatigue was observed as a cause of failures within a number of engineering components. The first reported fatigue investigations were carried out in 1830 by a German engineer, W. A. Albert, who made repeated loading tests on iron chains [3]. However at that time the best known instances of fatigue failures in service occured in the axles of stage coaches and later in those of rolling stock of the rapidly developing railway systems. Structural interests in fatigue arose from the increasing use of wrought iron structures, particularly bridges, which were replacing those of brick and stone in order to meet the demands of the expanding railway systems. Between 1849 and 1865 further work involving repeated-bending tests on beams was carried out by Hodgkinson [4] and Fairbairn [5] in England. Fairbairn conducted a series of experiments on the effect of repeated loads on wrought iron girders some 22 feet long and 16 inches deep. Fairbairn found that the load required to break the girder under repeated load conditions was 1/4th of that required under static load conditions. However, the earliest systematic research on fatigue was carried out by Wholer [6] who presented his results in terms of an S-N curve, which presents the number of loading cycles to failure (N_f) versus the applied cyclic stress value. This diagram is schematically shown in figure 2.1 and is today still a very important tool for design engineers. In 1911 the results of an extensive investigation was

reported to the Institution of Mechanical Engineers, London, by Eden, Rose and Cunningham [7] who had studied the effect of heat treatment, surface finish, form of test specimen and many other variables on the fatigue behaviour of both steels and non-ferrous metals. Gough [8] during the 'World War I' pointed out that increased endurance was to be found as a result of surface polishing of the connecting rods of aircraft engines.

Undoubtedly, many new materials were developed and exploited with little being known of their fatigue characteristics. At the same time the emergence of nuclear power, guided missiles, supersonic flight, space vehicles, satellites and sophisticated chemical processes have introduced new fatigue problems for the design engineer, or in many cases have tended to extend the capabilities of most established materials to their limits.

The diversity of the problem is reflected in the occurance of fatigue failures in bolted, riveted and welded steel and aluminium structural assemblies— the detail design of joints under fatigue loading has recieved considerable attention, reinforced and prestressed concrete beams, pressure vessels, bolts and screws, plain and rolling bearings, rock drills, fan blades and turbine discs, aircraft propellers, springs, pipe lines, railway rails, gears, steel dies, ship's hulls and agricultural machinery.

2.3 Fatigue Mechanisms

Fatigue damage results in progressive localized permanent structural change. It may result in cracking and subsequent fracture after a sufficient number of loading

cycles. Historically fatigue has been described as a two stage process. The first stage is related to the development of a crack, i.e. crack initiation, whereas the second stage describes crack propagation. Given the application of a suitable level of cyclic stress, cracks are initiated at the surface from pre-existing surface defects such as grain boundaries, triple points or inclusions. Depending upon the applied stress level once initiated these cracks may either continue to propagate or become non-propagating [9]. The *fatigue limit* may therefore be defined as a limiting stress below which cracks once created are unable to produce failure, i.e. are unable to propagate beyond crack arresting features within the microstructure. Failure may occur due to the individual growth of single cracks or as a result of the coalescence of several cracks depending upon the nature and history of the stress and material. Crack initiation is strongly dependent upon the ductility of a material, the applied stress level and the nature of the microstructure. Short fatigue crack propagation is largely influenced by the intensity of the mechanical driving force and the orientation and size of grains within the material.

Fine [10] suggested that the fatigue failure process may be divided into following stages;

- Cyclic plastic deformation prior to fatigue crack initiation,
- Initiation of one or more microcracks,
- Propagation or coalescence of microcracks to form one or more macrocrack,
- Propagation of one or more macrocracks and

- Final failure.

Forsyth [11] discussed fatigue as a mechanism of crack initiation and crack growth. He further divided crack growth into two stages; stage I crack growth and stage II crack growth. As the time period spent in the initiation of crack is usually significantly short with respect to the total life, Miller [9] has described fatigue as a mechanism of crack propagation.

2.4 Crack Initiation

Crack initiation during cyclic deformation generally occurs in regions where strain has become localized such as surface or sub-surface defects. Strain localization may occur at pre-existing stress concentrations such as notches, corrosion or etch pits and machining scratches. However under extremely good surface conditions cracks are likely to initiate at sites such as non-metallic inclusions, slip bands and grain boundaries. The mechanism and tendency for cracking at such sites is described individually in the following sections. Crack initiation is considered as a primary stage of fatigue damage.

Inclusions

Cracks can initiate from inclusions due to the following reasons;

a) cracking of matrix close to the inclusion

b) decohesion or debonding at inclusion/matrix interface

c) cracking of the inclusion itself.

Fine [10] has described different ways in which inclusions can affect fatigue crack initiation. Inclusions are often associated with the initiation of cracks as they act as obstacles to dislocaions pile-ups at the matrix/inclusion interface.

Johnson [12] also reported that for a 2219 T851 aluminium alloy inclusions cracked first after which the crack advanced into the matrix. An alternative mechanism was seen by Fine [10] for a 2024T4 aluminium alloy where Al_2CuMg and Al_7Cu_2Fe particles were found to initiate cracks within the matrix.

The role of inclusions as crack initiation points has also been discussed by several other authors. Brooksbank and Andrews [13] proposed that the internal stresses which may be generated around inclusions is due to differences in the thermal expansion coefficients of inclusion and matrix respectively. They considered the inclusions in terms of the stresses generated at the interface of matrix and inclusion on cooling.

Shih and Araki [14] investigated the effect of inclusions on crack initiation in high strength carbon steels and concluded that oxide inclusions were more damaging than other inclusions such as sulphides. Crack initiation was found to be dependent upon the size and shape of the inclusions. Further to this they described the existence of a critical minimum inclusion size for crack initiation. Spherical oxide inclusions larger than 20μm and embedded close to the surface of steel were potential nucleation sites for main crack. The critical minimum size however decreased if these oxide inclusions (Al_2O_3) were angular or of the stringer type aligned perpendicular to the stress axis.

Pickering [15] pointed out the importance of methods employed for assesing inclusions not only in terms of their size and distribution but their shape. The ease of formation of voids at the interface of the inclusion and matrix is very important for ductile failure of steels particularly those involving sulphide inclusions. Gladman [16] also favoured a similar view point to Pickering and concluded that the effect of sulphide inclusions on ductile fracture was consistent with the traditional views of void nucleation, growth and coalescence.

Khalifa [17] has investigated the effect of inclusions on the fatigue limit of a heat-treated carbon steel. He found that martensitic microstructures had a relatively low fatigue ratio defined as the ratio of the fatigue limit to the ultimate tensile strength, such behaviour was explained by the enhanced damaging effects of inclusions and impurities in the hard structures.

In a quenched and tempered medium carbon/molybdenum alloy steel containing (Al_2O_3) inclusions, up to 25μm in diameter, debonding between the particles and the matrix as well as cracking of the particles occured [18]. Eid and Thomason [18] performed calculations of the local stress near the inclusions and they demonstrated the importance of the elastic moduli. Particles harder than the matrix produce large tensile stress concentrations whereas softer ones, such as MnS, were not sources of fatigue cracks in this steel.

Slip Bands

The first work on fatigue crack initiation was conducted around 1900 by Ewing and Humphrey [19]. They prepared the surface of a specimen metallurgically and examined the surface grains with an optical microscope during the course of a fatigue test. They observed the formation of slip lines across grains, their broadening into bands and the eventual development of cracks in the broadened bands.

Later Thompson and Wadsworth [20] observed the formation, broadening and development of surface cracks in slip bands on copper and nickel. In 1933, Gough [8] studied crack initiation in single crystal aluminium and found that slip bands were the potent sites. Figure 2.2 schematically illustrates the formation of a surface crack by slip [21].

In 1950's Forsyth [22] observed the formation of intrusions and extrusions during fatigue tests and reported these features as the cause of crack initiation. A typical extrusion emanating from a slip band is shown in figure 2.3. Cottrell and Hull [23] later proposed a model for the development of intrusions and extrusions. The model illustrating the sequence involved in the operation is presented in figure 2.4.

More recent work [24-26] on ferrous and non ferrous materials has also supported the production of slip bands and their relation to crack initiation.

Cracking from slip bands has become debateable as Miller [2] suggested that in fact slip bands are cracks. Slip bands do appear at those places where cracks

already exist. He also pointed that further work needs to be done to gain a clearer understanding in order to evaluate which process takes place first i.e. a crack or slip band.

Grain Boundaries

Grain boundaries also offer a source of strain incompatibility, and help in the initiation of microcracks. Cooper and Fine [27] have studied the crack initiation in an iron of 99.93 wt.% purity. They observed that at high plastic strain amplitudes crack initiation was associated with grain boundaries.

Mughrabi [28] reported that for high cycle fatigue of copper polycrystals, crack initiation occurs not only in emerging persistant slip bands (PSBs) but also grain boundaries (GBs), at sites where PSBs impinge.

In a study of the fatigue of low carbon martensite it has been reported that crack initiation was associated with prior austenite grain boundries [29].

More recently Yates [30] demonstrated that grain boundaries of waspalloy acted as sites for short fatigue crack initiation.

2.5 Crack Propagation

Once a crack is initiated, it enters into a crack propagation phase. Crack propagation occurs as a result of the stress concentration which develops at the crack tip. This phase may be divided into three distinct stages as shown in figure 2.5.

2.5.1 Stage I Crack Propagation

Stage I cracks lie along the active slip planes which in general coincide with the maximum shear plane [31]. In the case of torsional loading these cracks grow parallel or perpendicular to the torque axis i.e. 45^0 to the direction of maximum normal stress. However in uniaxial loading stage I cracks propagate in planes coincident with the maximum shear stress which is oriented at 45^0 to the loading direction. Such cracks have a high initial growth rate which is subject to the influence of the material's microstructure. This stage of growth continues until the crack changes direction onto the tensile plane and stage II type growth begins. This stage of propagation may continue for one, two or three grain diameters and is a dominant feature of low-stress high cycle fatigue.

2.5.2 Stage II Crack Propagation

A crack enters the second stage when it changes its direction of propagation to that which is perpendicular to the maximum normal stress. The transition from stage I to stage II might occur as a result of strain incompatibility arising at grain boundaries/phase boundaries or on attaining a critical value of the ratio of tensile to shear stress [11]. This change depends upon stress level, stress state and material microstructure etc.

The different behaviour observed between stage I and stage II growth has led to the introduction of terms such as *short* cracks and *long* cracks. Stage II cracks are often classed as *long* cracks as their behaviour may be quantified by Linear Elastic

Fracture Mechanics (LEFM) analyses. In many cases this stage is characterised by the the appearance of striation markings on the fracture surface.

2.5.3 Stage III Crack Propagation

The third stage of propagation is known as final rupture. In this stage ductile tearing of the material takes place due to the nucleation of voids as illustrated in figure 2.5. The instability of the remaining ligament and inability to sustain the load results in a high growth rate during this period.

2.6 Fracture Mechanics

2.6.1 Introduction

Fracture mechanics has provided an important tool to the design engineer. It is developed on the basis that materials contain crack-like defects from which fast fracture may occur. It helps in calculating the maximum defect size for a given stress or the maximum permissible stress for a given intrinsic defect size. LEFM may be applied with confidence in situations where fracture occurs under essentially elastic conditions. This theory may be extended to materials exhibiting relatively small scale yielding prior to fracture. However for very tough materials which exhibit gross yielding prior to fracture, the use of LEFM is no longer valid. In such cases an Elastic Plastic Fracture Mechanics (EPFM) approach is adopted and parameters such as Crack-Opening Displacement (C.O.D) or the J- Integral are

often used.

2.6.2 Linear Elastic Fracture Mechanics

Linear Elastic Fracture Mechanics developed from the early work of Griffith [32] who sought to explain why the observed strength of a material is considerably less than the theoretical strength based on the forces between atoms. He concluded that real materials must contain defects and cracks which reduce their strength.

Based on the ideas above and further developments, principally by Irwin [33], LEFM has developed as an analytical approach to fracture. It relates the stress distribution in the vicinity of a crack tip to other parameters such as the nominal stress applied to the structure and the size, shape and orientation of the crack. Thus it permits a representation of the material's fracture properties, often in terms of a single parameter. Irwin observed while analysing the stress distribution at the crack tip in an infinite plate that the stresses were proportional to $(\pi a)^{1/2}$, where 'a' is the half crack length. On this basis, Irwin defined a *stress intensity factor, K* as

$$K = \sigma(\pi a)^{1/2} \tag{2.1}$$

The stress intensity factor is a means of characterising the elastic stress distribution near the crack tip and has units of MN-$m^{-3/2}$. In order to extend the applicability of LEFM beyond the case of a central crack in an infinite plate, K is usually expressed in the more general form as

$$K = Y\sigma(\pi a)^{1/2} \tag{2.2}$$

Where Y is a geometry factor and a is the half length of a central crack or the full length of an edge crack.

The stress intensity factor may be designated as K_I, K_{II} and K_{III} depending upon the mode of loading and crack extension.

There are three different modes of cracking, as shown in figure 2.6, which may be described as:

1) Mode I : this is known as the tensile or opening mode in which the tensile stress acts in the Y-direction i.e. perpendicular to the crack surfaces and causes them to move apart from each other.

2) Mode II : is known as the shear mode in which shear stresses act in the X-direction i.e. perpendicular to the crack tip resulting in edge-sliding of the crack surfaces.

3) Mode III : is also known as a shear mode in which shear stresses act in the Z-direction i.e. parallel to the crack tip and results in screw-sliding of the crack surfaces and hence causes tearing.

In cyclic loading, K varies over a stress intensity range ΔK , where

$$\Delta K = K_{max} - K_{min} \tag{2.3}$$

or

$$\Delta K = Y(\Delta\sigma)\sqrt{\pi a} \tag{2.4}$$

where $\Delta\sigma = \sigma_{max} - \sigma_{min}$

The simplest and most widely used expression which relates the stress intensity factor range to crack growth rate during cyclic loading is the Paris-Erdogan equation [34] expressed as:

$$da/dN = C(\Delta K)^m \tag{2.5}$$

Where da/dN is crack growth rate, mm/cycle, and C and m are material constants.

The manner in which crack growth rate varies during fatigue cycling is illustrated in figure 2.7. This graph shows that at low ΔK values (Region I) there is a threshold value of stress intensity range, ΔK_{th} , below which the crack will not propagate. The mid ΔK region (Region II) shows a linear behaviour between stress intensity range and crack growth rate and may be quantified by the Paris law. At higher ΔK values (Region III) crack growth increases towards the fracture toughness value, K_{IC}. As the crack grows, K_{max} increases and failure will occur when this exceeds the fracture toughness of the material, K_{IC}.

Equation 2.5 may be written as;

$$da/dN = C(Y.\Delta\sigma.\sqrt{\pi a})^m \tag{2.6}$$

For the calculation of fatigue lifetime, equation 2.6 may be integrated in the limits a_0 to a_f where a_0 is the initial crack length and a_f the failure crack length.

LEFM has extensively been used for the prediction of crack growth and hence fatigue lifetime in situations where applied stress levels are low and elastic condi-

tions at the crack tip dominate. In other words the plastic zone size at the crack tip is so small that it does not have a severe effect on the elastic stress fields at the crack tip. The principal reason for the wide application of LEFM analyses is that it enables the prediction of crack growth in large structures by studying small laboratory specimens under identical crack tip stress intensity conditions.

2.6.3 Elastic Plastic Fracture Mechanics

For most structures Linear Elastic Fracture Mechanics suffices to predict fatigue crack growth rates and hence lifetime. This is particularly the case where structures contain inherent defects having a depth greater than 0.5 mm. For components and structures where no pre-crack initially exists ΔK in equation 2.4 is essentially zero although a fatigue crack may initiate and grow. There exits therefore a limitation to the application of LEFM. The two principal limitations relate to the relative size of the crack length to the plastic zone size. The first of these limits relates to the definition of the stress intensity field at the tip of a sharp crack. Elastic analysis indicates a singularity condition at the crack tip but through the introduction of the cyclic yield stress, σ_{cy}, a plastic zone develops which blunts the crack. The limiting size of the plastic zone is typically one-fiftieth of the crack length. Given the $r_p \leq$ a/50 a second limitation exists, this being that the applied stress range should be less than 0.3 σ_{cy}. In order to resolve this problem where small scale yielding at the crack tip is exceeded, a new approach known as Elastic Plastic Fracture Mechanics (EPFM) has been developed. EPFM is therefore used in situations where cracking

is controlled by local plastic deformation at the crack tip.

The two most common approaches adopted to measure the extent of plastic deformation are; crack-tip opening displacement (CTOD) and the J-Integral.

Crack Tip Opening Displacement; This method was proposed by Dugdale [36] and developed by Wells [37]. It is based on the fact that under sufficiently high plasticity conditions failure is governed by the local deformations occuring at the crack tip and the extent of these deformations enables the measurement of crack tip opening displacement. CTOD may be approximated by;

$$\delta_c(CTOD) = \frac{K_{IC}^2}{E\sigma_y} \tag{2.7}$$

J-Integral: During the period in which CTOD was being developed in the UK an alternative approach was being developed by Rice [38] in the USA. This has become known as J- Integral approach and provides a means for describing the severity of conditions at a crack tip in a non-linear elastic material. ΔJ may be expressed as:

$$J = \int_\Gamma (Wdy - T\frac{\delta u}{\delta x} ds) \tag{2.8}$$

where W = the strain energy density

Γ = the path of the integral

T = a traction vector

u = the displacement vector

x, y = the rectangular co-ordinates

ds = an increment of the contour path and

$T(\frac{\delta u}{\delta x} ds)$ = the rate of work input.

Under linear elastic conditions, J is equivalent to Griffith's strain energy release rate concept and is related to the stress intensity factor used in LEFM where

$$\Delta J = \Delta K^2 / E' \tag{2.9}$$

The most common method of application of the *J-Integral* approach is to convert experimentally determined value of J_{IC} to equivalent G_{IC} or K_{IC} values. It has also been shown that J is related to the crack tip opening displacement. The following equations are frequently used to relate the various fracture toughness parameters;

$$K_{IC}^2 / E' = G_{IC} = J_{IC} = \lambda \sigma_y \delta_c \tag{2.10}$$

Where $E' = E$ for plain stress

and $E' = E/(1 - \nu^2)$ for plain strain

The energy relationships and applicability of both CTOD and J are given in Appendix A.

For gross yielding conditions crack growth models have been derived using parameters applicable to the bulk material. Tomkins [39] suggested a model based upon a shear decohesion approach which is expressed as;

$$da/dN = A(\Delta\sigma)^m . a \tag{2.11}$$

where A and m are material constants.

Solomon [40] and Ibrahim and Miller [41] proposed a modified version of this equation based upon the fact that in a large scale yielding situation plastic strain is probably the most important parameter controlling crack growth rather than the

applied stress;

$$da/dN = A(\Delta\epsilon_p)^m.a \tag{2.12}$$

Both of the above equations offer an advantage in that they are very simple to use although it should be noted that they have a limitation in that they may only be used to predict crack growth rate which is directly proportional to crack length and therefore can not account for the growth of short cracks which show purturbations in growth i.e. decelerations and accelerations resulting from the influence of the microstructure.

2.7 Short Crack Behaviour

As a result of the limitations of LEFM type analyses for short cracks having lengths comparable to the microstructural dimension the study of short crack growth behaviour has recently received wide attention.

Several researchers have suggested various definitions of the term '*short*' fatigue cracks. Suresh and Ritchie [42] suggested that cracks are defined as being short (i) when their length is small compared to relevant microstructural dimensions (a continuum mechanics limitation), (ii) when their length is small compared to the scale of local plasticity (a linear elastic fracture mechanics limitation), or (iii) when they are simply physically small (e.g. $\leq$ 0.5–1mm). Miller [43] considered the following short fatigue crack definition;

> The upper limit of a short crack is that length which can be calculated from LEFM anlayses, in which the stress intensity factor is the

threshold value and the maximum value of the cyclic stress is approximately equal to two-third of the cyclic yield stress of the material.

He suggested that for the two plain carbon steels studied, the lower and upper limit for a short crack appears to be 3 or 4 μm and 100 μm respectively.

However short cracks can be divided into three main classes [44]. Typical regimes of short cracks are shown in figure 2.8.

1) *Microstructurally Short Cracks (MSC)*; This regime covers those cracks whose lengths, a, are less than the dominant microstructural barrier length, d, and are largely influenced by the surrounding microstructure. These cracks are usually termed as Stage I, Mode II cracks as they grow on the planes of maximum resolved shear stress. Continuum fracture mechanics analyses are considered to be invalid in this regime.

2) *Physically Small Cracks (PSC)*; In this regime the lengths of cracks are greater than the dominant microstructural barrier length, d, but are of a length less than the minimum length, l, for which LEFM is valid. These cracks are usually known as Stage II, Mode I cracks as they grow in a direction perpendicular to the maximum normal stress. As these cracks do not suffer any major influence of the microstructure their growth rate increases in a linear manner with increase in crack length, continuum mechanics may be applied to them.

3) *Highly Stressed Cracks*; This class describes those cracks whose lengths are greater than the minimum length, l, for which LEFM is valid, but the applied stress level is greater than two-thirds of the cyclic yield stress for the material. These

cracks are classed as EPFM type cracks as they are developed under low cycle high stress conditions.

Brown [45] suggested that short and long cracks may be differentiated on the basis of the extent of plasticity ahead of the crack tip. A crack will be classed as short if its length is smaller than the size of the plastic zone at its tip.

High growth rates of this type of crack has seen scientists and engineers become more involved in an understanding of the contributing mechanisms and thereby develop suitable analytical models. A safe design procedure may therefore only be possible if S-N data is produced employing empirical and theoretical models which take into account the influences of variables on crack growth such as local plasticity, microstructure, crack tip environment, growth mechanisms, crack driving force and the effects such as closure.

It has been pointed out that short cracks initially grow at a faster rate but then slow down and halt temporarily or arrest depending upon the applied stress level, as they approach a barrier to their growth (e.g. a grain or phase boundary). If the applied stress is above the fatigue limit (a stress level limiting crack propagation), the crack slows for a while and then accelerates until failure occurs. However at the fatigue limit stress level, short crack growth behaviour is similar but the period of time spent at the barrier increases before the development of a long crack. If the stress level is below the fatigue limit a crack if initiated is arrested at successive barriers depending upon stress level and eventually becomes non-propagating. However such cracks may produce failure if they are forced to

overcome the barrier by, for example mechanical overloads or by chemical assistance i.e. corrosion, thereby attaining a threshold value (a_{th}) for the corresponding stress level. The short crack growth behaviour described dictates that as the stress level decreases the time period for crack retardation increases. This time period is therefore greatly dependent upon the crack driving force and the nature of the barrier. Such crack growth behaviour is illustrated in figure 2.9 [46].

Several researchers [47-51] have studied the behaviour of short cracks and their work is highly accredited. Lankford [52] reported that short crack deceleration occurs due to the blockage of the plastic zone. Morris [53] has made a similar comment in that the distance between the crack tip and the grain boundary is an influencing factor and controls the crack growth. Navarro and de los Rios [54] suggested that the intermittent decelerating and accelerating nature of short crack growth is dominated by the successive blocking of the plastic zone by slip barriers such as grain boundaries and subsequent initiation of slip in the next grain.

The studies conducted by Hunter and Fricke [55] on 6061-T6 aluminium alloy under high cycle fatigue conditions demonstrated that cracks exhibited decelerations on attaining a length of about 300 μm. Several cracks were observed using the plastic replication technique. de Lange [56] also carried out fatigue tests to study short crack growth behaviour in 26 ST aluminium alloy and 35 CD 4 steel. Cracks were seen to slow down for both alloys when they had traversed a distance of four or five grain diameters. He explained failure as a three stage process. Firstly initiation of a crack followed by the second stage which involves high initial growth

rates with subsequent slow growth due to the interaction of the crack tip with grain boundaries and a final high growth period resulting in rapid failure.

Lankford has studied the fatigue behaviour of a high strength steel AISI 4340 [57], a nickel base super alloy [58] and 7075-T6 aluminium alloy [59,60]. In the high strength steel crack growth retardations were seen around crack lengths of 4 μm and 20 μm which reflect the minimum and maximum prior austenite grain size respectively. In the case of the aluminium alloy he found that cracks slowed down when their lengths were close to the microstructural dimension i.e. the grain size, equivalent to 16 μm. He also attempted to understand the mechanism contributing to crack growth anomalies observed for short cracks and conducted fatigue tests in a dry nitrogen environment [60]. The crack growth trend observed showed that the environmental influence is not responsible for such anomalies. It has been reported previously by Lankford [52] and more recently by Smith [61] that the size of the crack tip plastic zone and that of the grain are important parameters influencing short crack growth. If the size of the plastic zone is greater than that of the grain then high growth is observed as the grain boundary does not exert any significant influence on growth.

Brown and Hicks [49] studied the short crack growth behaviour in a titanium alloy IMI 685 and suggested that the crack deceleration or acceleration pattern was associated with grain orientiation ahead of a growing crack. If there is a favourable orientation the crack will not slow down alternatively it might retard or arrest.

The study of short crack growth in a medium carbon steel [62,63] revealed an

initial high growth rate while a crack was growing through a ferrite grain followed by a period of slow growth when a crack reached a microstructural obstruction i.e. pearlite/ferrite interface in this case. Once the pearlite phase was overcome, the crack accelerated and continued its propagation. However, the presence of grain or phase boundaries significantly affect the propagation behaviour of cracks in polycrystalline materials [64].

Pearson [65] pointed out the fast crack growth observed in the early stages of growth in a study of short crack behaviour in an aluminium alloy. Other workers [66,67] suggest that a very small or negligible crack closure effect is responsible for this high growth rate.

For the safe design of engineering components and structures, it seems to be necessary that some microstructural aspects must be encorporated while analysing the short crack growth behaviour. Hobson [68] presented an empirical model, discussed later, based on this suggestion. Brown [45] and Taylor [69] reported the importance of an assessment of the microstructural parameter, d , as used in the above model. Taylor suggested that this parameter should be conservative and may be as great as 10 times the average grain size. Later he [70] described this valve in terms of the cyclic plastic zone, r_p , and gave a figure of $10r_p$.

With the outcome of such research it has become evident that short cracks play a key role in the fatigue process and their effect must be considered for developing crack growth models to be used for design purposes.

2.8 Short Fatigue Crack Growth Models

As previously stated, the crack growth rate of short cracks is initially high shows a decrease when cracks approach a microstructural obstruction. This differing behaviour from long cracks where an increase in crack length results in increase in crack growth rate offers severe limitations on the use of the simple Linear Elastic Fracture Mechanics. For adequate quantification of growth behaviour of such cracks previous work has suggested that the influence of microstructure or crack closure effect should be taken into account.

A model based on "grain boundary blockage" was presented by Chang et al [71]. He suggested that a crack can grow only when a critical strain energy at its tip is exceeded and thus an incubation period results for cracks when they approach grain boundaries. The crack length is assumed to be constant during this incubation period. This incubation period may be calculated using parameters such as the applied stress levels, crack length and the distance of the crack tip to the next grain boundary. This model was later modified by Morris et al [72] by removing the original constraint that crack length remains constant throughout the incubation period. He discussed crack growth behaviour across a grain boundary until a mature plastic zone is developed in the next grain. This model can describe crack retardations at grain boundaries but does not explain the fast crack growth rates observed by short cracks before reaching grain boundaries. In order to avoid this limitation he incorporated crack closure into the model. The closure stress was considered proportional to the distance from the crack tip to next grain

boundary. The combination of both incubation and closure gave fair agreement with experimental data.

Later Zurek et al [73] presented two models in extension of the ideas suggested by Morris et al [74] taking into account the effects of crack closure and microstructure. The first model encountered the crack closure effect and was based on the assumptions that the closure stress was directly proportional to the distance (X) from the crack tip to the next grain boundary. The crack closure stress, σ_{cc}, was given by the relationship:

$$\sigma_{cc} = \alpha.X.\sigma_{max}/2a \tag{2.13}$$

where 'a' is the crack length, α a material parameter and σ_{max} is the maximum applied stress. The crack growth was predicted by using the following equation:

$$da/dN = C\Delta K^n[1 - \alpha.X(1.12\sigma_{max})]^n \tag{2.14}$$

where c and n are material constants.

A second model used to describe the incubation period at a grain boundary was formulated as:

$$(da/dN)_m = da/dN[1 - \Delta N_i/\Delta N_p + \Delta N_i] \tag{2.15}$$

where $(da/dN)_m$ is the measured growth rate and is assumed to be a function of the power law growth rate da/dN, ΔN_p is the number of loading cycles spent in propagation as a crack moves across a grain and ΔN_i is the cycles during which

the crack is arrested at the grain boundary.

Chan and Lankford [75] presented a model for short crack growth characterization based on LEFM assumptions considering the variation in orientiation of grains and grain boundary effects. Short crack growth was expressed by the following equation:

$$da/dN = C_1 \Delta K^n [1 - (1 - \tau_b/\tau_a)(D - 2X/D)^m] \tag{2.16}$$

where C_1, n and m are constants, X is the distance of the crack tip from the nearest grain boundary, D is the grain diameter, τ_a and τ_b represent resolved shear stresses in adjoining grains a and b respectively. For a crack growing from grain a to b, it would be relatively easy to initiate slip in the next grain b if τ_b is greater that τ_a. However, when τ_b tends to zero the crack will arrest at the grain boundary.

The above models of Zurek [73] and Lankford [75] were successful when applied to their own results however as these models are based on LEFM assumptions it remains questionable whether they are applicable for short crack growth analyses.

Later, de los Rios et al [62] analysed high cycle torsional fatigue test data of a medium carbon steel using his newly proposed model. This model was based on the crack growth rate being proportional to the strength of the slip band. The crack growth rate was calculated by the following equation:

$$da/dN = f_s \tau_s (L_s - a)/G \tag{2.17}$$

where G is the shear modulus, f_s is the fraction of dislocations on the slip band

governing the crack extension process and L_s is the length of the slip band.

The shear stress τ_s acting on the slip band was given by the following expression:

$$\tau_s = Gn_s b/L_s \tag{2.18}$$

where b is the Burger's vector and n_s is the number of dislocations in a slip band.

This model gives an initial high growth rate when L_s is large but crack growth decreases to zero as its length becomes equivalent to slip band length. The model was successful in predicting crack growth rates for individual cracks when compared with data taken from acetate replicas. Lifetime predictions for a failure crack were however achieved by applying a statistical approach.

Later Hobson and Brown [68] proposed a model for analysing growth rates of microstructural short and physically small cracks respectively consisting of two equations.

The first equation considered the microstructural influence and introduced a parameter, d, to characterise it. This equation predicts decreasing crack growth rate with increasing crack length with growth eventually decreasing to zero as the crack length approaches the value of d. This equation is expressed as:

$$da/dN = C_1(d - a) \tag{2.19}$$

where C_1 is a constant and depends upon applied stress or strain, d is a microstructural barrier length such as grain size and a is the surface crack length.

The second equation represents continuum mechanics type growth and shows a direct proportional relationship between crack length and crack growth rate due

to a lack of microstructural influence. This may be written as:

$$da/dN = C_2 a - D \tag{2.20}$$

where C_2 is also a function of stress or strain and D is a constant describing the threshold crack growth rate.

These two equations may be integrated in the limits of surface roughness i.e. a_0 to d and d to failure crack length, a_f, being summed to predict total fatigue life.

Navarro and de los Rios [76] presented a single equation for the analysis of both microstructural short and physically small cracks. This model suggests that crack growth is proportional to the plastic displacement at the crack tip and may be expressed as:

$$da/dN = f\phi \tag{2.21}$$

where ϕ is the plastic displacement at the tip of the crack and the factor f has been interpreted as the fraction of dislocations on the slip band which participate in the process of crack extension. Both ϕ and f are dependent upon the applied stress level. ϕ may be calculated by;

$$\phi = \frac{2k}{G}\frac{\sqrt{1-n^2}\sigma.a}{n} \tag{2.22}$$

The Hobson-Brown model is explained in detail in chapter 6 where an analysis of the results of the present study has been carried out.

Chapter 3

Literature Review — Environment-Assisted Failure

3.1 Introduction

When a metallic component is exposed to an aggressive environment it may fail in a catastrophic manner. This failure may result from corrosion reactions alone or through the conjoint action of corrosion and applied stress, which may be of a static or cyclic nature. On the basis of the stress state and the role played by the environment in a particular metal-environment system these failures may be conveniently classified into the following categories:

a) Stress corrosion cracking

b) Hydrogen embrittlement

c) Corrosion fatigue

3.1.1 Stress Corrosion Cracking

Stress corrosion cracking(SCC) is a common failure process. It occurs when a metal is subjected to a corrosive environment in the presence of a static tensile stress. The stresses can be externally applied, but residual stresses often cause SCC failures.

Environments that cause SCC are usually aqueous and can be condensed layers of moisture or bulk solutions. Typically, SCC of an alloy is the result of the presence of a specific chemical species within the environment. Thus, the SSC of copper alloys is often due to the presence of ammonia or its derivatives in the environment, similarly chloride ions cause cracking in stainless steels and aluminium alloys. However an environment that causes SCC in one alloy may not cause cracking in another alloy. Changing the temperature, the degree of aeration, and/or the concentration of the ionic species may change an innocuous environment into one that causes SCC failure. Furthermore an alloy may be immune in one heat treatment condition but susceptible in another. Because of such variations the possible alloy-environment combinations that cause SCC is continually expanding and the possibilities are virtually infinite.

Stress corrosion cracking is a delayed failure process. That is, cracks initiate and propagate at a slow rate (for example 10^{-6} m/s) until the stresses in the remaining ligament of metal exceed the fracture strength. The sequence of events involved in the SCC process is usually divided into three stages:

- Crack initiation and stage I propagation

- Stage II or steady-state crack propagation
- Stage III crack propagation or final rupture

Many different mechanisms have been proposed to explain the synergistic stress-corrosion interactions that occur at the crack tip, and there may be more than one process which causes SCC. Proposed mechanisms have been classified into two basic catagories:

- Anodic mechanisms
- Cathodic mechanisms

During corrosion both anodic and cathodic reactions must occur, and the phenomenon that results in crack propagation may be associated with either of these reactions. In neutral aqueous solution the most common anodic reaction is that of active dissolution and removal of metal from the crack tip. Conversely the most common cathodic reaction is hydrogen evolution, which may lead to absorption, diffusion, and subsequent embrittlement.

3.1.2 Hydrogen Embrittlement

Hydrogen Embrittlement is a form of environmetally-assisted failure which results from the adsorption of hydrogen into the metal matrix. This process is accelerated by the presence of a residual or applied tensile load.

There are a number of theories for this type of degradation such as pressure, surface adsorption, decohesion, enhanced plastic flow, hydrogen attack and hydride

formation of which the first three are considered as the most important ones.

The *Pressure Theory* of hydrogen embrittlement is one of the oldest models for hydrogen damage [77]. This theory attributes hydrogen embrittlement to the diffusion of atomic hydrogen into the metal and its eventual accumulation at voids or other internal surfaces in the alloy. As the concentration of hydrogen increases at these microstructural discontinuties, a high internal pressure is developed that enhances void growth or initiates cracking.

The *Surface Adsorption Theory* suggests that hydrogen adsorbs on the free surfaces created adjacent to a crack thereby decreasing the surface energy and hence the work required for fracture [78]. Reduction in the work of fracture would thus enhance crack propagation at stress levels below those typically experienced for a particular alloy in a benign environment. There are many arguments against this model. The principal criticism is that it greatly underestimates the work of fracture and does not account for discontinuous crack growth that has been observed for hydrogen cracking.

The *Decohesion Theory* describes the effect on the cohesive force between force between atoms of the alloy matrix of hydrogen adsorption [79]. Sufficiently high hydrogen concentrations that accumulate ahead of a crack tip are assumed to lower the maximum cohesive force between metal atoms such that the local maximum tensile stress perpendicular to the plane of the crack then becomes equivalent to or greater than the lattice cohesive force and fracture results.

It has been reported that hydrogen embrittlement plays a vital role in the failure

of high strength materials such as steels, titanium and aluminium alloys immersed in sodium chloride solutions [80,81].

3.1.3 Corrosion Fatigue

Corrosion fatigue is another type of environment-assisted failure which occurs as a result of the conjoint action of an applied cyclic stress and a corrosive environment. It is generally suggested that in the presence of an aggressive environment cyclic stresses enhance both the crack initiation and propagation processes for a number of specific metal-environment systems. As a result specimens may fail at very low stresses when compared to tests conducted in an ordinary environment of air. Since the present study mainly concentrates on this particular failure process this topic has been explained in detail in the following sections.

3.2 Corrosion Fatigue

3.2.1 Introduction

The redution in fatigue lifetime of components as a result of the presence of an aggressive environment is becoming very common and can be catastrophic for engineering industries such as processing and energy generation. This has led to an important consideration to be encountered by a design engineer for safer designs.

Previous studies [82-87] have shown that fatigue strength decreases in air when compared to that observed for tests conducted within a vacuum for metals such as

copper, 70:30 brass, lead, molybdenum, aluminium and aluminium alloys. However most of the corrosion fatigue research has been conducted in aqueous or gaseous environments and has considered normal laboratory air as a reference environment. In the present study a similar approach has been adopted. The influence of a corrosive environment is illustrated by the S-N curves given in figure 3.1, which suggests an elimination of the fatigue limit associated with air fatigue testing of ferrous materials. This suggests that there is no 'safe' stress range within which the life should be infinite. It is however convenient to determine an 'endurance limit' namely the stress range below which the material will endure some specified number of loading cycles. An important point to be noted here is that corrosion fatigue lifetime is often prolonged at high stress levels due to retarded initiation resulting from crack blunting as shown by curve A [88]. Results obtained by conducting several fatigue tests on copper and its alloys [89,90] under wet conditions gave longer lifetimes than those tested in air. This beneficial effect was mainly seen at high stresses. Titanium showed a similar effect in another study in which the curve in distilled water was found to fall above that in air. In other systems the whole S-N curve is moved down to lower fatigue lifetimes as indicated by curve B. Previous work [91] and the present study [92] have confirmed both behaviours i.e. curve A and B respectively.

3.2.2 Early Studies

During World War I frequent failures of paravane towing ropes kept in a state of vibration in sea water were observed and was the first reported instance of corrosion fatigue. The first systematic investigation on this subject exploring the causes of such failures was carried out by Haigh [93-95].

Further detailed research in this area by McAdam [96] and later reviewed by Gough [97] is also highly accredited. After conducting a series of experiments McAdam warned of the use of certain alloy steels in place of ordinary steels subjected to cyclic loading. The reduction in corrosion fatigue strengths of various alloy steels in comparison to normal air fatigue has become a well known problem.

Early investigators of corrosion fatigue [98,99] favoured the stress concentration pit theory because physical examination of failed specimens revealed a number of very large cracks initiating from large hemisperical pits at the metal surface. Undoubtedly pitting of metals in aggressive environments leads to a reduction in fatigue life.

3.2.3 Failure Mechanisms

Like the process of air fatigue, corrosion fatigue also consists of two main stages. The first stage concerns that of crack initiation. Previous studies have demonstrated that the presence of an aggressive environment reduces the time period required for the nucleation of cracks. This time period has been mentioned as 10 per cent of the total lifetime unlike 90 per cent stated for air fatigue [88,100],

although this is not exclusively the case as cracks may initiate in a very small fraction of lifetime spending the remaining lifetime in propagation. The simultaneous action of a corrosive environment and a cyclic stress also increases the density of cracks when compared to that observed in air. The possible mechanisms involved in corrosion fatigue crack initiation are explained in the following section. Crack initiation is sometimes assisted by a chemical process which produces chemical notches, i.e. pits. This stage plays a vital role in failure. This is due to the fact that once a crack is nucleated it develops sufficient stress intensification for continued crack growth. The second stage which concerns crack propagation shows purturbations in short crack growth due to microstructural features such as grain or phase boundaries up to a certain crack length. Beyond which a linear relationship might exist between crack length and growth rate for systems where SCC is not operative. Failure usually occurs as a result of the coalescence of a number of individual cracks depending upon the nature of stress and metal-environment system.

3.2.4 Crack Initiation

In smooth specimens crack initiation occurs at the surface which is exposed to the environment resulting in strain localization. This stage usually covers a short period of lifetime but shows a strong dependence upon the stress history and metal-environment combination however much of the corrosion fatigue life is spent in the propagation of cracks.

Corrosion fatigue crack initiation in an aqueous environment may occur as a result of any of the following electrochemical processes:

a) Pitting

b) Preferential dissolution

c) Film rupture

d) Surface energy lowering- (Rebinder's approach)

The possibility of any of the above mechanisms for crack initiation strongly depends upon the metal-environment system.

There are at least three major electrochemical and/or environmentally related conditions that affect crack initiation. These include; (1) active dissolution (unfilmed); (2) passivity (ultra-thin films) and (3) presence of a bulk oxide film on the surface either pre-existing or formed during corrosion fatigue.

Pitting

Pitting may be defined as a localized chemical attack by an aggressive environment at certain 'sensitive' points of the metal surface e.g. inclusions. Pitting is considered as a major mechanism for crack initiation in corrosion fatigue. Pits can be seen very easily on the surface of the metal during the course of a test.

The earliest work of McAdam [101] on pre-pitted steel clearly indicated that pits act as chemical notches which result in early crack initiation and hence lower the fatigue limit. McAdam also showed that where pre-pitting by corrosion reduced the in-air fatigue life, pre-pitting followed by testing in the same corrosive environment produced a further reduction of fatigue strength. The most signifi-

cant reduction of fatigue strength occured after the first few days of pre-corrosion, extended corrosion times up to 300 days caused little further reduction of fatigue strength. This is understandable because although a small pit produces a significant stress intensification by a factor of about 3 for an hemispherical pit, the stress intensification will remain the same if the pit remains hemispherical as it deepens but increases to only about 3.5 if it deepens and becomes hyperbolic in shape [88]. Thus high stress concentration factors will only arise for narrow, sharp tipped and relatively long pits which are probably geometrically indistinguishable from cracks. Jaureneuax et al [102] performed experiments (similar to McAdam's work) on AISI 316 stainless steel and obtained a significant reduction in fatigue limit for pre-pitted specimens relative to normal specimens tested under similar conditions.

In a later study Evans and Simnad [103] conducted a systematic investigation of corrosion fatigue and concluded that the corrosive environment served primarily to initiate surface stress raisers in the form of pits which eventually developed into cracks.

Corrosion fatigue studies of BS 4360 50D steel carried out in NaCl solution by Hodgekeiss [104] and Congleton et al [105] provided evidence of crack initiation associated with the pitting process. Nakasone et al [106] observed that 90 percent of the incipient cracks formed in HT 60 structural steel in aerated 1.0M H_2SO_4 + 1.0M Nacl solution were positively associated with pits.

Corrosion fatigue studies of mild steel in 0.6M Nacl solution have reported that

crack nucleation occurs as a result of the formation and coalescence of micropits created at and around non-metallic inclusions [107].

Although pitting plays a significant role in crack initiation it is not exclusively a pre-requisite for corrosion fatigue cracking and cracking may occur even in the absence of pitting. For example corrosion pits are not essential for enhanced crack initiation as shown by Simnad and Evans [103] and Duquette and Uhlig [108] who tested steel in acid solution and obtained corrosion fatigue in the absence of pitting. Akid [24] showed that pitting was a function of solution pH value with corrosion fatigue cracking arising from pitting in pH 6 solutions and from slip band dissolution in pH 2 solutions. McAdam [101] also pointed out that corrosion fatigue lifetimes were the same as those for tests conducted in air for steel specimens subjected to fatigue in an environment of 3 per cent NaCl + NaOH at pH 12 even though the presence of hemispherical pits was evident. This may have occured as a result of pit geometry and also the presence of thick protective oxide layer on the surface of the specimens causing blocking of slip movements. Fatigue tests carried out on high purity aluminium specimens in a tap water [109] produced a large number of pits but there was no significant evidence of their association with crack initiation.

Preferential Dissolution

The tendency of a metal to dissolve in a solution depends upon the ease with which its atoms may be oxidised. This results in the formation of positively charged metal ions flowing into the solution.

Preferential dissolution often occurs as a result of chemical inhomogenity. It has been reported [110] that low carbon steel in nitrate solution is susceptible to preferential dissolution along grain boundaries due to solute segregation along these boundaries. Duquette and Uhlig [108] have pointed out that the role of preferential dissolution is to effectively unlock otherwise blocked slip processes thereby accelerating the intrusion-extrusion phenomenon thus causing premature crack initiation.

Evans and Duquette [111] suggested that any stress applied causes atoms to move to the crack tip region. These atoms are believed to be electrochemically more active than other atoms of the matrix and will tend to dissolve preferentially.

Hoar and Hines [112] demonstrated that a relationship between the rate of metal dissolution and the rate of application of strain exists. A large increase in metal dissolution rate does occur but only for certain metals which include iron.

It has also been shown by Hahn et al [113] and Masuda et al [114] that controlled dissolution of a polycrystalline copper surface during cyclic deformation (under load control) results in broadening of the PSBs as well as enhanced growth of both the number and the height of PSBs when compared to specimens cyclically deformed in laboratory air. In polycrystals however crack initiation and early propagation were in general primarily confined to grain boundaries. When single crystals were tested PSB formation was also enhanced, although the broadening of the PSBs resulted in a delay in crack initiation and fatigue lifetimes that were observed to be even longer than for those observed in air [115]. These experiments

demonstrated that there is a significant interaction between the development and growth of PSBs and corrosion.

Laird and his co-workers [116,117] have performed experiments on single crystals of copper, both unfilmed (actively dissolving) and filmed (corrosion resulting in a bulk oxide film). For unfilmed specimens (active corrosion), an increase in the number of PSBs was reported and the spacing of the PSBs was decreased and preferential dissolution of the PSBs was observed which is in agreement with the results of Duquette and co-workers [113-115,118-120].

In another study of the corrosion fatigue behaviour of copper Yan et al [116,117] pointed out that there are strong interactions between simultaneous corrosion and cyclic straining in that enhanced corrosion was observed. They confirmed the results of Duquette et al [113-115,118-120] in that enhanced dissolution is caused by the emergence of mobile dislocations, specifically enhanced dissolution of metal atoms associated with those dislocations that form the PSBs. This study also concluded that below a critical preferential corrosion rate, corrosion has no appreciable effect on fatigue resistance [116]. A similar result had been reported for carbon steels [108], although Yan and Laird indicated that the critical corrosion rate was specific to PSBs rather than a general corrosion rate.

Film Rupture Mechanism

This mechanism depends upon the applied stress/strain level and may only be applicable in an environment where any surface films formed are insoluble in nature. It suggests that during cyclic loading an oxide film formed on the specimen surface

is damaged mechanically by the slip steps emerging from beneath the surface causing dissolution of the more anodically-active bare metal exposed to the corrosive environment. This may result in rapid dissolution and/or the development of a stress concentration leading to crack nucleation at the point of rupture.

An interesting study by Kondo et al [121] indicated that the fatigue lifetimes of steels subjected to corrosion fatigue conditions in a steam environment decreases with the decrease of frequency but only up to a certain critical value. An improved life was observed at frequencies below a critical value of 1 cpm (0.016 Hz). This phenomenon is likely as a result of the time-dependent film repair process during the tensile half of the fatigue cycle. Thus the ratio of the rate of film rupture to rate of film repair determines the reduction or improvement in fatigue lifetime as a function of the frequency of loading.

Beital and Bowles [118] have reported that a significant delay in crack initiation may occur in specimens tested under oxide film coating conditions. Hahn and Duquette [113] have also demonstrated the association of crack initiation with the rupture of protective films by fatigue-generated deformation.

Surface Energy Lowering - The Rebinder's Approach

There have also been suggestions that the environment may lower the surface energy of a metal or alloy (the so-called "Rebinder Effect") resulting in enhanced deformation and possibly easy crack initiation [123].

The Rebinder mechanism is based on the assumption that the surface energy of a solid immersed in a solution may be lowered by the chemisorption or adsorp-

tion of some chemical species present in the environment. Rebinder [124] while suggesting this mechanism pointed that the adsorption of certain species from solution facilitiate the process of slip thus providing assistance in more active work hardening and cavity formation leading to early creation of incipient cracks.

Benedicks [125] reported that the wetting of metal surfaces by liquid environments could be responsible for a number of environment sensitive mechanical properties including corrosion fatigue by a reduction in the surface energy of the solid leading to a dilation of surface atomic bonds thus facilitating the slip process. According to this worker, the effect should increase with decreasing surface tension of the liquid thus pointing to a marked effect of strong surface active agents such as oleic acids.

Laird et al [126] in quoting the suggestion made by Karpenko that the mechanism of corrosion fatigue may be dependent on applied stress level pointed out that at high stresses (i.e. lifetimes of 10^4 - 10^5 cycles) crack initiation is attributed to hydrogen adsorption at cathodic sites with subsequent embrittlement; at moderate stresses (long lives 10^5-10^6 cycles) environment adsorption promotes crack initiation through a surface energy reduction at highly stressed anodic sites and at low applied stresses (lives greater than 10^6 cycles) crack initiation is promoted by the destruction of a protected oxide film due to a lowering of the electrode potential in highly stressed anodic areas.

The above opinion gained some weight when Petch [127] demonstrated that the adsorption of hydrogen on a metal surface may reduce the interatomic attraction

between atoms resulting in a lowering of the surface energy.

3.2.5 Crack Propagation

Once a crack is initiated by one of the possible processes mentioned above it may continue to propagate until failure of the specimen occurs depending upon its stress concentration relative to other cracks present. The crack propagation behaviour in many cases simulates that observed for air fatigue but crack growth rate is increased due to the synergistic action of the corrosive environment and cyclic stress.

It is very difficult to fully understand the exact mechanism contributing to corrosion fatigue crack growth. It has been suggested however that, depending upon the specific metal-environment system, aqueous corrosion fatigue crack growth is controlled by *anodic dissolution* (AD) or *hydrogen embrittlement* (HE) at the crack tip which in turn is governed by the prevailing electrochemical reactions.

In the case of anodic dissolution the fresh metal surface at the crack tip dissolves and passes into solution. The anodic reaction which occurs in ferrous materials, equation 3.1 involves the oxidation of metal atoms to metal ions. Simultaneously, depending upon the solution pH, a cathodic reaction involving the reduction of dissolved oxygen to hydroxyl ions, or reduction of hydrogen ions to gaseous hydrogen, takes place on the crack sides or on the external surface acting as a cathode, equation 3.2. In neutral or alkaline solutions, equation 3.2 controls the corrosion rate and the overall reaction is given by equation 3.3. The total reaction for iron is described by

$$Fe \longrightarrow Fe^{++} + 2e \tag{3.1}$$

$$1/2O_2 + H_2O + 2e \longrightarrow 2OH^-; pH > 7 \tag{3.2}$$

$$2Fe + O_2 + 2H_2O \longrightarrow 2Fe(OH)_2 \tag{3.3}$$

However where conditions are such that hydrogen embrittlement may result equation 3.2 is replaced by equation 3.4 . This cathodic reaction represents the redution of hydrogen ions to atomic hydrogen which may control the crack growth when the pH of the solution falls below 7.

$$H^+ + e \longrightarrow H(adsorbed); pH < 7 \tag{3.4}$$

Scott [128] reported that oxygen is consumed as it diffuses down the crack enclave resulting in the formation of an insoluble metal hydroxide and a strong acid.

$$Fe^{++} + 2Cl^- \longrightarrow FeCl_2 \tag{3.5}$$

$$FeCl_2 + 2H_2O \longrightarrow Fe(OH)_2 + 2HCl \tag{3.6}$$

These hydrolysis reactions enhance the acidity of the solution at the crack tip thereby creating conditions whereby hydrogen ion reduction, equation 3.4, can proceed at a significant rate promoting hydrogen formation within the crack. The hydrogen atoms produced can combine to form molecular hydrogen or diffuse into the metal.

Several research workers have quoted their views in an attempt to explain the mechanisms involved in corrosion fatigue crack growth. For example, Dervinis et al [129] pointed out that corrosion fatigue testing of an Al-Li alloy 2090 in 3.5 percent NaCl solution resulted in reductions in fatigue life of up to four orders of magnitude. The major mechanism for corrosion fatigue in this case appeared to be hydrogen embrittlement. Austen and McIntyre [130] also considered hydrogen embrittlement while explaining the corrosion fatigue results of a high strength steel.

Ford [131] employed the anodic dissolution process with success to explain fatigue crack propagation rates in an Al-7.0 percent Mg alloy in 3 percent NaCl solution. The anodic dissolution of localized slip has also been suggested in the study of corrosion fatigue behaviour of 316L alloy tested in chloride solutions [132].

More recently Akid [91] pointed out that anodic dissolution controlled torsional corrosion fatigue crack growth in a low strength low alloy steel (BS 4360 50B) exposed to 3.5 percent NaCl solution.

3.3 Variables Affecting Corrosion Fatigue

Corrosion fatigue crack growth may be affected by a number of variables generally classified into the following three categories:

a) Loading variables

b) Environmental variables

c) Metallurgical variables

The influence of each category will be briefly described below.

3.3.1 Effect of Loading Variables

Effect of Stress Amplitude/Stress Intensity Factor Range; In general, a low amplitude of cyclic stress/stress intensity permits greater opportunity for involvement of the environment and favours larger environmental effects in the failure process. Where stresses/stress intensities are sufficiently high, environmental interaction may be reduced, because the mechanical crack driving force becomes dominant. However stress amplitude must be considered together with mean stress, frequency and crack length which governs the nature of the crack tip chemistry. For the stress intensity factor range, stress must be considered in conjunction with the crack size in determining the stress-intensity factor range. Low stress/stress-intensity levels may allow adequate time for environmental interaction however if the frequency is high the crack tip may be exposed to the environment for only a very short period of time thus, only limited environmental action may take place.

Effect of Frequency; Cyclic frequency generally shows little/no effect on fatigue behaviour in non-aggressive environments whereas in aggressive environments fatigue strength is strongly influenced by a change in frequency. For most materials, the frequency dependence of corrosion fatigue is thought to result from the fact that the interaction of a material and the environment is essentially a time-dependent process. Low frequencies, especially at low stress amplitudes allow more time for interaction of the environment with the material causing greater damage. Conversely, high frequencies, particularly when a high stress amplitude is involved tend not to affect fatigue life.

In general, the total duration of the test is an important factor since corrosion is time-dependent [101,133,134]. It has been said that a given time produces greater damage at a high frequency, but a given number of cycles results in greater damage at low frequencies. Endo and Miyas [135] reported that for low alloy steels in fresh water a frequency of 1450 cycles/min (24 Hz) caused failure in 10^6 cycles or 11.5 hours, but at a frequency of 5 cycles/min (0.08 Hz) failure took place after after 1.1 $\times 10^5$ cycles or 360 hours.

Barsom [136] has also reported the effect of frequency. He showed that a decrease of frequency resulted in an accelerated corrosion fatigue crack growth. Scott [137] suggests that change of frequency determines the time available for passivation and hence environmental interaction. The influence of frequency on corrosion fatigue crack growth rate is shown in figure 3.2 [138].

Effect of Mean Stress/Stress Ratio; High tensile mean stress will increase the duration that the crack will open which may enhance corrosion fatigue damage during each cycle. Corrosion fatigue crack growth rates are generally enhanced by an increase in the stress ratio, R , which is the ratio of the minimum stress to the maximum stress.

Figure 3.3(a) shows an example taken from the structural steel-sea water system for a range of R ratios from 0.1 to 0.85 . It is apparent that positive R ratios (indicating high mean tensile stresses superimposed on the cyclic stress) significantly enhance crack propagation rates, in this particular case the effect saturates between R = 0.5 and 0.7 . Negative R ratios, which indicate compressive stresses

operate for a proportion of the stress cycle, have been shown to have no effect on crack growth rate [128].

Effect of Stress-Wave Form; The cyclic stress wave form affects the influence of an aggressive environment. Prolonged exposure at peak stress contributes to accelerated crack growth. A typical behaviour is shown in figure 3.3(b).

Atkinson and Lindley [139] suggested that 'positive saw-tooth" wave shape may be more damaging than others under identical frequency conditions due to its slow rise time. Barsom [136], who tested a 12Ni-5Cr-3M0 steel in 3.5 percent NaCl solution with R=0 at 0.1 Hz has reported that only those wave-shapes with slow rise times, i.e. sinusoidal, triangular and positive saw-tooth, show enhanced crack growth rates. Other forms such as negative saw-tooth, and skewed with fast rise times gave results identical to the air fatigue data.

Effect of Loading Mode; The change in loading mode may significantly affect the corrosion fatigue crack growth behaviour.

Magnin et al [132] while presenting a comparison of corrosion fatigue results of 316L stainless steel alloy with stress corrosion cracking behaviour, suggested that the tension-compression test was much more severe that the cyclic tensile stress and induces damage which can occur even if stress corrosion cracking was not observed. The damaging effect due to tension-compression tests can be explained in terms of a localization of the plastic deformation and of the anodic dissolution which occur in this case. During the first cycles the multiplication of the slip lines induces an increase of the anodic current density i.e. fatigue slip bands promote a localization

of the dissolution process.

Yoda [140] studied stress corrosion cracking (SCC) behaviour of a high strength steel in water and 3.5 percent salt water under modes I, II and III loading. The results showed that the susceptibility of this material to stress corrosion cracking was considerable for mode I but negligibly small for mode II and mode III. This suggests that mode I corrosion fatigue crack growth may also be assisted by SCC for metal-environment systems prone to stress corrosion cracking.

3.3.2 Effect of Environmental Variables

Influence of Chemical Activity of the Environment; Corrosion fatigue resistance of a material significantly decreases by increasing the chemical activity of the environment, for example by lowering the pH of a solution or by increasing the corrodent concentration. Conversely an improvement may be observed on decreasing the chemical activity.

Parkins [141] suggested that for corrosion fatigue studies of aluminium in 3.5 per cent NaCl solution, the increase in pH value from 7 to 10 changed the form of dissolution from that of preferential to the case of general corrosion. Radd et al [142] conducted fatigue tests in 3% NaCl solution, at a pH above 12.1 the results showed that a fatigue limit was regained and this limit increased at still higher pH values. These investigators suggested that corrosion fatigue results from the formation of differential aeration cells which produce pits on the metal surface and that a high pH value provides a barrier, in the form of ferrous hydroxide, to the

diffusion of oxygen from within the bulk solution.

Congleton and Craig [88] pointed that an increase in pH of 3.5% NaCl solution from 7 to 10 resulted in rapid corrosion fatigue crack initiation in BS 4360 50D steel. A typical figure illustrating pH effects on this metal-environment system is shown in figure 3.4.

Corrosion fatigue tests performed on mild steel specimens in distilled water and in various concentrations of KCl have shown that solutions ranging from 0.025M to 2.0M have virtually identical effects on corrosion fatigue lives however at concentrations below 0.025M the effect approaches that of distilled water, although corrosion rates increase in an almost linear manner with solution ion concentration [143]. A typical example illustrating the influence of corrodent concentration on corrosion fatigue resistance of 13Cr steel is shown in figure 3.5 [144].

Effect of Temperature; Temperature can affect corrosion in a number of ways. If the corrosion rate is completely governed by the elementary process of metal oxidation the corrosion rate increases exponentially with an increase in temperature. This relationship is reflected in the Arrhenius expression:

$$r = Aexp(-E/RT) \tag{3.7}$$

where r is the corrosion rate, A is a pre-exponential factor, E is the activation energy, R is the gas constant and T the absolute temperature.

Corrosion fatigue crack growth rates tend to increase with increasing temperature. There are indications that the rate-controlling process for crack growth may be thermally activated.

Gould [145] conducted corrosion fatigue tests on mild steel in artificial sea water at constant temperatures of 15, 25, 35 and 45^{0}C showing there to be a significant effect of temperature, with fatigue life being approximately halved when the temperature was raised from 15 to 35^{0}C. A similar effect has also been discussed by Dugdale [146]. The influence of temperature may be seen from figure 3.6.

Influence of Electrode Potential; Electrode potential like loading frequency strongly influences corrosion fatigue crack propagaion in aqueous environments. Controlled changes in the potential of a specimen can result in either the complete elimination of corrosion fatigue or dramatic brittle fracture depending upon the nature and rate of the corrosion reactions prevailing at the particular applied potential.

For steels that crack by hydrogen embrittlement when stressed in aqueous solutions, corrosion fatigue cracking may be increased on the application of high cathodic polarization potentials. For each steel stressed at constant ΔK in aqueous chloride [147,148] at the free corrosion potential the crack growth rate is about three times faster than that reported for air and is enhanced by a factor of five at a very high cathodic potential. For the low strength steel BS4360:50D intermediate potentials appear to be mildly beneficial.

3.3.3 Effect of Metallurgical Variables

Effect of Chemical Composition; Alloys which show good general corrosion or SCC resistance often show increased resistance to corrosion fatigue susceptibility. For

example, chromium steels generally show better resistance to corrosion fatigue than carbon steels [149]. Wescott [99] pointed out that chromium is the most effective alloying element for increasing the corrosion fatigue strength in the absence of hydrogen sulphide and nickel is the most effective in the presence of hydrogen sulphide.

Effect of Microstructure and Heat Treatment; Microstructural characteristics such as grain size and second-phase particles can affect corrosion fatigue behaviour. Materials having small grains are generally more resistant to crack initiation because stress concentrations occuring at the surface are lower when compared to the coarse grained material.

Corrosion fatigue behaviour is significantly affected by heat treatment processes that alter the microstructure and distribution of alloying and impurity elements, for example, quenched and tempered steels are much susceptible to corrosion fatigue. Wescott [99] suggested that internal stress resulting from heat-treatment (hardening and tempering) has a deleterious effect on the corrosion fatigue limits than for plain-carbon and medium alloy steels. Therefore steels in heat treated condition suffer greater damage than when in a normalized, annealed or hot rolled condition.

3.4 Preventive Measures for Corrosion Fatigue

The presence of an aggressive environment generally reduces the fatigue strength of a component. The corrosion fatigue life of a component may be increased by

taking into account one or combination of the following measures.

Design Considerations

The importance of design in minimising air fatigue failure is well known, and similar considerations naturally apply in designing for corrosion fatigue conditions. Design is also important in combating corrosion; in particular, it is necessary to avoid crevices, for example in joints where stagnation may arise owing to inaccessibility to air and the development of an anodic area or, in the case of a closed system where inhibitors are being used, bimetallic corrosion, preferential corrosion of two phase alloys etc.

Choice of Material

For permanent solutions a new material may be selected. The substitution of a more corrosion resistant material, e.g. Monel metal or stainless steel, is often advocated. However this is not necessarily always the correct remedy; a 15 percent chromium steel for instance is prone to failure in corrosion fatigue because of the disruption of the normally protective surface film.

Inducing Surface Compressive Stresses

The protection of steel against corrosion fatigue has been one of the major preoccupations of corrosion engineers. The beneficial effect of inducing a compressive stress in the surface of the steel applies to corrosion fatigue as well as air fatigue. For example, improvement in corrosion fatigue strength has been obtained by shot

peening [150], and nitriding [151]. Inglis and Lake [151,152] found that the corrosion fatigue limit of nitrided steel to be 68 percent of the in-air endurance limit when tested in river water for 170 million cycles.

Cathodic/Anodic Protection

Zinc cathodically protects steel by sacrificial action, a method that can also be achieved by applying a potential more negative than the free corrosion potential of the metal. This method has been shown to be effective on mild steel in 3 per cent NaCl solution [153]. At an applied potential of 0.49V (vs S.H.E) or below, the fatigue life of specimens became constant and the fatigue limit observed in air was restored.

An interesting variant of cathodic protection is anodic protection which relies on the preservation of a passive protective film on the surface of the material. Cowley, Robinson and Kerrich [154] have shown that this method can be successfully applied to plain carbon and stainless steels in an oxidising environment. The improvement is greatest with the stainless steels which rely on a protective oxide film for their corrosion resistance. In some cases the fatigue strength is greater than in air, and the superior protection is afforded by the anodically formed film compared with the air-formed film. There are limitations to its applications, for example, if crevice conditions exist in certain areas, accelerated attack may result at these points.

Coatings

Electro-plated coatings often improve resistance to corrosion fatigue. Allsop [155] noticed a significant improvement in endurance limit (10^6 cycles) of a zinc-plated 0.63 percent carbon steel wire tested in sea-water with zero mean stress when compared with unplated material. Similar comments are given by Harvey [156]. Whittaker and Liddiard [157] who reported that sufficient protection to corrosion fatigue was obtained when metal coatings were given to aluminium alloys.

Use of Inhibitors

Inhibitors have been shown to be beneficial. The concentration of inhibitors required for protection differ for stressed and unstressed systems. It has been suggested that a higher concentration of inhibitors was required for stressed systems in order to protect against uniform corrosion [158,159]. This is due to the additional effect of mechanical breakdown of the films in the presence of the stress. This has also been confirmed by the work of Gould and Evans [160] while studying corrosion fatigue behaviour of drawn mild steel wires in a KCl solution with and without K_2CrO_4 additions.

3.5 Electrochemical Studies

The corrosion of metals in the presence of an aqueous solution occurs as a result of electrochemical reactions. The corrosion process defines the occurance of cathodic and anodic reactions at the surface of a metal. Many research workers

have shown considerable interest in conducting electrochemical tests for corrosion studies. These tests offer a number of advantages:

1) they allow a study of the mechanisms involved in the corrosion process.

2) they facilitate an acceleration of corrosion process, for example, they can be used to increase or control the oxidizing potential of an envoirnment enabling the determination of specific characteristics of a metal such as passivity to be small without the addition of chemical oxidizing agents.

3) corrosion rate measurements may be conducted without specimen removal from the environment or significant disturbance.

However there are some limitations of these tests such as :

1) it is necessary for the environment to be an electrolyte.

2) resistance drops through insulating layers and dilute electrolytes severely limit corrosion measurements.

3) all electrodes in use must be in intimate contact with the environment.

4) the corrosion rate being measured will be average over the entire specimen often and that of a filmed surface.

5) the electrodes must be isolated keeping themselves free from electric contact.

The electrochemical corrosion rate may be determined by estimating the corrosion current using polarization and linear polarization resistance methods and applying Faraday's Law.

The first method may employ three different techniques for the estimation of corrosion currents: The specimen may be polarized cathodically to potentials at

least 50mv more negative than the free corrosion potential taking sufficient data points to allow a determination of the cathodic Tafel slope. The cathodic Tafel line may be extrapolated back to the free corrosion potential line where the point of intersection with free corrosion potential line gives the value of corrosion current density i.e. i_{corr}. The second technique is similar to first with the exception that the specimen is polarized anodically to potentials greater than 50mv more positive than the free corrosion potential. A third technique involves both cathodic and anodic polarization and is conducted as described with the corrosion current , i_{corr}, being obtained at the intersection of the extrapolated anodic and cathodic Tafel lines. These three techniques are shown in figure 3.7.

The second method used for corrosion current determination is known as *Linear Polarization Resistance.* This method is based on the application of only a small potential to the specimen. By measuring the current produced by this change a potential-current density plot is obtained which is approximately linear in the region within 10mv of the free corrosion potential.

The Polarization Resistance, R_p, of a corroding electrode is defined as the slope of a potential (E)-current density (i) plot at the free corrosion potential E_{corr} and has the units of $ohm.cm^2$.

$$R_p = (\partial \Delta E / \partial i), \Delta E = 0 \tag{3.8}$$

whereΔE = E - E_{corr} is the polarization from the corrosion potential and i is the current density corresponding to a particular value of ΔE.

From the Polarization Resistance, R_p, the corrosion current density, i_{corr}, can be calculated using the relationship [161].

$$i_{corr} = B/R_p \tag{3.9}$$

Where B involves both the anodic and cathodic Tafel slopes (b_a, b_c): as given;

$$B = b_a b_c / 2.303(b_a + b_c) \tag{3.10}$$

b_a and b_c may be determined by adopting the single sweep procedure as described by Mansfeld [161] or by a method of curve fitting to the Linear Polarization Resistance curve or using the polarization curve performing another experiment.

The advantage of polarization measurements are the possibility of recording instantaneous corrosion rates and the use of this technique for on-line monitoring of a large number of processes in which corrosion might cause problems [162].

In another approach *Faraday's Law* may be applied for the corrosion current density, i_{corr}, estimation. This law may be presented as equation 3.11.

$$i = \frac{zFW}{M} \tag{3.11}$$

Where i is the corrosion current, z is the valence charge on the cation, F Faraday's constant, W is the weight loss, and M is the atomic weight of iron.

The corrosion current, i, is proportional to the metal dissolution occurring as a result of corrosion. The amount of dissolution may be determined by considering loss in weight of metal or the ferrous ion(Fe^{++}) concentration in the solution.

More recently, there has been considerable interests in methods to evaluate the tendency of the materials to exhibit selective area corrosion i.e. pitting or crevice corrosion by means of polarization techniques. The method adopted is one in which an increasing potential is applied until the specimen reaches the transpassive or pitting region [163]; the potential sweep is then reversed and return of the current to the passive region is recorded. The characteristics of this current-potential hysteresis curve are thought to be related to the tendency of the material to pit or show crevice corrosion in the environment in question.

3.6 Environment-Assisted Fatigue Crack Growth Models

3.6.1 Introduction

It seems appropriate to shed some light on the types of corrosion fatigue crack growth described by Austen and Walker [164] before discussing crack growth models . He described these processes as; True Corrosion Fatigue (TCF) and Stress Corrosion Fatigue (SCF):

True Corrosion Fatigue identifies the behaviour where fatigue crack growth rates are enhanced by the presence of an aggressive environment through a synergistic action of corrosion and cyclic loading. This is also known as corrosion fatigue below K_{ISCC} and applies to materials which do not stress corrode such that $K_{ISCC} \geq K_{IC}$. Where K_{ISCC} is a threshold stress intensity factor for stress corrosion

under mode I loading and K_{IC} is related to the critical stress intensity, K , for fracture [165] as shown in figure 3.8(b). Here the environment accelerates fatigue crack growth below K_{ISCC}, a common scenario for low-to-moderate strength alloys that are either immune to SCC or exhibit high K_{ISCC} and low da/dt. This type of behaviour was discussed by Barsom based on the data for a maraging steel exposed to 3 per cent NaCl [136,166], where a substantial corrosion fatigue effect was seen below the static load threshold (K_{ISCC}) but only for those loading waveforms that include a slow deformation rate to maximum stress intensities. True corrosion fatigue has been observed in aluminium alloys [86,167-171]. This type of corrosion fatigue crack growth behaviour is illustrated in figure 3.9(a).

Stress Corrosion Fatigue is also known as 'corrosion fatigue above K_{ISCC}' and is shown in figure 3.9(b). It describes static load stress corrosion cracking under fatigue conditions which occurs whenever the stress intensity in the fatigue cycle is above K_{ISCC}. Such behaviour is possible for those material-environment systems which are susceptible to stress corrosion cracking and environmental influence is seen after reaching K_{ISCC}. This type of behaviour may be characterised by a 'bump' with a plateau of growth rates as observed in stress corrosion crack growth. Stress corrosion fatigue has been observed in both steels [172-175] and titanium alloys [176].

The final and the most common type of crack growth behaviour pertains to material-environment systems which exhibit Stress Corrosion Fatigue(SCF) above K_{ISCC} and also True Corrosion Fatigue(TCF) at all stress intensity values. A

mixed behaviour is represented schematically in figure 3.9(c). Either true corrosion fatigue or stress corrosion fatigue could be induced in a material. For example Meyn [177] showed that this change in mechanism could be seen for a titanium alloy by changing the frequency and R ratio of the cyclic loading. Similar results have also been observed in other investigations on steels [164].

3.6.2 Long Cracks

Only within the last few decades has an extensive study on the influence of aggressive environment on the fatigue strength of metals been carried out. Modelling of the environment-assisted crack growth is therefore limited to a few poineer workers [137,173,178-183].

Wei and Landes [173] first proposed a superposition model which summed the stress corrosion component of crack growth with air fatigue crack growth. Whenever K exceeds K_{ISCC} during cyclic loading and the fatigue crack propagation component developed in a reference environment. This model can be expressed as;

$$(da/dN)_{cf} = (da/dN)_r + \int da/dt K(t) dt \qquad (3.12)$$

where $(da/dN)_{cf}$ is the rate of fatigue crack growth in an aggressive environment, $(da/dN)_r$ is the rate of fatigue crack growth in an inert environment and the integral term is the environmental contribution obtained from sustained load crack growth observed in the same environment. Such an approach is applicable when type b behaviour is observed (see figure 3.9(b)), since it predicts that below K_{ISCC} level there is no environmental effect. This model takes no account of synergis-

tic interactions between corrosion and fatigue, nevertheless good agreement was obtained between the experimental and predicted lifetimes. Also the effects of frequency, R ratio, and wave-shape were also satisfactorily predicted [173,178].

A related approach has been adopted to account for frequency effects on the corrosion fatigue behaviour of α-brass tested in a tarnishing solution of ammonia [179]. In this case it is postulated that a film forms at the tip of the crack in each cycle and the thickness of this film per cycle is estimated on the basis of macroscopic kinetics. Superposition of the corrosion reaction upon the mechanical process of crack advance may be shown by

$$da/dN = 8/\pi[(K_{max}/E)^2 - (K_{th}/E)^2)] + b(f) \qquad (3.13)$$

where b(f) represents the amount of tarnish formed per cycle, a function of the frequency, f. A fair agreement between the observed and predicted lifetimes was obtained using this approach. Later Austen and Walker [164] suggested a model known as 'The Process Competetion Model'. The basis of this model is that the processes of the stress corrosion and fatigue (or true corrosion fatigue) are mutually competitive, not additive as in the Wei and Landes model [173]. It is assumed that the crack will propagate by the fastest available mechanism pertinent to the prevailing stress intensity. This implies that corrosion fatigue crack growth curves can be constructed by combining fatigue and stress corrosion (See figure 3.8 (a,b)) and simply taking the fastest rate throughout. The model may be presented as;

$$(da/dN)_{cf} = max[(da/dN)_r.(da/dt)1/f] \qquad (3.14)$$

where $(da/dN)_{cf}$ and $(da/dN)_r$ represent fatigue crack growth in aggressive en-

vironment and inert environment respectively and the final term accounts for the aggressive environmental contribution.

These workers while studying the behaviour of 835M30 steel in 3.5% NaCl suggested that the process competetion model may be used to construct corrosion fatigue crack growth curves for any combination of stress ratio and frequency. This facility may have a value in terms of material selection for optimum resistance to corrosion fatigue and calculation of lifetimes for design purposes.

The corrosion fatigue crack growth behaviour above K_{ISCC} has also been quantified by Gallagher and Wei [180]. They presented the following model;

$$(da/dN)_{cf} = (da/dt)_{env} + (da/dN)_r . f \qquad (3.15)$$

where $(da/dt)_{env}$ is a time-dependent component of crack advance and is strongly dependent on the wave-shape, the maximum stress intensity, the stress intensity range and the environment used. The factor f denotes the frequency of loading.

Gallagher [180] studied the fatigue behaviour of 4340 steel in 3.5 percent NaCl solution and showed that the effect of changing the frequency on corrosion fatigue cracking was adequately predicted by using this model. The loading pattern used was fully reversed and sinusoidal so that only during part of loading cycle was the stress intensity level above K_{ISCC}.

Barsom [136] explored the influence of changes in both stress intensity and frequency on the 'below K_{ISCC}' corrosion fatigue behaviour of a 12Ni-5Cr-3Mo steel in 3 percent NaCl solution. His results showed that as the frequency was decreased from 600 cpm to 6 cpm, the environmental effects on crack growth rates

increased. He calculated crack growth rate using the following equation;

$$(da/dN) = D(t)(\Delta K)^2 \tag{3.16}$$

where D(t) is a constant for any given frequency and is a function of time, t. It is dependent upon the particular metal-environment system. In air D(t) was constant and also independent of frequency. Its value increased with the decrease of frequency a maximum was observed at 6 cpm (0.1 Hz).

He also pointed out that the stress wave-form is very important as sinusoidal, triangular or positive saw tooth wave-forms resulted in an increase in D(t) values three times higher than observed in air. However, crack growth rate was not affected by other wave forms such as square and negative saw-tooth type.

3.6.3 Short Cracks

Most of the work to date on corrosion fatigue has been carried out with long LEFM type cracks. Recently more interests has been shown in short crack studies as it has been recognised that under corrosion fatigue conditions small cracks of an 'equal stress intensity' propagate much faster than long cracks [24,184,185]. Gangloff [185] reported that below a crack length value of 3 mm environmental enhancement was significant.

Hodgkiess [104] carried out corrosion fatigue tests on a structural steel in sea water and suggested that this environment was more influential on crack initiation than on the relatively short crack propagation. He pointed out that the enhanced crack propagation rates in sea water are considered to be due to anodic dissolution

at the crack tip with hydrogen embrittlement playing a minor role.

Speidel [186] demonstrated that high strength aluminium alloys in an over-aged condition may show large reduction in fatigue life due to intergranular small crack initiation and propagation when subjected to an aqueous sodium chloride environment. However crack tip opening strain was considered to play a major role producing high growth rates of small cracks developed in aluminium alloys under moist air conditions [187].

Nakai et al [188] reported rapid growth rates observed for short cracks while testing HY130 steel in 3.5 percent sodium chloride solution. They suggested that with an increase in crack length, growth rates for short cracks converged to those of long cracks. Short cracks propagated at a rate up to a factor of two faster than long cracks. Gangloff and Ritchie [189] demonstrated that in a steel/purified hydrogen gas system high growth rates for small cracks when compared to long cracks seemed to be due to the lack of crack closure effect.

Several other researchers proposed that environmental effects can increase the growth rates of short cracks in aggressive environments [190-192]. Gangloff [190-192] who conducted corrosion fatigue tests on high strength AISI 4340 steels in aqueous 3 percent NaCl solution suggested that corrosion fatigue short crack propagation rates increased up to two orders of magnitude than corresponding rates of long cracks at the same ΔK level, although the behaviour in inert environments was essentially similar.This phenomenon is not completely understood but preliminary analyses have indicated that effect could be attributed to differences in the

local crack tip environment of long and short cracks, resulting mainly from different electrochemically active surface-to-volume ratios of the cracks arising from the influence of crack length on the solution renewal rate in the crack tip region [190,192,193].

Few quantitative models have been developed to analyse corrosion fatigue short crack growth behaviour taking into account a mechanism of hydrogen embrittlement or dissolution.

Although studying physically short cracks the modelling of Gangloff and Ritchie [189] is worth noting. They suggested a model based on hydrogen embrittlement and presented the following equation;

$$da/dN = \phi(C_h).(\Delta K)^2 \tag{3.17}$$

where C_h depends upon stress level, time and crack length. C_h is a measure of the quantity of adsorbed hydrogen and this factor represents the chemical driving force available for environmental crack growth. ΔK in this case represents the mechanical driving force and ϕ is a constant.

Turnbull and Newmann [195] proposed a mathematical model considing a number of factors such as mass-transport theory, electrochemical reaction rates at the crack tip and on the crack walls and film rupture mechanisms for anodic dissolution controlled corrosion fatigue.

In another model Ford and Hudak [196], while analysing the results obtained from the tests conducted on stainless steel in water environment at different temperatures, suggested that film rupture followed by slip dissolution was responsible

for crack growth.

Akid [91] working on the study of corrosion fatigue of microstructure dependent and physically-short crack growth of a low strength low-alloy steel in 3.5% NaCl solution considered a linear summation model. He proposed that for torsional loading anodic dissolution at the crack tip was the major electrochemical reaction contributing to crack advance . The most significant effect observed was an elimination of the in-air fatigue limit. An explanation given for this was that an additional chemical driving force was available for crack growth at sub-fatigue limit stresses and that dissolution allowed growth beyond crack arresting features associated with the microstructure. He presented the following model;

$$(da/dN)_{env} = (da/dN)_{air} + (da/dN)_{diss} \tag{3.18}$$

and

$$(da/dN)_{diss} = (Mi_a/zF\rho).1/\omega \tag{3.19}$$

In the above equation M is the atomic weight of the corroding metal i.e. Fe, i_a is anodic dissolution current, z is the charge on the cation i.e. Fe^{++}, F is the Faraday's constant, ρ is the metal density and ω is the cyclic frequency.

The above summation equation gave fare agreement with the experimental results while calculating crack growth rates and fatigue lifetimes based on the Hobson-Brown [68] and Navarro-de los Rios [76] models.

More recently Sun [26] performed long life corrosion fatigue tests in neutral 0.6M NaCl solution fog to understand the behaviour of short fatigue crack growth in Al - Li alloy. He observed a large reduction in short fatigue crack growth resistance

and suggested that hydrogen embrittlement resulting from hydrogen diffusion was its main cause. He proposed a crack growth model which assumes that hydrogen diffuses to the PSB where it lowers the friction stress. This assumption was based on previous work by Petch [127]. A reasonable agreement between experimental and predicted fatigue lifetimes was observed.

Chapter 4

Experimental Work

4.1 Introduction

As previously stated, the principal aim of this research was to gain an understanding of the influence of an aggressive environment upon the initiation and growth of short fatigue cracks. In order to achieve this the following experimental programme was undertaken.

- Characterisation of microstructure.
- Determination of the monotonic uniaxial and cyclic torsional stress-strain properties.
- Determination of base-line, short fatigue crack growth characteristics in air.
- Assessment of the short fatigue crack growth behaviour under corrosion fatigue conditions.

- Determination of environment-assisted critical (threshold) crack lengths necessary to cause subsequent air fatigue failure at stresses below the 'in-air' fatigue limit.
- Evaluation of corrosion charateristics of the given metal-environment system using electrochemical studies.
- Evaluation of the influence of adsorbed hydrogen on the monotonic uniaxial and cyclic torsional properties.

4.2 Material

The material used for all tests was a silico-manganese spring steel (BS 250A53). This is a high carbon low alloy steel in the quenched and tempered condition used for the manufacture of railway track clip fastenings.

4.2.1 Chemical Composition

The actual cast chemical composition for this material is as shown in table 4.1 . Also given in this table is the British Standard specification for 250A53.

4.2.2 Heat Treatment

In order to develop the required metallurgical and mechanical properties, the material was hardened and tempered. The hardening was conducted by heating the material to an austenitising temperatue of 950^0C for 15 minutes followed by quench-

ing in oil. Tempering was then carried out at a temperature of 450^{0}C with a hold time of 30 minutes. A similar heat-treatment was performed to obtain a larger prior austenite grains by increasing the austenitising temperature to 1100^{0}C while tempering was done at the same temperature that of first heat treatment.

4.2.3 Microstructure

The microstructures obtained from the given heat-treatments were analysed using an image analysis system. The microstructure resulting from the first heat treatment was designated as 'standard' and is mainly used in the present study. Whereas that obtained from the second heat treatment was labelled as 'large'. The prior austenite grain size of both microstructures was measured using the Mean Linear Intercept method. The results of these analyses are presented in chapter 5.

4.2.4 Mechanical Properties

The majority of the present research was carried out using the 'standard' Prior Austenite Grain (PAG) mirostructure of which the mechanical properties as given in table 4.2 correspond to an average hardness for this material of 480 Hv. Tensile tests were conducted using a MAYES servo-electric machine and an ASTM standard configuration test specimen [197]. Similar tests were repeated using specimens pre-charged with hydrogen in order to determine the influence of adsorbed hydrogen.

4.3 Test Facilities

4.3.1 Test Specimen

To acquire an understanding of the behaviour of short fatigue crack growth a smooth hour-glass shaped fatigue specimen, figure 4.1, was used for this research.This specimen was chosen to meet the following requirements:

- development of a small stress concentration at the area of minimum cross-section in order to cause cracking within a restricted area.
- easy to polish and localized replication.
- provision of good fixture facilities for a corrosion cell.
- easy to handle i.e. fitting and removal from grips.

Similar designs have been employed in previous studies [24-26,200,201] and proved successful in obtaining short crack growth data.

4.3.2 Test Machine

The torsional fatigue testing facility used in this study, figure 4.2(a), is a strain controlled machine and provides facilities for both high strain low-cycle and low strain high-cycle fatigue testing. A low-speed drive is used for high strain cycling to avoid thermal effects and this drive consists of a reversible 3-phase motor driving a 3000:1 reduction gear through a stepped pulley system. During cycling the reduction gear is coupled directly to the specimen holder. The high speed drive is

used for low strain long-endurance cycling. This high-speed drive facility involves a variable dc motor which drives a variable throw crank and a connecting rod. The connecting rod is attached to the specimen holder via a fine control link. The length of the connecting rod can be adjusted to compensate for the movement of the fine control and to adjust for zero mean shear strain.

For brevity only a brief explaination is given here however further information may be obtained from Reference [200].

Measuring Systems and their Calibration

The applied torque is measured using a load cell made of solid cylindrical EN25 steel bar connected in series with the specimen. Since the load cell operates well within its elastic limit,the applied torque is proportional to its surface strain and this strain is measured by means of four resistance strain gauges arranged such that the system is sensitive to torsion but insensitive to axial loads and temperature changes. The load cell was calibrated by hanging dead weights on to a load arm and recording the output from a strain gauge bridge indicator. This calibration is represented by the following equation.

$$y = 1.006x - 1.875 \times 10^{-2} \tag{4.1}$$

where x is the applied load in Nm, and y the output of the strain gauge bridge indicator.

The angular displacement is measured by a Cam-Linear Variable Displacement Transducers (LVDT) arrangement. Two cams are fixed on the specimen at a

given gauge length upon which the LVDTs locate. The twist produced in the specimen by the application of torque is transmitted to the transducers via the cams. The voltage output from the two LVDTs are recorded and the resultant signal is represented as the angle of twist over the entire gauge length section. For calibration purpose an angular movement of the cams was produced by rotating the input shaft via a gear box which had a reduction ratio of 3000:1. The following equation illustrates the calibration of LVDTs.

$$y = 0.828x - 8.25 \times 10^{-2} \tag{4.2}$$

where x represents the angular displacement in degrees and y the reading on digital multimeter in volts.

Instrumentation and Control

The instrumentation employed for recording measurements from the fatigue testing machine is illustrated in figure 4.2(a). An X-Y pen recorder was used to plot hysteresis loops as a back up enabling calculation of stress and strain values. A microcomputer was interfaced with the machine for recording information such as torque, angle of twist, number of loading cycles, frequency and temperature during the tests. Computer control facilitated in switching off the motor (and solution circulation pump in corrosion fatigue tests) at a preset number of cycles to allow for replication of the specimen. The machine was also stopped on attaining a 10 per cent drop in the stabilized load described as a failure criteria in this study. Periodic checks were made between data recorded and values obtained from signal

analyser which gave a good correlation.

4.3.3 Specimen Grips

New specimen grips were designed and made in order to achieve the following aims:

a) providing a cotter-pin arrangement for easy fixing and removal of specimen from the grips thus replacing the existing through-specimen-pin arrangement.

b) the reduction in the size of the cavities to fit specimen ends due to the change in the specimen design.

4.3.4 Transducer Cams and Mountings

New transducer cams and mountings were designed for the present work. These cams were made of plastic whereas the mountings for holding LVDTs were made of stainless steel. The mountings were designed in such a way that the transducers were resting on the cams at points on the profile along the central axis of the specimen. The use of plastic for the manufacture of cams allowed for their use in both air and corrosive environments. The cams were fixed on the specimen using a jig which allowed reproducable accurate location and gauge length.

4.3.5 Environment Circulation System

This system was designed and built for pumping the corrosive solution from a reservoir to a corrosion cell fitted onto the specimen. An air pump allowed aeration of the test solution. The corrosion cell was designed in such a way that it

should provide a leak free fitting and also be easy to remove from the specimen for replication purposes.

4.4 Specimen Preparation

4.4.1 Surface Finishing

After machining, the hour-glass gauge length section was polished to a mirror image surface finish (Ra = 0.25μm). This procedure involved two main steps. In the first step coarse polishing was accomplished using emery papers with increasingly finer grit i.e. 320, 600, 800, 1000 and 1200. Before changing from one grade to another it was ensured that scratches from the previous paper had been removed. Each time the specimen was washed and dried using acetone to avoid the contamination of the previous coarse grade particles. After polishing with the finest emery paper i.e. 1200 grit the specimen was examined under the metallurgical microscope to ensure that all scratches were unidirectional and due only to the last emery paper used. The final polishing was completed by cloth polishing using diamond pastes of 30, 6, 3, 1 and 0.25μm respectively. Again after cloth polishing the specimen was observed under the microscope to examine its surface. This operation was completed when a mirror image surface finish was obtained.

4.4.2 Etching

In order to study the interaction between microstructual features such as PAG boundaries, tempered martensite, non-metallic inclusions and short fatigue cracks the standard PAG material specimen was etched with 0.5 percent Nital for 35 seconds at room temperature. However an alternative etchant made of following reagents was used for etching the large PAG material specimen as this produced improved results; 100 ml Methanol, 10 ml Picric acid, 20 drops Hydrochloric acid and 20 drops Teepol (wetting agent).

This etching was also performed at room temperature but for a time period of about 57 seconds.

4.4.3 Reference Marking

In all crack growth tests where surface replication of the specimen was used for crack size determination reference marks were made within the gauge length. These marks were made using a Vicker's Microhardness Indentor on four locations i.e. top, bottom , front and rear side of the specimen circumference located at a distance 3mm each side of the minimum diameter of specimen. These indentations produce impressions on replicas which help in locating the position of cracks especially in the early stages of life where cracks are extremely small and difficult to differentiate from each other.

4.5 Crack Growth Monitoring

4.5.1 Plastic Replication Technique

This technique was used in the present study to obtain information on crack development and growth behaviour. The technique involves the following procedure;

A sheet of cellulose acetate material having a thickness of 0.035 mm is cut into pieces of approximately 23 mm long and 12 mm wide. There are two major limitations in deciding the size of the acetate piece used. First is concerned with its length and if longer than the mentioned size, the ends overlap whilst wrapping around the specimen and thus create difficulties in detaching it from the specimen's surface. However the use of short lengths develops a problem of incomplete surface replication. The second limitation involves that of the width of the piece used, piece wider than 12 mm results in buckling and gives incomplete coverage of the surface. At the time of replication the specific area of specimen is sprayed with acetone and immediately a piece of acetate sheet is placed on the specimen's top surface with the help of a tweezer. After this a few drops of acetone are again sprayed to the inside at the replica contact point of both ends of acetate piece. This helps in wrapping the remaining part of the piece itself with the specimen by a mechanism of capillary action, at the same time surface tension keeps it firmly on the specimen. One precaution has to be taken here in that no acetone drop should fall on the outer surface of acetate piece as acetone may dissolve and damage the replica. After drying within 2-3 minutes, the piece is removed from the specimen's surface

using sellotape and fixed onto a microscope glass slide for subsequent microscopical examination. As it is difficult to replicate all the specimen with one replica the specimen's specific area is assumed to be divided into two parts i.e. upper half and bottom half. Once the upper half surface replication is completed , the same procedure is repeated for for bottom half of the specimen's surface. The number of replicas taken in a test depends upon the expected fatigue lifetime of that specimen.

This technique has been used in this and previous studies having the following advantages:

- it is an efficient method of detecting cracks of a few microns length.
- it helps in relating the influence of microstructures on crack initiation and growth .
- it provides an excellent permanent record of each test from the start to end.
- it allows an estimate of crack density.
- no use of electronic / sophisticated equipment and hence no possible dangers of repairs .
- finally it is an economic technique.

4.5.2 Direct Observation

Although in previous studies the surface replication technique provided good results allowing the relationship between microstructure and crack development to be studied it was difficult to obtain a suitable image from the replica which clearly

showed the microstructure. This created a problem in relating the crack growth with microstructure. It was therefore necessary in a few tests for the specimen to be removed from the machine and examined directly under the microscope. This method was quite helpful in understanding the mechanism involved in stage I / stage II crack growth particularly under corrosion fatigue conditions.

4.5.3 Image Analysis System

Replicas made during a fatigue test were examined using an in-house Image Analysis System . This system consists of a high-resolution metallurgical microscope, an image capturing monitor, a camera for relaying to an image from the replica to the image capturing board incorporated within a personal computer. The system software offers a number of measuring options which include crack length, area and volume fraction. The results of measurements carried out are displayed on the PC monitor and can be permanantly stored on a hard or floppy disc. The microscope also provides a facility of auto-exposure photography by the replacement of video camera by a standard 35mm photographic camera.

4.6 Fatigue Tests

4.6.1 Test Procedure

In-air Tests

Transducer cams were fixed to the polished hour-glass fatigue test specimen at a set gauge length using a special purpose jig. The specimen was then fitted in the fatigue test machine via the cotter-pin arrangement. A torque of specific range and zero mean value was applied to the specimen as explained in section 4.3.2. LVDTs were then brought to a central position on the cams and electonically zeroed. Load application and zeroing of LVDTs was achieved using the local mode of the programmable switch circuit. When a test was ready to run this mode was changed to the remote setting allowing for control using software loaded on a BBC microcomputer. This enabled information such as applied torque, angular displacement, number of loading cycles, frequency (5 Hz) and temperature to be recorded at pre-selected intervals. The machine was also stopped automatically for replication purpose at pre-determined intervals. The first replica was taken just before any load application on the specimen i.e. zero cycles, for reference purposes. Further replication depended upon the expected fatigue lifetime and was kept short during the stages of crack initiation and early growth. Tests were continued until the specimen broke or reached a stage close to fracture.

Corrosion Fatigue Tests

Corrosion fatigue tests were conducted at 5 Hz in a solution of 0.6M NaCl made by using laboratory grade sodium chloride and de-ionized water. This solution was aerated and circulated from and to a reservior via a corrosion cell fitted on to the specimen. The same test procedure as described above was adopted for these tests. The test was stopped at pre-selected intervals and the corrosion cell removed for replication purposes. This procedure was completed within 10 minutes. Corrosion fatigue tests conducted with and without replication under otherwise identical conditions confirmed no significant effects on fatigue life of stopping the test for replication purposes.

Intermittent Air Fatigue/Corrosion Fatigue Tests

All of these tests were carried out at stress levels below the 'in-air' fatigue limit using a similar procedure to that described for the previous studies. For these sub-fatigue limit tests cracks were seen to initiate, grow and arrest. The specimen was the Fatiguen subjected to corrosion fatigue cycling at the same applied stress level. The resulting non-propagating cracks were monitored for any further propagation that may occur as a result of the influence of the environment. A typical test procedure is shown in figure 4.3. The crack length obtained after the introduction of the last environment was considered as a critical crack length for that particular stress level. The majority of these tests involved the use of 'standard' PAGs material. However a few tests on 'large' PAGs material were conducted to understand the

relative importance of microstructural features in controlling fatigue crack growth.

Failure Criteria

Previous studies have described several criteria used to explain the failure of a specimen. For example Zachariah [201] adopted a crack length criteria in which he mentioned a particular crack length at failure. However other research workers [202,203] used a specific percentage of reduction in applied load as the failure criteria. Ibrahim [202] used a 5 percent figure and Mohammad [203] presented this value as 10 percent. In recent studies [24-26,198] similar approach of reduction in applied load has been used. Based on the above mentioned criteria a drop in 10 per cent applied torque was chosen as the failure criteria of the specimens for the present study.

4.7 Electrochemical Tests

4.7.1 Introduction

These tests were conducted to determine the corrosion characteristics of the given metal-environment system. The results obtained from these tests were considered in the development of a corrosion fatigue crack growth model.

4.7.2 Test Equipment

The polarization measurements were carried out using a standard multineck polarization cell. This typical polarization cell consists of the following main parts:

a) the specimen acting as a working electrode

b) a Standard Calomel reference electrode

c) two platinum auxiliary electrodes

d) a thermometer and

e) aeration / de-aeration facilities

The results obtained from the test were recorded on a personal computer connected to the polarization cell via a computer controlled autostat. The whole apparatus is shown in figure 4.2(b).

4.7.3 Test Procedure

The specimens acting as the working electrode was made from the same material as that used for fatigue studies described as standard PAG in section 4.2.3 having a surface area of $1.11cm^2$. The surface of the specimen was prepared in a manner identical to that of the fatigue test specimens. After polishing the surface the specimens were cleaned with teepol and washed with de-ionized water. Finally these specimens were ultrasonically cleaned in acetone and dried.

Electrochemical tests for polarization studies were conducted in an aerated 0.6M NaCl solution pH 6.0 in accordance with ASTM standard practices G59-78 [204] and G5-82 [205]. The information obtained from these experiments were automatically recorded using a personal computer. The validity of the results taken from autostat/computer facility was confirmed by comparing with the results of similar tests determined by using Solatron digital multimeters connected with the

cell.

4.8 Evaluation of Hydrogen Embrittlement

In order to evaluate the role of mechanisms such as anodic dissolution and/or hydrogen embrittlement in corrosion fatigue crack growth the following series of tests were conducted:

a) *Air fatigue tests*: These tests involved the use of hydrogen pre-charged specimens. Three fatigue specimens having a mirror-image surface finish were charged with hydrogen at a cathodic potential of -1.25V using an electrochemical cell and autostat. Two specimens were charged in 0.6M NaCl solution pH6 for a period of 10 and 24 hours respectively. A third specimen was charged with hydrogen for 24 hours but within a 0.6M NaCl solution pH2 in order that a higher concentration of hydrogen ions was available. Immediately after the completion of hydrogen charging each especimen was dried and cycled in air under torsional at a stress level of 854 MPa for 5 million cycles at a frequency of 5Hz. These tests were designated as HF1, HF2 and HF3 respectively.

b) *Corrosion fatigue tests*: These tests were conducted in which the specimen was subjected to an applied cathodic potential. Three corrosion fatigue tests were carried out at a stress level of 851 MPa for 0.5 million cycles at a frequency of 5Hz and under an applied potential of -1.25V. The first two tests were conducted in 0.6M NaCl pH6 and 0.6M NaCl pH2 solutions respectively. A third test involved the use of a specimen which contained a few non-propagating cracks resulting from

the HF3 test (see section 5.6.2) and was conducted in 0.6M NaCl pH6 solution. These tests were denoted as CP1, CP2 and CP3 respectively.

c) Tensile tests: The first of these tests was performed on normal 'uncharged' material. Two other tests were carried out using specimens pre-charged with hydrogen in a 0.6M NaCl pH6.0 solution at a potential of -1.25V for a period of 24 and 100 hours respectively. These tests were labelled as NT1, PT1 and PT2 respectively.

Chapter 5

Results

5.1 Introduction

This chapter presents the results obtained from the present investigations conducted on a 250A53 steel. Preliminary information was gained on the metallurgical microstructure and mechanical properties of the material. The relationship between stress and strain under cyclic loading conditions was also studied and the results of fatigue endurance data in the form of S-N curves for both laboratory air and aggressive environments are presented. Section 5.5 describes the initiation and growth behaviour of short cracks studied under different test conditions namely; air fatigue, corrosion fatigue, and intermittent air fatigue/corrosion fatigue. In the following section the informatoin obtained for this metal-environment system from polarization experiments have been given. Finally the results obtained from tests conducted to evaluate the effects of hydrogen adsorption are presented.

5.2 Microstructure

The silico-manganese spring steel used in this study was heat treated to a condition representative of a railway clip component. A microstructure of lath martensite surrounded by prior austenite grain (PAG) boundaries was seen. A large number of non-metallic inclusions were observed lying within the matrix as well as along the PAG boundaries. A microprobe analysis of these inclusions was carried out to estimate their chemical composition. A second heat treatment was conducted to provide a similar tempered martensite microstructure but with a variation in PAG size. The PAG size measurements of both heat treatments were carried out using the Mean Linear Intercept method. The average prior austenite grain sizes were found to be around 30 μm and 60 μm for standard and large grain microstructures respectively [207]. The standard microstructure is shown in figure 5.1(a) whereas a schematic illustrating the prior austenite grain boundaries and martensite laths is shown in figure 5.1(b).

5.3 Cyclic Stress-Strain Behaviour

The cyclic stress-strain response of this material under fully reversed torsional loading was determined by conducting a multi-step test. In torsional loading the shear stress is proportional to the applied torque. The values of stabilized torque and angular displacement were considered for construction of the cyclic stress-strain curve. Shear stress and shear strain were calculated using equations 5.1 and

5.2 respectively.

$$\Delta\tau = \frac{\Delta T.(m+3)}{2\pi r_0^3} \tag{5.1}$$

where $\Delta\tau$ is the shear stress range for a given value of ΔT, m is the slope of the logΔT-log$\Delta\theta$ plot and r_0 is the minimum radius of the specimen.

The relationship between strain and angular displacement in an hour-glass specimen was presented by Brown and Carbonell [208] as;

$$\phi = \frac{\tau_0}{Gr_0}\int_{-l}^{+l}\left(\frac{r_0}{r}\right)^4 \delta x + \frac{\gamma_{0p}}{r_0}\int_{-l}^{+l}\left(\frac{r_0}{r}\right)^{\frac{3+n}{n}} \delta x \tag{5.2}$$

where γ_{0p} is the plastic strain at the minimum section, l the gauge length, r_0 the minimum radius and n the value of hardening exponent for the material.

The value of r in the gauge length range i.e. between -l and l may be given by the equation;

$$r = r(x) = r_0 + R - \sqrt{R^2 - x^2} \tag{5.3}$$

where R is the radius profile for the hour-glass specimen, in this case R = 98mm.

For comparison shear strain values were calculated using the Ramberg-Osgood relationship [45].

$$\gamma = (\tau/G) + (\tau/k)^{1/n} \tag{5.4}$$

where G is the shear modulus, n is the hardening exponent and k is the intercept of the y-axis of a line drawn through the plastic range of the cyclic stress-strain curve.

For this material the cyclic stress-strain response is given by the equation [206];

$$\gamma = (\tau/825) + (\tau/600)^{1/0.1} \tag{5.5}$$

The above calculated data of shear stress range and shear strain range was then plotted and is shown in figure 5.2. This figure clearly shows three different regions; a linear relationship between $\Delta\tau$ and $\Delta\gamma$, region I, which represents the elastic behaviour of the material, the slope of this part being the shear modulus. Region II describes a non-linear relationship referred to as the elastic-plastic regime, this regime is characterised by a variation in slope, m. The final region III represents the plastic regime. This part may be expressed by the following expression;

$$\Delta\tau = A(\Delta\gamma_p)^{\alpha} \tag{5.6}$$

where A and α are material constants. $\Delta\gamma_p$ is given in percent and shear stress range in MPa.

5.4 S-N Curves

The fatigue endurance data of smooth specimens was obtained by conducting tests under fully reversed torsional loading at room temperature within two environments notably laboratory air and an aerated 0.6M NaCl solution. This data is presented in table 5.1. The number of cycles to failure (N_f) was based on a 10 percent reduction in the applied stabilized load. S-N curves for in-air and corrosion fatigue conditions are shown in figure 5.3.

The S-N curve for air fatigue studies shows that a limiting stress exists below which cracks once initiated are unable to propagate to produce a failure crack; this is represented by a *fatigue limit* stress. A shear stress range of 915 MPa ($\Delta\gamma$ = 1.24 %) is suggested for this material. An equation based on Coffin [209] and

Manson [210] type relationship is given by;

$$\Delta\gamma_t.(N_f)^{0.1363} = 9.875 \tag{5.7}$$

However Basquin [211] proposed another equation using stress rather than strain. Thus the above type equation may be expressed as;

$$\Delta\tau.(N_f)^{0.0449} = 1.83 \times 10^3 \tag{5.8}$$

The S-N curve for corrosion fatigue studies suggests a reduction/elimination of the 'in-air' fatigue limit. The influence of an aggressive environment is seen in a progressive decrease of the S-N curve when compared to that of the air fatigue curve. Although a corrosion fatigue limit may not exist an endurance limit corresponding to a fatigue life of 10^7 cycles has been evaluated equivalent to 179 MPa ($\Delta\gamma = 0.21$ %).

In a similar procedure to that used for the air fatigue S-N data two endurance laws were developed for corrosion fatigue.

$$\Delta\gamma_t.(N_f)70.3677 = 73.44 \tag{5.9}$$

and

$$\Delta\tau.(N_f)^{0.3348} = 3.912 \times 10^4 \tag{5.10}$$

5.5 Crack Initiation and Growth

5.5.1 Air Fatigue Tests

Crack growth tests were carried out at stress levels of 1106 MPa, 1008 MPa, 915 MPa, 900 MPa and 815 MPa. Crack initiation and growth behaviour was studied by examining surface replicas taken of the specimen during the course of a fatigue test. Crack initiation was seen to occur at non-metallic inclusions. Microprobe analysis of non-metallic inclusions suggested that inclusions having higher proportions of elements such as Si and Al were more damaging than other inclusions in this material. Mode II shear cracks nucleated from these inclusions and propagated along the plane of maximum resolved shear stress coincident with the longest length of the inclusion. Such cracks showed an initial high growth rate followed by a deceleration in growth as they approached prior austenite grain (PAG) boundaries. After overcoming the first grain boundary cracks accelerated and showed a further deceleration on approaching the next grain boundary. This oscillatory pattern was noted for crack lengths of a few grain diameters. A major retardation in growth was seen at a crack length equivalent to about four prior austenite grains. This period of slow crack growth showed a strong dependence upon the applied stress level and decreased with an increase in the value of stress. An increase in crack growth rate with increase in crack length up to failure was observed when a crack had crossed the major deceleration barrier. Where the applied stress level was below the fatigue limit cracks were seen to retard and arrest at microstructural barriers

i.e. prior austenite grain boundaries. Typical initiation and growth behaviour is shown in figure 5.4 .

Crack growth behaviour was studied by measuring crack lengths corresponding to a specific number of applied loading cycles. After collecting data from a test a plot of surface crack length(a) versus number of cycles(N) was obtained. A comparison of different 'a' versus 'N' curves for the major/failure cracks at various stress levels is shown in figure 5.5. In this figure the behaviour of a non-propagating crack is also provided.

From the above data crack growth rates were calculated using a secant method;

$$(da/dN)_i = (a_{i+1} - a_i)/(N_{i+1} - N_i) \tag{5.11}$$

where a_i and a_{i+1} are two consecutive crack lengths at N_i and N_{i+1} number of cycles respectively. As the crack growth rate calculated by the above equation represents the growth at the mid point of the two consecutive crack lengths mentioned above, an average crack length was obtained by using the simple relation;

$$(a_{av})_i = (a_i + a_{i+1})/2 \tag{5.12}$$

The crack growth results of individual air fatigue tests are presented in appendix 'C'. The analysis of these results is described in the next chapter.

5.5.2 Corrosion Fatigue Tests

Corrosion fatigue crack growth tests were conducted at stress levels of 900 MPa, 854 MPa, 817 MPa, 601 MPa and 404 MPa. In this series of tests crack growth

was also monitored using acetate replicas. Crack initiation was associated with a localized chemical pitting process occuring at non-metallic inclusions. Microprobe analysis of those non-metallic inclusions which appeared most susceptible to pitting indicated there to be a distinct association with the elements; S, Al, Mn and Si. On exposure of the specimen to the environment pitting occured readily although the degree to which this occured depended upon the applied stress level. The sites of pits were quite obvious during the test. As cycling continued, pits developed along the shear mode plane at a rate which decreased as they approached a length equivalent to the mean prior austenite grain (PAG) size. After progressing beyond the PAG boundary a stage II, mode I crack developed at the ends of the pit. These cracks propagated in a manner similar to that observed in air fatigue tests, that is, showing decelerations and accelerations at crack lengths equivalent to multiples of the prior austenite grain size until eventual rapid growth led to failure. Although the microstructural barriers offer a resistance to crack growth it appears that they are less effective when compared to growth under in-air conditions. This is attributed to the presence of an additional driving force being of a chemical nature. An important difference noted here was that the transition from the short crack regime to that of the long crack regime occured when the crack was growing in mode I as opposed to mode II growth observed for air tests. The length at which this transition occured was however consistent with that exhibited in air fatigue tests. Crack initiation and development under these conditions is illustrated in figure 5.6. An additional feature of corrosion fatigue tests was a significant increase in

the number of cracks initiated for a particular stress level. The number of initiated cracks in a test showed a stress dependency and obeyed the following relationship;

$$N_a = 2.123 \times 10^{-10}(\Delta\tau)^{4.104} \tag{5.13}$$

or

$$N_a = 209.14(\Delta\gamma)^{4.201} \tag{5.14}$$

where N_a is the number of cracks initiated up to the failure stage at an applied shear stress or strain range.

At low stresses failure of a specimen took place due to the growth of individual cracks. However as the stress level increased coalescence of a small number of cracks resulted which contributed to the final failure of the specimen. The number of cracks taking part in the failure process may be expressed as;

$$N_{cl} = 6.057(\Delta\gamma)^{2.7383} \tag{5.15}$$

where N_{cl} is the number of cracks which coalesce to form the failure crack at a given stress/strain level.

As with air fatigue studies crack lengths developed under corrosion fatigue conditions were measured for each stress level. Crack lengths of the failure/major crack representing each stress was then plotted against number of loading cycles. The results of these tests are tabulated in appendix 'D' and plotted in figure 5.7.

5.5.3 Intermittent Air Fatigue/Corrosion Fatigue Tests

This series of tests was carried out at stress levels below the 'in-air' fatigue limit, i.e. 900 MPa, 853 MPa, 815 MPa and 600 MPa. As the applied stress level was below the fatigue limit, cracks initiated, propagated and eventually arrested as a result of prolonged air fatigue cycling. The resulting non-propagating cracks were re-propagated by the introduction of a specific period of corrosion fatigue cycling, for example, 5000 cycles. Crack lengths were monitored to assess crack re-propagation. Where cracks were observed to have re-propagated they were subject to air fatigue cycling, until crack arrest or failure occured, see figure 5.8. The number of corrosion fatigue cycles introduced in order to produce a crack of such a length that subsequent in-air fatigue failure at the sub-fatigue limit stress may occur was seen to be dependent upon both the applied stress level and crack length. A typical example illustrating crack initiation and development under intermittent air fatigue/corrosion fatigue conditions is presented in figure 5.8.

The results of these tests are given in appendix 'E' and plotted in figure 5.9. In this figure the letter 'E' has been used to denote the introduction of a period of corrosion fatigue cycling. In order to confirm the role of prior austenite grain boundaries an intermittent air fatigue /corrosion fatigue test was conducted using a specimen having a large prior austenite grain size microstructure. As it was difficult to reveal the martensite microstructure using acetate replicas, the specimen was removed from the test rig in order to observe the surface directly under the microscope. Observations directly from the specimen helped in understanding

the role played by the PAG boundaries, in particularly when a crack arrests and changes its path from mode II to mode I. Such an example is shown in figure 5.10 where arrow marks indicate the PAG boundaries. Table 5.2 presents the lengths of arrested cracks prior to corrosion fatigue cycling.

5.6 Electrochemical Tests

Electrochemical tests were performed to determine the electrochemical behaviour of the given metal-environment system. Initially the free corrosion potential, E_r , was recorded with time. The results of this test, see figure 5.11, showed that the free corrosion potential became more negative as time increased with the potential dropping quickly but later becoming almost constant. Further additional tests were conducted, namely anodic and cathodic polarization curves, to estimate the corrosion current, i_{corr}. A comparative study of the resulting corrosion current was made by conducting polarization tests at varying potential scan rates. Polarization data suggested that the value of i_{corr} dropped with a decrease in the scan rate. The corrosion current determined from this plot was later used in equation 6.18 to calculate a dissolution rate for the metal. The results of these polarization experiments are shown in figure 5.12.

5.7 Evaluation of Hydrogen Effects

5.7.1 Hydrogen Pre-charged Fatigue Tests

Three air fatigue tests were carried out at a stress level of 850 MPa (i.e below the 'in-air' fatigue limit) using specimens pre-charged with hydrogen. Two specimens were pre-charged in neutral 0.6M NaCl solution for a period of 10 and 24 hours respectively. A third specimen was pre-charged for 24 hours but using a 0.6M NaCl solution having a pH of 2. Each specimen was tested in air for 5 million cycles. No apparent cracking was seen in the first two tests, that is for charging times of 10 and 24 hours. But the third test resulted into a few non-propagating cracks. These cracks which had lengths of about 50 μm, were initiated from non-metallic inclusions and similar to those obtained from air fatigue tests. Any effect of hydrogen charging would be expected to occur early in the fatigue tests as hydrogen diffusion from the specimens will occur with prolonged testing times. In order to ensure a sufficient supply of atomic hydrogen throughout the fatigue cycling cathodic polarization was applied during corrosion fatigue testing, see below.

5.7.2 Corrosion Fatigue Tests Under an Applied Cathodic Potential

In a further test series three corrosion fatigue tests were conducted at a stress level of 854 MPa. In this case specimens were subjected to an applied cathodic potential of -1250 mV. All tests were fatigued for half a million cycles i.e. about 5 times

the life of the corrosion fatigue test (CF3) carried out at this stress level. These tests did not reveal any signs of cracking, as was the case for the test conducted at pH2. Furthermore no effect of excessive cathodic polarization was observed despite one specimen being used which contained a non-propagating crack obtained from a previous test (see section 5.7.1).

5.7.3 Pre-charged Tensile Tests

One tensile test was carried out using a standard, uncharged specimen. Other tests tests involved the use of specimens pre-charged with hydrogen for 24 and 100 hours tively. The results achieved from these tests indicated that mechanical properties were affected for pre-charged specimens when compared with that of a standard specimen. The period of pre-charging time played an influential role, a point to be discussed in chapter 7. The results of these tests may be found in table 4.2 and figure 5.13.

Chapter 6

Crack Growth Modelling and Analysis

6.1 Introduction

This chapter is concerned with the development of suitable crack growth models for both in-air and corrosion fatigue tests carried out in the present study. The approach is based on the application /modification of existing models previously employed in a number of studies [24,25,212]. These models were later used to predict air fatigue and corrosion fatigue lifetimes.

applicationIt is now clearly evident that a Linear Elastic Fracture Mechanics (LEFM) approach to the quantification of defects which are subject to large plastic deformations or have a length comparable to the microstructural dimension of the material provides severe limitations as a result of the lack of small scale yielding. An effort is therefore being made to provide an adequate analysis of

the microstructurally-dependent short fatigue cracks regime by developing models which incorporate microstructural parameters. Recently, two such models which describe the oscillatory nature of short crack observed in air fatigue studies have been proposed by Hobson and Brown [68] and Navarro and de los Rios [76]. In the present study the former of these models has been employed in a modified form for the analysis of the fatigue results.

6.2 Air Fatigue Modelling

6.2.1 Short Crack Growth Equation

A crack growth equation which describes microstructural-short crack growth has previously been described by Hobson [198] and is given in equation 6.1 ;

$$(da/dN)_{sa} = C_{sa}(d_i - a) \tag{6.1}$$

where the constant for short crack growth in air, C_{sa} is a material constant and d represents a microstructural parameter. This parameter may be described as a distance between two consecutive microstructural barriers and may for example be equated to the size of a grain. Such a barrier offers a resistance to the propagation of a crack resulting in crack deceleration as the crack approaches such an obstacle. In order to determine the value of the parameter d , crack growth rates of those cracks which showed marked decelerations in growth were plotted against average crack lengths. A least squares regression fit was applied to these points and the value of the intercept at zero crack growth rate was determined. The value

of the intercept was considered to correspond with the value of d. The values of d determined for each crack showed some variation which reflects a variation observed in the grain size of the material. An average value of d was then calculated from this data and compared with the average prior austenite grain size. A fair agreement was observed between these two results. Given that the average prior austenite grain (PAG) size was representative of the value of 'd' this value was therefore used in the analysis of the crack growth data. The value C_{sa} in equation was calculated for each successive pair of data points of crack length and crack growth rate which exhibited a deceleration in growth. See Appendix B for detailed analysis. Constants were calculated for individual cracks for tests conducted at different stress levels. At a particular stress level a scatter in the values of 6.1 this onstant was observed which suggested that all cracks did not propagate at the same rate. Some cracks propagated at a faster rate than others due to the size of the grain and the orientation of the grain with respect to the resolved shear stress. It was therefore decided that a conservative approach to assessing fatigue crack growth rates would be to use an average value of those constants corresponding to the cracks having the highest growth rates. A relationship between the averaged constant at individual strain level was then determined and is given in equation 6.2;

$$C_{sa} = A(\Delta\gamma_t)^{\alpha} \tag{6.2}$$

The values of this constant, C_{sa} , are given in table 6.1.

Experimental results suggest that the short crack growth regime exists over

about four prior austenite grain diameters, i.e. 120 μm, and crack decelerations occured when a crack approached each PAG boundary. It therefore seemed appropriate to model this regime by determining individual short crack growth equations for the first four grains. Hence the equations developed may be presented in a single equation of the form;

$$(da/dN)_{sa} = A_i(\Delta\gamma_t)^{\alpha_i}(d_i - a) \tag{6.3}$$

, where i = grain number i.e. 1, 2, 3 and 4

$A_i = 4 \times 10^{-6}, 1.4 \times 10^{-6}, 8 \times 10^{-7}$ and 3×10^{-7} (for grains 1-4 respectively)

and α_i = 8.7055, 8.0108, 7.9048 and 7.7924 (for grains 1-4 respectively)

with d_i = 30, 60, 90 and 120 μm.

Based on these equations short crack growth rate calculations were made. A comparison with experimental growth rates is presented in figure 6.1.

6.2.2 Long Crack Growth Equation

When a crack overcomes the dominant decelerating barrier its growth characteristics exhibit fewer perturbations at which point it is considered that a transition from short to long crack growth has occured. This regime represents a continuing acceleration in crack growth as the crack length increases.

A long crack growth equation may be written as;

$$(da/dN)_{la} = C_{la}a - D_t \tag{6.4}$$

The coefficient for long crack growth in air , C_{la} , given in the above equation is a function of stress or strain and its value may be obtained by applying linear

regression analyses to the crack length-crack growth data for those cracks having a length greater than the short-long transition length. An equation showing the relationship between this coefficient and applied strain level was then determined which may be expressed by the following equation;

$$C_{la} = B(\Delta\gamma_t)^{\beta} \tag{6.5}$$

The values of the coefficient, C_{la}, are presented in table 6.1.

The constant, D_t , represents a threshold crack growth rate. This is a function of strain level at which the fatigue limit assumes a growth rate approaching zero ($\Delta\gamma_{fl}$). This would be expected when the length of a crack equates that of the short crack-long crack transition length , d_m , i.e. 120 μm in the case of the present study. D_t was therefore calculated using the following equation;

$$D_t = B(\Delta\gamma_{fl})^{\beta} d_m \tag{6.6}$$

The long crack growth equation may therefore be expressed as;

$$(da/dN)_{la} = 3.02 \times 10^{-5}(\Delta\gamma_t)^{2.6123} a - 6.37 \times 10^{-3} \tag{6.7}$$

The crack growth rate was calculated by using equation 6.7 and then plotted on experimental results as shown in figure 6.1.

6.2.3 Fatigue Lifetime Calculations

Fatigue lifetime was calculated by adding together individual lifetimes spent within both the short crack and long crack growth regimes. Individual lifetimes were obtained by integrating equation 6.3 and equation 6.7 in the range a_0 to d_m and

d_m to a_f respectively, where a_0 was a typical value for the surface roughness for the polished specimen, i.e. 0.25μm and a_f was the failure crack length taken as equal to half of the diameter of the specimen (4mm). A comparison of experimental and predicted fatigue lifetimes is presented in table 6.2 and shown in figure 6.2.

6.3 Corrosion Fatigue Modelling

6.3.1 A Modified Hobson's Model

Corrosion fatigue crack development suggests that a chemical pitting process was operative in the early stages of cracking. A predictive model was therefore proposed for corrosion fatigue which included the following three stages;

1) Pit development

2) environmental-assisted short fatigue crack growth

3) environmental-assisted long fatigue crack growth

The pit development stage may be described by the following equation;

$$(da_p/dN)_{pcf} = C_p(a_{tl} - a_p) \tag{6.8}$$

where a_{tl} = stage I - stage II transition length, in this case equivalent to one prior austenite grain, i.e. 30 μm.

and a_p = pit length, μm.

Experimental observation indicated that once created, a pit continued to propagate until it reached a prior austenite grain boundary where a transition to a stage II- mode I crack occured. Analysis of this stage was carried out for pit lengths up

to a length equal to the average prior austenite grain size. The pitting constant C_p was determined using a similar approach adopted for the determination of C_{sa} in air fatigue modelling. The relationship between C_p and strain level may be represented by the following equation;

$$C_p = 5.735 \times 10^{-4}(\Delta\gamma_t)^{2.5143} \tag{6.9}$$

Pit propagation rates calculated using equation 6.8 are plotted in figure 6.3.

Once a crack was initiated from the original pit-like defect its growth rate behaviour was similar to that observed for air fatigue studies and therefore a similar analytical procedure was adopted for the development of short and long crack growth equations.

Short crack growth equations may be expressed as;

$$(da/dN)_{scf} = C_{scf}(d_i - a) \tag{6.10}$$

or

$$(da/dN)_{scf} = K_i(\Delta\gamma_t)^{b_i}(d_i - a) \tag{6.11}$$

where i = grain number i.e. 2, 3 and 4

$K_i = 4.198 \times 10^{-4}, 2.277 \times 10^{-4}$ and 1.51×10^{-4} and

$b_i = 2.8916$, 3.2788 and 2.8757 for grains 2, 3 and 4 respectively.

Corrosion fatigue long crack growth data was analysed adopting the same procedure for long cracks propagating in air. The long crack equation is given in equation 6.12;

$$(da/dN)_{lcf} = C_{lcf}a - D \tag{6.12}$$

or

$$(da/dN)_{lcf} = 5.392 \times 10^{-5}(\Delta\gamma_t)^{1.993}a - 3.051 \times 10^{-4} \qquad (6.13)$$

The constants for pit development C_p , corrosion fatigue short crack growth C_{scf} and corrosion fatigue long crack growth C_{lcf} are given in table 6.3. Calculated growth rates based on equations 6.8, 6.10 and 6.12 are plotted in figure 6.3.

The total corrosion fatigue life was determined by first calculating the number of cycles spent propagating the pit/crack in each individual stage (based on the integration of individual equations) and then summing up according to equation 6.14.

$$N_t = N_p + N_s + N_l \qquad (6.14)$$

where N_p , N_s and N_l represent lifetimes for pitting, short and long crack growth respectively. The results of these predictions are given in table 6.4 and a comparison with experimental lifetimes is illustrated in figure 6.4.

6.3.2 A Superposition Model

A second model for the prediction of corrosion fatigue crack growth was proposed based on the summation of two terms. The first of these terms describes crack growth resulting in air and is a strain-dependent term; essentially this is considered to be the *mechanical driving force.* The second term expresses the crack driving force resulting from chemical interactions of the metal and the aqueous chloride environment. As previously discussed this driving force is seen to be responsible for enhanced crack propagation rates and the propagation of cracks beyond crack

arresting barriers at 'in-air' sub fatigue limit stresses. This second term is described as a *chemical driving force.* The superposition model may be expressed by the following equation;

$$(da/dN)_{cf} = (da/dN)_a + (da/dN)_e \tag{6.15}$$

where $(da/dN)_a$ represents crack growth rate in air as calculated through the equations given in section 6.2 and $(da/dN)_e$ represents environmental crack growth rate and may be evaluated by equation 6.16 or 6.17;

$$(da/dN)_{se} = 2.46 \times 10^{-2}(\Delta\gamma_t)^{2.305}a^{-0.612} \tag{6.16}$$

and

$$(da/dN)_{le} = 2.702 \times 10^{-5}(\Delta\gamma_t)^{1.4250}a \tag{6.17}$$

Equation 6.16 was developed using environmental growth rate obtained by subtracting air fatigue crack growth rates from corrosion fatigue crack growth rates for cracks of identical length at different stress levels. This equation involved the use of decreasing environmental crack growth rate with increasing crack length. Equation 6.17 was obtained from regression analyses of increasing environmental crack growth rates versus crack length.

This approach has been adopted in an attempt to charaterise the behaviour of a crack under the simultaneous action of the environment and cyclic stress which otherwise can not be modelled simply by employing a constant dissolution rate as obtained from Faraday's law;

$$da/dt = M.i_{corr}/z.\rho.F \tag{6.18}$$

where da/dt is crack growth in μm/second and i_{corr} is the anodic dissolution corrosion current in mA/cm^2.

Equation 6.18 represents a time dependent crack growth rate which may be transformed to a cycle dependent term by incorporating the frequency of fatigue cycling;

$$(da/dN)_e = (da/dt).1/f \tag{6.19}$$

Prediction of corrosion fatigue lifetime

In order to incorporate an additional factor due to the environmental crack growth, term $(da/dN)_e$, herein denoted as E , equation 6.15 requires some modification.

An equation for corrosion fatigue pit/short crack growth (scf) is given by;

$$(da/dN)_{scf} = (da/dN)_{sa} + E \tag{6.20}$$

or

$$(da/dN)_{scf} = C_{sa_i}(d_i - a) + E \tag{6.21}$$

This equation was integrated in limits of the surface roughness, a_0 (0.25 μm) and a_t to predict lifetime within the pit development/short crack region.

where a_t represents a length corresponding to transition from dissolution controlled growth to hydrogen embrittlement dominated crack growth.

Similarly corrosion fatigue long crack growth equation may be expressed by equation 6.22.

$$(da/dN)_{lcf} = (da/dN)_{la} + E \tag{6.22}$$

or

$$(da/dN)_{lcf} = C_{la}a - D + E \tag{6.23}$$

where $(da/dN)_{la}$ is given in equation 6.7 and E is given in equation 6.17.

The lifetime for this region is obtained by integrating equation 6.23 in the limits of a_t and a_f where a_f is the failure crack length.

The crack growth rate calculated using equations 6.20 and 6.22 are plotted in figure 6.5 and the calculated lifetimes in comparison to experimental lifetimes are shown in figure 6.6.

Chapter 7

Discussion

7.1 The Fatigue Limit

Fatigue tests conducted in air indicated that a limiting stress exists below which cracks if initiated become non-propagating. This limiting stress is known as the *fatigue limit* and a value of 915 MPa ($\Delta\gamma_t = 1.24$ %) is suggested for this material under fully reversed torsional loading. The arrest of cracks at sub-fatigue limit stresses occurs because the mechanical driving force associated with the crack is insufficiently large to overcome the microstructural barriers i.e. prior austenite grain boundaries in this case and initiate slip in the adjacent grains. The lengths of non-propagating cracks vary depending upon the level of sub-fatigue limit stress applied. It is usually suggested that stresses below this limit represent a 'safe stress range' for design purposes. The present study allows a comment on this statement suggesting that this is only true in situations where service conditions are such that only non-aggressive environments such as air are encountered. In

actual practice this is not often the case. The present study involving intermittent air fatigue/corrosion fatigue tests offers a warning on declaring a 'safe stress range' unless the exclusion of the aggressive environment can be ensured. These tests suggest that for this metal-environment system non-propagating cracks obtained at stress levels close to the 'in-air' fatigue limit as a result of air fatigue cycling can be made to propagate by the introduction of an aggressive environment for a very short time period i.e. 5000 cycles or about 15 minutes (see section 7.3.3).

Corrosion fatigue tests however performed in 0.6M NaCl solution showed that there is a strong influence of this environment on the fatigue properties of this material. An elimination of the 'in-air' fatigue limit appears to result and there is no longer a 'safe' stress range as long as the conjoint action of cyclic stress and environment continues. An endurance limit based on a specified number of loading cycles may however be obtained for design purposes. A stress level of 177 MPa ($\Delta\gamma = 0.2$ %) is suggested as an endurance limit for 10^7 cycles.

7.2 Crack Initiation Behaviour

7.2.1 Air Fatigue

Crack initiation in air is seen to take place almost exclusively at non-metallic inclusions. It appears that debonding at the matrix/inclusion results because of a high strain incompatibility at the interface. Metallographic examination of the material indicated the presence of a large number of inclusions of varying size and

shape. Inclusions having relatively high percentages of elements such as Si and Al were seen as potent sites for crack initiation. The damaging effect of non-metallic inclusions becomes more significant in high hardness materials, in particular when hardness values are above 40 HRC [213]. It has been reported that the size and shape of the refractory type inclusions is an important consideration for fatigue life. Large inclusions were more harmful than small inclusions and angular-shaped ones more harmful than spheroidal shapes. Borek et al [214] pointed that in fatigue studies of a high hardness material cracks were initiated by hard refractory oxides of Si, Mg and Al.

In the present study cracks initiated preferentially along the longitudinal axis of the specimen i.e. along one of the two mutually perpendicular planes of maximum resolved shear stress. Crack density showed a strong dependence upon the applied stress level and multiple crack initiation was observed at high stresses as more grains are likely to be plastically deformed.

7.2.2 Pit Development

Experimental observations indicate that a 'pit development' mechanism appears to be operative prior to short crack propagation, although it cannot be ruled out that crack propagation is concealed by dissolution processes occurring at the pit sites. A pitting process will therefore be discussed as a base for cracking under corrosion fatigue conditions.

Fatigue tests conducted in 0.6M NaCl solution show a strong metal-environment

interaction which results in early crack initiation and growth. Non-metallic inclusions dissolve in preference to the matrix due to their chemical sensitivity and inhomogenous nature. Microprobe analysis of the non-metallic inclusions susceptible to chemical attack indicated that they were rich in elements like S, Al, Mn and Si. Pits result from strain-assisted dissolution of these inclusions sites. The dissolution of these inclusions can result in the formation of H_2S which creates a favourable condition for pits to continue their growth i.e. sulphides act to catalyse the anodic dissolution reaction. Once created these pits propagate along the plane of maximum shear stress coincident with the longitudinal axis of the specimen. A decrease in growth occurs on approaching a microstructural barrier, i.e. a prior austenite grain boundary. The number of pits developed is stress dependent and a marked increase in pitting was seen at high stress levels i.e. close to the 'in-air' fatigue limit which suggested that the stress intensity associated with the inclusions accelerates the pitting process. Figures 7.1 illustrates the propensity of pit development leading to mode I crack initiation at different stress levels. This figure clearly shows that pits having lengths 30-60 μm were more likely to develop mode I cracks. From the results of pit propagation rates an assessment of the anodic dissolution current has been made. Based on the values of a and N of failure/major crack i_{corr} was calculated for different stress levels. Figure 7.2(a) shows that the corrosion current decreases with the increase of pit length and the maximum corrosion current associated with a pit increases with the applied stress/strain level as shown in figure 7.2(b). As corrosion fatigue tests were restricted to stress levels up

to the fatigue limit stress it is not possible at present to suggest the shape of this plot beyond $\Delta\gamma_t$ values of 1.2 %. However it is expected that a limiting current density will exist as the process is charge transfer controlled.

7.2.3 Corrosion Fatigue Crack Initiation

After overcoming the microstructural barrier i.e. prior austenite grain boundary, stage II/mode I cracks were developed from the ends of pits. These cracks continued their growth in the same tenslie mode (ie. mode I). The number of cracks developed in a test was not equivalent to the number of pits initiated which suggests that crack propagation is attributed to the existance of favourable conditions ahead of the tip of the pit. A typical sequence illustrating pitting and crack development is shown in figure 5.6.

7.3 Crack Growth Behaviour

Crack growth was significantly enhanced in corrosion fatigue tests where an additional *chemical* driving force was operative along with the *mechanical* driving force. This mechanical driving force is considered to control crack growth in air fatigue. The mechanisms involved in crack growth for air fatigue, corrosion fatigue and intermittent air fatigue/corrosion fatigue will be discussed in detail below;

7.3.1 Air Fatigue

Cracks which nucleate at non-metallic inclusion sites continue their growth in the mode II plane of maximum shear stress. Depending upon the applied stress level crack may retard and/or arrest on encountering a prior austenite grain boundary. Crack propagation beyond these microstructural barriers occurs when the stress concentration at the tip of a crack is sufficient to induce slip within the adjacent grains. The degree of slow growth, or whether or not arrest occurs, depends upon such factors as the orientiation of adjacent grains, grain size and the nature of the fatigue load. Shear cracks experience a number of decelerations and accelerations while progressing through prior austenite grains. The time spent in crossing microstructural barriers was dependent upon the applied stress level. At high stresses cracks slow down for only a short period of time whereas around the fatigue limit stress the general growth pattern was similar except that a significant period of time was consumed in propagation beyond barriers and into adjacent grains. On attaining an average crack length of around 120 μm, equivalent to four times the average prior austenite grain size, a dominant deceleration in crack growth was observed which is accounted for by the crack attaining a suitable aspect ratio. Once a crack overcame this major barrier it continued to propagate until failure of the specimen took place. Cracks therefore experienced a significant influence of microstructure during the mode II/stage I growth which is almost absent during the mode I/stage II growth. It is worth noting that not all cracks which initiated in a test were able to continue propagating until failure. Failure resulted either

from the growth of a single crack or was caused by the coalescence of individual small cracks. Despite the large number of cracks which developed, most were seen to arrest at various stages of a test. This suggests that a favourable orientation might be necessary for continued crack propagation although load shedding is also possible. Similarly a variation in crack growth rate is observed for individual cracks which highlights the role of variation in grains size and orientation.

7.3.2 Corrosion Fatigue

Experimental results obtained from corrosion fatigue tests indicated there was a significant influence of the aggressive evironment at all stress levels applied in this study. This differs somewhat to the results given in a previous study for a low carbon steel [24] where a little influence was seen at high stresses. Figure 5.3 shows that the applied stress level plays a vital role in promoting the environment's aggressiveness. From the crack growth results of these tests, figures 6.3, it appears that like air fatigue the early stages of crack growth exhibit an oscillatory pattern up to a particular crack length. A significant difference with respect to air fatigue studies was observed in that the transition from short to long crack growth, i.e. from microstructural dependent to continuum mechanics type growth, occured in mode I crack growth. The purturbations observed in corrosion fatigue short crack growth indicate that there is still an influence of the microstructue although the degree to which retardation occurs was decreased suggesting that the role of the environment is one which causes a reduction in barrier strength. In these tests a

transition from short to long crack growth was seen to take place around 120 μm which coincides with that observed in air fatigue.

All corrosion fatigue tests were conducted at sub-fatigue limit stresses. Although the applied stress alone was insufficient for crack propagation it is sufficient to break surface oxide films which enable the process of dissolution to occur and hence short crack growth has been attributed to the simultaneous action of chemical and mechanical driving forces. The broadening of pits and cracks implies that a mechanism of strain-assisted dissolution enables a crack to grow beyond a microstructural barrier which would otherwise have arrested under equivalent air fatigue conditions. On attaining a critical crack length the stress associated with the crack tip is sufficient to activate the dislocation source in the next grain and thereby produce a mechanical dominated event contributed to crack growth. The proposed mechanism of strain-assisted dissolution which causes a crack to grow through the prior austenite grain boundary may be favoured by features such as increased dislocation density at the crack tip and chemical hetrogenity between the matrix and prior austenite grain boundary. The role of strain-assisted dissolution as the major process contributing to corrosion fatigue short crack growth was evaluated by conducting additional experiments in which non-propagating cracks of around 50-60 μm in length, obtained from air fatigue cycling, failed to propagate under corrosion fatigue when an applied cathodic potential was applied during the test. This suggests clear evidence of the role of dissolution in light of the fact that cycling, with an applied cathodic potential, was continued to a lifetime 5 times

that of the actual corrosion fatigue lifetime at an identical stresss level.

When a crack is deemed to be long, i.e. when its growth may be quantified by continuum mechanics, the contribution from the chemical driving force may no longer be associated purely with strain-assisted dissolution. It appears from the experimental data that in-air and corrosion fatigue crack growth rates still differ at long crack lengths. In this respect a mixed-mechanism incorporating strain-assisted dissolution and hydrogen embrittlement may be operative. A possible explanation for this may be that; at long crack lengths acidification of the solution in the vicinity of the crack tip occurs as a result of limited oxygen diffusion to the crack tip region and a pH gradient can exist between the bulk solution and the crack tip solution. In addition to this a triaxial stress state at the crack tip promotes hydrogen adsorption ahead of the crack tip thus embrittling the material. A significant effect of hydrogen was observed in tensile tests using pre-charged specimens which may provide some support to the suggestion made above. From figure 6.3 it can be seen that a difference between air and corrosion fatigue crack growth rates exists at crack lengths greater than 300 μm. Assuming that the dissolution rate is a function of crack length and decreases as crack length increases relative to the mechanical driving force, the contribution arising from hydrogen effects must be considered in order to predict total crack growth rates. The influence of the environment with respect to crack size has been reported in previous studies [215,195]. Turnbull, for example suggests that as crack depth increases, the increased potential drop causes a diminished dissolution rate.

7.3.3 Intermittent Air Fatigue/Corrosion Fatigue

These tests were conducted at stress levels below the 'in-air' fatigue limit. Initial prolonged fatigue cycling in air resulted in the initiation of cracks which eventually became non-propagating halting at prior austenite grain boundaries. Figure 5.8(a) illustrates that a non-metallic inclusion of angular shape is more detrimental in terms of crack initiation site in that it may initiate cracks in both planes of maximum shear stress, a comment also made in a previous study [213]. This non-propagating crack resumed propagation during the introduction of corrosion fatigue cycling, for a period of 5000 cycles. It was seen that a pit was created from which a stage I crack developed and appears that the growth of this crack was controlled by dissolution as may be seen from the broadening of crack, figure 5.8(b). This crack again arrested when subjected to the next stage of air fatigue cycling. A second interval of corrosion fatigue cycling was then applied in order to repropagate the crack. An additional 5000 corrosion fatigue cycles were applied resulting in crack propagation. In this case a stage II/mode I crack developed, again assisted by anodic dissolution, see figure 5.8(c). On returning to 'in-air' cycling the crack continued its growth until failure of the specimen occured. A different crack growth behaviour between that of corrosion fatigue and air fatigue was seen, see figure 5.8(d), where a broadening of the corrosion fatigue crack illustrates the role of anodic dissolution. It is suggested that continued air fatigue crack growth up to failure is only possible when a crack has attained a critical (threshold) crack length. The number of corrosion fatigue intervals applied in a test to obtain this

critical crack length was a function of the applied stress level and crack length. For example, at stress levels close to the 'in-air' fatigue limit the introduction of one or two corrosion fatigue intervals was sufficient for subsequent air fatigue crack growth to continue. At the low stress level of 600 MPa 32 corrosion fatigue periods were introduced for a period of either 5000 or 10000 cycles. It is interesting to note that the total number of corrosion fatigue cycles, i.e. 230000, in this intermittent test is quite similar to the actual corrosion fatigue lifetime, i.e. 226000 cycles, at an identical stress level. This is understandable in the sense that crack arresting microstructural features offer a high resistance in air and are only overcome when the strain-assisted dissolution process is greater than that offered by the barriers.

Intermittent tests offer an understanding of the type of mechanism active during corrosion fatigue short crack growth. It is suggested that strain-assisted dissolution plays a key role in short crack growth under corrosion fatigue conditions for the following reasons;

- a triaxial stress state associated with the tensile loading which favours hydrogen adsorption is not achieved during shear crack propagation.
- the cyclic frequency used during these tests was sufficiently high that the possibility of hydrogen diffusion to a region ahead of the crack tip is limited.
- crack growth rates obtained during each interval of corrosion fatigue cycling in intermittent tests were almost identical to those obtained for full immersion tests, see figure 7.3. This observation cannot be explained in terms of a hydrogen adsorption mechanism as the introduction of corrosion fatigue

cycling was for extremely short time periods i.e. around 15 minutes, which it is suggested is insufficient time for hydrogen saturation to be achieved.

7.4 Stage I - Stage II Transition

A significant difference between air and corrosion fatigue cycling was seen in the transition from a crystallographic-stage I to non-crystallographic-stage II crack growth. Tests conducted in air at or above the fatigue limit showed that this transition occurred when a crack had grown to an average shear crack length of 120 μm. This crack length corresponded to four prior austenite grains assuming an average prior austenite grain size of 30 μm. In corrosion fatigue tests however this transition from shear crack to mode I crack growth occured at much shorter crack lengths. This transition was observed, on average, when a crack reached a prior austenite grain boundary i.e. 30 μm length.

The earlier transition observed in corrosion fatigue may have occured as a result of the following reasons [207]:

1. in-depth shear crack growth due to strain-assisted dissolution produced an appropriate aspect ratio at an early stage unlike shear cracks obtained under air fatigue loading which had long surface lengths and shallow depths;

2. the broadened crack shape, resulting from dissolution effects, enabled a crack to propagate along slip planes that otherwise would not have been in a favourable orientation under air fatigue conditions;

3. if crack closure effects are considered during stage I crack growth then any contribution from this mechanism will be smaller for corrosion fatigue tests than for that during air fatigue i.e. shorter shear crack length in corrosion fatigue tests resulting in reduced crack face rubbing.

The above comparison of transition lengths in air and corrosion fatigue tests were representative of failure cracks. In corrosion fatigue tests the stage I - stage II transition seemed to be very influencial in producing failure. For example, those cracks which had shortest mode II - mode I transition lengths of the order of one grain were more damaging than others having longer transition lengths. Those cracks whose transition lengths were very long, i.e. 100-300 μm, obtained from the coalescence of a number of closely located pits were least influencial in stage II cracking and it was often observed that they were unable to propagate to failure. This may be possible due to two factors. Firstly, that such cracks had not attained a suitable aspect ratio and secondly, more rubbing of the shear faces was experienced and hence larger closure effects were operative.

In order to confirm the relation of prior austenite grain boundary to stage I - stage II transition and also to crack retardation and arrest, an additional intermittent air fatigue/corrosion fatigue test was conducted. In this test the material had been given a heat treatment procedure which resulted in larger prior austenite grains, averaging 60 μm. Figure 5.10 shows that a prior austenite grain boundary not only caused a crack to arrest but also acted as a point at which the mode II - mode I transition occured. Previously, it has been also been suggested that this

transition occurred at grain boundaries [216] and Forsyth [9] related this stage I - stage II transition to a point where reversal of dislocation movement is prevented. He also pointed out that this transition occured when the ratio of shear stress to tensile stress had attained a critical value.

7.5 Threshold Crack Growth

As previously discussed, intermittent air fatigue/corrosion fatigue tests not only assisted in understanding the actual mechanism contributing to corrosion fatigue short crack growth but were also adopted as a method of determining long LEFM crack threshold values. Such cracks were obtained by applying corrosion fatigue conditions to non-propagating cracks up to a point at which subsequent in-air fatigue cycling, at the sub-fatigue limit stress, produced continued crack growth in air.

Threshold crack lengths are predicted using equation 6.7 in which a threshold growth rate of 1×10^{-5} μm/cycle has been considered. These calculated threshold crack lengths are given in table 5.2 in comparison to experimentally determined values from intermittent air fatigue/corrosion fatigue tests. Figure 7.4 illustrates a Kitagawa-Takahashi [217] diagram constructed by using short and long crack growth equations of air fatigue, where additional points represent experimental results of intermittent tests. A good correlation exists between theoretical and experimentally determined threshold crack lengths and also between crack growth rates for crack lengths above the respective threshold crack length. It therefore

appears from these test results that the formulation of short and long crack growth equations from smooth specimens is a suitable method for predicting LEFM threshold crack lengths and growth rates.

7.6 Electrochemical Studies

Theses studies were conducted to establish base line electrochemical data for the metal-environment system under study. Initially the variation of the free corrosion potential, E_r, was studied with time. It was seen that E_r dropped (i.e. became more negative) shortly after immersion, however the rate of decrease in potential reduced as the time of immersion increased. After a long immersion period, 24 hours, an almost steady state was observed, where no significant change in potential was observed. A typical time-E_r relationship is shown in figure 5.11.

In a further study of the electrochemical behaviour of this metal-environment system, anodic and cathodic polarization experiments were performed which were then used to determine the corrosion current, i_{corr}. These tests were conducted at a very fast scan rate (10000 mV/min) in the cathodic region and varying anodic scan rates of 10, 500 and 1000 mV/min. Fast sweep rates to cathodic potentials was used in an attempt to prevent/disrupt film formation before an anodic scan was started. A significant difference in i_{corr} values was obtained as scan rate varied. The i_{corr} was seen to be influenced by the sweep rate and decreased as the sweep rate decreased. Again it may be suggested that the reduction in corrosion current values observed while reducing the sweep rate may be attributed to the time available for

a film to form on the surface of the specimen. It is therefore unlikely that an estimate of the actual corrosion current generated at the crack tip i.e. bare metal surface may be derived from simple polarization methods. The surface condition of the specimen significantly influences any electrochemical measurements made [218,219,220]. Other workers [221] have suggested the use of a scratching electrode technique to determine suitable anodic-dissolution currents. The values of the corrosion current obtained from this study is far higher than those obtained from the present study and previous work [24].

7.7 Fractography

7.7.1 Air Fatigue

It is evident from figure 7.5(a) that at low stress levels a single crack is dominant in the failure process and that stage I cracking is of pure shear where stage II cracking is of mixed type i.e. shear and tensile. The rubbed fracture faces seen in this picture illustrates the presence of a shear mode. Figure 7.5(b) presents a clearer picture of stage I cracking, however at higher stress levels it seems that more than one crack contributes to failure by a mechanism of multiple initiation as shown in figure 7.6(a). Figure 7.6(b) suggests that more crack opening is occuring as little rubbing is evident in the stage II crack growth as observed at lower stress levels.

7.7.2 Corrosion Fatigue

At low stress levels it is quite obvious that pitting played a key role in the initiation of cracks. The presence of the environment causes cracking at low stress levels due to stress concentration associated with pits as shown in figure 7.7(a). In addition to this at high stress levels multiple initiation is seen for corrosion fatigue in comparison to that observed at high stresses in air fatigue, see figure 7.7(b). This may be due to the presence of corrosion pits which tells us that the environment plays a greater role in the early development and growth of cracks. At high magnification it appears that the fracture surface is heavily pitted particularly in the initiation region as shown in figure 7.7(c).

7.7.3 Intermittent Air Fatigue/Corrosion Fatigue

Intermittent tests were carried out at various stress levels. At comparatively low stresses, i.e. 815 MPa, it is considered that cracks develop at inclusion/matrix interfaces but do not extend beyond this region because of the limited crack tip stress intensity. At higher stress levels close to the in-air fatigue limit, i.e. 900 MPa, cracks initiate and propagate within the matrix but then arrest at microstructural barriers. The result of this is that corrosion fatigue crack propagtion was required at an early stage in the life of the crack for the the lower stress level. Figure 7.8(a) shows that at low stress level corrosion fatigue was required at an early stage when the crack was small, around 30 μm, whereas at a higher stress, figure 7.8(b), corrosion fatigue was introduced when the crack had arrested after attaining a long

shear mode length, around 100 μm.

7.7.4 Normal and Pre-charged Tensile Tests

A comparative study was made of the fracture surfaces of normal and pre-charged tensile specimens at low and high magnifications, see figures 7.9 and 7.10. It can be seen from figure 7.9 that for an uncharged specimen initiation occurs within the center of the specimen. In hydrogen pre-charged specimens initiation sites occur closer to the edge of the specimen.

At high magnification as illustrated in figure 7.10, the fracture surface of the uncharged specimen shows ductile/transgranular cracking and evidence of microvoid coalescence. In pre-charged specimens fractures are of a mixed type. A proportion of the area is ductile/transgranular while the remainder is brittle i.e. intergranular. The proportion of the intergranular fracture increases as the time for pre-charging increases indicating an increase in the amount of hydrogen adsorbed within the material.

7.8 Effect of Hydrogen

In order to evaluate the role of hydrogen in this metal-environment system, three different series of tests were carried out. In the first series fatigue specimens were pre-charged with hydrogen and tested under torsional loading conditions. After prolonged air fatigue cycling at sub-fatigue limit stress no apparent cracking was observed, which suggested that there was no influence of diffused hydrogen under

such loading conditions. A second series of tests involved tensile tests on pre-charged specimens. The results of these tests indicated a significant effect of hydrogen on the mechanical properties which were affected severely, see table 4.2. As discussed in the previous section, the fracture surfaces of these specimens showed that the amount of interganular cracking increased with an increase in the period of pre-charging.

In the final series, corrosion fatigue tests were conducted with the specimen subject to an applied cathodic potential of -1.25 V (vs SCE). As with pre-charged fatigue tests no effect of hydrogen was noted. No cracking was observed despite specimens being fatigued within the environment for a period 5 times that of the ordinary corrosion fatigue test. In a similar procedure a specimen which contained a few non-propagating shear cracks of lengths around 50 μm, originated from previous cycling in air was also tested under an applied potential conditions. These cracks also did not show any sign of re-propagation. It may therefore be suggested that there is no influence of hydrogen on stage I/mode II cracking.

7.9 Crack Growth Models

Empirical models for air and corrosion fatigue studies were developed. A decrease in crack growth rate was observed with the increase in crack length for short crack regime. After progressing beyond the dominant microstructural barrier where a crack is assumed to behave in a manner similar to that of long LEFM type cracks, a linear relationship between calculated growth rate and crack length existed. The

crack growth curves generated using theses models showed a good correlation with the experimental data as may be seen in figure 6.1 and 6.3. From figure 6.3 it is apparent that the environment is important in the early stages of crack growth.

As far as the role of environment in corrosion fatigue crack growth is concerned, it was initially suggested that strain-assisted dissolution was responsible for crack growth enhancement [207]. However analyses of both air and corrosion fatigue results indicated that it was not the only mechanism which contributed to corrosion fatigue crack growth. The non-conservative predictions made by using an environmental term in the superposition model based on the electrochemeical test test results also suggested that corrosion fatigue failure is more consistent with a mixed mechanism of anodic dissolution and hydrogen embrittlement. An attempt has therefore been made to develop a superposition model which represents such behaviour. Here the environmental term is described as a 'chemical driving force'. Based on experimental results it seems that this driving force is initially high and then decreases until it reaches a transition length (mode II - mode I). This regime which has already been suggested as pit development may be a dissolution-controlled event. However after passing this transition length, the chemical driving force seems to increase in a linear manner. This regime which is mode I crack growth appears to be governed by mixed mechanisms of strain-assisted dissolution and hydogen embrittlement. The proportion of either of these two mechanisms may be related to the length of a mode I crack. It is therefore suggested that as the mode I crack length increases the contribution from strain-assisted dissolution

decreases and that from hydrogen embrittlement increases. The crack growth predictions made by using this superposition model gave a reasonable agreement with the experimental results.

Chapter 8

Conclusions and Future Work

8.1 Conclusions

The following conclusions may be drawn from the present study of short fatigue crack growth behaviour in a silico-manganese spring steel under both air and aggressive environmental (0.6M NaCl solution) conditions;

1) Crack initiation in air was associated with non-metallic inclusions which showed a strong dependence upon the applied stress level with multiple crack initiation being observed at high stress levels. Cracks propagated almost exclusively along one of the two mutually perpendicular planes of maximum resolved shear stress.

2) Short fatigue cracks exhibited high initial growth rates and subsequent deceleration as they approached microstructural barriers such as prior austenite grain boundaries. After overcoming the first barrier cracks accelerate beyond this but are then subject to a further deceleration on reaching the next barrier. This os-

cillatory nature of crack growth continues up to a length equivalent to about four prior austenite grains.

3) A transition from a short to long crack is suggested when a crack has attained a length equal to around 120μm, i.e. four prior austenite grains, beyond which little influence of microstructure is seen and cracks continued growing up to failure.

4) Cracks once initiated become non-propagating when the applied stress level is below the fatigue limit. The lengths of these non-propagating cracks were consistent with multiples of the prior austenite grain size.

5) Chemical pitting at non-metallic inclusions sites resulted in favourable conditions for the initiation of corrosion fatigue cracks. Once initiated pits continued to propagate in a shear mode and depending upon their associated stress intensity they developed into stage II/mode I cracks after traversing 1-2 prior austenite grains.

6) Short corrosion fatigue cracks propagate in a mode I plane and show perturbations in growth i.e. decelerations and accelerations similar to that observed in air fatigue tests. A short to long crack transition occured during mode I growth at a crack length almost equivalent to that observed in air fatigue studies.

7) Pitting and hence crack density increased with an increase in the applied stress level.

8) Broadening of pits/stage I cracks resulting from strain-assisted dissolution causing an early stage I-stage II transition, when compared to that observed in air fatigue. At low stresses, failure takes place due to the growth of individual cracks.

At high stresses i.e. close to the 'in-air' fatigue limit failure occurs due to crack coalescence which is seen to occur around or after 60% of the total lifetime.

9) Corrosion fatigue failure may be described as a three stage process, namely; pit development, environment-assisted short crack growth and environment-assisted long crack growth. It is suggested that strain-assisted dissolution is primary responsible for short crack growth. As crack length increases it is considered that a hydrogen embrittlement mechanism becomes operative.

10) Intermittent air fatigue/corrosion fatigue type tests have been shown to provide a suitable technique for establishing LEFM long crack thresholds from smooth specimens.

8.2 Future Work

The present study has allowed an insight into the mechanisms involved in the initiation and propagation of short fatigue cracks in both environments of air and 0.6M NaCl solution. Additional work which would further assist in understanding the role of the environment in the development and growth of short fatigue cracks is suggested below;

1) Influence of solution temperature

The temperature of a solution has been shown to have an adverse effect on corrosion fatigue crack growth as chemical reaction rates increase with increasing solution temperature. The influence of the anodic dissolution reaction may therefore be studied by conducting tests at different temperatures.

2) Influence of frequency

A significant enhancement in corrosion fatigue crack growth may be observed under low frequency conditions where greater time is available for an environment to interact with the material. A useful extension of this study would be to increase the time available for hydrogen adsorption through a change in the cyclic frequency.

3) Influence of loading mode

It has been suggested that hydrogen uptake is little influenced by torsional loading. A useful series of tests would therefore be one which involved a similar study under uniaxial push-pull loading conditions.

4) Effect of cathodic polarization

Current studies have shown that applied cathodic polarization eliminates the anodic dissolution reaction and prevents crack propagation despite hydrogen evolution occuring at the crack tip. An interesting test would therefore be one in which cathodic polarization was applied to a specimen containing a mode I-stage II crack under torsional loading conditions.

Bibliography

[1] S. H. Avner: (1976) Introduction to Physical Metallurgy, McGraw Hill.

[2] K. J. Miller: (1991) "Metal fatigue — past, current and future", Twenty-seventh John Player lecture, Proc. Inst. Mech. Engrs., London.

[3] L. P. Pook: (1976) The Role of Crack Growth in Metal Fatigue, The Metals Society, London.

[4] E. A. Hodgkinson: (1849) "command paper", No. 1123, HMSO, London.

[5] W. Fairbairn: (1864) "Experiments to determinethe effects of impact, vibratory action and long continued changes of load on wronght- iron girders", Phil. Trans. Roy. Soc. , 154, pp 311-325.

[6] A. Wholer: (1871) "Wholer's experiments on the strength of metals", Engineering, 11, pp 199-200.

[7] E. M. Eden, W. N. Rose and F. L. Cunningham: (1911) "The endurance of metals-experiments on rotating beams at University College, London", Proc. Inst. Mech. Engrs., London, Parts 3-4, pp 839-974.

[8] H. J. Gough: (1926) The Fatigue of Metals, Scott, Greenwood and Son, London.

[9] K. J. Miller: (1985) "The short fatigue crack problem", Fatigue Engng. Mater. Struct., 5, pp 223-232.

[10] M. E. Fine: (1980) "Fatigue resistance of metals", Metall. Trans. A, 11, pp 365-379.

[11] P. J. E. Forsyth: (1961) "Two stage process of fatigue crack growth", Proc. Crack Propagation Symp., Cranfield, Vol 1, pp76-94.

[12] H. H. Johnson and P. C. Paris: (1968) "Sub critical flaw growth", Engng. Fract. Mech., pp 3-45.

[13] D. Brooksbank and K. W. Andrews: (1972) "Stress fields around inclusions and their relation to mechanical properties", JISI, 210, pp 246-255.

[14] T. Y. Shih and T. Araki: (1973) "The effect of non-metallic inclusions and microstructures on the fatigue crack initiation and propagation in high strength carbon steels", Trans. ISIJ , 13, pp 11-19.

[15] F. B. Pickering: (1973) "The need for inclusions assessment", Steel Times Annual Reviews, pp 99-110.

[16] C. Gladman: (1975) "Sulfide inclusion in steel", ASM Materials/Metal Working Technology Series, No. 6, Metal Park, Ohio, USA.

[17] T. A. Khalifa: (1988) "Effect of inclusion on the fatigue limit of a heat treated carbon steel", Mat. Sc. & Eng. A, 102, pp 175-180.

[18] N. M. A. Eid and P. F. Thomason: (1979) "The nucleation of fatigue cracks in a low alloy steel under high-cycle fatigue conditions and uniaxial loading", Acta Met., 27, pp 1239-1249.

[19] J. A. Ewing and J. C. W. Humphrey: (1903) "The fracture of metals under repeated alternations of stress", Phil. Trans. Roy. Soc., A200, pp 241-250.

[20] N. Thompson and N. J. Wadsworth: (1958) "Metal fatigue", Adv. Phys. (Philos. Mag. Suppl.), 7, pp 72-169.

[21] W. A. Wood: (1958) "Formation of fatigue cracks", Phil. Mag., 3, pp 692-699.

[22] P. J. E. Forsyth: (1951) "Some metallographic observations on the fatigue of metals", J. Inst. Metals, 80, pp 181-186.

[23] A. H. Cottrell and D. Hull: (1957) "Extrusion and intrusion by cyclic slip in copper", Proc. Roy. Soc., A 242, pp 211-213.

[24] R. Akid: (1987) "The initiation and growth of short fatigue cracks in aqueous saline environment", Ph.D. Thesis, University of Sheffield.

[25] W. Zhang: (1991) "Short fatigue crack growth under different loading systems", Ph.D. Thesis, University of Sheffield.

[26] S. Y. Sun: (1991) "Long life corrosion fatigue in an aluminium-lithium alloy", Ph.D. Thesis, University of Sheffield.

[27] C. V. Cooper and M. E. Fine: (1983) "Fatigue crack initiation in iron", in Defects, Fracture and Fatigue, eds. G. C. Sih and J. W. Provan, pp 183-194.

[28] H. Mughrabi: (1983) "A model of high-cycle fatigue crack initiation at grain boundaries by persistant slip bands", ibid, pp 139-146.

[29] T. Kunio et al: (1979) "The role of prior austenite grains in fatigue crack initiation and propagation in low-carbon martensite", Fatigue Fract. Engng. Mater. Struct., 2, pp 237-249.

[30] J. R. Yates: (1990) "An investigation of geometry and data analysis procedures for short crack growth in waspalloy at 19^0C", Final report for brochure B1J1-81D SMP 1058/3.

[31] H. O. Fuchs and R. I. Stephens: (1980) Metal Fatigue in Engineering, Wiley-Interscience Publication, New York.

[32] A. A. Griffith: (1921) "The phenomena of rupture and flow in solids", Phil. Trans. Roy. Soc., London, A221, pp 163-197.

[33] G. R. Irwin: (1957) "Fracture mechanisms", J. App. Phys., 24, pp 361-364.

[34] P. C. Paris and F. Erdogan: (1963) "A critical analysis of crack propagation laws", J. Basic engng., Trans. ASME, series D, 85, pp 528-534.

[35] R. O. Ritchie: (1977) "Influence of microstructure on near-threshold fatigue crack propagation in ultra-high strength steel", Metal Science, 11, pp 368-381.

[36] D. S. Dugdale: (1960) "Yielding of steel sheets containing slits", J. Mech. Phys. Solids, 8, pp 100-108.

[37] A. A. Wells: (1962) "Unstable crack propagation in metal: Damage and post fracture", Proc. Crack Propagation Symp., Cranfield, Vol. 1, pp 210-230.

[38] J. R. Rice: (1968) Fracture, Vol II, ed. H. Liebowitz, Academic press, New York.

[39] B. Tomkins: (1968) "Fatigue crack propagation, an analysis", Phil. Mag., 18, pp 1041-1066.

[40] H. D. Solomon: (1972) "Low cycle fatigue crack propagation in 1018 steel", J. Mater., 7, pp 299-306.

[41] M. F. E. Ibrahim and K. J. Miller: (1980) "Determination of fatigue crack initiation life", Fatigue Engng. Mater. Struct., 2, pp 351-360.

[42] S. Suresh and R. O. Ritchie: (1984) "Propagation of short fatigue cracks", Int. Met. Rev., 29(6), pp 445-475.

[43] K. J. Miller: (1984) "The propagation behaviour of short fatigue cracks", in Subcritical Crack Growth due to Fatigue, Stress Corrosion and Creep, ed. L. H. Larsson, Elsevier Applied Science Publishers, pp 151-166.

[44] K. J. Miller: (1987) "The behaviour of short fatigue cracks and their initiation part-I; a review of two recent books", Fatigue Fract. Engng. Mater. and Struct., 10(1), pp 75-91.

[45] M. W. Brown: (1986) "Interfaces between short, long and non-propagating cracks", The Behaviour of Short Fatigue Cracks, eds. K. J. Miller and E. R. de los Rios, pp 423-439.

[46] K. J. Miller: (1987) "The behaviour of short fatigue cracks and their initiation - part II; a general summary", Fatigue Fract. Engng. Mater. Struct., 10(2), pp 93-113.

[47] K. Tanaka , M. Hojo and Y. Nakai: (1983) "Crack initiation and early propagation in 3 pct silicon", Fatigue Mechanisms, Advances in quantitative Measurement of Physical Damage, ASTM STP 811, pp 207-232.

[48] D. Taylor and J. F. Knott: (1981) "Fatigue crack propagation behaviour of short cracks; the effect of microstructure", Fatigue Engng. Mater. Struct., 4(2), pp 147-155.

[49] C. W. Brown and M. A. Hicks: (1983) "A study of short fatigue crack growth behaviour in titanium alloy IMI 685", Fatigue Engng. Mater. Struct., 6, pp 67-75.

[50] C. W. Brown and J. E. King: (1986) "The relevance of microstructure influences in the short crack regime to overall fatigue resistance", Small Fatigue Cracks, Published by the Met. Soc. Inc., pp 73-95.

[51] C. W. Brown and D. Taylor: (1984) "The effect of texture and grain size on the short fatigue crack growth rates in Ti-6Al-4V", in Fatigue Crack

Threshold Concepts, eds. D. L. Davidson and S. Suresh, AIME, Philadelphia, pp 433-446.

[52] J. Lankford: (1985) "The influence of microstructure on the growth of small fatigue cracks", Fatigue Fract. Engng. Mater. Struct., 8, pp 161-175.

[53] W. L. Morris: (1980) "The non-continuum crack tip deformation behaviour of surface microcracks", Metall. Trans. A, 11, pp 1117-1123.

[54] A. Navarro and E. R. de los Rios: (1988) "Short and long fatigue crack growth; a unifield model", Phil. Mag. A, 57(1), pp 15-36.

[55] M. S. Hunter and W. M. G. Fricke, Jr.: (1956) "Fatigue crack propagation in aluminium alloy", Proc. ASTM, 56, pp 1038-1046.

[56] R. G. de Lange: (1964) "Plastic replica methods applied to a study of fatigue crack propagation in steel 35 CD 4 and 26 ST Aluminium Alloy", Trans. AIME, 230, pp 644-648.

[57] J. Lankford: (1977) "Initiation and early crack growth of fatigue cracks in high strength steel", Engng. Fract. Mech., 9, pp 617-624.

[58] J. Lankford, T. S. Cook and G. P. Sheldon: (1981) "Fatigue microcrack growth in a nickel-base super alloy", Int. J. Fract., 17, pp 143-155.

[59] J. Lankford: (1982) "The growth of small fatigue cracks in 7075-T6 aluminium alloy", Fatigue Engng. Mater. Struct. , 5, pp 233-248.

[60] J. Lankford: (1983) "The effect of environment on the growth of small fatigue cracks", Fatigue Engng. Mater. Struct., 6, pp 15-31.

[61] R. A. Smith: (1983) "Short fatigue cracks" ASTM-STP 811, pp 264-279.

[62] E. R. de los Rios, Z. Tang and K. J. Miller: (1984) "Short crack fatigue behaviour in a medium carbon steel", Fatigue Engng. Mater. Struct., pp 97-108.

[63] E. R. de los Rios, H. J. Mohammad and K. J. Miller: (1985) "A micromechanics analysis for short fatigue crack growth", Fatigue Engng. Mater. Struct., 8, pp 49-64.

[64] P. Lukas and L. Kunz: (1985) "The mechanism of fatigue crack propagation", Ko Vove Materials, 23(6), pp 701-714.

[65] S. Pearson: (1975) "Initiation of fatigue cracks in commercial aluminium alloys and the subsequent propagation of very short cracks", Engng. Fract. Mech., 7(2), pp 235-247.

[66] J. L. Breat, F. Murdy and A. Pineau: (1983) "Short crack propagation and closure effect in a 508 steel", Fatigue Engng. Mater. Struct., 6, pp 349-358.

[67] K. Tanaka and Y. Nakai: (1983) "Propagation and non-propagation of short fatigue cracks at sharp notch", Fatigue Engng. Mater. Struct., 6, pp 315-327.

[68] P. D. Hobson and M. W. Brown: (1986) "Two phases of short crack growth in a medium carbon steel", The Behaviour of Short Fatigue Cracks, eds. K.

J. Miller and E. R. de los Rios, pp 441-459.

[69] D. Taylor: (1986) "Fatigue of short cracks: The limitations of fracture mechanics", The Behaviour of Short Fatigue Cracks, eds. K. J. Miller and E. R. de los Rios, pp 479-490.

[70] D. Taylor and J. F. Knott: (1981) "Fatigue crack propagation behaviour of short cracks; the effect of microstructure", Fatigue Engng. Mater. Struct., 4, pp 147-155.

[71] R. Chang, W. L. Morris and O. Buck: (1979) "Fatigue crack nucleation at intermetallic particles in alloys - A dislocation pile-up model", Scripta Met., 13, pp 191-194.

[72] W. L. Morris, M. R. James and O. Buck: (1981) "Growth rates models for short surface cracks in Al 2219-T851", Metal. Trans. A, 12, pp 57-64.

[73] A. K. Zurek, M. R. James and W. L. Morris: (1983) "The effect of grain size on fatigue growth of short cracks", Metal. Trans. A, 14, pp 1697-1705.

[74] W. L. Morris, M. R. James and O. Buck: (1983) "A simple model of stress intensity range threshold and crack closure stress", Engng. Fract. Mech., 18, pp 871-877.

[75] K. S. Chan and J. Lankford: (1983) "A crack tip model for the growth of small fatigue cracks", Scripta Metall. , 17, pp 529-532.

[76] A. Navarro and E. R. de los Rios: (1988) "A microstructurally- short fatigue crack growth equation", Fatigue Engng. Mater. Struct., 11(5), pp 383-396.

[77] C. A. Zapffe and C. E. Sims: (1941) "Hydrogen-embrittlement, internal stress and defects in steel", Trans. AIME, 145, pp 225-271.

[78] N. J. Petch and P. Stables: (1952) "Delayed fracture of metals under static load", Nature, 169, pp 842-843.

[79] A. R. Troiano: (1960) "The role of hydrogen and other interstitials in the mechanical behaviour of metals", Trans. ASM, 52, pp 54-80.

[80] B. F. Brown: (1966) "A new stress corrosion cracking test for high strength alloys", Mater. Res. Stand., ASTM , 6, pp 129-133.

[81] M. H. Peterson, B. F. Brown, R. L. New Begin and R. E. Grover: (1967) "Stress corrosion cracking of high strength steels and titanium alloys in chloride solutions at ambient temperatures", Corrosion , 23, pp 142-148.

[82] H. J. Gough and D. G. Sopwith: (1932) "Atmospheric action as a factor in fatigue of metals", J. Inst. Metals, 49, pp 93-112.

[83] K. U. Snowden: (1964) "The effect of atmosphere on the fatigue of lead", Acta Met., 12, pp 295-303.

[84] J. A. Roberson: (1965) "Environmental influences on the fatigue of molybdenum", Trans. AIME , 233, pp 1799-1800.

[85] N. J. Wordsworth: (1959) Internal Stress and Fatigue in Metals, eds. Rassweiler and Grube, Elsevier, Amsterdam, pp 382-396.

[86] T. Broom and A. Nicholson: (1961) "Atmospheric corrosion-fatigue of age-hardened aluminium alloys", J. Inst. Metals, 89, pp 183-190.

[87] W. Engelmaier: (1968) "Fatigue behaviour and crack propagation in 2024-T3 aluminium alloy in ultra high vacuum and air", Trans. Met. Soc. AIME, 242, pp 1713-1718.

[88] I. Congleton and I. H. Craig: (1982) "Corrosion fatigue" in Corrosion Processes, ed. R. N. Parkins, pp 209-269.

[89] N. P. Inglis: (1957) "Recent advances in metallic materials of construction for use in the chemical industry", Chem. and Indus. (London), pp 180-189.

[90] J. B. Cotton and B. P. Downing: (1957) "Corrosion resistance of titanium to sea water", Trans. Inst. Mar. Engrs., 69(8), pp 311-319.

[91] R. Akid and K. J. Miller: (1988) "The initiation and growth of short fatigue cracks in an aqueous saline environment" in Environment - Assisted Fatigue, EGF Publication 7, eds. P. M. Scott and R. A. Cottis, Mechanical Engineering Publications, London, pp 415-434.

[92] R. Akid and G. Murtaza: (1991) "Corrosion fatigue crack growth modelling of a high strength steel subjected to fully reversed torsional loading" in Life Predictions of Corrodible Structures , Cambridge, Sept. 23-26, NACE, to be published.

[93] B. P. Haigh: (1917) "Experiments on the fatigue of brasses", J. Inst. Metals, 18, pp55-77.

[94] B. P. Haigh: (1929) "Chemical action in relation to fatigue in metals", Trans. Inst. Chem. Engrs., 7, pp 29-48.

[95] B. P. Haigh and B. Jones: (1930) "Atmospheric action in relation to fatigue in Pb", J. Inst. Metals, 43, p. 271.

[96] D. J. McAdam: (1926) "Stress - strain relationships and corrosion fatigue of metals", Proc. ASTM , 26, pp 224-254.

[97] H. J. Gough: (1932) "Corrosion fatigue of metals", J. Inst. Metals, 49, pp 17-92.

[98] D. J. McAdam, Jr. and G. W. Geil: (1941) "Pitting and its effect on the fatigue limit of steels corroded under various conditions", Proc. ASTM , 41, p. 696.

[99] B. B. Wescott: (1938) "Fatigue and corrosion fatigue of steels", Mech. Engg., 60, pp 813-829.

[100] T. S. Sudarshan, T. S. Srivatsan and D. P. Harveyii: (1990) "Fatigue processes in metals — role of aqueous environments", Engng. Fract. Mech., 36(6), pp 827-852.

[101] D. J. McAdam: (1931) "Influence of water composition on stress corrosion", Proc. ASTM, 31, pp 259-278.

[102] G. E. Journeuax, J. W. Martin and D. E. Talbot: (1977) "The role of electrochemistry in corrosion fatigue", in Mechanisms of Environment-sensitive Cracking of Materials, Metal Society Publication, pp 322-333.

[103] U. R. Evans and M. T. Simnad: (1947) "The mechanism of corrosion fatigue of mild steel", Proc. Royal Soc., A188, pp 372-392.

[104] T. Hodgkiess: (1977) "Corrosion fatigue of structural steel in sea water", in Mechanisms of Environment Sensitive Cracking of Materials, Metal Society Publication, pp 348-358.

[105] J. Congleton: (1983) "Some electrochemical and microstructural aspects of corrosion fatigue", ASTM STP 801, pp 367-389.

[106] Y. Nakason, K. Tasuji and H. Kitagawa: (1980) in Mechanical Behaviour of Materials, Proc. third international conf. held in Cambridge, eds. K. J. Miller and R. F. Smith, ICM3 , vol. 2, p. 345.

[107] G. P. Ray, R. A. Jarman and J. G. N. Thomas: (1985) "The influence of non-metallic inclusions on the corrosion fatigue of mild steel", Corrosion Science, 25(3), pp 171-184.

[108] D. J. Duquette and H. H. Uhlig: (1969) "The critical reaction rate for corrosion fatigue of a 0.18% carbon steel and the effect of pH", Trans. ASM, 62, pp 839-845.

[109] H. J. Gough and D. J. Sopwith: (1932) "The behaviour of a single crystal

of aluminium under alternating torsional stresses while immersed in a slow stream of tap water", Proc. Roy. Soc., A 135, pp 392-411.

[110] J. Flis and J. C. Scully: (1968) "The role of interstitial and substitutional impurities in stress corrosion cracking of low carbon steel in nitrate solution", Corrosion, 24, pp 326-334.

[111] D. Withwham and U. R. Evans:(1950) "Corrosion fatigue—The influence of disarrayed metal", JISI, 165, pp 72-79.

[112] T. P. Hoar and J. G. Hines: (1956) "The stress-corrosion cracking of austenitic stainless steels", JISI, 182, pp 124-143.

[113] H. N. Hahn and D. J. Duquette: (1979) "The effect of heat treatment on the fatigue and corrosion fatigue behaviour of a CuNiCr alloy", Metall. Trans. A, 10, pp 1453-1460.

[114] H. Masuda and D. J. Duquette: (1975) "The effect of surface dissolution on fatigue crack nucleation in polycrystalline copper", Metall. Trans. A, 6, pp 87-94.

[115] H. N. Hahn and D. J. Duquette: (1978) "The effect of surface dissolution on fatigue deformation and crack nucleation in copper and copper 8% aluminium single crystal", Acta Metall., 26, pp 279-287.

[116] B. D. Yan, G. C. Farrington and C. Laird: (1985) "Strain localization in single crystals of copper cycled in 0.1M perchloric acid solution under potential control", Acta Metall., 33, pp 1533-1545.

[117] B. D. Yan, G. C. Farrington, C. Laird: (1985) "The interaction of simultaneous cyclic straining and aqueous corrosive attack in the behaviour of persistant slip bands", Acta Metall., 33, pp 1593-1600.

[118] H. N. Hahn: (1977) Ph.D. Dissertation, Rensselaer Polytechnic Institute, Troy , New York.

[119] C. Garcia and D. J. Duquette: (1985) Corrosion of Nickel Based Alloys, ed. R. C. Scarbury (Philadelphia , PA: ASTM), p. 127.

[120] C. Garcia, D. J. Duquette: (1986) "Modelling envoirnmental effects on crack growth processes", eds. R. H. Jones, W. W. Gerberich (Warrendale, PA, The Metallurgical Society - American Institute of Mining, Metallurgical and Petroleum Engineers, p. 343.

[121] T. Konda, T. Kikuyama, H. Nakajima, M. Shindo and R. Nagasaki: (1972) "Corrosion fatigue of ASTM A-302B steel in high temperature water, the simulated nuclear reactor environment", in Corrosion Fatigue: Chemistry, Mechanics and Microstructure, NACE-2, pp 539-549.

[122] G. A. Beital and C. Q. Bowles: (1971) "Influence of anodic layers on fatigue-crack initiation in aluminium", J. Met. Soc., 5, pp 85-91.

[123] S. P. Lynch: (1979) "Mechanisms of fatigue and environmentally-assisted fracture", in Fatigue Mechanisms, ASTM STP 675, ed. J. T. Fong, philadelphia, PA, pp 174-213.

[124] P. A. Z. Rebinder, Physi K, 72, p 191: (1931) (Quoted by J. M. West, Electrodisposition and corrosion process - 2nd edition , Van- Nostrand Reinhold Publication), p. 166.

[125] C. Benedicks: (1948) Pittsburgh Int. Conf. on Surface Reactions, p. 196.

[126] C. Laird and D. J. Duquette: (1972) "Mechanisms of fatigue crack nucleation", Corrosion Fatigue: Chemistry Mechanics and Microstructure, NACE-2, pp 88-115.

[127] N. J. Petch: (1956) "The lowering of fracture-stress due to surface adsorption", Phil. Mag., 1, pp 331-337.

[128] P. M. Scott: (1979) "Effect of environment on crack propagation", Developments in Fracture Mechanics-1, ed. G. C. Chell, pp 221-257.

[129] C. P. Dervenis, E. I. Meletis and R. F. Hochman: (1988) "Corrosion fatigue in Al-Li alloy 2090", Mat. Sc. & Engg. A, 102, pp 151-160.

[130] I. M. Austen and P. McIntyre: (1979) "Corrosion fatigue of high strength steel in low-pressure hydrogen gas", Metal Science, 13, pp 420-428.

[131] F. P. Ford: (1978): "Quantitative examination of slip - dissolution and hydrogen embrittlement theory of cracking in aluminium alloy", Metal Science, 12, pp 326-334.

[132] T. Magnin, D. Desjardins and M. Puiggali: (1989) "The influence of mechanical test condition on corrosion fatigue", Corrosion Science, 29(5), pp

567-576.

[133] D. J. McAdam, Jr.: (1930) "The influence of stress range and cycle frequency on corrosion", Proc. ASTM, 30, pp 411-447.

[134] D. J. McAdam, Jr.: (1931) "Influence of stress on corrosion", AIME Tech. Pub., No. 417, pp 1-39.

[135] K. Endo and Y. Miyas: (1958) "Effects of cycle frequency on corrosion fatigue strengths", Bull. Japan Soc. Mech. Engg., 1, pp 374-380.

[136] J. M. Barsom: (1972) "Effect of cyclic stress form on corrosion fatigue crack propagation below K_{ISCC} in a high yield strength steel", Proc. Conf. on Corrosion Fatigue , NACE-2, pp424-434.

[137] P. M. Scott: (1979) "Corrosion fatigue in pressure vessel steels for light water reactors", Metal Science, 13, pp 396-401.

[138] J. M. Barsom: (1971) "Corrosion-fatigue crack propagation below K_{ISCC}", Engng. Fract. Mech., 3, pp 15-25.

[139] J. D. Atkinson and T. C. Lindley: (1979) "Effect of stress wave form and hold-time on environmentally assisted fatigue crack propagation", Metal Science, 13, pp 444-448.

[140] M. Yoda: (1988) "Stress corrosion cracking under Mode I, II and III loading", Engng. Fract. Mech., 30(4), pp 461-467.

[141] R. N. Parkins: (1980) "Aqueous environmental influences in corrosion fatigue", Proc. First UK-USSR Seminar, Corrosion Fatigue , eds.R. N. Parkins and Ya. M. Kolotyrkin, pp 36-46.

[142] F. J. Radd, L. H. Crowder and L. H. Wolfe: (1960) "Effect of pH in the range 6.6-14.0+ on the aerobic corrosion fatigue of steel", Corrosion , 16, pp 415-418.

[143] A. J. Gould: (1933) "The influence of solution concentration on the severity of corrosion fatigue", Engineering, 136, pp 453-454.

[144] A. J. McEvily: (1977) "Current aspects of fatigue", Metal Science, 11, pp 274-284.

[145] A. J. Gould: (1936) "The influence of temperature on the severity of corrosion fatigue", Engineering, 141, pp 495-496.

[146] D. S. Dugdale: (1962) "Corrosion fatigue of sharply notched steel specimens", Metallurgia, 65, pp 27-28.

[147] M. H. El Haddad, T. H. Hopper and B. Mukherjee: (1981) "Review of new developments in crack propagation studies", J. Test. Eval., 9, pp 65-81.

[148] J. P. Gallagher: (1970) "Corrosion fatigue crack growth rate behaviour above and below K_{ISCC}", Report NRL-7064, Naval Research Laboratory.

[149] Metals Handbook, Corrosion, Vol. 13.

[150] M. T. Simnad and U. R. Evans: (1947) "The mechanism of corrosion fatigue of steel in acid solution", JISI, 156, pp 531-539.

[151] N. P. Inglis and G. F. Lake: (1931) "Corrosion-fatigue of mild steel and chromium-nickel austenitic steel in river tees water", Trans. Faraday Soc., 27, pp 803-808.

[152] N. P. Inglis and G. F. Lake: (1932) "Corrosion-fatigue tests of nitrided steel and nickel-plated steel in river tees water", Trans. Faraday Soc., 28, pp 715-721.

[153] D. J. Duquette and H. H. Uhlig: (1968) "Effect of dissolved oxygen and NaCl on corrosion fatigue of 0.8 % carbon steel", Trans. ASM, 61, pp 449-456.

[154] W. E. Cowley, F. P. A. Robinson and J. E. Kerrich: (1968) "Anodic protection for the control of corrosion fatigue", British Corrosion Journal, 3, pp 223-237.

[155] R. T. Allsop: (1953) "The effect of stress in electrodeposits upon the corrosion-fatigue properties of spring steel", Coil Spring J., 32, pp 5-10.

[156] W. E. Harvey: (1930) "Zinc as a protective coating against corrosion fatigue of steel", Metals and Alloys, 1, pp 458-461.

[157] E. A. G. Liddiard, J. A. Whittaker and H. King: (1962) First International Congress on Metallic Corrosion, Butterworths, London, p. 482.

[158] F. N. Speller, I. B. McCorkle and P. F. Mumma: (1928) "Influence of corrosion accelerators and inhibitors on fatigue of ferrous metals", Proc. ASTM, 28, pp 159-167.

[159] F. N. Speller, I. B. McCorkle and P. F. Mumma: (1928) "The influence of corrosion accelerators and inhibitors on fatigue of ferrous metals", Proc. ASTM, 29, pp 238-249.

[160] A. G. Gould and U. R. Evans: (1939) "A scientific study of corrosion-fatigue preliminary report on experiments at Cambridge University", Iron and Steel Inst. Special Report, 24, pp 325-342.

[161] F. Mansfeld: (1973) "Tafel slopes and corrosion rates from polarization resistance measmurements", Corrosion, 29, pp 397-402.

[162] F. Mansfeld: (1976) "The polarization resistance technique for measuring corrosion currents", Advances in Corrosion Science and Technology, eds. M.G. Fontana and R.W. Staehle, Plenum Press, New York, Vol. 6, pp 163-262.

[163] B. E. Wilde: (1972) "A critical appraisal of some popular laboratory electromechanical tests for predicting the localized corrosion resistance of stainless alloys in sea water", Corrosion, 28, pp 163-262.

[164] I. M. Austen and E. F. Walker: (1977) "Quantitative understanding of the effects of mechanical and environmental variables on corrosion fatigue crack growth behaviour", Conf. Inst. Mech. Engrs., London, pp 1-10.

[165] P. McIntyre: (1973) "The relationship between stress corrosion cracking and sub-critical flaw growth in hydrogen and hydrogen sulphide gases", Proc. Int. Conf. on Stress Corrosion Cracking and Hydrogen Embrittlement of Iron Base Alloys , France, eds. R. W. Staehle, J. Hotchmann, R. D. McCright and J. E. Slater, NACE - 5, pp 788-797.

[166] J. M. Barsom: (1969) "Mechanisms of corrosion fatigue below K_{ISCC}", Int. J. Fract. Mech., 7, pp 163-182.

[167] M. J. Horden: (1966) "Fatigue behaviour of aluminium in vacuum", Acta Metall., 14, pp 1173-1178.

[168] R. P. Wei: (1968) "Fatigue-crack propagation in a high-strength aluminium alloy", Int. J. Fract. Mech., 4, pp 159-170.

[169] J. A. Feeney, J. C. McMillan and R. P Wei: (1970) "Enviromental fatigue crack propagation of aluminium alloys at low stress intensity levels", Metall. Trans., 1, pp 1741-1757.

[170] A. Hartmann: (1965) "On the effect of oxygen and water vapor on the propagation of fatigue cracks", Int. J. Fract. Mech., 1, pp 167-188.

[171] F. J. Bradshaw and C. Wheeler: (1966) "The effect of environment on fatigue crack growth in aluminium and some aluminium alloys", Appl. Mater. Res., 5, pp 112-120.

[172] E. P. Dahlberg: (1965) "Fatigue-crack propagation in high-strength 4340 steel in humid air", Trans. ASM, 58, pp 46-53.

[173] R. P. Wei and J. D. Landes: (1969) "Correlation between sustained-load and Fatigue Crack Growth in high strength Steels", Mater. Res. Std., 9, pp 25-27.

[174] W. A. Van Der Sluys: (1965) "Effect of repeated loading and moisture on the fracture toughness of SAE 4340 steel", J. Basic Engng., 87, pp 363-373.

[175] J. P. Gallagher and J. M. Sinclair: (1969) "Environmentally assisted fatigue crack growth rates in SAE 4340 steel", J. Basic. Engng., 91, pp 598-602.

[176] R. W. Judy, Jr. , T. W. Crooker, R. E. Morey, E. A. Lange and R. J. Goode: (1966) "Low-cycle fatigue-crack propagation and fractographic investigation of Ti-7Al-2Cb-1Ta and Ti-6Al-4V in air and in aqueous environments", Trans. ASM, 59, pp 195-207.

[177] D. A. Meyn: (1971) "An analysis of frequency and amplitude effects on corrosion fatigue crack propagation in Ti-8Al-1Mo-1V", Metall. Trans., 2, pp 853-865.

[178] G. A. Miller, S. J. Hudak and R. P. Wei: (1973) "The influence of loading variables on environment enhanced fatigue crack growth in high strength steels", J. of Test. and Eval., 1, pp 524-531.

[179] A. J. McEvily and R. P. Wei: (1972) "Fracture mechanics and corrosion fatigue", in Corrosion Fatigue: Chemistry, Mechanics and Microstructure, NACE-2, pp 381-393.

[180] J. P. Gallagher and R. P. Wei: (1972) "Corrosion fatigue crack propagation in

steels", Proc. Int. Conf. on Corrosion Fatigue, NACE-2, Connecticut, USA, pp 409-423.

[181] P. Marshall: (1977) "The influence of low oxygen and contaminated sodium environments on fatigue behaviour of solution treated AISI 316 stainless steel", Proc. Conf. on The Influence of Environment on Fatigue, Inst. Mech. Engrs., London, pp 27-36.

[182] H. D. Solomon: (1972) Proc. 2nd. Int. Conf. on Corrosion Fatigue; eds. O. J. Devereaux, A. J. McEvily and R. W. Staehle, NACE, p. 331, 420, 553.

[183] S. Kawai and K. Kasai: (1985) "Considerations of allowable stress of corrosion fatigue (focused on the influence of pitting)", Fatigue Fract. Engng. Mater. Struct., 8(2), pp 115-127.

[184] R. Holder: (1977) "Environmental effects on fatigue crack initiation and propagation in a cast steel", Conf. Inst. Mech. Eng. London, UK., pp 37-41.

[185] R. P. Gangloff and R. P. Wei: (1986) "Small crack-environment interaction: The hydrogen embrittlement perspective", Small Fatigue Cracks, eds. R. O. Ritchie and J. Lankford, pp 239-264.

[186] M. O. Speidel: (1975) "Stress corrosion cracking of aluminium alloy", Met. Trans., 6A, pp 631-651.

[187] J. Lankford and D. L. Davidson: (1984) "Near-threshold crack tip strain and crack opening for large and small fatigue cracks", in Fatigue Crack Growth Threshold Concepts, eds. D. Davidson and S. Suresh, AIME, pp 447-463.

[188] Nakai et al: (1986) "Short crack growth in corrosion fatigue for a high strength steel", Engng. Fract. Mech., 24, pp 433-444.

[189] R. P. Gangloff and R. O. Ritchie: (1984) "Environmental effects novel to the propagation of short cracks", Fundamentals of Deformations and Fracture , eds. B. A. Bilby , K. J. Miller and J. R. Willis, pp 529-558.

[190] R. P. Gangloff: (1983) in Advances in Crack Length Measurement, ed. C. J. Beevers, p 175.

[191] R. P. Gangloff: (1981) in Fatigue Crack Growth Measurement and Data Analysis, eds. Hudak and Bucci, STP 738, ASTM, p 120.

[192] R. P. Gangloff: (1981) "The criticality of crack size in aqueous corrosion fatigue", Res. Mech. Lett., 1, pp 299-306.

[193] R. P. Gangloff: (1984) in Embrittlement by the Localized Crack Environment, ed. R. P. Gangloff, AIME.

[194] B. F. Jones: (1982) "The influence of crack depth on the fatigue crack propagation rate for a marine steel in sea water", J. Mater. Sc., 17(2), pp 499-507.

[195] A. Turnbull and R. C. Newmann: (1986) "The influence of crack depth on crack electrochemistry and fatigue crack growth", in Small Fatigue Cracks, p 283.

[196] F. P. Ford and S. J. Hudak: (1986) "Potential role of the film rupture mechanism on environmentally assisted short crack growth", Small Fatigue Cracks

, eds. R. O. Ritchie and J. Lankford, pp 289-308.

[197] Annual Book of ASTM Standards, 1985, Vol. 03.01, E8M.

[198] P. D. Hobson: (1985) "The growth of short fatigue cracks in a medium carbon steel", Ph. D. thesis, University of Sheffield.

[199] C. Wang: (1991) "The effect of mean stresses on short fatigue crack growth behaviour", Ph. D. thesis, University of Sheffield.

[200] K. P. Zachariah and K. J. Miller: (1974) "Fatigue testing rig", Engineering, 214, pp 563-565.

[201] K. P. Zachariah: (1974) "Fatigue crack initiation and stage I propagation", Ph. D. thesis, University of Sheffield.

[202] M. F. E. Ibrahim: (1981) "Early damage accumulation in metal fatigue", Ph. D. thesis, University of Sheffield.

[203] H. J. Mohammad: (1986) "Cumulative fatigue damage under varying stress range conditions", Ph. D. thesis, University of Sheffield.

[204] "Conducting potentiodynamic polarization resistance measurements", Annual Book of ASTM Standards, ASTM, G59-78, 1978.

[205] "Standard reference method for making potentiostatic and potentiodynamic anodic polarization measurements", Annual Book of ASTM Standards, ASTM, G5-82, 1982.

[206] R. Akid: (1988) First Report to Pandrol International Ltd.

[207] R. Akid and G. Murtaza: (1990) "Environment-assisted short fatigue crack growth of a high strength steel", in Short Fatigue Cracks, ed. K. J. Miller, ESIS, MEP Publications, London, to be published.

[208] E. P. Carbonell and M. W. Brown: (1986) "A study of short crack growth in torsional low cycle fatigue for a medium carbon steel", Fatigue Engng. Mater. Struct., 9, pp 15-53.

[209] L. F. Coffin: (1954) "A study of the effects of cyclic thermal stress on ductile metal", Trans. ASME, 76, pp 931-950.

[210] S. S. Manson: (1954) "Behaviour of materials under conditions of thermal stress", N.A.C.C.T.N., 2933.

[211] O. H. Basquin: (1910) "The exponential law of endurance tests", Proc. ASTM, Vol 10.

[212] K. Hussain: (1990) "Short and long fatigue crack growth in C-Mn steel used for industrial ventilation fans", Ph. D. thesis, University of Sheffield.

[213] D. H. Breen and E. M. Wene: (1978) "Fatigue in machines and structures – ground vehicles", in Fatigue and Microstructure, ASM, pp 57-99.

[214] F. Borik et al: (1963) "Fatigue properties of an ausformed steel", ASM Trans., 56, pp 327-338.

[215] R. A. Cottis: (1986) "The corrosion fatigue of steels in saline environments: Short cracks and crack initiation aspects", in Small Fatigue Cracks, eds. R. O. Ritchie and J. Lankford, pp 265-268.

[216] M. W. Parsons and K. J. Pascoe : (1976) "Observation of surface deformation, crack initiation and crack growth in low cycle fatigue under biaxial stress", Mater. Sc. & Engng., 22, pp 31-50.

[217] H. Kitagawa and S. Takahashi: (1976) "Applicability of fracture mechanics to very small cracks", 2nd Int. Conf. on the Mechanical Behaviour of Materials, Boston, USA, ASM, pp 627-631.

[218] D. M. Brasher: (1967) "Stability of the oxide film on metals in relation to inhibition of corrosion. I. Mild steel in presence of aggressive anions", Br. Corr. J., 2, pp 95-103.

[219] G. K. Glass: (1986) "The effect of a change in surface conditions produced by anodic and cathodic reactions on the passivation of mild steel", Corr. Sc., 26, pp 441-454.

[220] C. D. Kim and B. E. Wilde: (1970) "The influence of cathodic pretreatment on the anodic dissolution kinetics of stainless steels in dilute acid media", Corr. Sc., 10, pp 735-744.

[221] J. Congleton, R. A. Oleih and R. N. Parkins: (1983) "Some electrochemical and microstructural aspects of corrosion fatigue", in Mechanics, Metallurgy, Electrochemistry and Engineering, ASTM STP 801, pp 368-389.

Table 4.1: Chemical composition of the material.

Element	BS 250A53(EN 45) (wt. %)	Actual, Cast No=D 8550 (wt. %)
C	0.52 -0.57	0.56
Si	1.8 - 2.1	1.85
Mn	0.8 - 1.0	0.81
Cr	0.2 - 0.3	0.21
Mo	0.01 - 0.06	0.025
Ni	0.3 max	0.151
S	0.05 max	0.024
P	0.05 max	0.026
Fe	remainder	remainder

Table 4.2 : Mechanical properties

Specimen condition	Tensile strength (MPa)	Elongation (%)	Reduction in area (%)	Fracture stress (MPa)
Uncharged	1571.2	11.1	29.50	1430.7
Pre- charged (24 hours)	1459.5	6.0	5.56	1434.3
Pre- charged (100 hours)	1412.0	2.0	0.69	1412.0

Table 5.1: Endurance results.

a) Air fatigue

Test No.	Shear stress range (MPa)	Shear strain range (%)	No. of cycles to failure (N_f)
AF14	1106	2.22	66300
AF1	1070	1.93	173000
AF10	1030	1.68	376000
AF15	1008	1.57	577500
AF8	915+	1.24	4850800
AF6	900	1.20	2025000*
AF7	853	1.10	5540000*
AF4	815	1.03	1381500*
AF11	601	0.73	9000000*

* = Unbroken

+ = Fatigue limit.

b) Corrosion fatigue

Test No.	Shear stress range (MPa)	Shear strain range (%)	No. of cycles to failure (N_f)
CF4	900	1.20	77000
CF3	854	1.10	99800
CF1	817	1.03	107000
CF5	601	0.73	226000
CF6	404	0.49	902000

Table 5.2: Summary of intermittent test results

Test No.	Shear stress range (MPa)	PAGS	Arrested crack length prior to CF cycling	Experimental threshold crack length	Theoretical threshold crack length, (Eq. 6.7)
IF12	600	30	29, 44, 60, 99, 120	464-508	483
IF4	815	30	84, 130	167-232	195
IF7	853	30	29, 69, 102	128	164
IF6	900	30	crack (a) 81, (b) 120	108-132	131
IGS 2	600	60	42, 69, 111		

CF = Corrosion Fatigue.

PAGS = Prior Austenite Grain Size.

Table 6.1: Coefficients for short and long crack growth equations (air).

Shear stress range (MPa)	Total shear strain range (%)	Short crack growth, (Eq. 6.3) C_{sa} (d_1)	Short crack growth, (Eq. 6.3) C_{sa} (d_2)	Short crack growth, (Eq. 6.3) C_{sa} (d_3)	Short crack growth, (Eq. 6.3) C_{sa} (d_4)	Long crack growth, (Eq. 6.7) C_{la}
1106	2.22	4.14×10^{-3}	8.33×10^{-4}	4.34×10^{-4}	1.50×10^{-4}	2.42×10^{-4}
1070	1.93	1.22×10^{-3}	2.71×10^{-4}	1.44×10^{-4}	5.03×10^{-5}	1.68×10^{-4}
1030	1.68	3.66×10^{-4}	8.93×10^{-4}	4.83×10^{-4}	1.70×10^{-5}	1.17×10^{-4}
1008	1.57	2.03×10^{-4}	5.20×10^{-5}	2.82×10^{-5}	1.00×10^{-5}	9.81×10^{-5}
915	1.24	2.6×10^{-5}	7.80×10^{-6}	4.3×10^{-6}	1.60×10^{-6}	5.29×10^{-5}

Table 6.2: A comparison between experimental and predicted air fatigue lifetimes.

Shear stress range (MPa)	Shear strain range (%)	Predicted lifetime, (Cycles) N_s	Predicted lifetime, (Cycles) N_l	Predicted lifetime, (Cycles) N_t	Experimental lifetime, (Cycles) N_f
1106	2.22	35068	15442	50510	66300
1070	1.93	105535	23004	128538	173000
1030	1.68	314769	34891	349660	376000
1008	1.57	537604	43335	580939	577500
915	1.24	3449849	166373	3616222	4850800

N_s = Short crack growth lifetime.

N_l = Long crack growth lifetime.

N_t = Total lifetime.

Table 6.3: Coefficients for pit development, short and long crack growth equations (environment, 0.6M NaCl solution)

Shear stress range (MPa)	Total shear strain range (%)	Pit development (Eq. 6.8) C_p	Short crack growth, (Eq. 6.11) C_{scf} (d2)	Short crack growth, (Eq. 6.11) C_{scf} (d3)	Short crack growth, (Eq. 6.11) C_{scf}(d4)	Long crack growth, (Eq. 6.13) C_{lcf}
900	1.20	9.071×10^{-4}	7.112×10^{-4}	4.140×10^{-4}	2.552×10^{-4}	7.754×10^{-5}
854	1.10	7.287×10^{-4}	5.553×10^{-4}	3.112×10^{-4}	1.990×10^{-4}	6.520×10^{-5}
817	1.03	6.178×10^{-4}	4.573×10^{-4}	2.510×10^{-4}	1.640×10^{-4}	5.719×10^{-5}
601	0.73	2.599×10^{-4}	1.689×10^{-4}	8.110×10^{-5}	6.110×10^{-5}	2.879×10^{-5}
404	0.49	9.540×10^{-5}	5.330×10^{-5}	2.190×10^{-5}	1.940×10^{-5}	1.301×10^{-5}

Table 6.4: A comparison between experimental and predicted corrosion fatigue lifetimes.

Shear stress range (MPa)	Total shear strain range (%)	Experimental lifetimes (Cycles)	Predicted lifetimes (Cycles) M-H-M	Predicted lifetimes (Cycles) S-M
900	1.20	77000	74916	85591
854	1.10	99800	92168	104442
817	1.03	107000	107970	121115
601	0.73	226000	251130	245528
404	0.49	902000	694558	509774

M-H-M = Modified Hobson's Model.

S-P = Superposition Model.

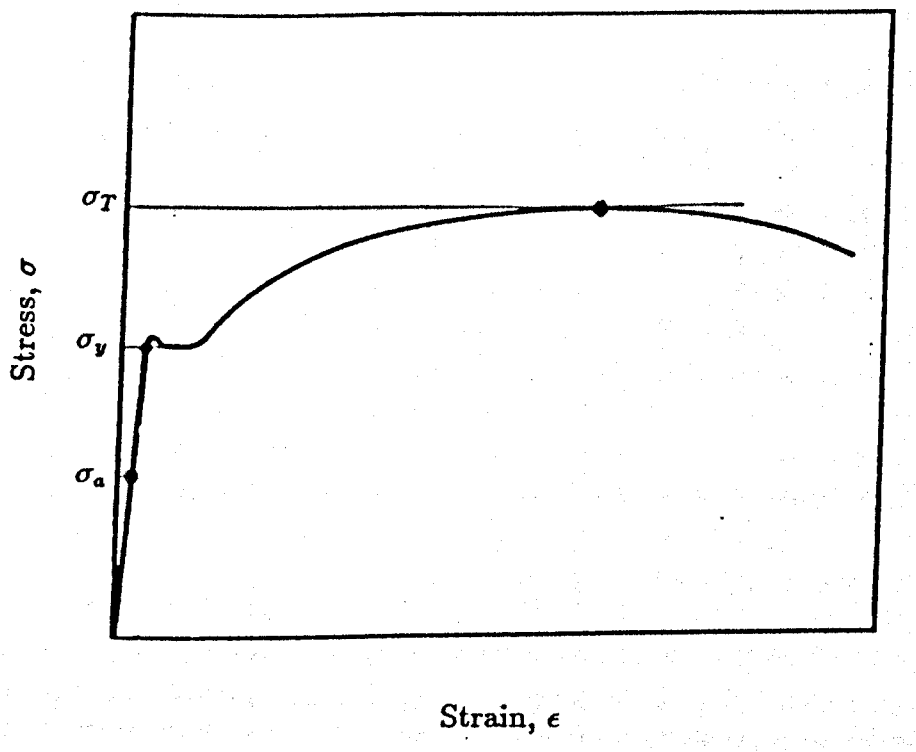

Figure 1.1: A schematic of the tensile stress-strain curve.

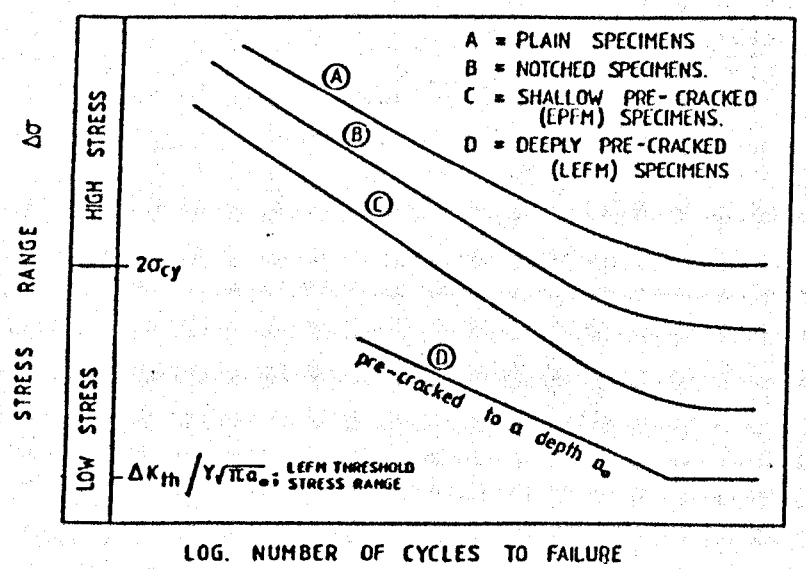

Figure 2.1: S-N curves for plain, notched and pre-cracked specimens. [Ref. 44]

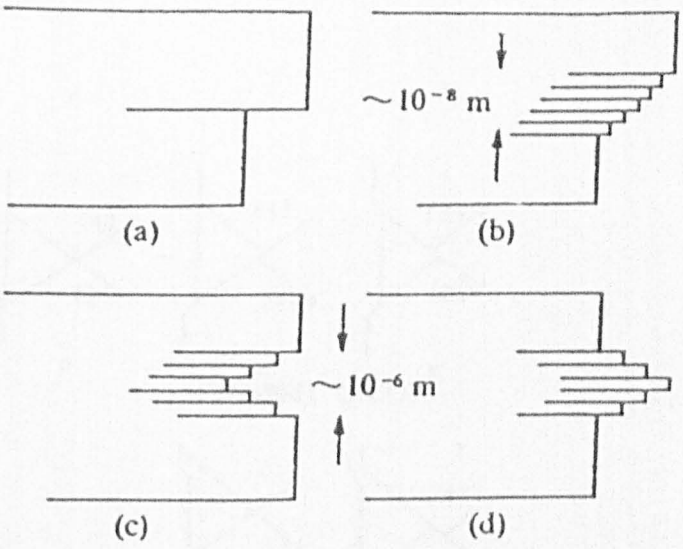

Figure 2.2: Formation of a surface crack by slip under different loading conditions; static slip: a) optical microscope, b) electron microscope and Fatigue slip: c) notch, d) peak. [Ref. 21].

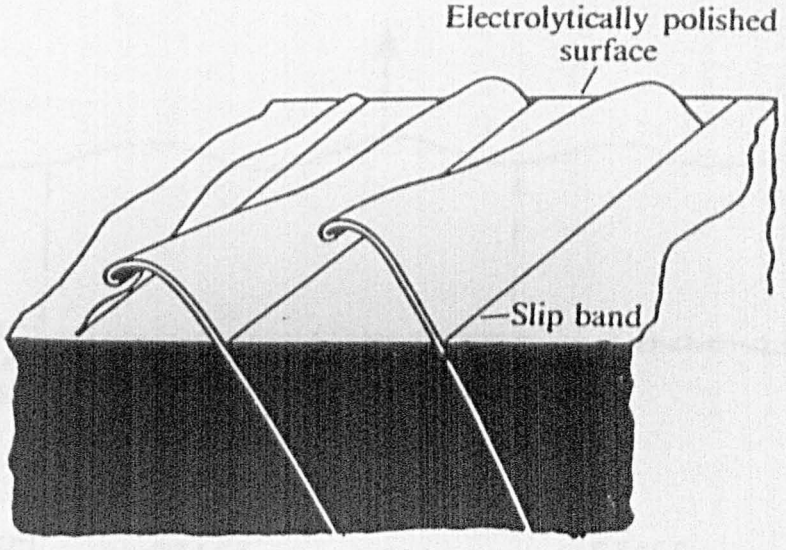

Figure 2.3: A schematic of slip band extrusion [Ref. 22].

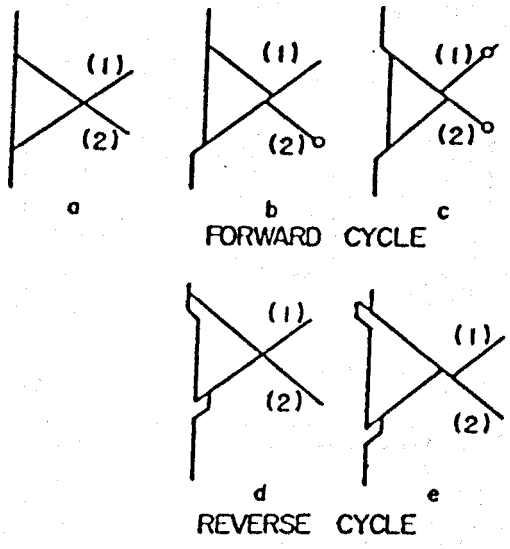

Figure 2.4: Model for the formation of intrusions and extrusions. [Ref. 23].

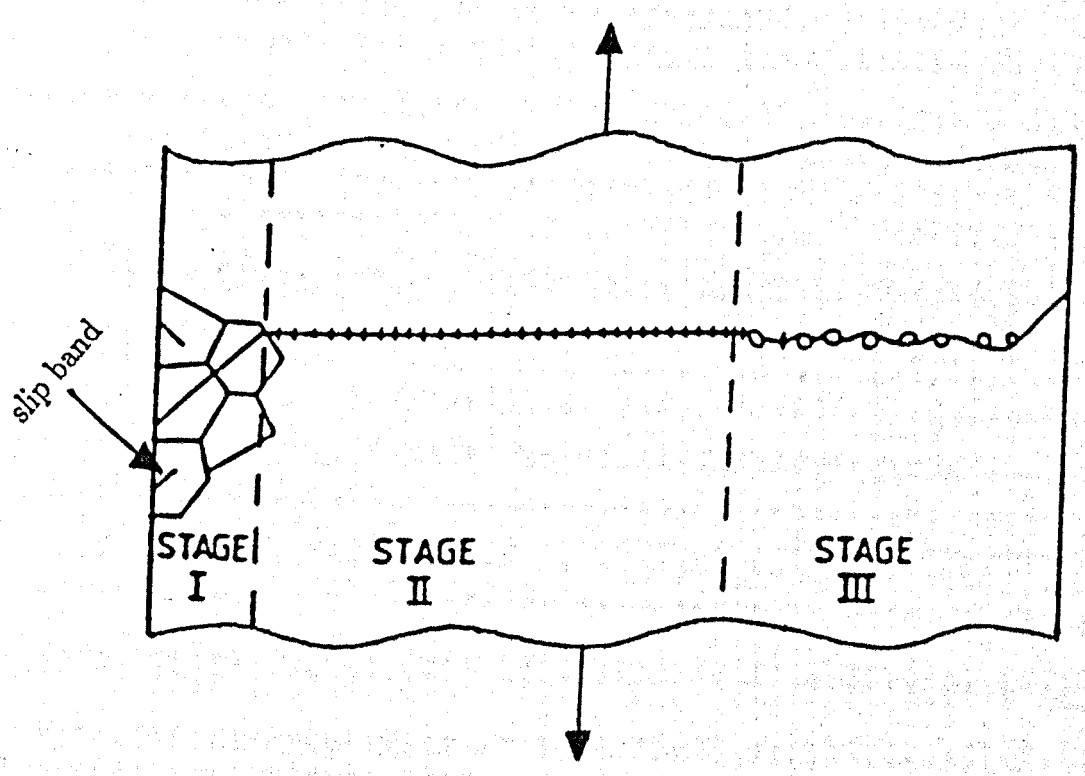

Figure 2.5: A schematic of the different fatigue crack propagation stages under uniaxial loading conditions.

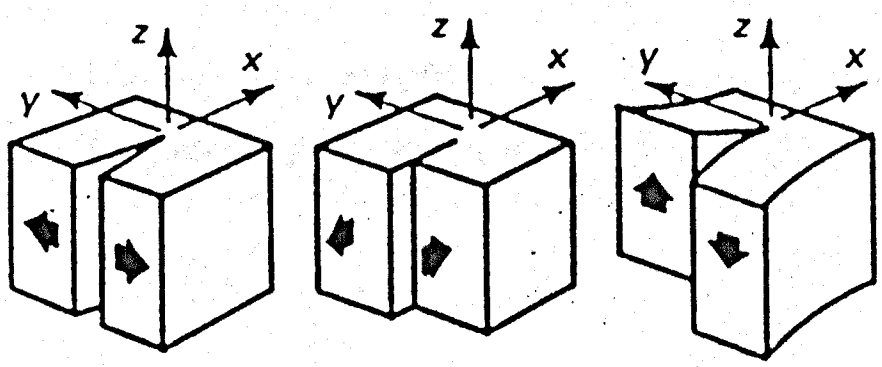

Figure 2.6: Modes of crack deformation.

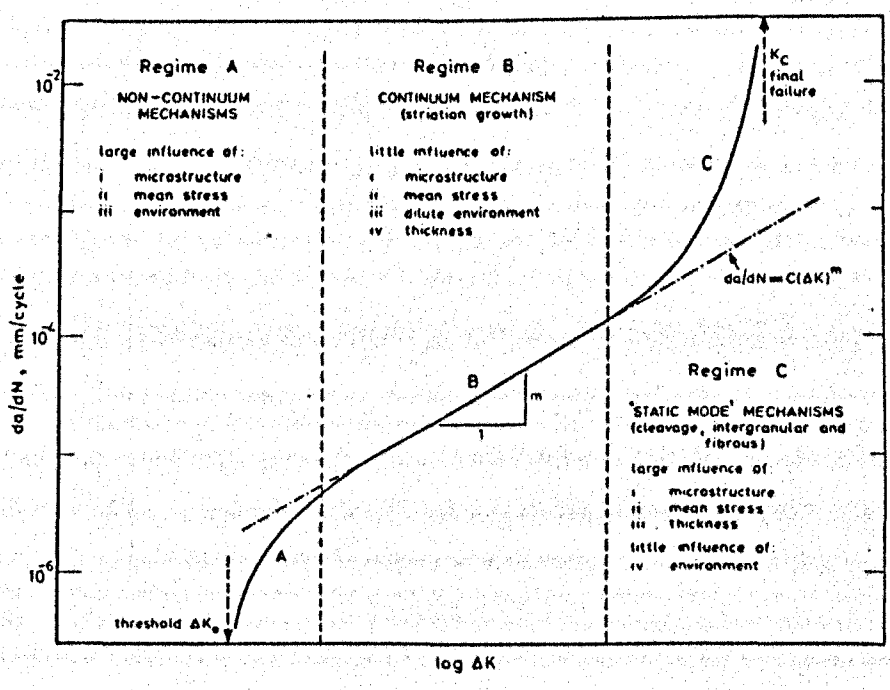

Figure 2.7: Fatigue curve representing crack growth rate versus stress intensity factor range for a pre-cracked specimen. [Ref. 35]

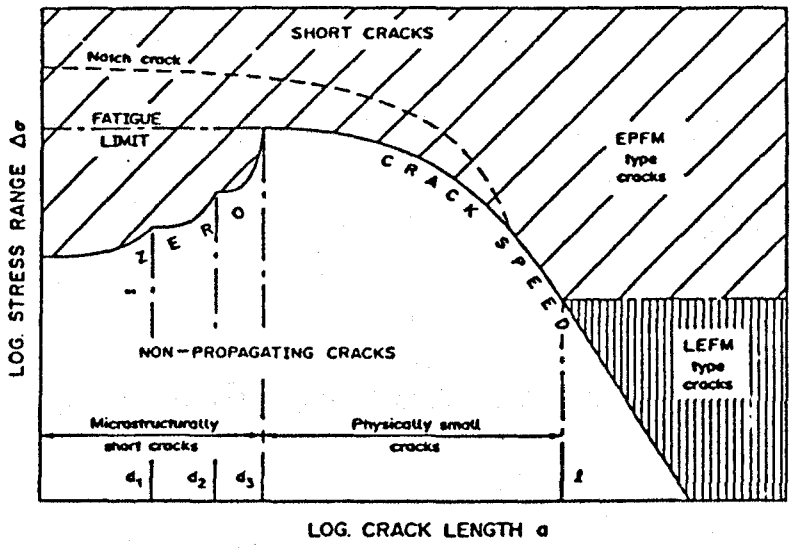

Figure 2.8: Three regimes of short crack behaviour [Ref. 44].

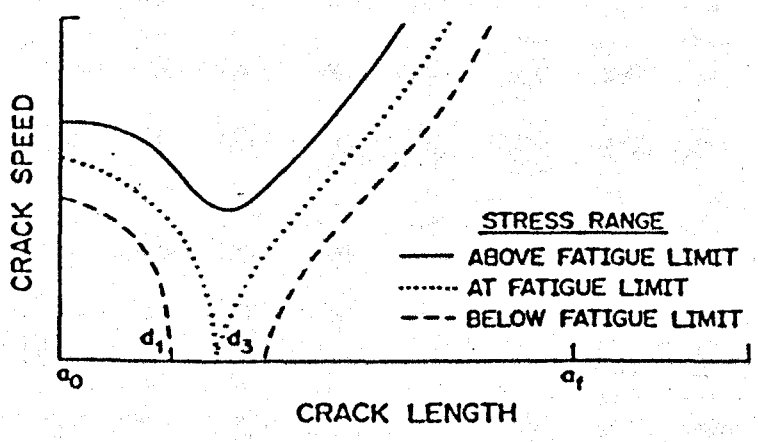

Figure 2.9: Short crack growth behaviour at different stress levels around the fatigue limit [Ref. 46].

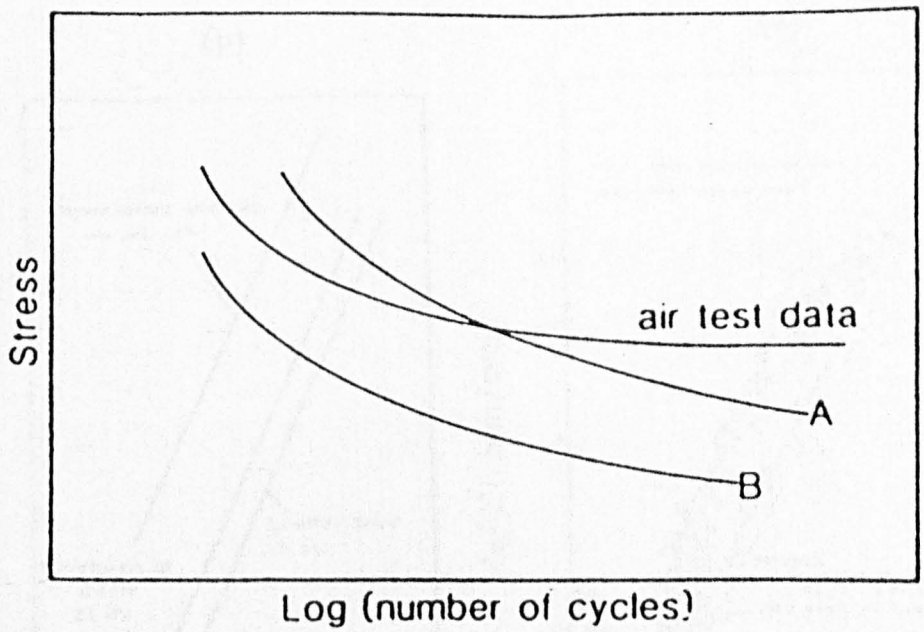

Figure 3.1: Schematic of air and corrosion fatigue S-N curves; A-Corrosion fatigue showing retarded initiation at high stress, B- Corrosion fatigue showing a general lowering of the fatigue strength [Ref. 88].

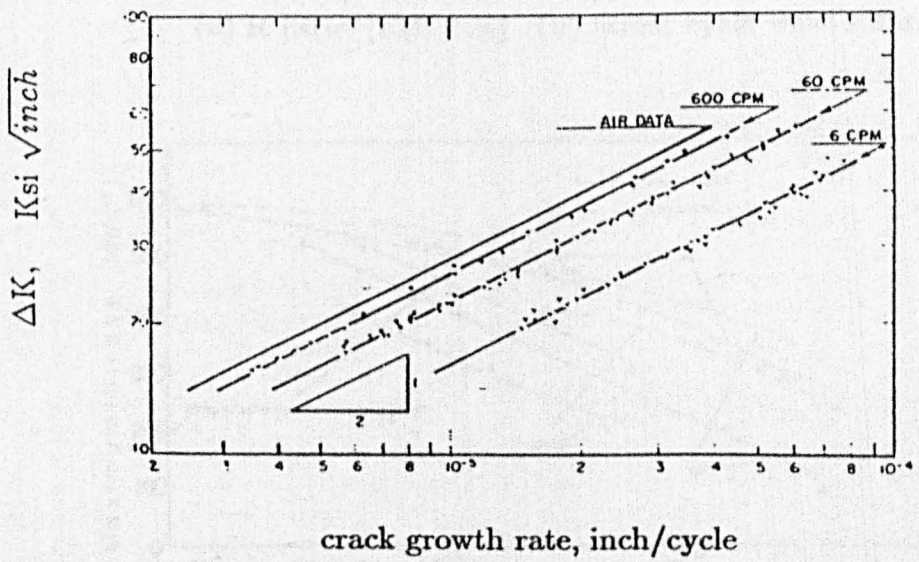

Figure 3.2: Influence of test frequency on corrosion fatigue crack growth. [Ref. 138].

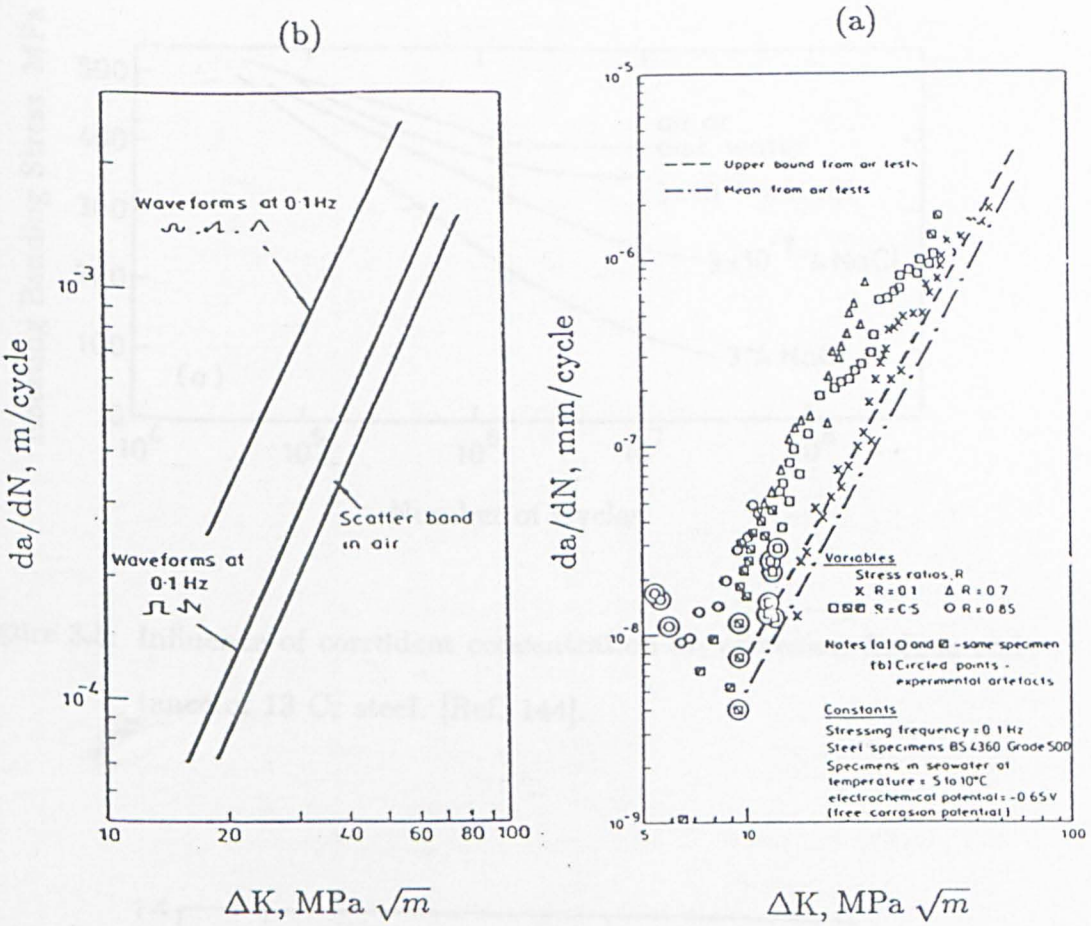

Figure 3.3: Effect of loading variables on corrosion fatigue crack growth; (a) R ratio [Ref. 128] (b) stress cycle wave form. [Ref. 138].

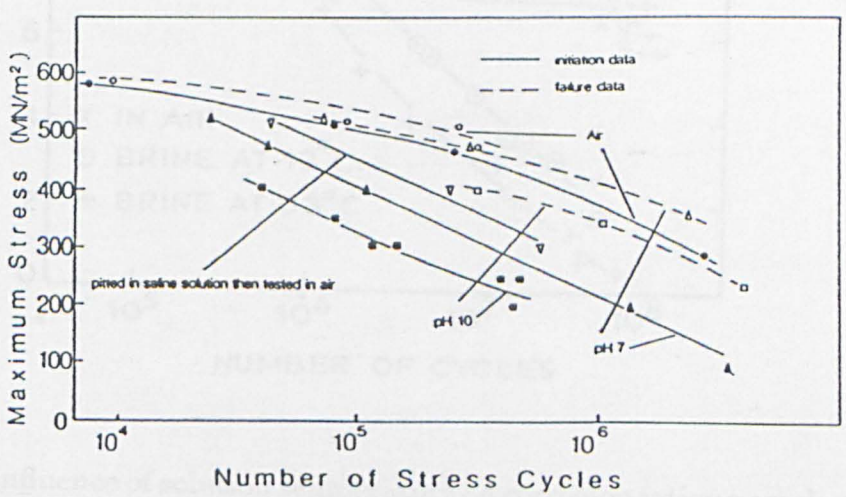

Figure 3.4: Corrosion fatigue failure and initiation results of BS 4360/50D tested in 3.5% NaCl solution; [Ref. 88].

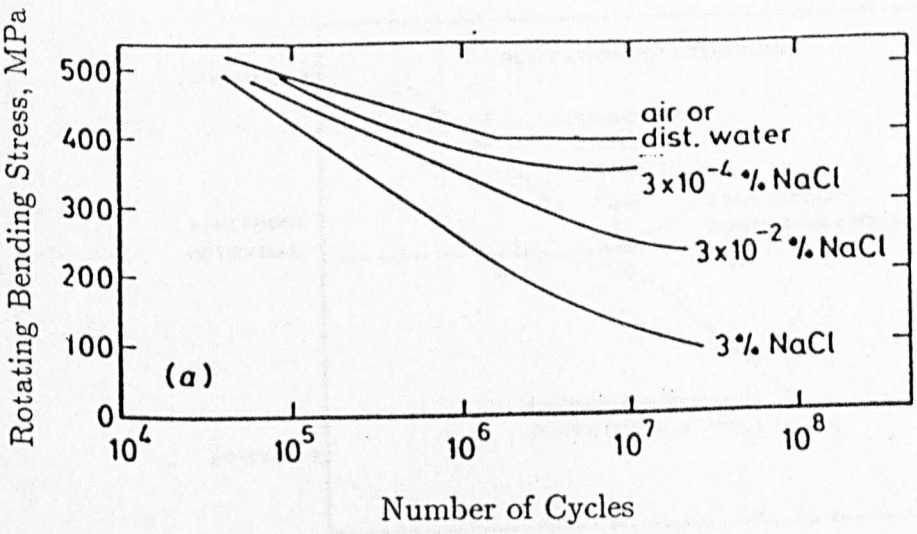

Figure 3.5: Influence of corrodent concentration on corrosion fatigue resistance of 13 Cr steel. [Ref. 144].

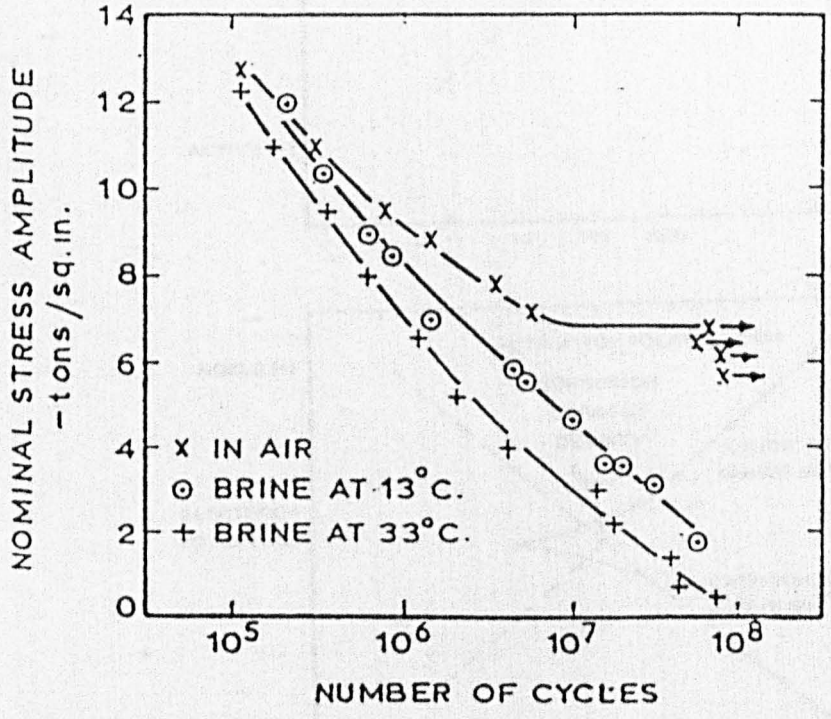

Figure3.6: Influence of solution temperature on corrosion fatigue crack growth. [Ref. 146].

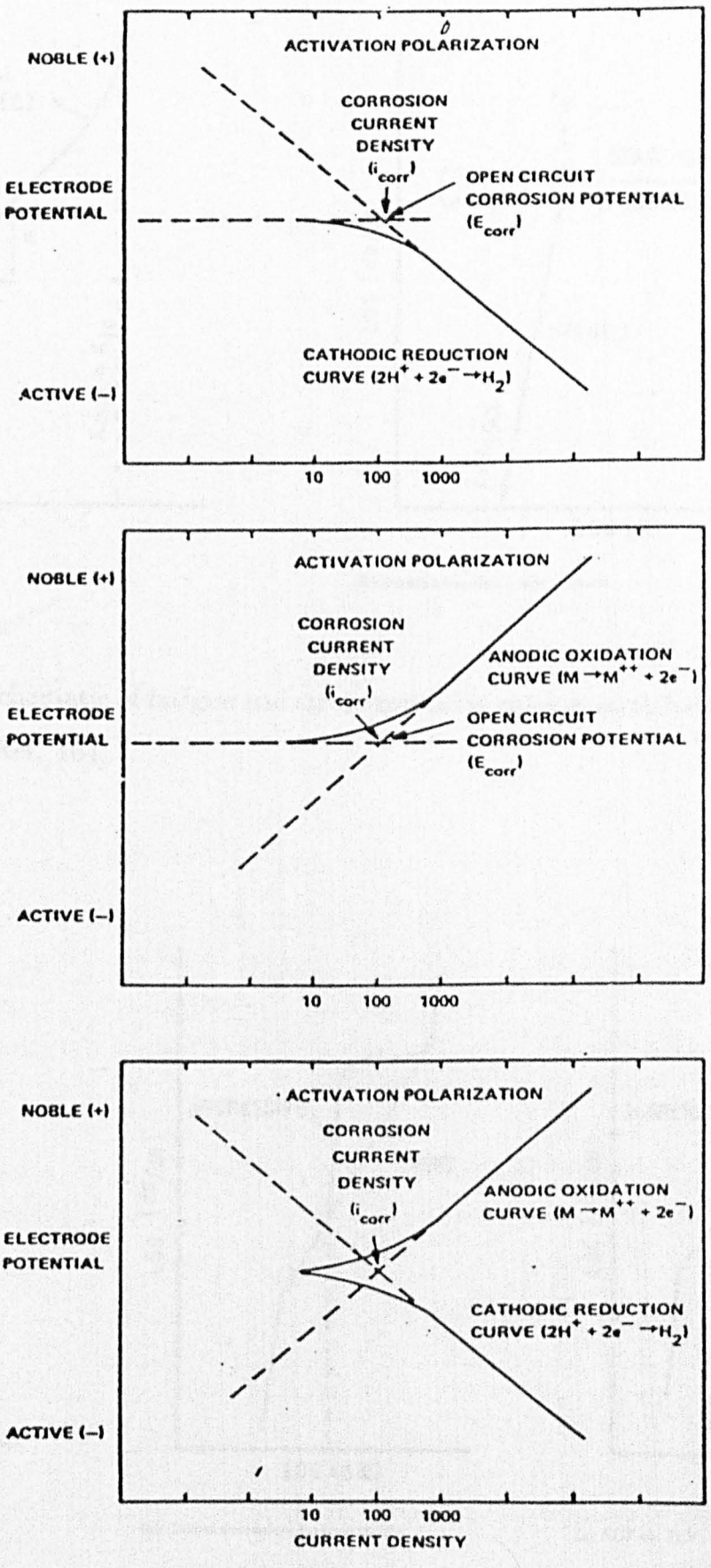

Figure 3.7: An illustration of methods used to estimate corrosion current density, i_{corr}.

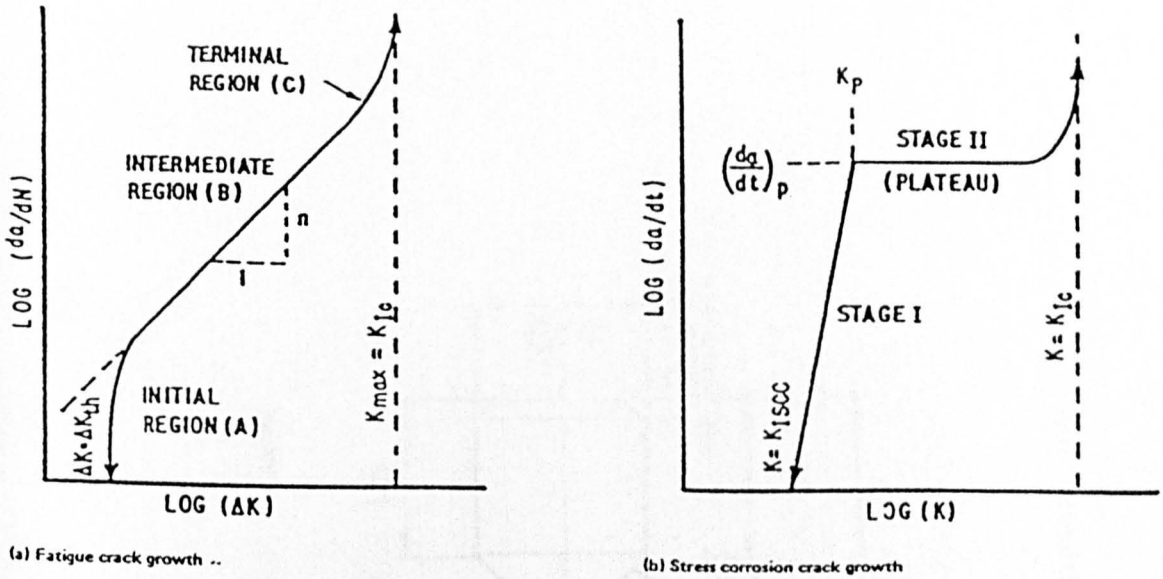

Figure 3.8: Schematic of fatigue and stress-corrosion crack growth behaviour. [Ref. 164].

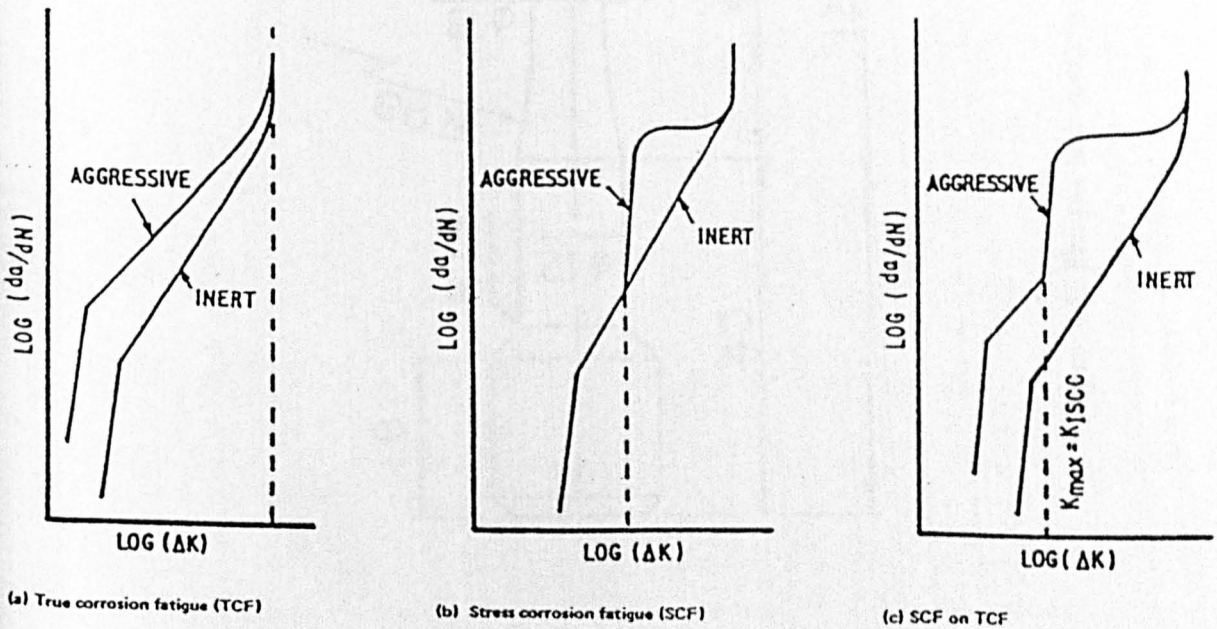

Figure 3.9: A schematic illustrating of the influence SCC processes on corrosion fatigue crack growth. [Ref. 164].

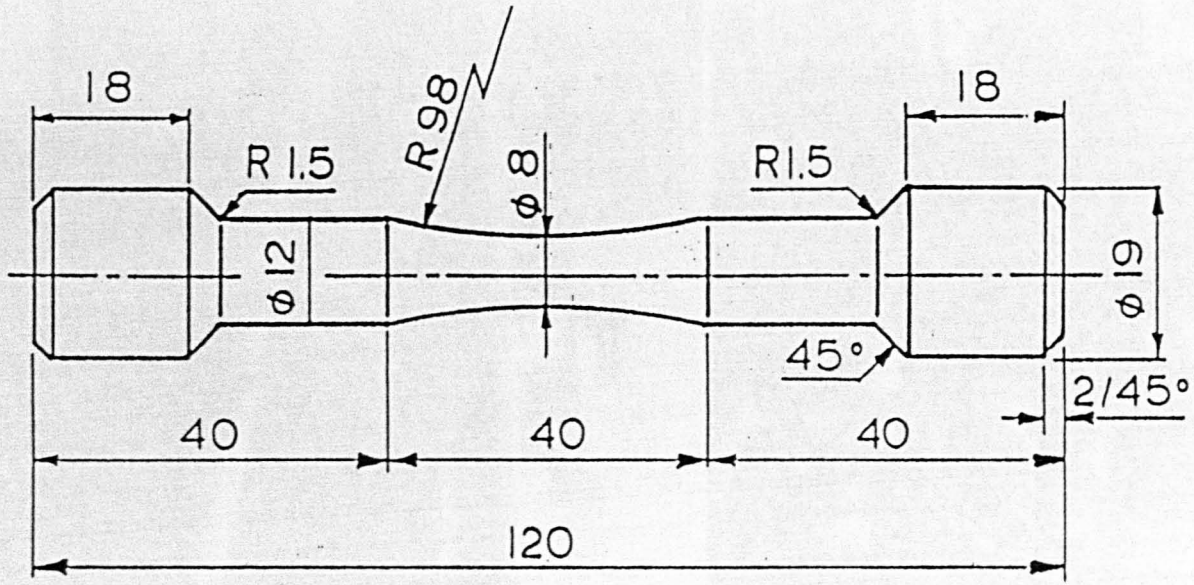

Figure 4.1: Fatigue test specimen configuration. All dimensions in ; mm

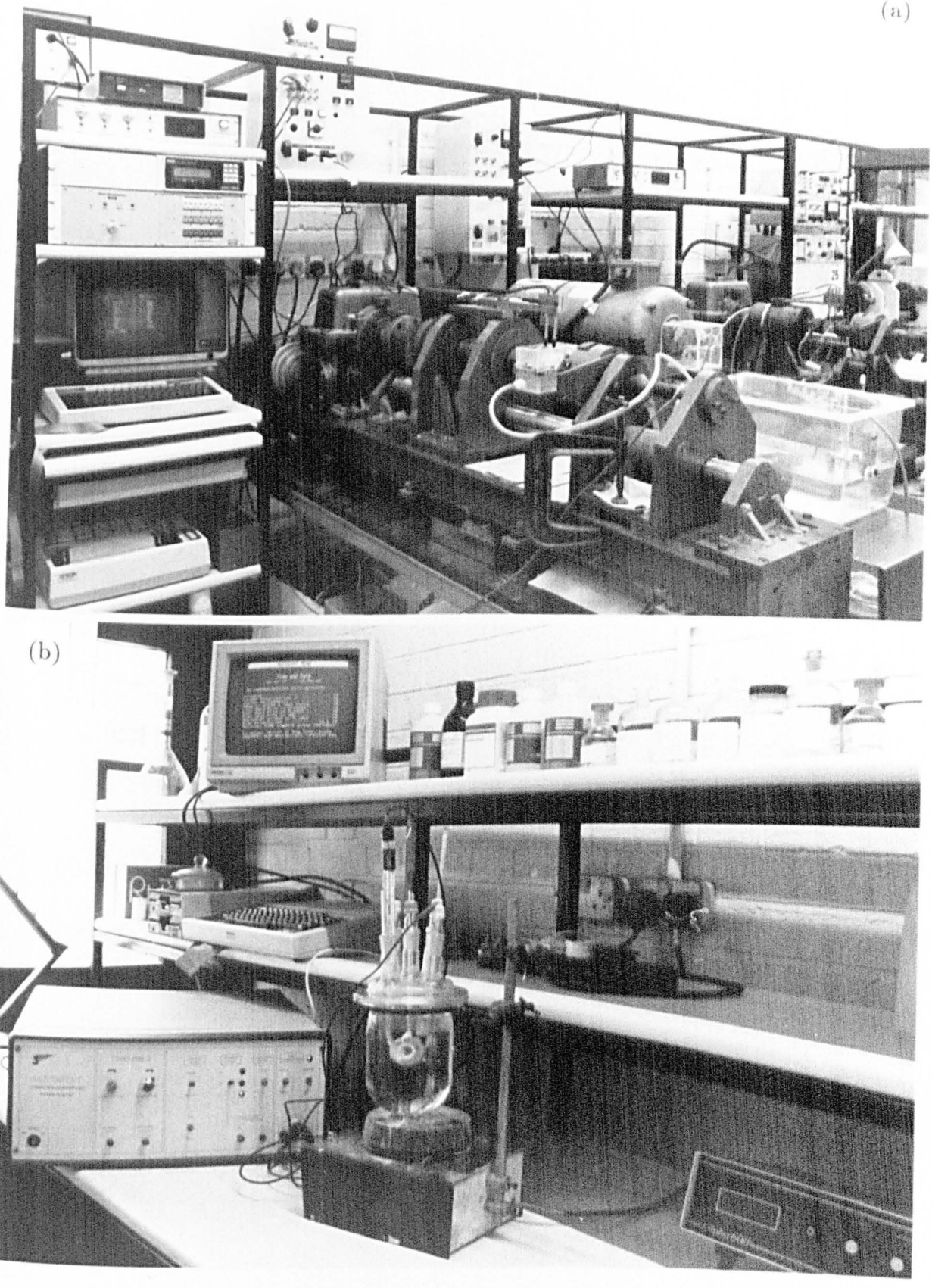

Figure 4.2: (a) Fatigue test rig.

(b) Electrochemical test apparatus.

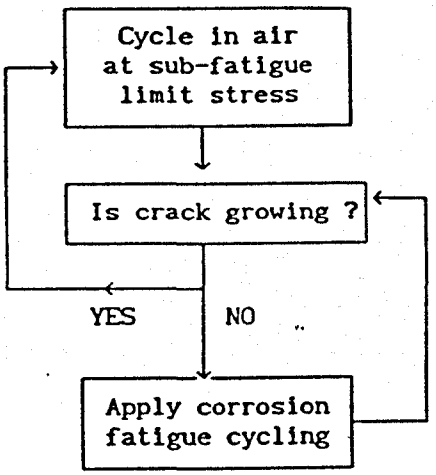

Figure 4.3: Intermittent air fatigue/corrosion fatigue testing sequence.

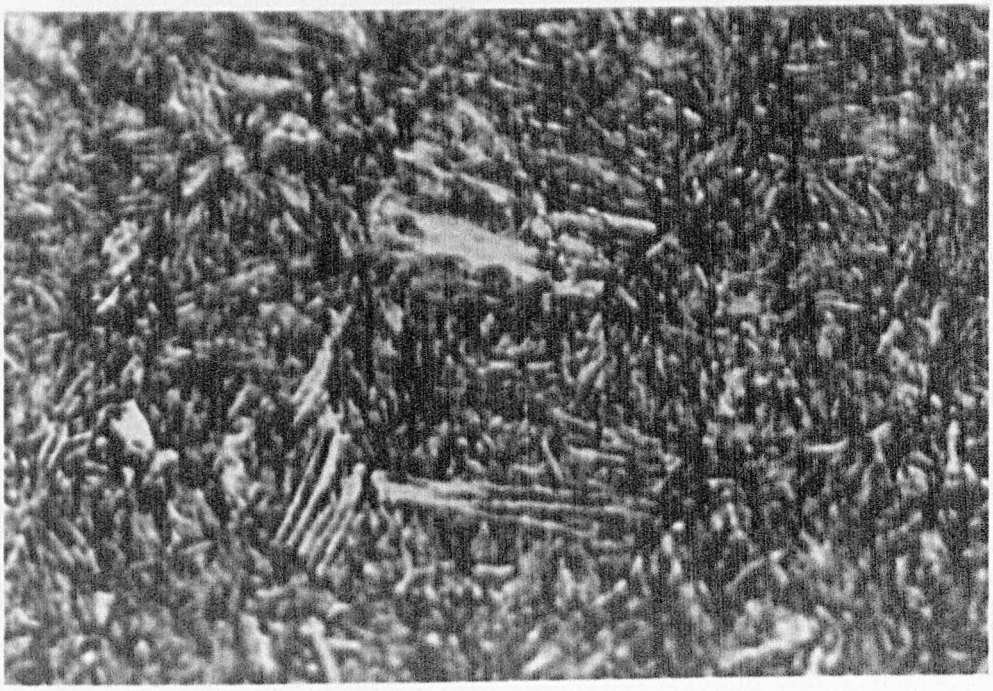

(a) $20\mu m$

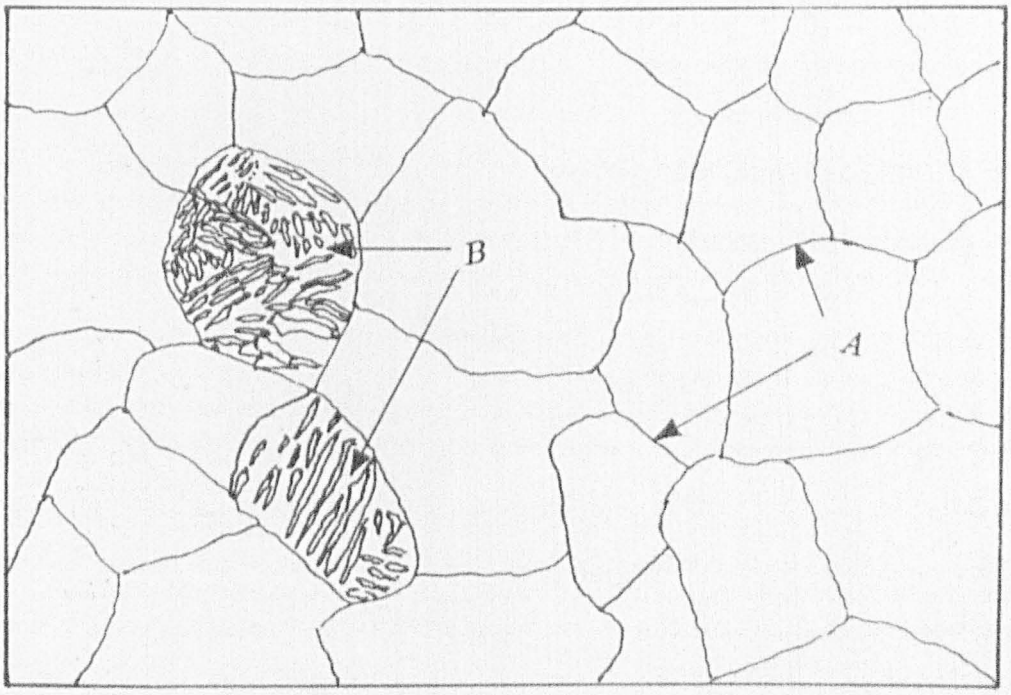

(b)

Figure 5.1: Material microstructure showing standard prior austenite grain size;
(a) Photomicrograph, (b) Schematic; A: Prior austenite grain boundaries,
B: Martensite laths.

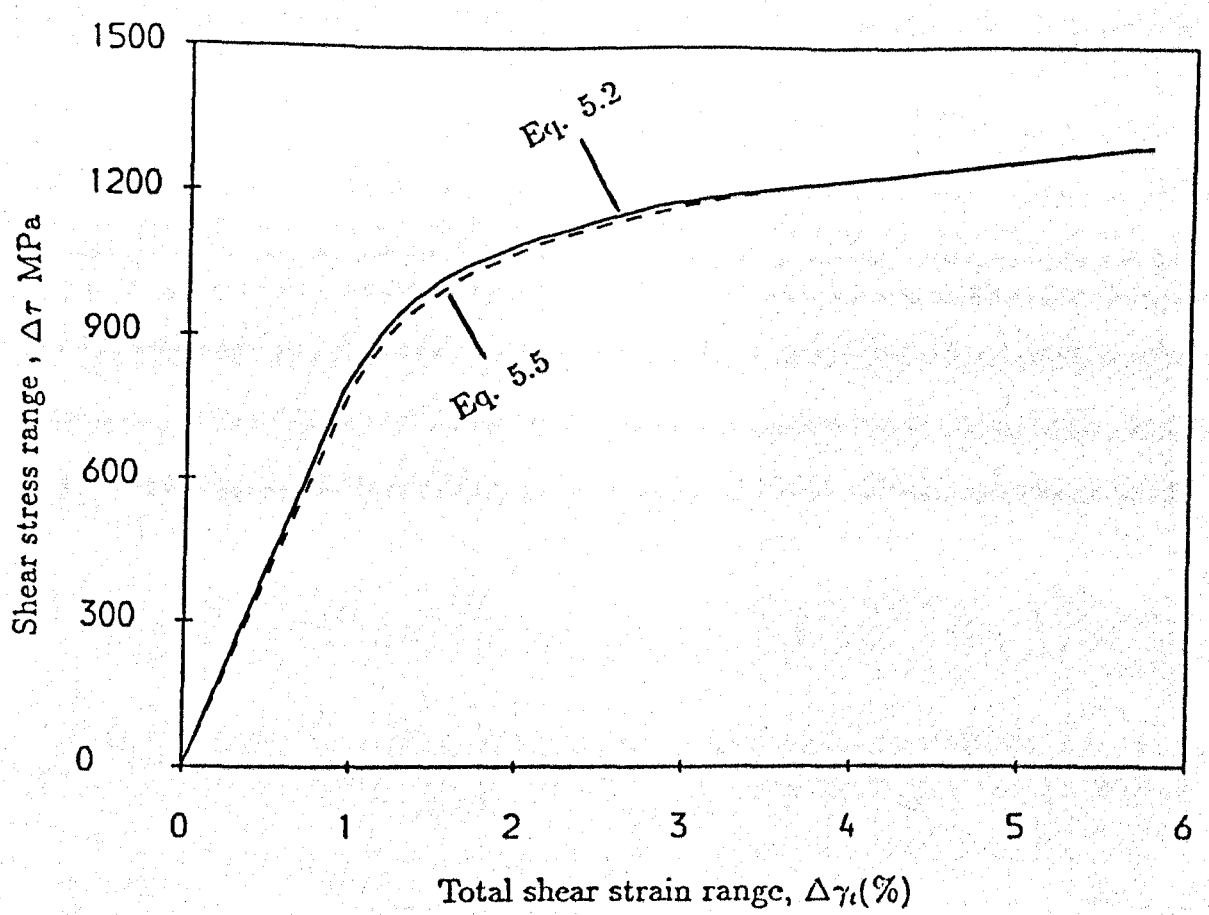

Figure 5.2: Cyclic shear stress-shear strain curve.

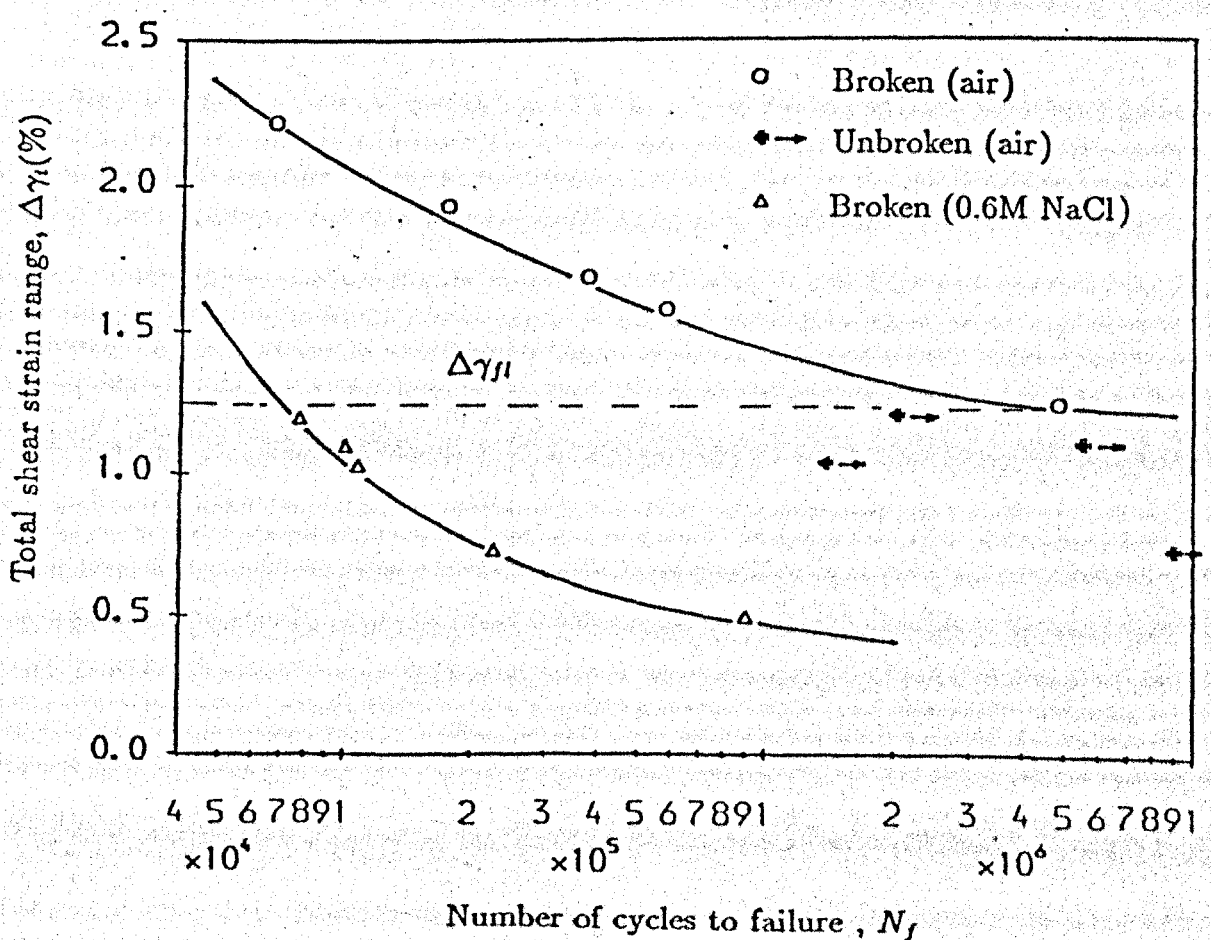

Figure 5.3: S-N curves.

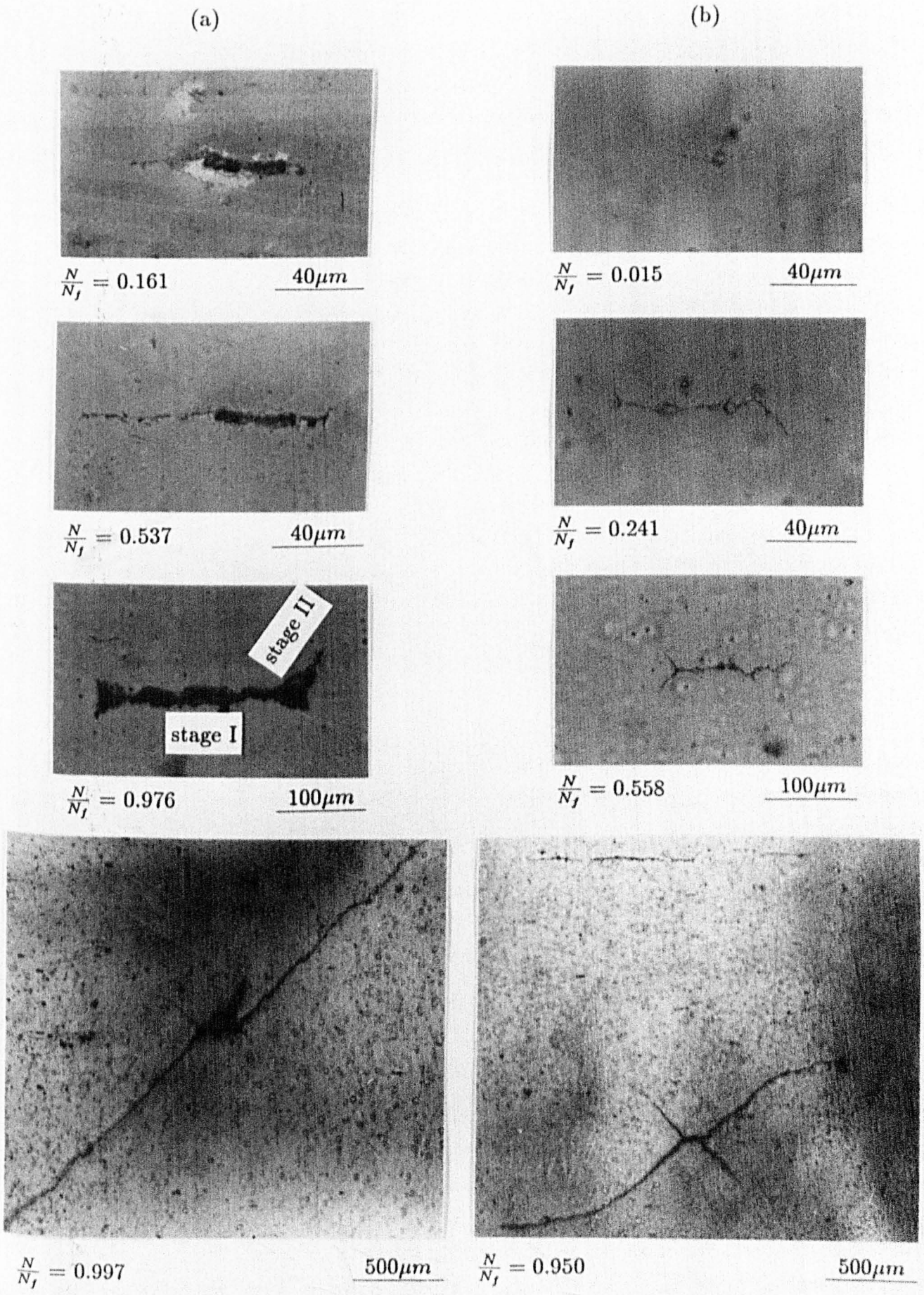

Figure 5.4: Typical air fatigue crack initiation and growth behaviour.

(a) $\Delta\tau = 915$ MPa, (b) $\Delta\tau = 1106$ MPa.

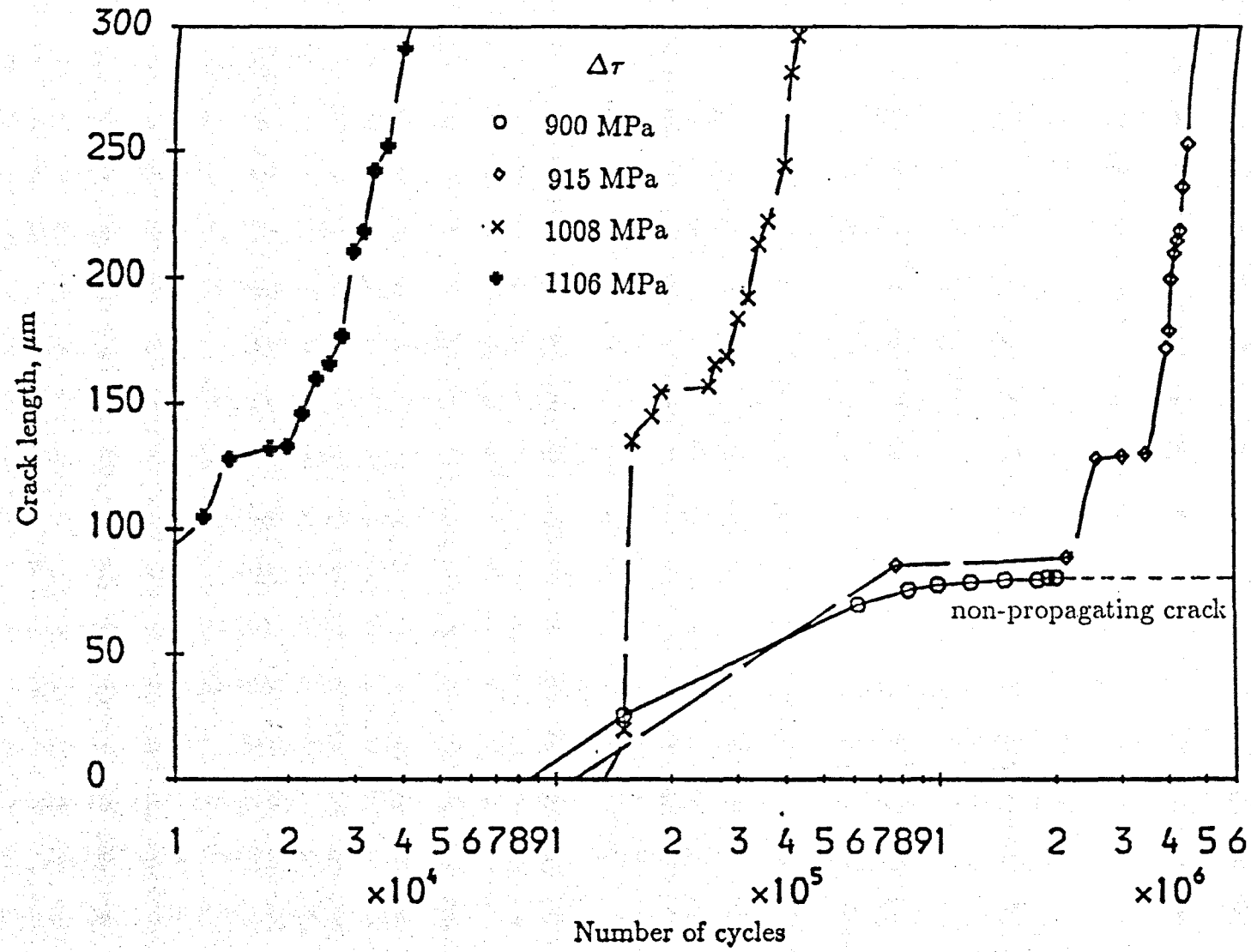

Figure 5.5: Air fatigue a versus N curves.

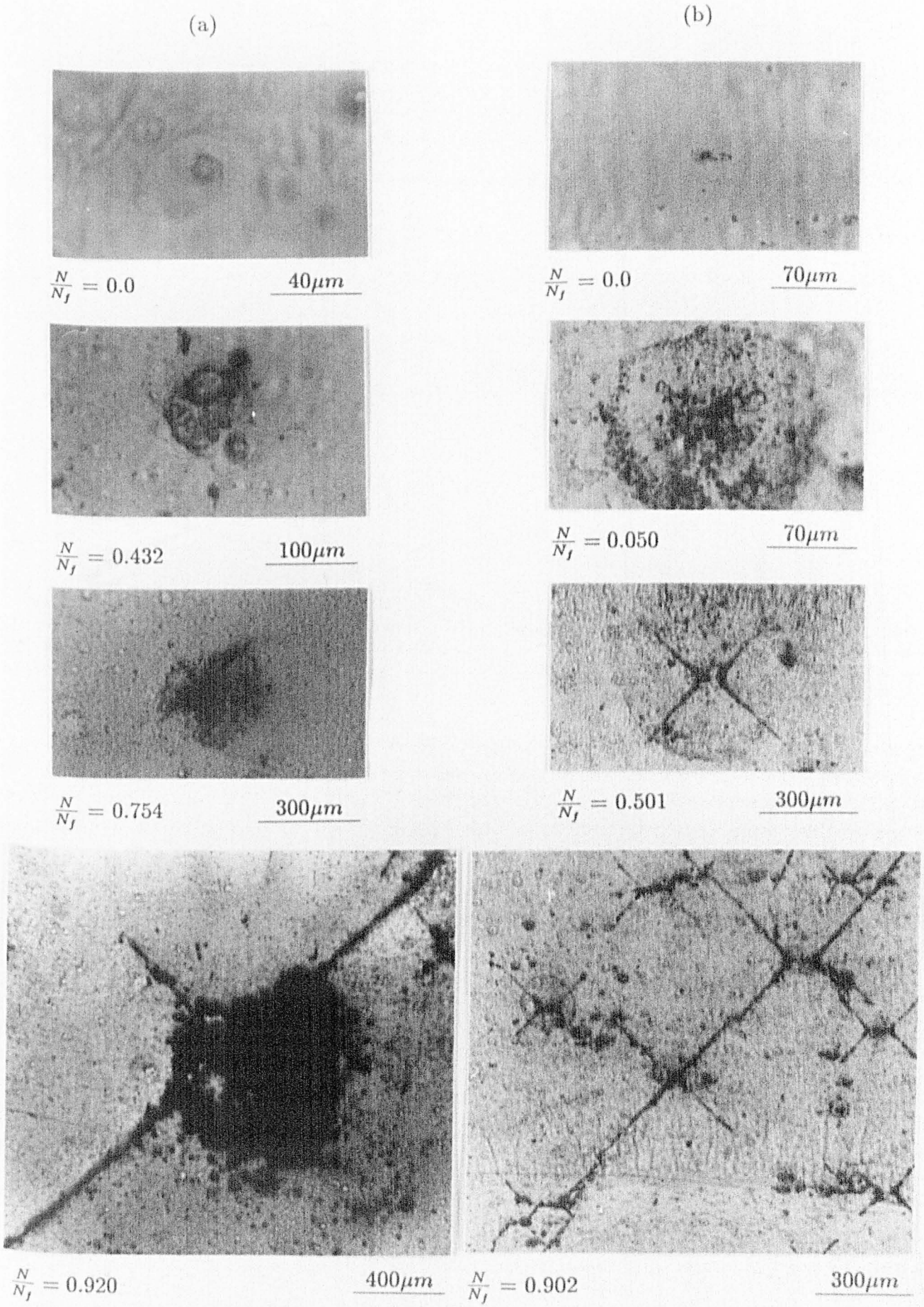

Figure 5.6: Corrosion fatigue crack development and growth behaviour.

(a) $\Delta\tau = 404$ MPa, (b) = $\Delta\tau = 900$ MPa.

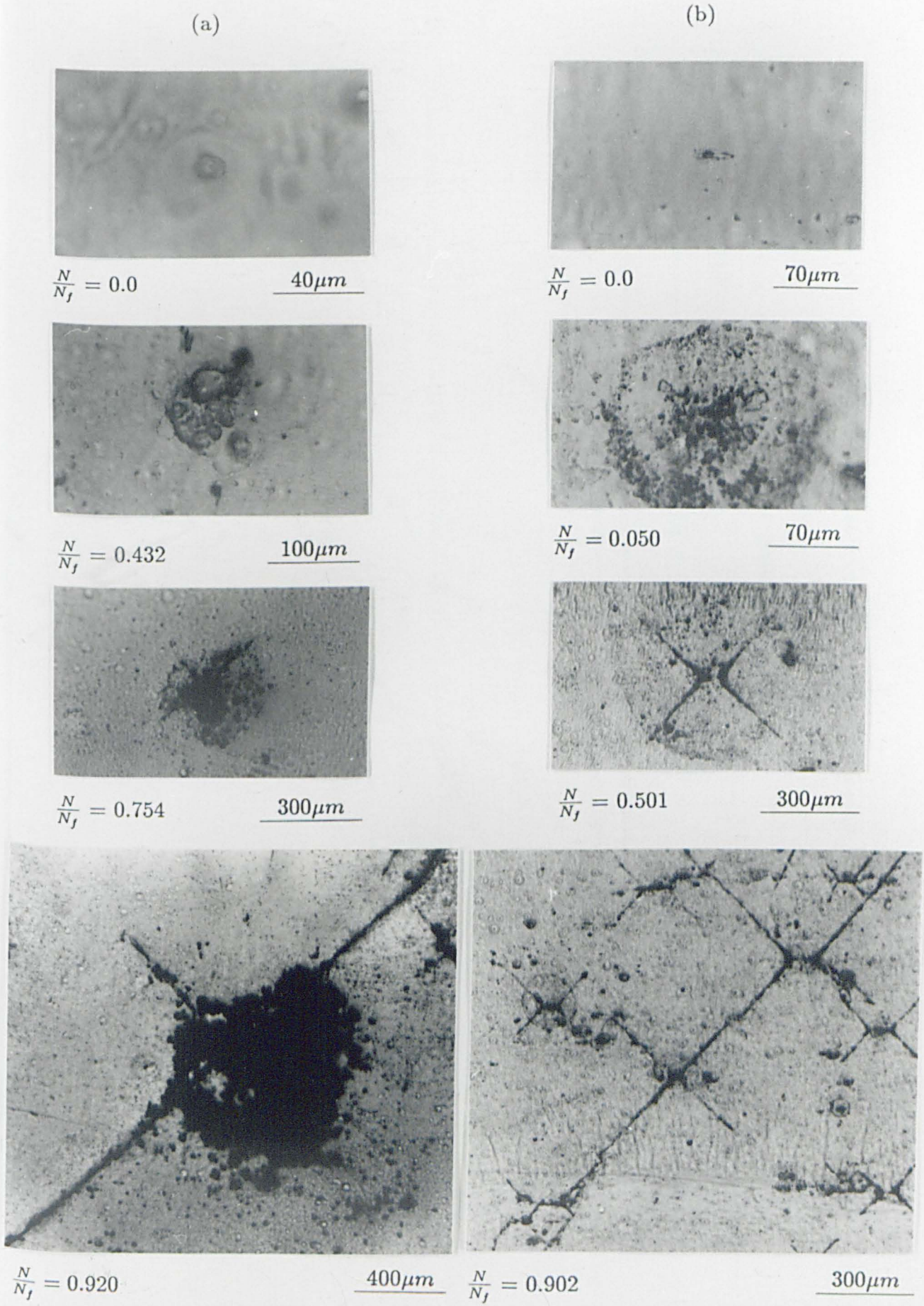

Figure 5.6: Corrosion fatigue crack development and growth behaviour.

(a) $\Delta\tau = 404$ MPa, (b) $= \Delta\tau = 900$ MPa.

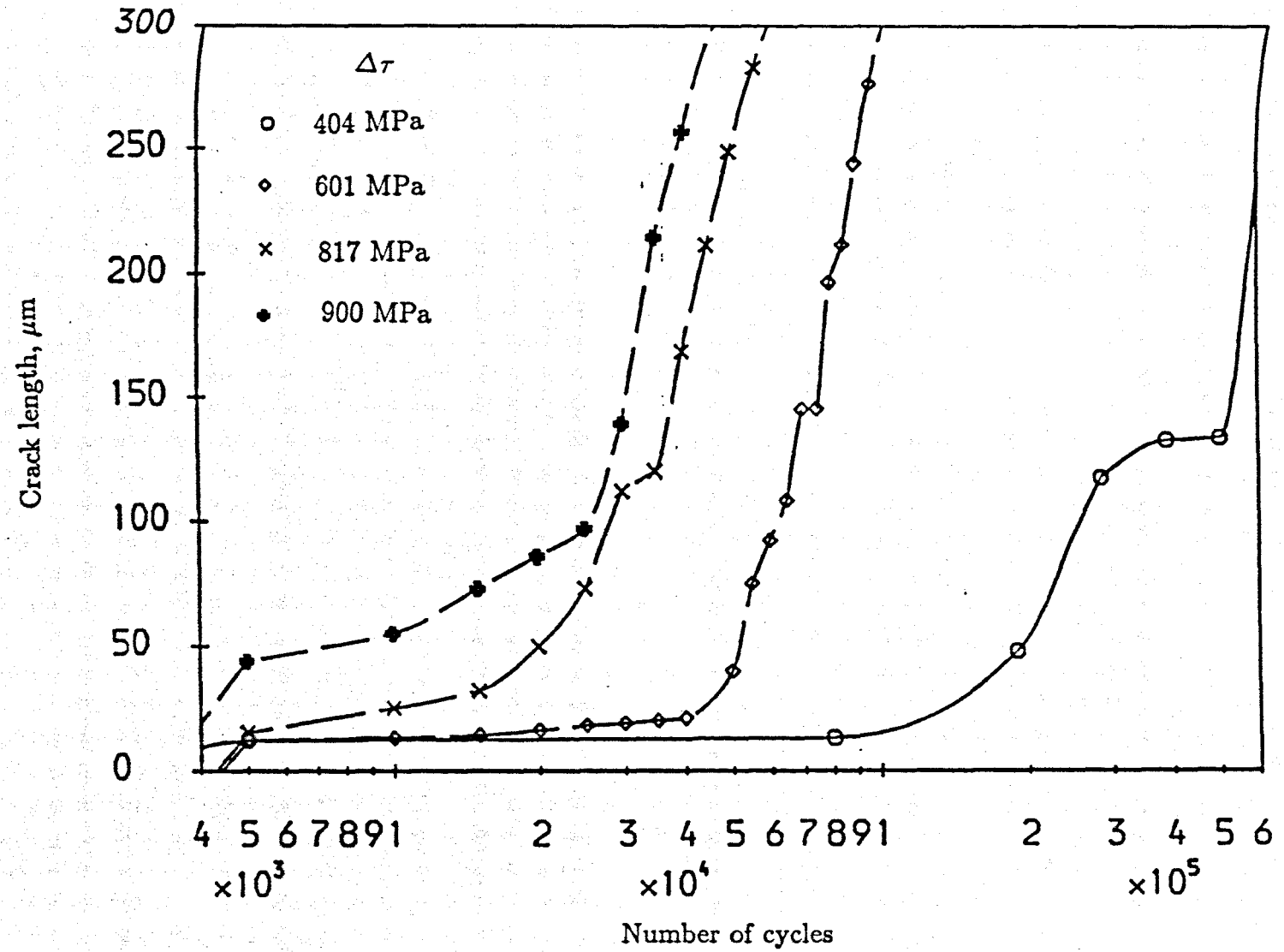

Figure 5.7: Corrosion fatigue a versus N curves.

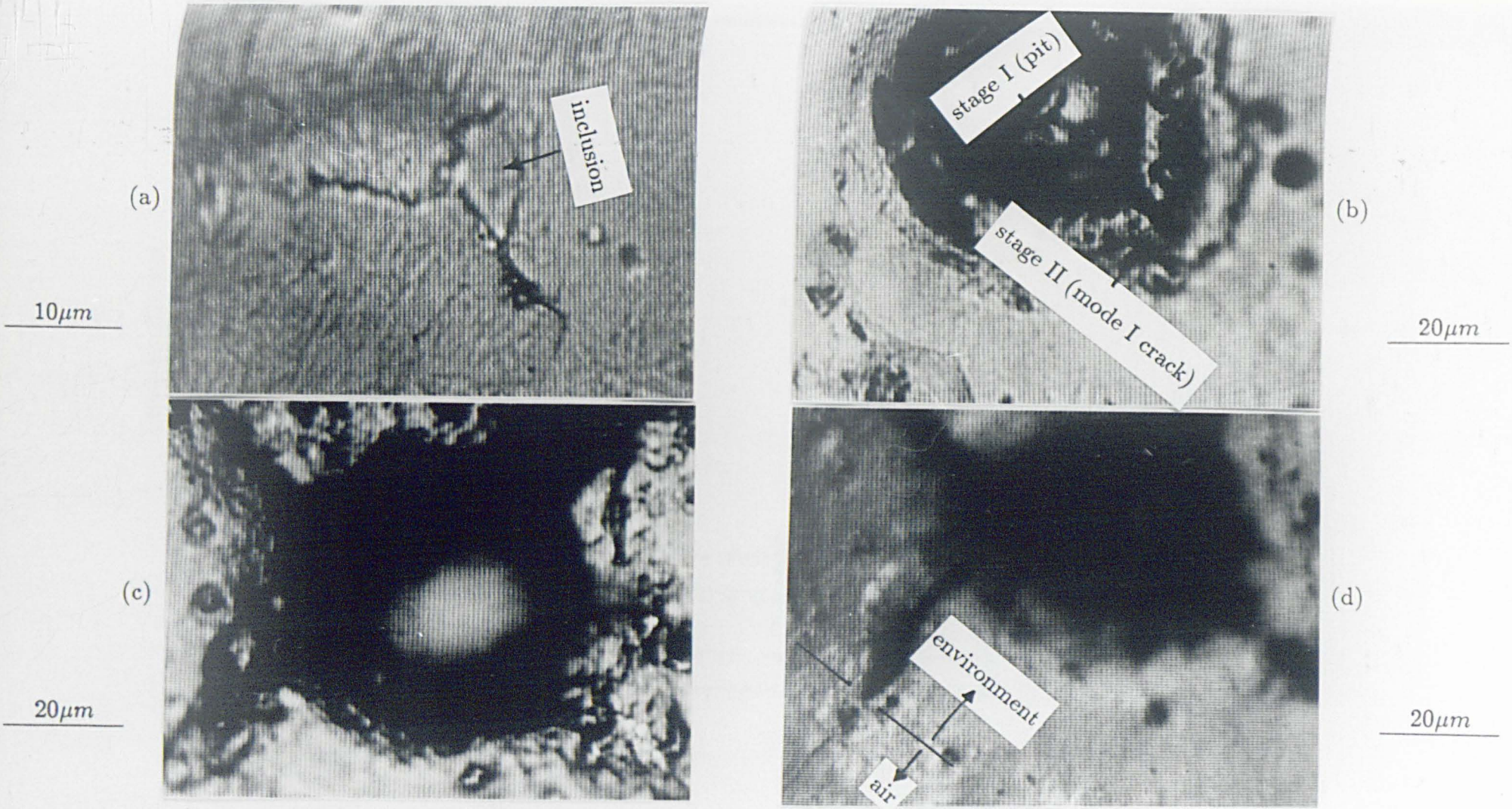

Figure 5.8: Typical crack initiation and development during an intermittent test. $\Delta\tau$ = 853 MPa: (a) 3.67 $\times 10^6$ cycles in air; (b) 3.67 $\times 10^6$ cycles in air + 5000 cycles in 0.6M NaCl solution; (c) 5.53 $\times 10^6$ cycles in air + 15000 cycles in 0.6M NaCl solution; (d) as (c) + 85000 cycles in air.

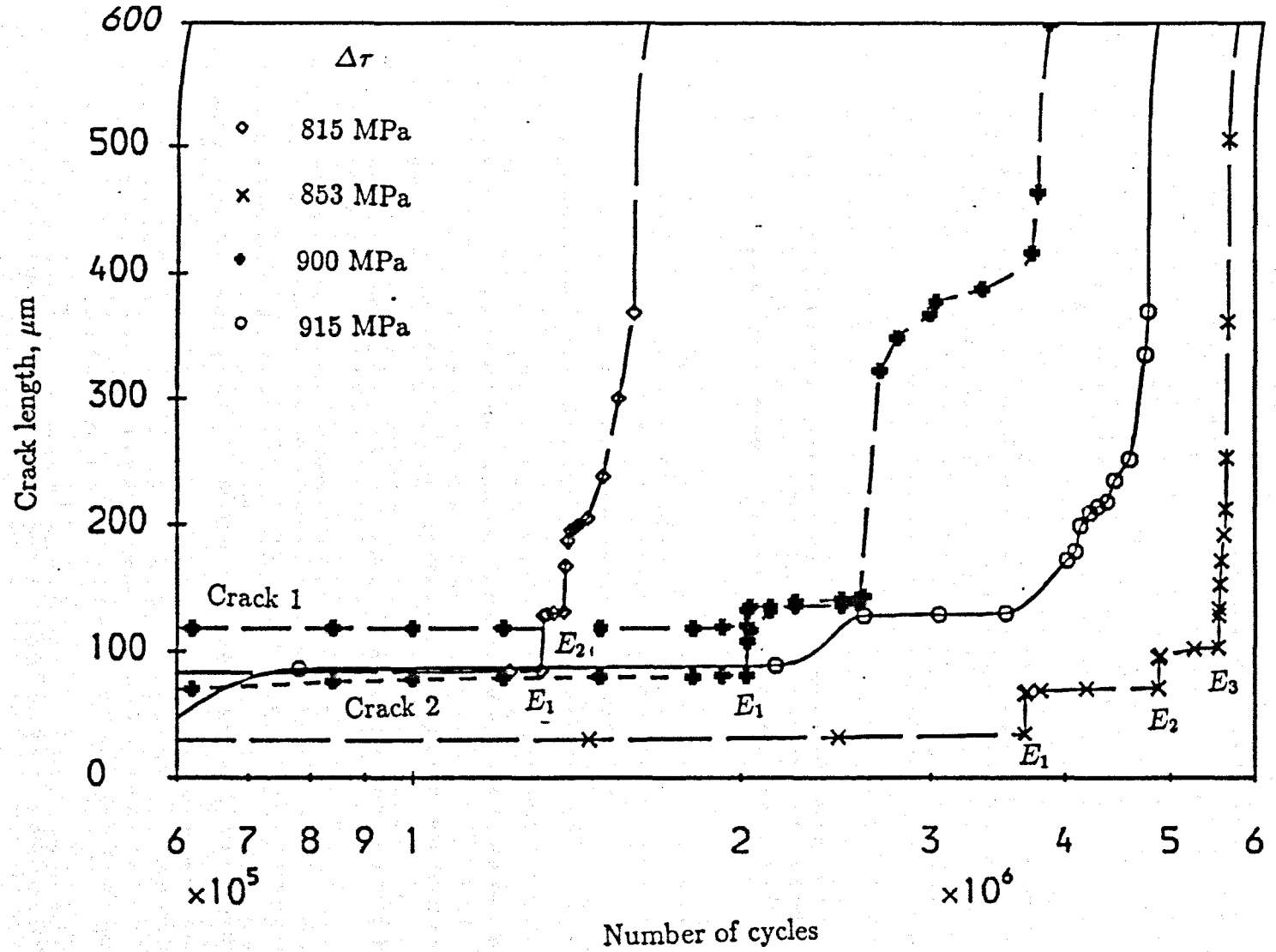

Figure 5.9: a versus N curves for air fatigue and intermittent air fatigue/corrosion fatigue tests.

Note: E denotes 5000 cycles under corrosion fatigue conditions.

Figure 5.10: Micrograph showing transition from stage I to stage II cracking after previous arrest at prior austenite grain boundaries (arrowed).

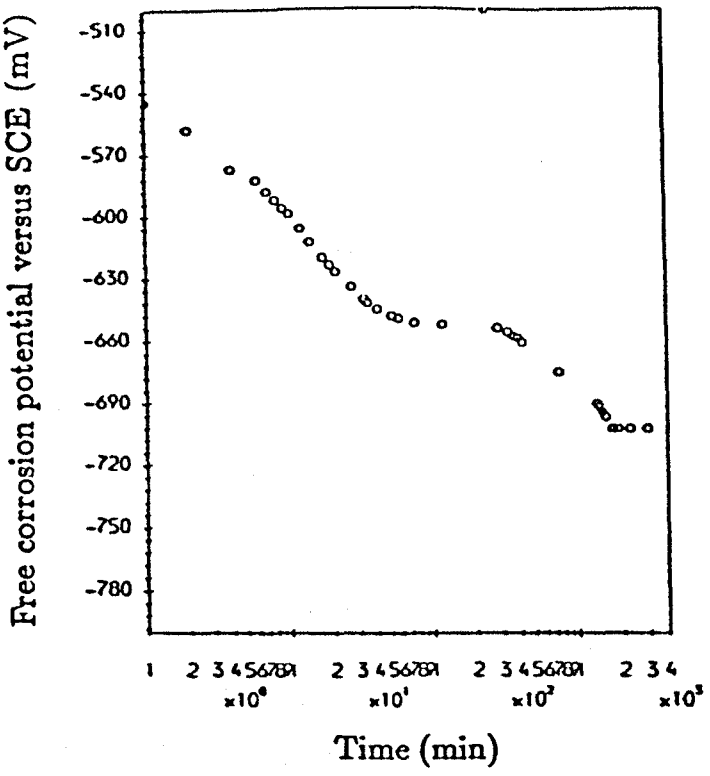

Figure 5.11: Influence of time of immersion on free corrosion potential.

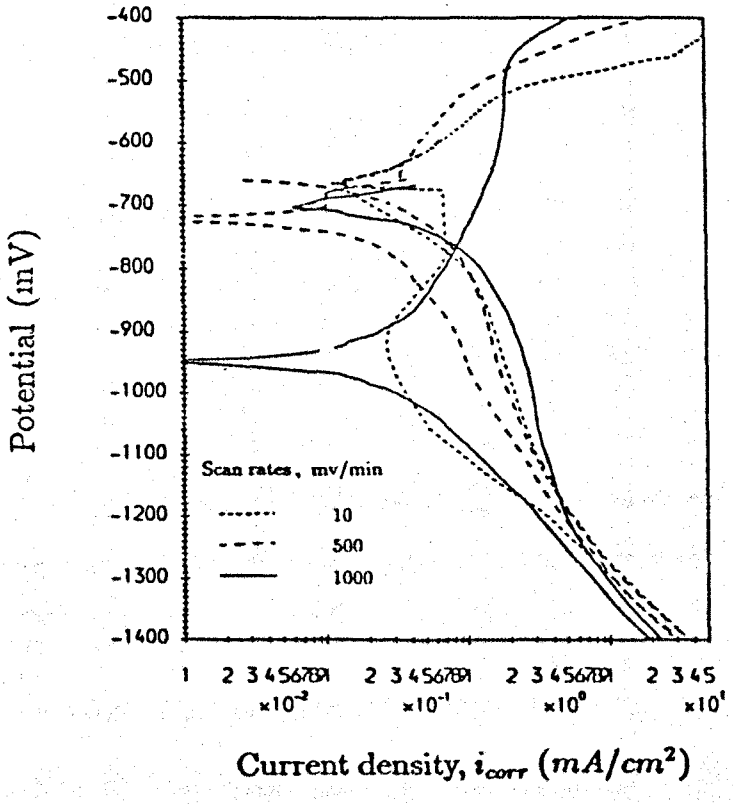

Figure 5.12: Effect of variation in scan rate on corrosion current, i_{corr}.

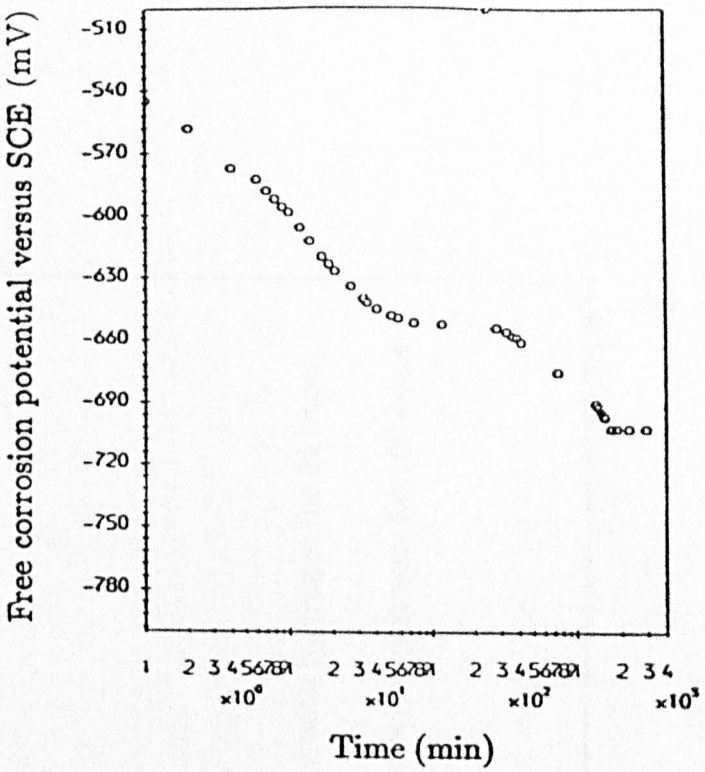

Figure 5.11: Influence of time of immersion on free corrosion potential.

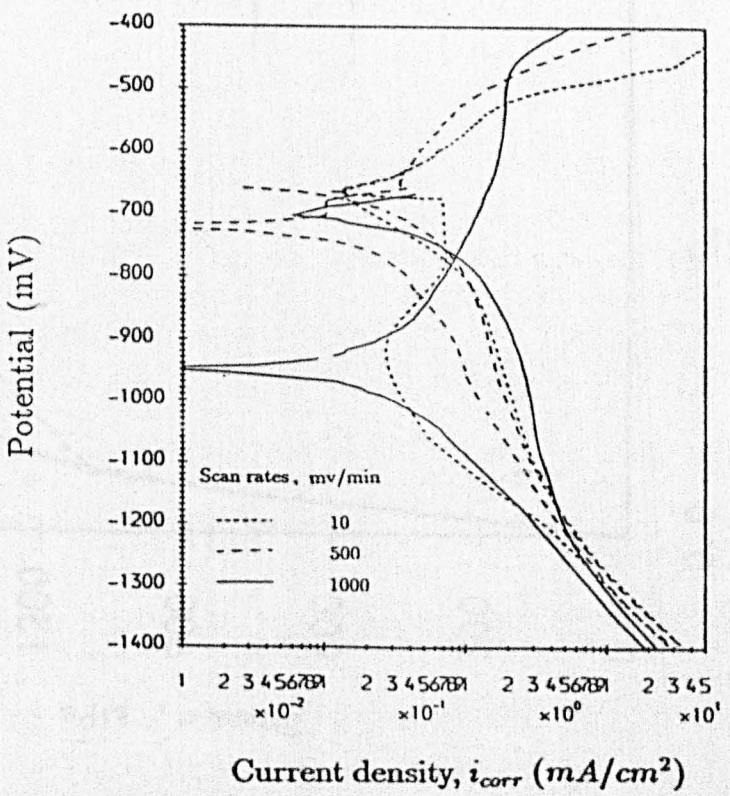

Figure 5.12: Effect of variation in scan rate on corrosion current, i_{corr}.

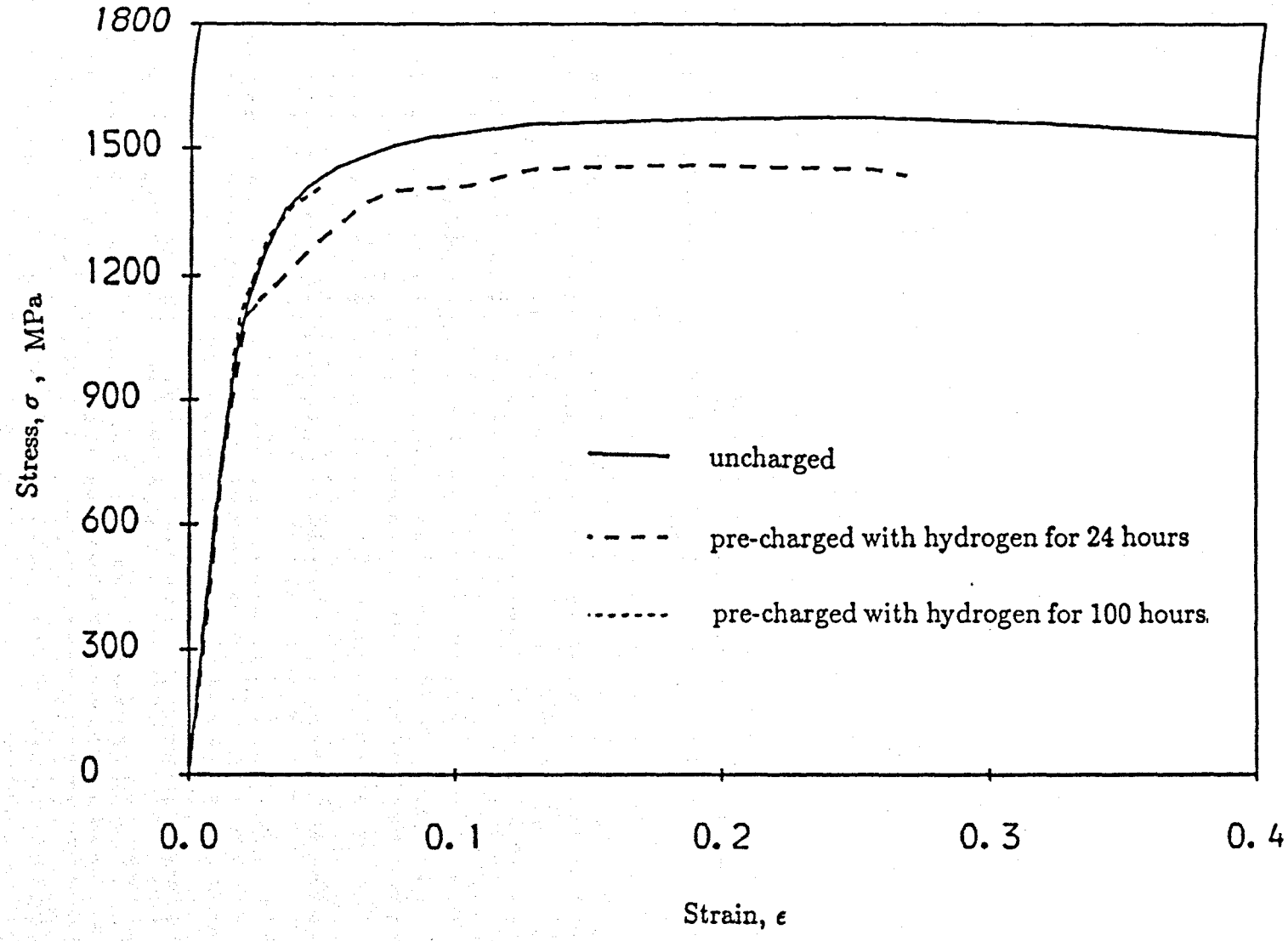

Figure 5.13: Tensile tests stress-strain curves.

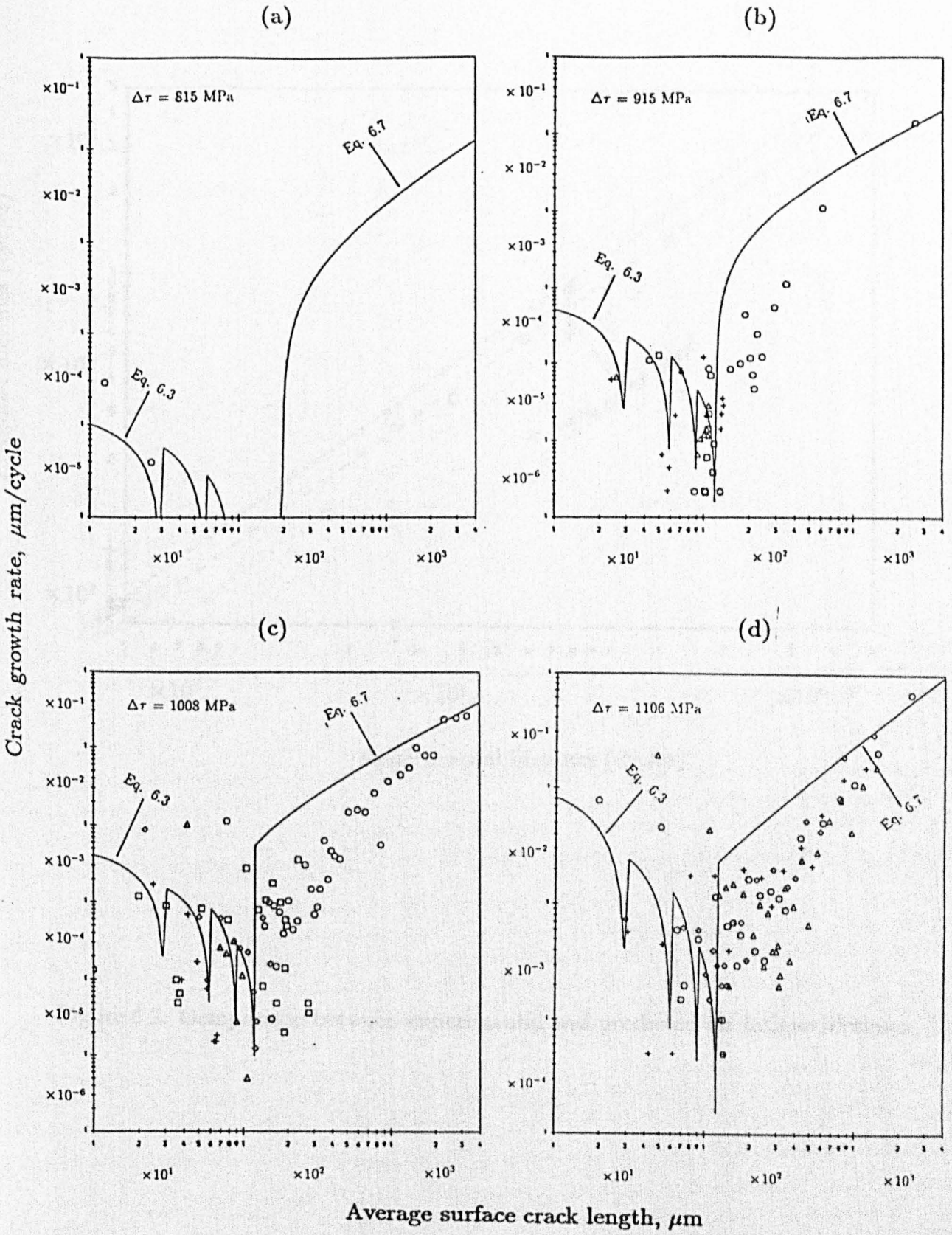

Figure 6.1: Air fatigue crack growth curves.

Note: each symbol represent an individual crack.

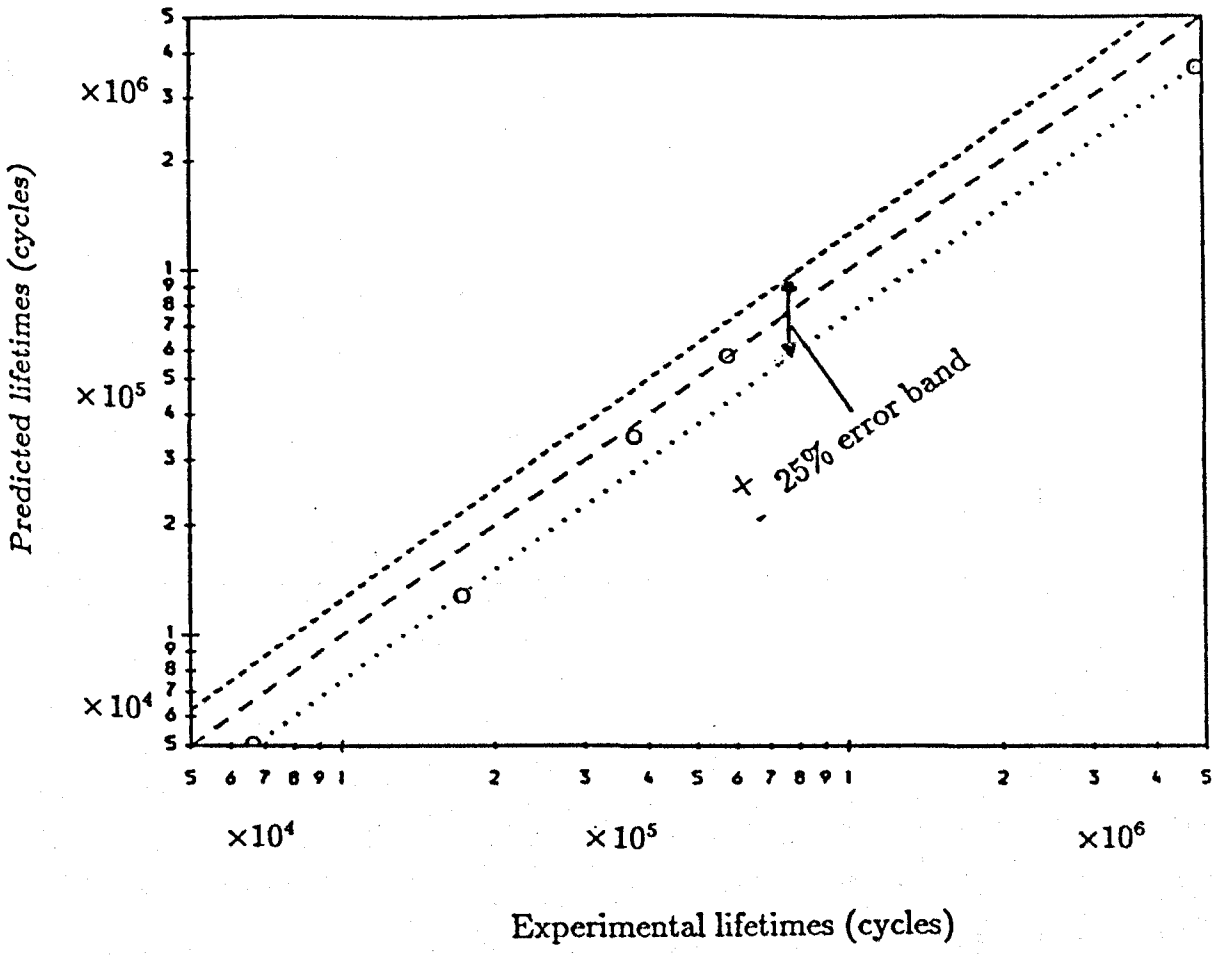

Figure 6.2: Comparison between experimental and predicted air fatigue lifetimes.

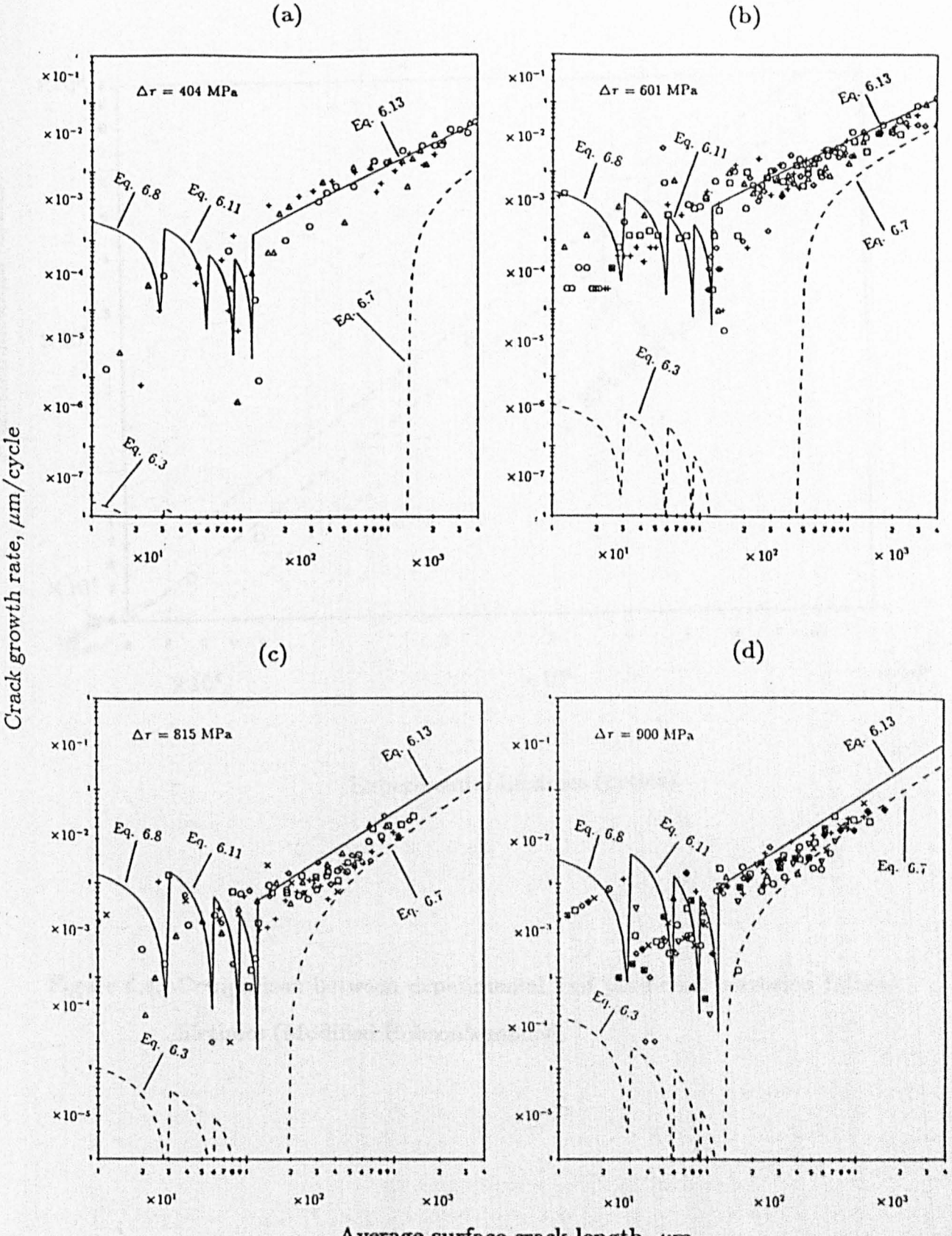

Figure 6.3: Corrosion fatigue crack growth curves;

Note: each symbol represent an individual crack.

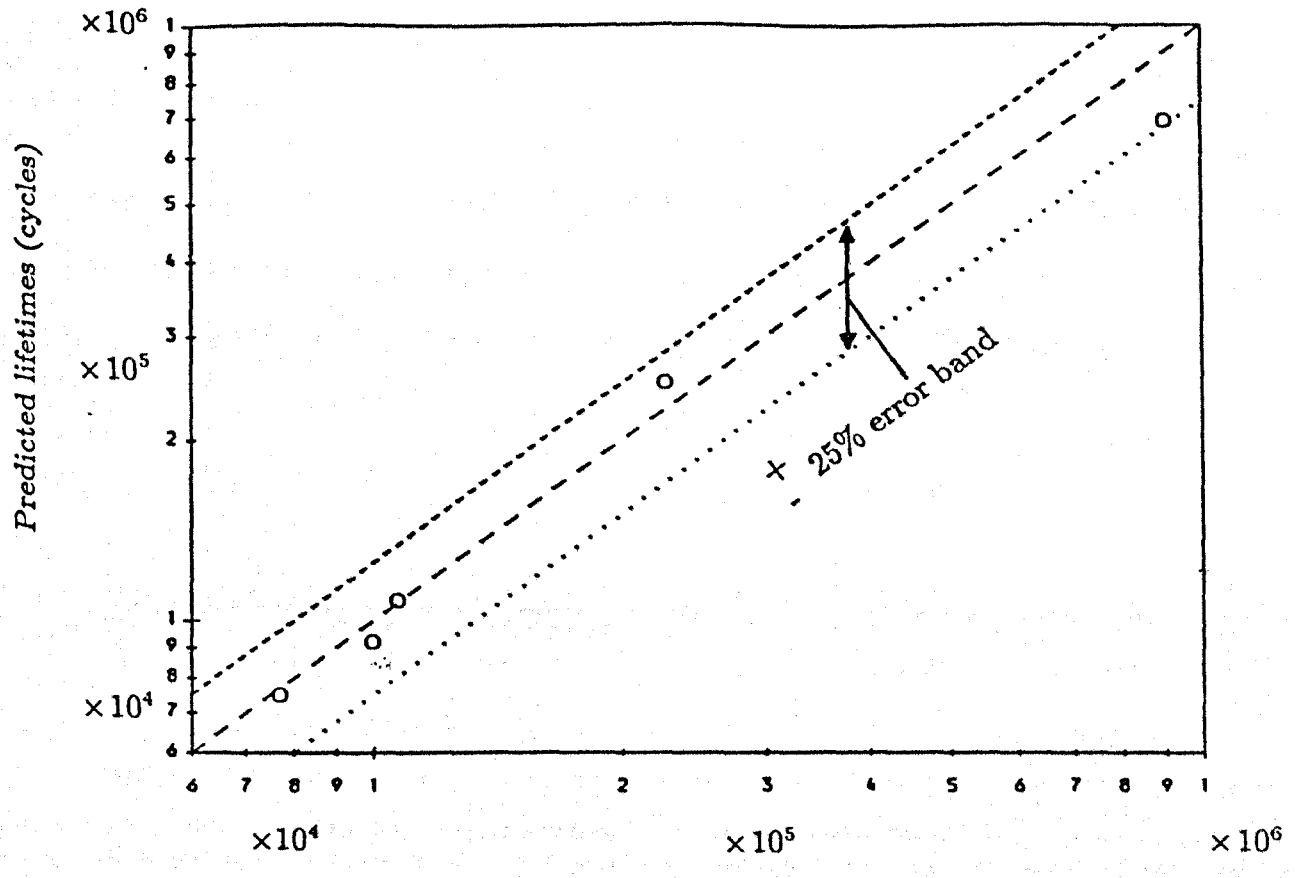

Figure 6.4: Comparison between experimental and predicted corrosion fatigue lifetimes (Modified Hobson's model).

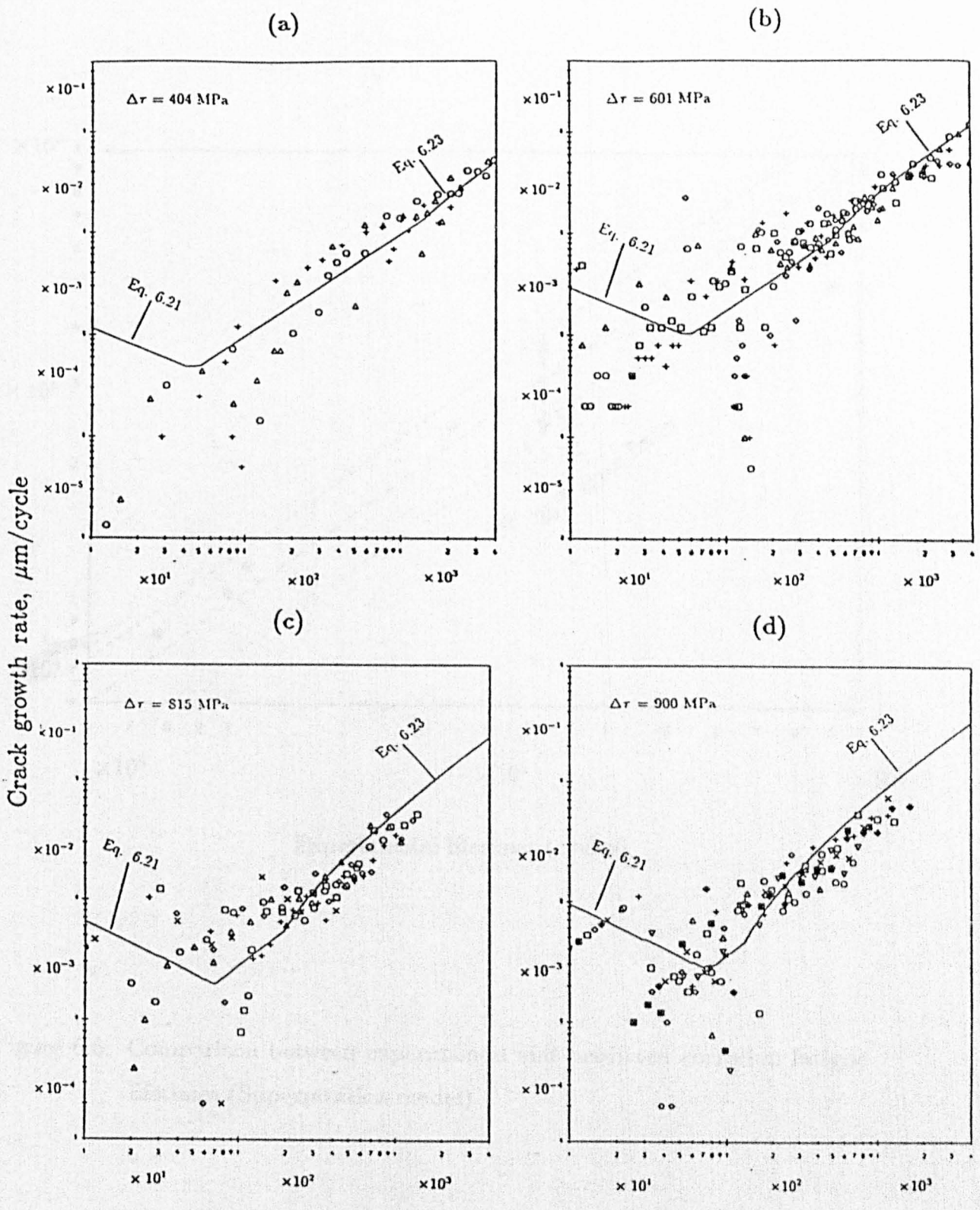

Figure 6.5: Corrosion fatigue crack growth curves;

Note: each symbol represent an individual crack.

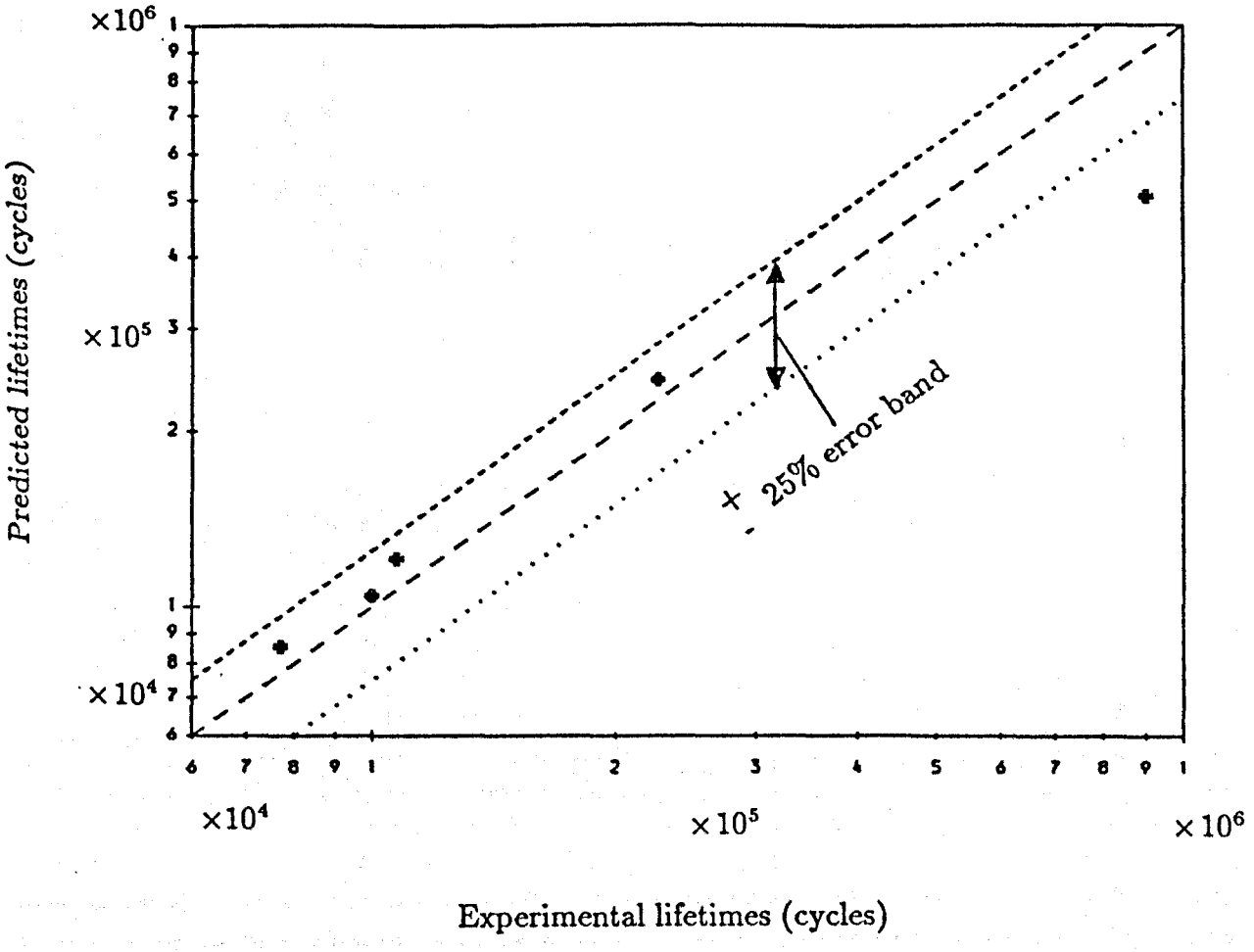

Figure 6.6: Comparison between experimental and predicted corrosion fatigue lifetimes (Superposition model).

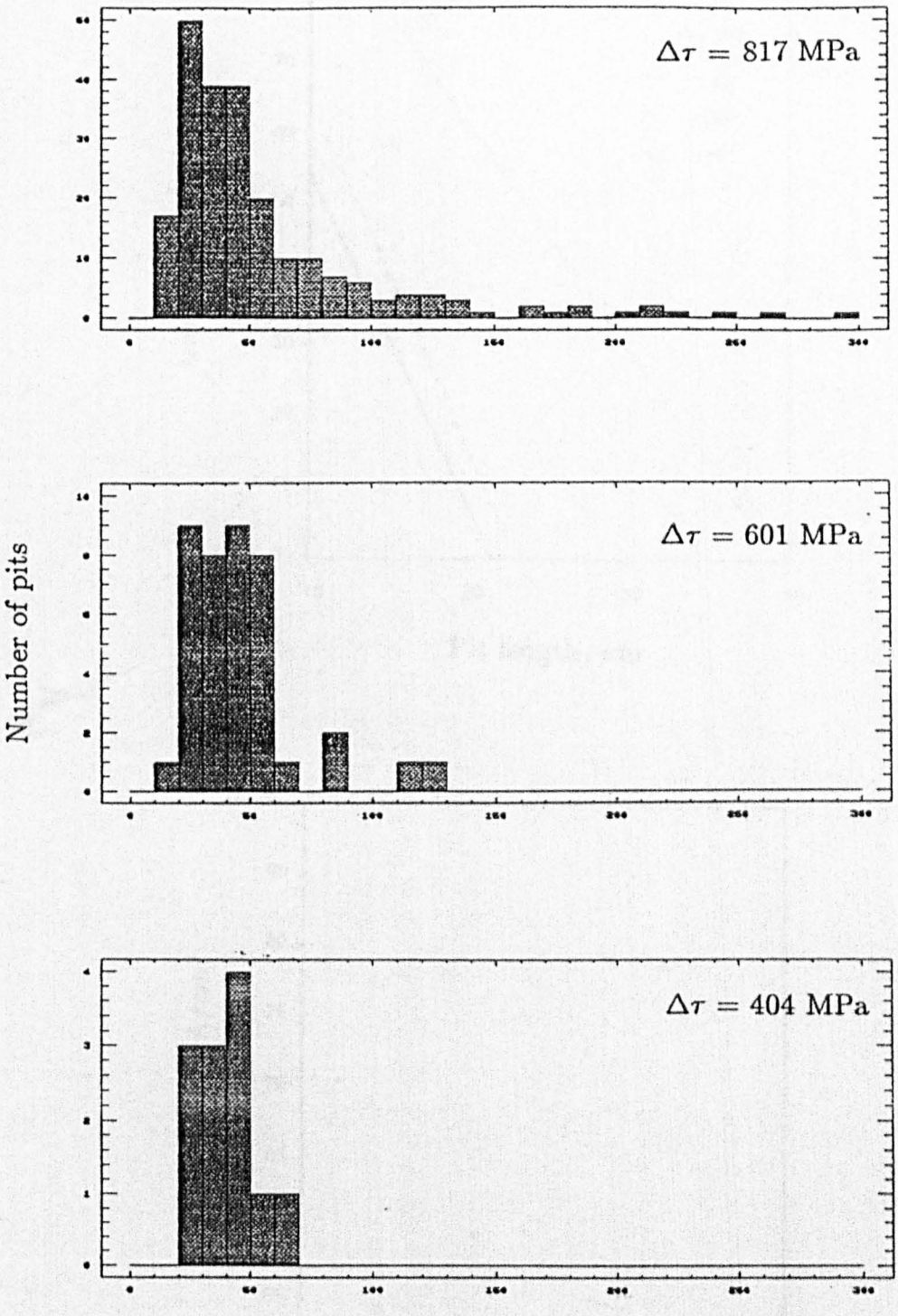

Figure 7.1: Histograms illustrating number of pits developed leading to crack initiation at different stress levels.

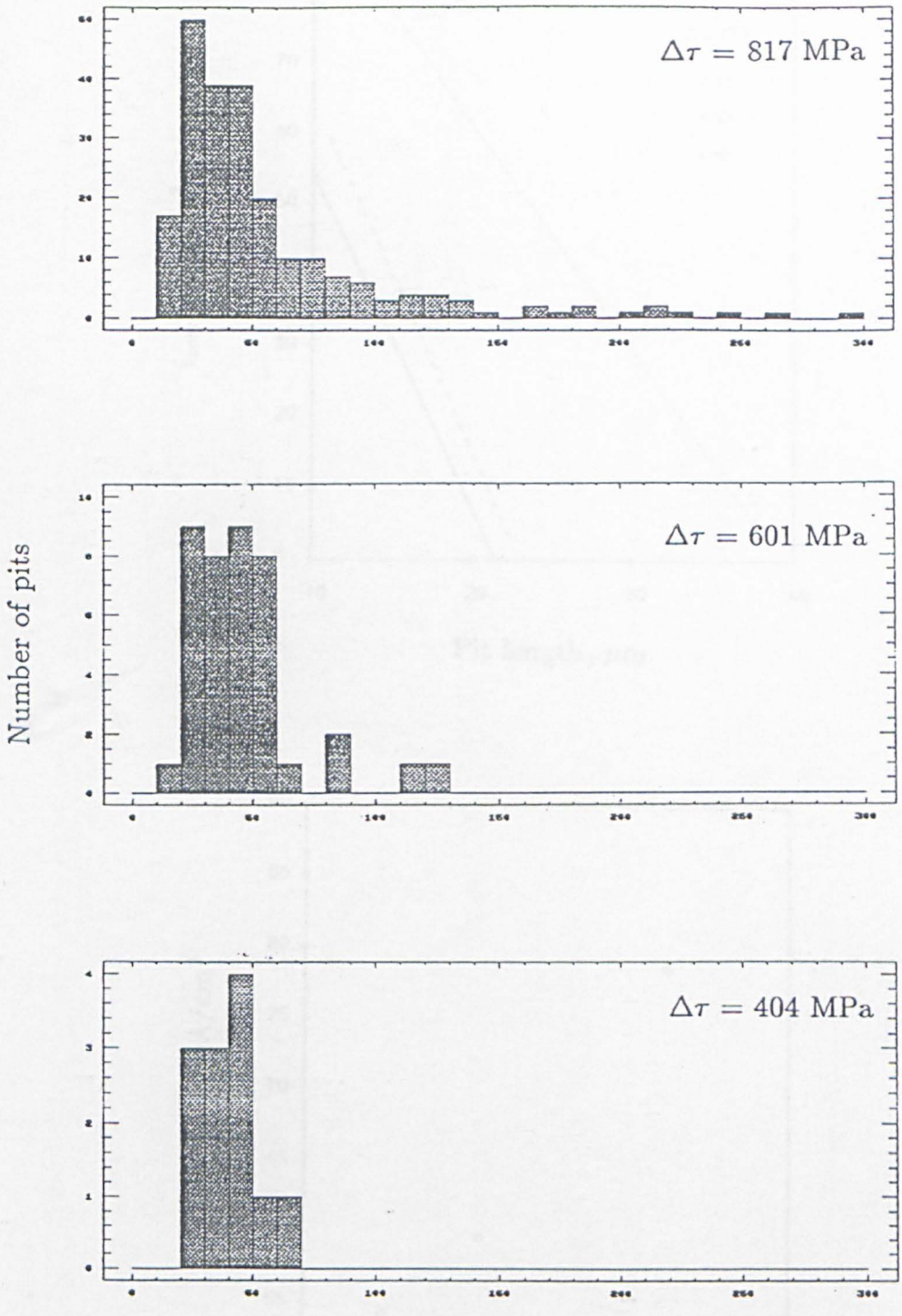

Figure 7.1: Histograms illustrating number of pits developed leading to crack initiation at different stress levels.

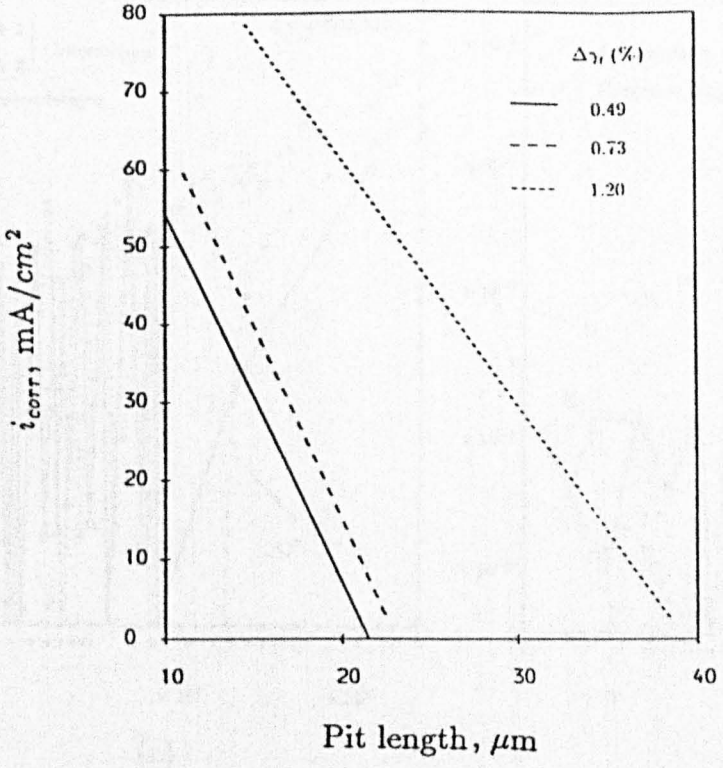

(a)

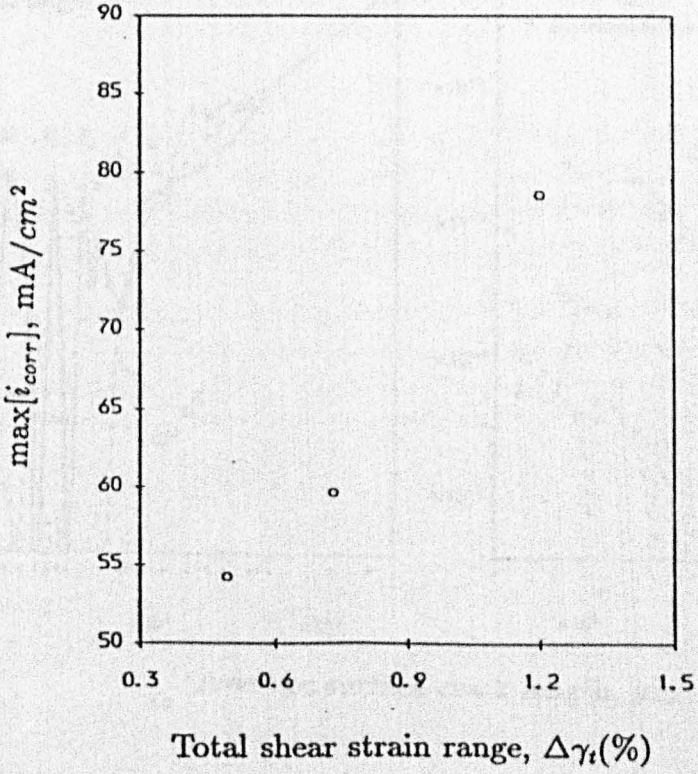

(b)

Figure 7.2: (a) Variation in i_{corr} with the pit length; (b) Relationship between max[i_{corr}] and total shear strain range.

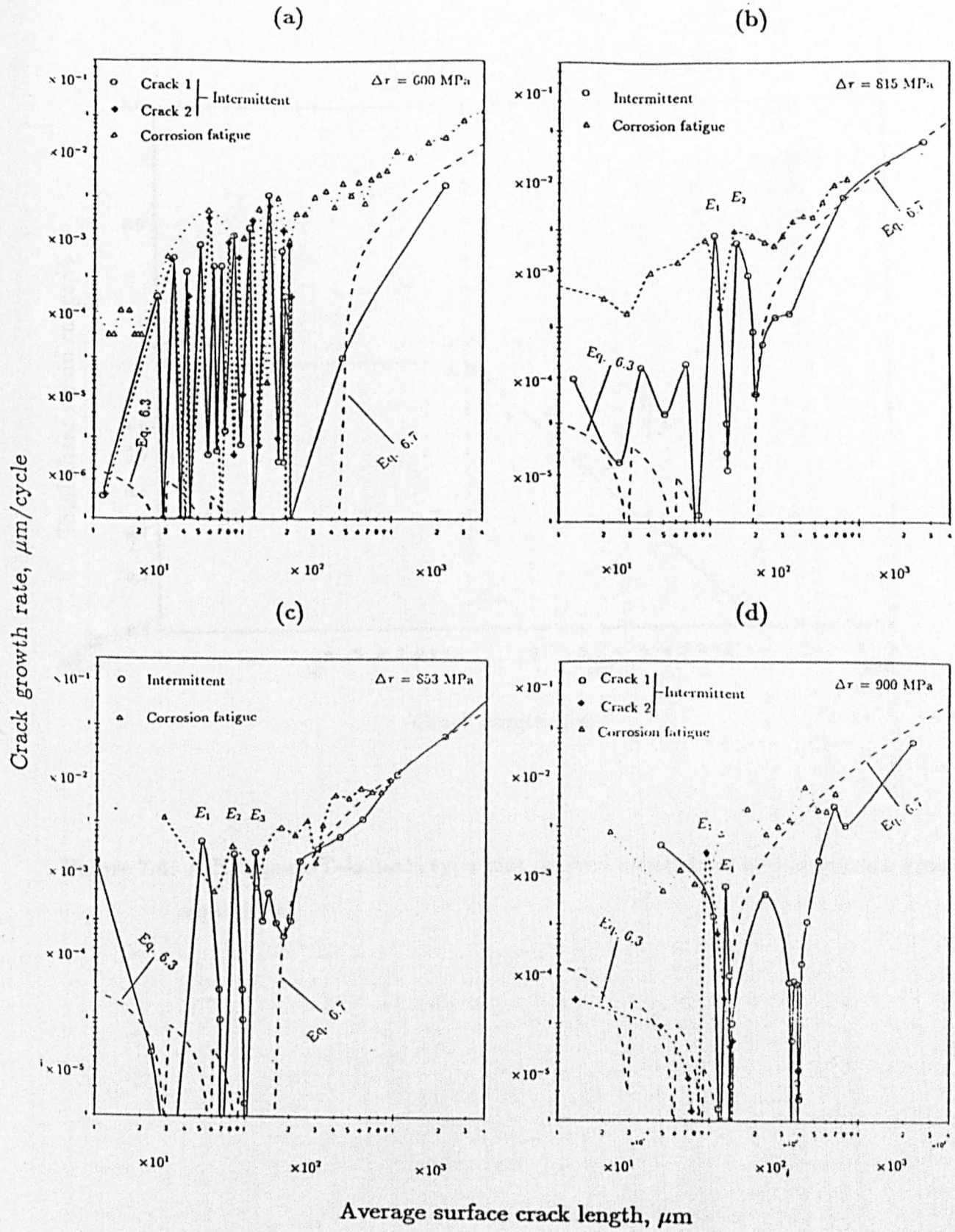

Figure 7.3: Intermittent air fatigue/corrosion fatigue crack growth curves.

Note: In figure (a) all intermittent crack accelerations were due to environment, up to a length of 212 μm.

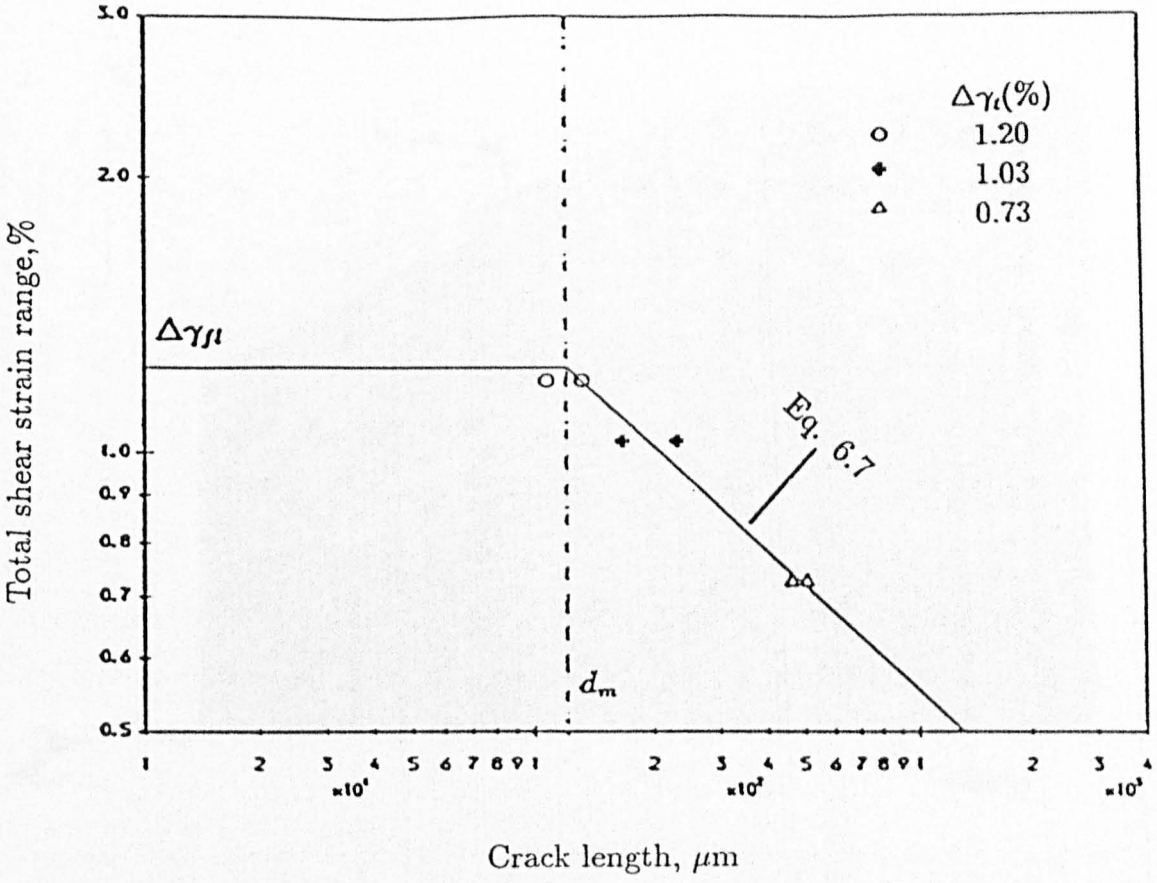

Figure 7.4: A Kitagawa-Takahashi type plot derived using short and long crack growth equations.

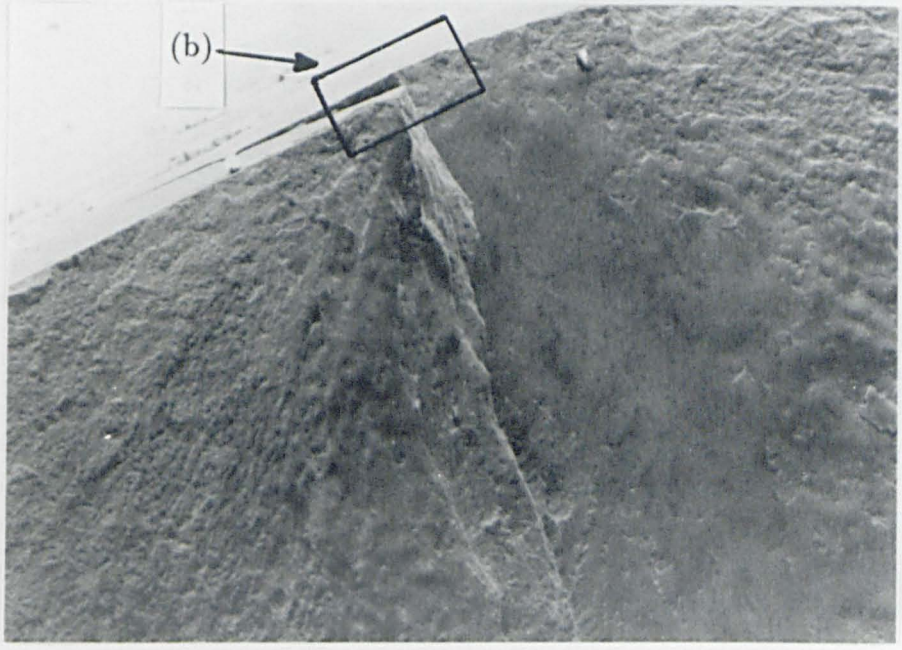

(a) $100\mu m$

(b) $5\mu m$

Figure 7.5: Fracture surfaces of air fatigue test specimen ; $\Delta\tau = 915$ MPa

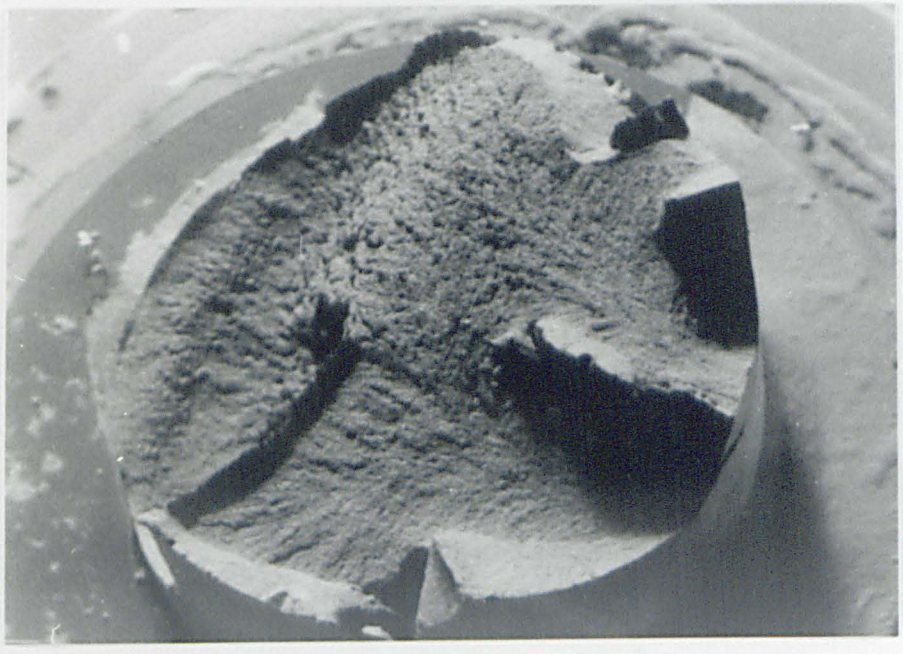

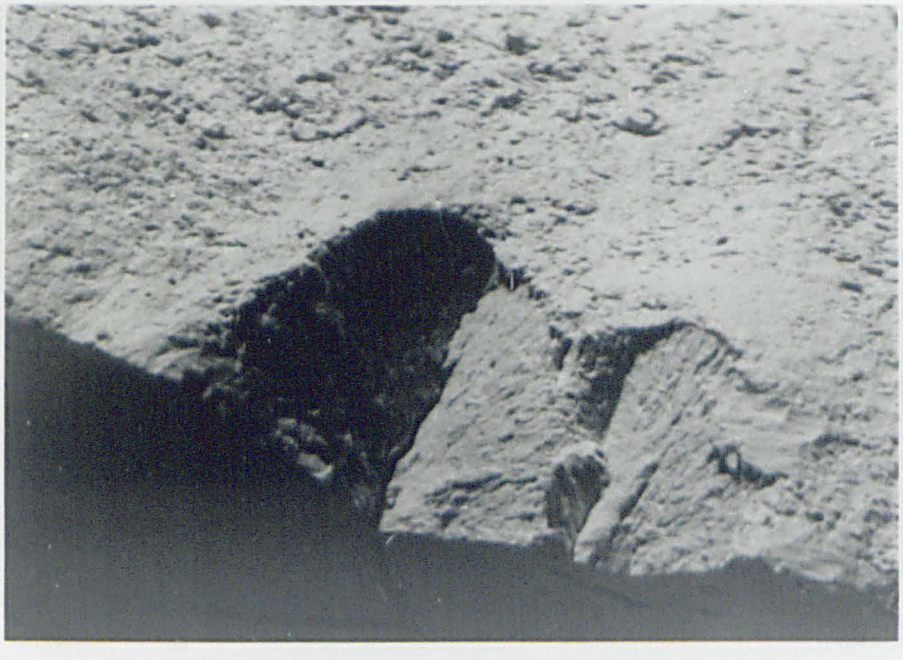

Figure 7.6: Fracture surfaces of air fatigue test specimen; $\Delta\tau = 1106$ MPa

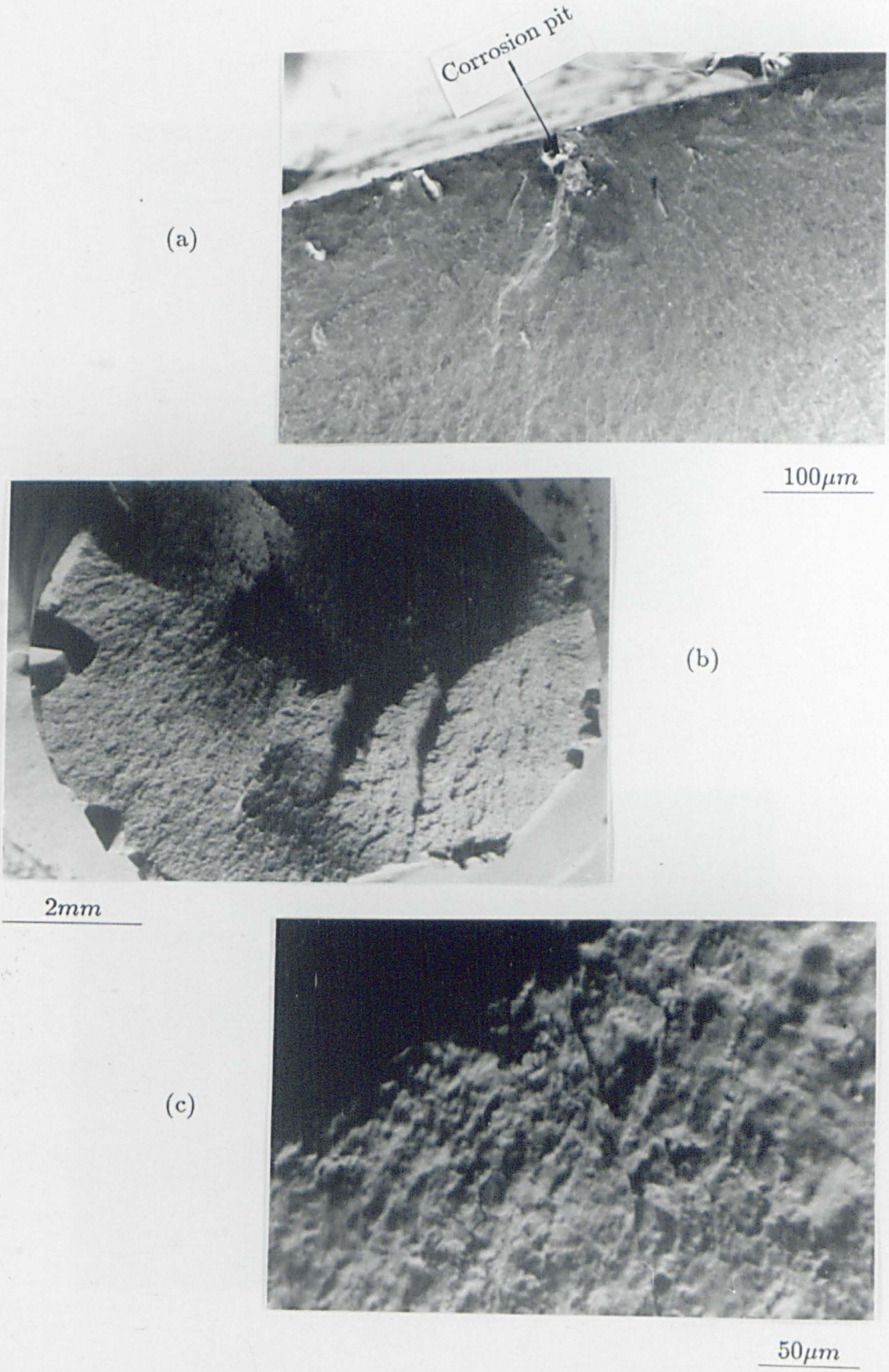

Figure 7.7: Fracture surfaces of corrosion fatigue test specimens;

(a) $\Delta\tau = 404$ MPa, (b)&(c) $\Delta\tau = 900$ MPa.

(a) $90\mu m$

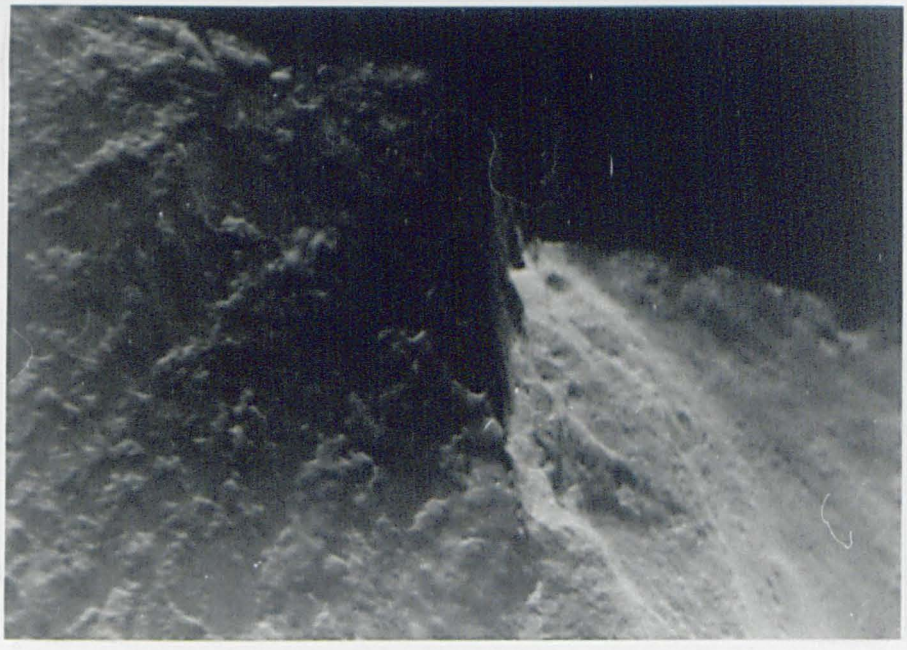

(b) $120\mu m$

Figure 7.8: Fracture surfaces of intermittent air fatigue/corrosion fatigue test specimens; (a) $\Delta\tau = 815$ MPa, (b) $\Delta\tau = 900$ MPa.

Normal

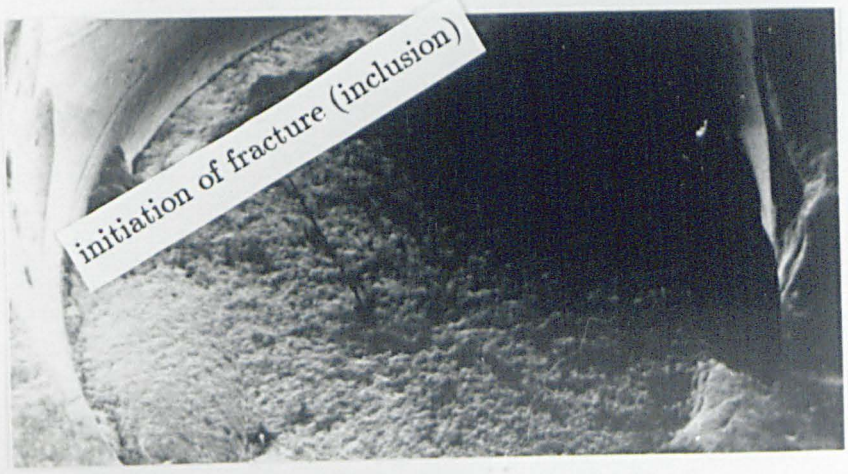

1mm

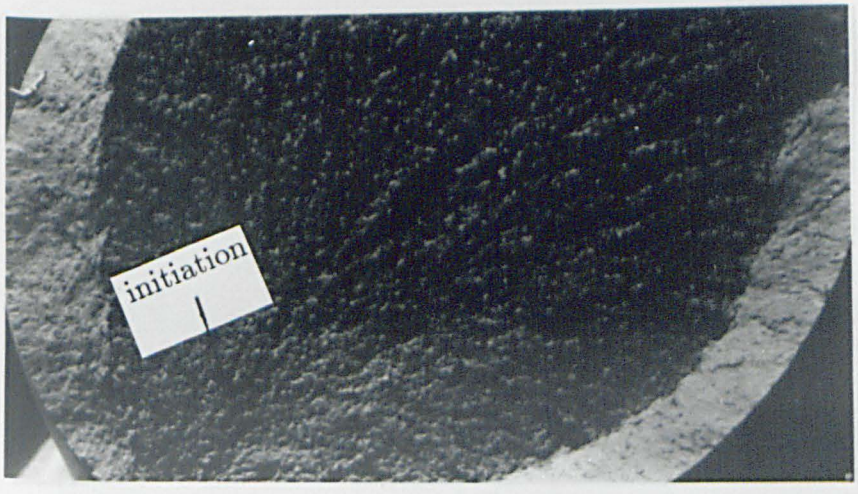

Pre-charged with hydrogen for 24 hours

1mm

Pre-charged with hydrogen for 100 hours

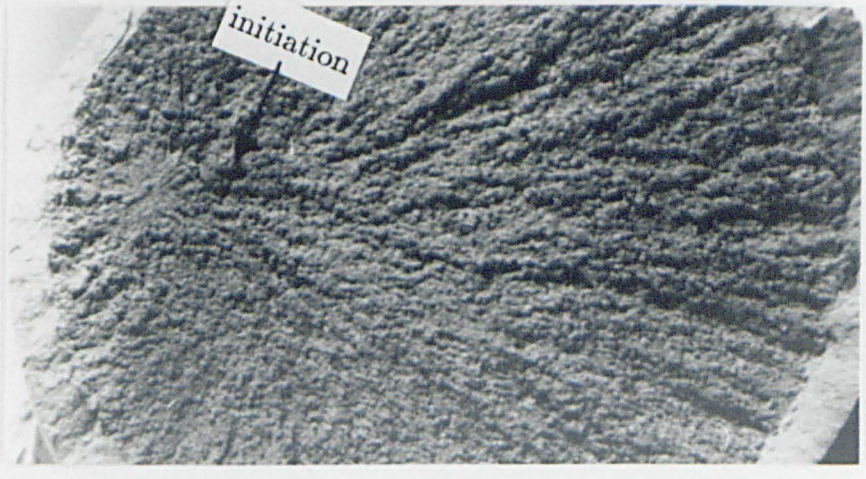

1mm

Figure 7.9: Fracture surfaces showing crack initiation sites of tensile specimens tested under various conditions.

Normal

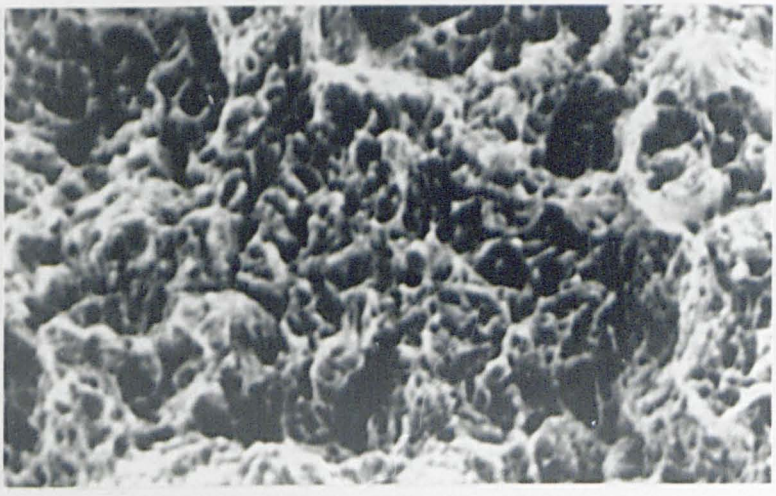

$20\mu m$

Pre-charged with hydrogen for 24 hours.

$20\mu m$

Pre-charged with hydrogen for 100 hours.

$20\mu m$

Figure 7.10: Fracture surfaces of tensile specimens tested under various conditions.

Appendix A

Elastic-Plastic Fracture Mechanics

Crack tip Opening Displacement, δ, is a direct measure of the state of the crack tip material in terms of a parameter closely associated with it. It is, however, very difficult to measure directly, but its value can be inferred from standard tests laid out in BS5762 [A1].

Using the Dugdale crack model, the crack tip opening displacement (CTOD) for a crack of length 2a in an infinite thin plate subjected to uniform tension δ in a material where plastic deformation occurs at the crack tip is given by [A2]:

$$\delta = \frac{8\sigma_y a}{\pi E} ln(sec\frac{\pi\sigma}{2\sigma_y}) \text{ ——————— (A1)}$$

expanding the secant term and keeping only the first term results in

$$\delta = \frac{\pi\sigma^2 a}{E\sigma_y} \text{ ——————— (A2)}$$

At very low stresses the above equation may be simplified to give

$$\delta = \frac{K^2}{E\sigma_y} \text{ ——————— (A3)}$$

The strain energy release rate expressed by equation (A4);

$$G = \frac{\pi a\sigma^2}{E} \text{ ——————— (A4)}$$

may be defined as the rate of transfer of energy from the elastic stress field of the cracked structure to the inelastic process of crack extension and represents the crack extension force. The critical value of G which makes the crack propagate to fracture, G_c, is called the fracture toughness of the material.

Dividing the above equation by σ_y we get

$$\frac{G}{\sigma_y} = \frac{\pi a\sigma^2}{E\sigma_y}$$

or

$$G = \frac{\pi a \sigma^2}{E \sigma_y} . \sigma_y$$

Now we can write it as;

$$G = \sigma_y \delta$$

Therefore, unstable fracture occurs when

$$G_{IC} = \lambda \sigma_y \delta_c$$

The factor λ depends upon the exact location at which CTOD is determined. It has been suggested [A3] that $\lambda \approx 2.1$ provides compatibility with LEFM conditions and that $\lambda \approx 1.0$ applies to conditions of extensive plasticity.

In order to overcome the difficulty of measuring and predicting crack tip opening displacements, an approximate method of characterising the crack tip plastic zone may be sought by using the J - contour integral [A4]. It is based on the finding that for a two - dimensional crack situation, the sum of the strain energy density and the work terms along a path completely enclosing the crack tip are independent of the path taken. This is shown in figure 1.

The energy line integral J is defined for either elastic or elastic-plastic behaviour as follows:

$$J = \int_\Gamma (W dy - T \frac{\delta u}{\delta x} ds)$$

where W is the strain energy density, Γ is the path of the integral which encloses the crack, T is a traction vector normal to the integral path, u is the displacement

vector, ds is an increment of the contour path and $T(\frac{\delta u}{\delta x} ds)$ is the rate of work input from the stress field into the area enclosed by Γ.

Being path-independent the J-integral can be determined by suitable stress analysis where σ and ϵ are established by finite element analysis around the contour enclosing the crack. Since J is path-independent we may choose the most convenient path, usually the specimen boundary.

The J integral can be interpreted as the potential energy difference between two identically loaded non-linear elastic specimens having slightly different crack lengths. This is illustrated in figure 2. From this it follows that

$$J = -\frac{\delta u}{\delta a}$$

J uniquely characterizes the crack tip field under elastic- plastic conditions, provided there is some strain hardening. Furthermore, for small scale yielding J can be directly related to the strain energy release rate, G, and hence to K i.e.

$$J = G = \frac{K^2}{E}$$

Despite difficulties in estalishing the precise meaning of J as applied to a description of the growth of cyclically stressed (non-stationary) cracks. Dowling [A5] and Dowling and Beglay [A6] proposed a power law correlation of fatigue crack growth rates under elastic-plastic conditions to the range of J i.e.

$$\frac{da}{dN} \propto (\Delta J)^{m'}$$

Provided such analysis is fundamentally justified, the use of ΔJ does present a first approach to characterizing the growth of short cracks which are comparable

in size to the extent of local yielding. However the validity of the ΔJ is often questioned since it appears to contradict a basic assumption in the definition of J — that the stress is propotional to the current plastic strain [A4]. This follows because J is defined from the deformation theory of plasticity, which does not allow for the elastic unloading and non-proportional loading effects which accompany crack advance [A7].

Crack tip opening displacement is used as an alternative treatment of elastic-plastic fatigue crack growth, which is not subject to the restriction required by non-linear elasticity. It is feasible to correlate rates of fatigue crack growth to the range of δ, i.e. the cyclic CTOD, $\Delta\delta$,

$$\frac{da}{dN} \propto \Delta\delta \text{ ——— (elastic-plastic)}$$

$$\frac{da}{dN} \propto \frac{\Delta K^2}{2\sigma_y E} \text{ ——— (linear elastic)}$$

Approaches based on J and δ are basically equivalent for proportional loading and are of course valid under both elastic-plastic and linear elastic conditions. Therefore they are generally applicable to a continuum description of the growth rate behaviour of cracks that are considered small because their size is comparable with the scale of local plasticity. For such short cracks the use of EPFM rather than LEFM may thus be expected at least in part to normalize differences in behaviour between long and short cracks. However, the short crack problem is not simply a break down in the application of LEFM since the use of elastic-plastic analyses cannot totally normalize differences between short and long cracks. Although elastic-plastic analysis is certainly important, differences in the behaviour of long

and short cracks can also be attributed to the microstructural, environmental and closure effects [A8].

References:

[A1] British Standard BS 5762, 1979.

[A2] G. T. Hahn and A. R. Rosenfeld: (1965) Acta Metall., 13, p. 293.

[A3] A. A. Wells: (1970) Eng. Fract. Mech., 1, p. 399.

[A4] J. R. Rice: (1968) J. Appl. Mech., 35, p. 379.

[A5] N. E. Dowling: (1976) in Cracks and fracture, STP 601, ASTM, p. 96.

[A6] N. E. Dowling and J. A. Beglay: (1976) in Mechanics of crack growth, STP 590, ASTM, p. 82.

[A7] J. W. Hutchinson and P.C. Paris: (1979) in Elastic-plastic fracture, STP 668, p. 37.

[A8] S. Suresh and R. O. Ritchie: (1984) Int. Met. Rev., 29 (6), p. 445.

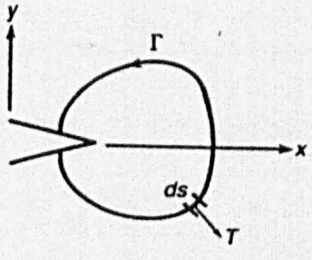

Fig. 1: Sketch of Γ contour drawn around a crack tip to define the J-integral .

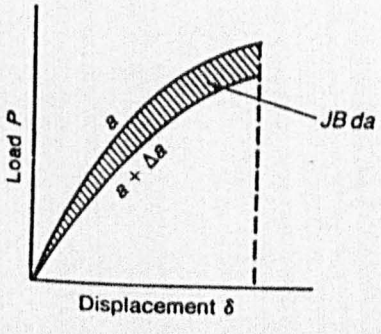

Fig. 2: Physical interpretation of the J-integral.
Note: B is the specimen thickness.

Appendix B

Crack Growth Modelling - Determination of Coefficients

The constant C_{sa} in equation 6.1 was calculated using experimental data points of crack length and crack growth rate which exhibited a deceleration in growth with an increase in crack length by applying the following expression assuming that equation 6.1 is valid;

$$C_{sa} = \frac{\frac{da}{dN}}{d_i - a_{av}}$$

In this study this condition arose when a crack was progressing towards a microstructural barrier, i.e. a prior anstenite grain boundary. The values of this constant calculated for different cracks at a particular stress level, showed some variation due to the variation in crack speed, this in turn is related to the microstructure i.e. grain size and orientation. Later a power law regression was applied to the derived values of C_{sa} and the total shear strain range ($\Delta\gamma_t$) appropriate to that constant thereby giving the values of A and α as given in equation 6.2. The experimental results indicated that there was a variation in deceleration of cracks while approaching each prior austenite grain boundary up to an average of four prior austenite grains suggesting this as the limit of the short crack regime. Therefore by repeating the above procedure constants A and α were calculated for each prior austenite grain and hence four equations were developed to represent short crack gowth. These constants for individual grains are given in section 6.2.1.

The coefficient for long crack growth equation, C_{la}, given in the equation 6.4 was taken as the slope of linear regression drawn through plots of crack length versus crack growth rate data (linear) for cracks showing an acceleration in growth for lengths greater than the dominant microstructural barrier, d_m. The constant, C_{la}, representing the failure/major crack was determined for each stress level. This

enabled the determination of the constants B and β given in equation 6.5 again adopting a power regression analysis to the data of C_{la} and total shear strain range.

The constant, C_p, used in the pit development equation (Eq. 6.8) for corrosion fatigue crack growth modelling was determined using the approach discussed above for C_{sa} determination. The only difference in this case was the use of a transition length, a_{tl}, representing transition from pit growth to mode I cracking which in this case corresponded to the first prior austenite grain.

Appendix C

Air Fatigue Crack Growth Results

Air fatigue crack growth data; Test No. : AF14;
$\Delta\tau$ = 1106 MPa, $\Delta\gamma_t$ = 2.22%, N_f = 66,300

No. of Cycles "N"	*Crack Length "a" (μm)*	*Av. Crack Length "a_{av}" (μm)*	*Crack Growth Rate "da/dN" (μm/cycle)*
Crack No. 1			
000	00	19.5	7.79×10^{-2}
500	39	50.5	4.60×10^{-2}
1000	62	65.0	5.99×10^{-3}
2000	68	69.5	1.50×10^{-3}
4000	71	73.0	2.00×10^{-3}
6000	75	90.0	5.00×10^{-3}
12000	105	116.5	1.15×10^{-2}
14000	128	130.0	9.99×10^{-3}
18000	132	132.5	5.00×10^{-4}
20000	133	139.5	6.49×10^{-3}
22000	146	153.0	6.99×10^{-3}
24000	160	163.0	3.00×10^{-3}
26000	166	171.5	5.50×10^{-3}
28000	177	193.5	1.65×10^{-2}
30000	210	214.0	4.00×10^{-3}
32000	218	230.0	1.20×10^{-2}
34000	242	247.0	3.33×10^{-3}
37000	252	271.5	1.30×10^{-2}
40000	291	308.0	1.13×10^{-2}
43000	325	338.5	9.00×10^{-3}
46000	352	427.5	3.77×10^{-2}
50000	503	606.0	5.14×10^{-2}
54000	709	792.5	8.35×10^{-2}
56000	876	986.5	0.1105000
58000	1097	1406.0	0.206000
61000	1715	2375.0	0.6600000
63000	3035	--	--

Air fatigue crack growth data; Test No. : AF14;
$\Delta\tau$ = 1106 MPa, $\Delta\gamma_t$ = 2.22%, N_f = 66,300

No. of Cycles "N"	*Crack Length "a" (μm)*	*Av. Crack Length "a_{av}" (μm)*	*Crack Growth Rate "da/dN" (μm/cycle)*
	Crack No. 2		
000	00	47.5	0.1900000
500	95	106.0	4.40×10^{-2}
1000	117	123.0	1.20×10^{-2}
2000	129	136.0	1.40×10^{-2}
3000	143	144.0	2.00×10^{-3}
4000	145	152.5	1.50×10^{-2}
5000	160	178.5	1.23×10^{-2}
8000	197	208.0	5.50×10^{-3}
12000	219	229.0	1.00×10^{-2}
14000	239	245.0	3.00×10^{-3}
18000	251	259.5	8.49×10^{-3}
20000	268	280.0	4.00×10^{-3}
26000	292	296.0	4.00×10^{-3}
28000	300	304.5	4.50×10^{-3}
30000	309	311.0	2.00×10^{-3}
32000	313	315.5	2.50×10^{-3}
34000	318	3390	1.40×10^{-2}
37000	360	365.0	3.33×10^{-3}
40000	370	384.5	9.66×10^{-3}
43000	399	435.5	2.43×10^{-2}
46000	472	485.5	6.75×10^{-3}
50000	499	556.0	2.85×10^{-2}
54000	613	667.0	5.40×10^{-2}
56000	721	802.0	8.09×10^{-2}
58000	883	947.0	4.26×10^{-2}
61000	1011	1119.5	0.1085000
63000	1228	1383.0	0.1550000
65000	1538	---	---

Air fatigue crack growth data; Test No. : AF14;
$\Delta\tau$ = 1106 MPa, $\Delta\gamma_t$ = 2.22%, N_f = 66,300

No. of Cycles "N"	*Crack Length* "a" (μm)	*Av. Crack Length* "a_{av}" (μm)	*Crack Growth Rate* "da/dN" (μm/cycle)
Crack No. 3			
0000	00	9.5	2.37×10^{-3}
8000	19	30.5	5.75×10^{-3}
12000	42	42.5	5.00×10^{-4}
14000	43	52.0	4.50×10^{-3}
18000	61	61.5	5.00×10^{-4}
20000	62	79.5	1.75×10^{-2}
22000	97	114.5	1.75×10^{-2}
24000	132	134.5	5.00×10^{-4}
34000	137	143.0	4.00×10^{-3}
37000	149	179.0	2.00×10^{-2}
40000	209	234.5	1.70×10^{-2}
43000	260	274.5	9.66×10^{-3}
46000	289	328.5	1.97×10^{-2}
50000	368	430.5	3.12×10^{-2}
54000	493	514.5	2.15×10^{-2}
56000	536	596.0	5.99×10^{-2}
58000	656	838.5	0.1216670
61000	1021	1173.5	0.1525000
63000	1326	—	—

Air fatigue crack growth data; Test No. : AF14;
$\Delta\tau$ = 1106 MPa, $\Delta\gamma t$ = 2.22%, N_f = 66,300

No. of Cycles "N"	*Crack Length* "a" (μm)	*Av. Crack Length* "a_{av}" (μm)	*Crack Growth Rate* "da/dN" (μm/cycle)
Crack No. 4			
0000	00	29.5	7.37×10^{-3}
8000	59	71.5	6.25×10^{-3}
12000	84	90.0	5.99×10^{-3}
14000	96	101.0	2.50×10^{-3}
18000	106	107.5	1.50×10^{-3}
20000	109	113.0	4.00×10^{-3}
24000	123	125.0	9.99×10^{-4}
28000	127	129.0	2.00×10^{-3}
30000	131	134.0	3.00×10^{-3}
32000	137	139.0	2.00×10^{-3}
34000	141	151.5	6.99×10^{-3}
37000	162	172.5	6.99×10^{-3}
40000	183	188.0	3.33×10^{-3}
43000	193	217.5	1.63×10^{-2}
46000	242	282.0	2.00×10^{-2}
50000	322	350.5	1.42×10^{-2}
54000	379	396.0	1.70×10^{-2}
56000	413	466.0	5.30×10^{-2}
58000	519	583.5	4.30×10^{-2}
61000	648	837.0	0.1890000
63000	1026	1319.5	0.2935000
65000	1613	--	--

Air fatigue crack growth data; Test No. : AF15;
$\Delta\tau$ = 1008 MPa, $\Delta\gamma_t$ = 1.57%, N_f = 577,500

No. of Cycles "N"	Crack Length "a" (μm)	Av. Crack Length "a_{av}" (μm)	Crack Growth Rate "da/dN" (μm/cycle)
Crack No. 1			
0000	00	10.0	1.33×10^{-4}
150000	20	77.5	1.15×10^{-2}
160000	135	140.0	5.00×10^{-4}
180000	145	150.0	9.99×10^{-4}
190000	155	156.0	3.07×10^{-5}
255000	157	161.5	9.00×10^{-4}
265000	166	167.5	1.50×10^{-4}
285000	169	176.5	7.49×10^{-4}
305000	184	188.0	4.00×10^{-4}
325000	192	202.5	1.05×10^{-3}
345000	213	217.5	4.50×10^{-4}
365000	222	233.0	5.78×10^{-4}
403000	244	262.5	3.03×10^{-3}
415000	281	288.5	1.50×10^{-3}
425000	296	303.0	7.00×10^{-4}
445000	310	316.5	8.66×10^{-4}
460000	330	330.5	1.50×10^{-3}
470000	338	354.0	6.39×10^{-3}
475000	370	375.0	2.00×10^{-3}
480000	380	394.0	4.66×10^{-3}
486000	408	416.0	4.00×10^{-3}
490000	424	451.5	3.66×10^{-3}
505000	479	516.5	1.50×10^{-2}
510000	554	594.0	1.60×10^{-2}
515000	634	671.5	1.50×10^{-2}
520000	709	774.5	2.62×10^{-2}
525000	840	854.0	5.60×10^{-3}
530000	868	961.0	3.72×10^{-2}
535000	1054	1166.5	4.49×10^{-2}
540000	1279	1334.5	5.54×10^{-2}
542000	1390	1489.5	9.94×10^{-2}
544000	1589	1708.0	7.93×10^{-2}
547000	1827	1946.5	7.96×10^{-2}
550000	2066	2299.0	0.2330000
552000	2532	2776.0	0.2440000
554000	3020	3278.0	0.2580000
556000	3536	4524.0	0.4942500
560000	5513	---	---

Air fatigue crack growth data; Test No. : AF15;
$\Delta\tau$ = 1008 MPa, $\Delta\gamma_t$ = 1.57%, N_f = 577,500

No. of Cycles "N"	Crack Length "a" (μm)	Av. Crack Length "a_{av}" (μm)	Crack Growth Rate "da/dN" (μm/cycle)
Crack No. 2			
0000	00	07.0	2.33×10^{-4}
60000	14	20.0	1.20×10^{-3}
70000	26	30.5	9.00×10^{-4}
80000	35	35.5	9.99×10^{-5}
90000	36	36.5	5.00×10^{-5}
110000	37	37.5	6.66×10^{-5}
125000	38	52.5	8.28×10^{-4}
160000	67	79.0	5.99×10^{-4}
200000	91	105.0	2.80×10^{-3}
210000	119	127.0	7.99×10^{-4}
230000	135	135.5	8.33×10^{-5}
242000	136	143.0	1.07×10^{-3}
255000	150	159.0	1.80×10^{-3}
265000	168	168.5	5.00×10^{-5}
285000	169	179.0	9.99×10^{-4}
305000	189	150.0	2.04×10^{-5}
403000	191	191.5	1.42×10^{-4}
410000	192	193.5	5.99×10^{-4}
415000	195	197.5	5.00×10^{-4}
425000	200	236.0	3.60×10^{-3}
445000	272	274.0	5.00×10^{-5}
525000	276	276.5	3.70×10^{-5}
552000	277	277.5	3.70×10^{-5}
579000	278	---	---
Crack No. 3			
0000	00	8.0	1.60×10^{-3}
10000	16	42.0	1.04×10^{-2}
15000	68	70.0	2.66×10^{-4}
30000	72	77.0	2.22×10^{-4}
75000	82	86.0	3.20×10^{-4}
100000	90	90.5	2.85×10^{-5}
135000	91	98.5	2.15×10^{-4}
265000	106	106.5	5.12×10^{-6}
460000	107	---	---

Air fatigue crack growth data; Test No. : AF15;
$\Delta\tau$ = 1008 MPa, $\Delta\gamma_t$ = 1.57%, N_f = 577,500

No. of Cycles "N"	Crack Length "a" (μm)	Av. Crack Length "a_{av}" (μm)	Crack Growth Rate "da/dN" (μm/cycle)
Crack No. 4			
0000	00	22.0	8.80×10^{-3}
5000	44	50.5	6.49×10^{-4}
25000	57	57.5	9.99×10^{-5}
35000	58	70.5	6.25×10^{-4}
75000	83	87.0	3.20×10^{-4}
100000	91	95.5	2.57×10^{-4}
135000	100	107.5	2.30×10^{-4}
200000	115	118.0	7.05×10^{-5}
285000	121	121.5	1.25×10^{-5}
365000	122	123.5	2.85×10^{-5}
470000	125	136.0	6.28×10^{-4}
505000	147	153.0	1.62×10^{-4}
579000	159	---	---
Crack No. 5			
0000	00	6.0	1.84×10^{-4}
65000	12	25.0	1.73×10^{-3}
80000	38	38.5	9.99×10^{-5}
90000	39	42.5	7.00×10^{-4}
100000	46	49.0	1.71×10^{-4}
135000	52	57.0	7.69×10^{-5}
265000	62	63.5	1.53×10^{-5}
460000	65	65.5	1.53×10^{-5}
525000	66	66.5	1.85×10^{-5}
579000	67	---	---

Air fatigue crack growth data; Test No. : AF8;
$\Delta\tau$ = 915 MPa, $\Delta\gamma t$ = 1.24%, N_f = 4,850,800

No. of Cycles "N"	*Crack Length "a" (μm)*	*Av. Crack Length "a_{av}" (μm)*	*Crack Growth Rate "da/dN" (μm/cycle)*
Crack No. 1			
0000	00	43.0	1.10×10^{-4}
780800	86	87.5	2.18×10^{-6}
2155800	89	108.5	8.66×10^{-5}
2605800	128	128.5	2.22×10^{-6}
3055800	129	129.5	2.12×10^{-6}
3525800	130	151.0	8.48×10^{-5}
4020800	172	175.5	9.99×10^{-4}
4090800	179	189.0	4.44×10^{-4}
4135800	199	204.0	1.17×10^{-4}
4220800	209	211.5	7.14×10^{-5}
4290800	214	216.0	4.70×10^{-5}
4375800	218	226.5	2.42×10^{-4}
4445800	235	243.5	1.21×10^{-4}
4585800	252	293.5	5.53×10^{-4}
4735800	335	352.0	1.13×10^{-3}
4765800	369	615.0	1.09×10^{-2}
4810800	861	2630.0	0.1415200
4835800	4399	---	---
Crack No. 2			
000000	00	26.0	6.65×10^{-5}
780800	52	52.5	7.27×10^{-7}
2155800	53	71.5	8.22×10^{-5}
2605800	90	91.5	6.66×10^{-6}
3055800	93	95.5	1.06×10^{-5}
3525800	98	101.0	1.21×10^{-5}
4020800	104	104.5	1.42×10^{-5}
4090800	105	105.5	2.22×10^{-5}
4135800	106	106.5	1.17×10^{-5}
4220800	107	108.0	2.85×10^{-5}
4290800	109	---	---

Air fatigue crack growth data; Test No. : AF8;
$\Delta\tau$ = 915 MPa, $\Delta\gamma_t$ = 1.24%, N_f = 4,850,800

No. of Cycles "N"	*Crack Length "a" (μm)*	*Av. Crack Length "a_{av}" (μm)*	*Crack Growth Rate "da/dN" (μm/cycle)*
Crack No. 3			
000000	00	24.0	6.14×10^{-5}
780800	48	52.5	6.54×10^{-6}
2155800	57	57.5	2.22×10^{-6}
2605800	58	59.0	4.44×10^{-6}
3055800	60	65.0	2.12×10^{-5}
3525800	70	100.0	1.22×10^{-4}
4020800	130	130.5	1.42×10^{-5}
4090800	131	131.5	2.22×10^{-5}
4135800	132	133.5	3.52×10^{-5}
4220800	135	136.0	2.85×10^{-5}
4290800	137	---	---
Crack No. 4			
000000	00	50.0	1.24×10^{-4}
780800	100	100.5	7.27×10^{-7}
2155800	101	101.5	2.22×10^{-6}
2605800	102	102.5	2.22×10^{-6}
3055800	103	103.5	2.12×10^{-6}
3525800	104	105.5	6.06×10^{-6}
4020800	107	107.5	1.42×10^{-5}
4090800	108	108.5	2.22×10^{-5}
4135800	109	112.0	7.05×10^{-5}
4220800	115	116.0	3.88×10^{-6}
4735800	117	117.5	9.09×10^{-6}
4845800	118	---	---

Appendix D

Corrosion Fatigue Crack Growth Results

Corrosion fatigue crack growth data; Test No. : CF4;
$\Delta\tau$ = 900 MPa, $\Delta\gamma t$ = 1.20%, N_f = 77,000

No. of Cycles "N"	*Crack Length "a" (μm)*	*Av. Crack Length "a_{av}" (μm)*	*Crack Growth Rate "da/dN" (μm/cycle)*
Crack No. 1			
0000	00	22.0	8.80×10^{-3}
5000	44	49.5	2.20×10^{-3}
10000	55	64.0	3.60×10^{-3}
15000	73	79.5	2.60×10^{-3}
20000	86	91.5	2.24×10^{-3}
25000	97	118.0	8.39×10^{-3}
30000	139	176.5	1.50×10^{-2}
35000	214	235.0	8.39×10^{-3}
40000	256	281.0	1.00×10^{-2}
45000	306	335.5	1.18×10^{-2}
50000	365	428.0	2.52×10^{-2}
55000	491	528.0	1.48×10^{-2}
60000	565	601.0	1.44×10^{-2}
65000	637	691.0	2.16×10^{-2}
70000	745	---	---
Crack No. 2			
0000	00	21.5	8.59×10^{-3}
5000	43	60.5	6.99×10^{-3}
10000	78	80.0	7.99×10^{-4}
15000	82	94.5	5.00×10^{-3}
20000	107	136.5	1.18×10^{-2}
25000	166	196.0	1.20×10^{-2}
30000	226	256.5	1.22×10^{-2}
35000	287	334.5	1.90×10^{-2}
40000	382	414.5	1.30×10^{-2}
45000	447	---	---

Corrosion fatigue crack growth data; Test No. : CF4;
$\Delta\tau$ = 900 MPa, $\Delta\gamma t$ = 1.20%, N_f = 77,000

No. of Cycles "N"	*Crack Length "a" (μm)*	*Av. Crack Length "a_{av}" (μm)*	*Crack Growth Rate "da/dN" (μm/cycle)*
Crack No. 3			
0000	00	16.0	6.39×10^{-3}
5000	32	37.0	2.00×10^{-3}
10000	42	74.0	1.28×10^{-2}
15000	106	110.5	1.80×10^{-3}
20000	115	138.5	9.39×10^{-3}
25000	162	190.0	1.12×10^{-2}
30000	218	242.0	9.59×10^{-3}
35000	266	311.0	1.80×10^{-2}
40000	356	403.5	1.90×10^{-2}
45000	451	500.0	1.96×10^{-2}
50000	549	635.0	3.43×10^{-2}
55000	721	816.5	3.82×10^{-2}
60000	912	1008.0	3.83×10^{-2}
65000	1104	1256.5	6.10×10^{-2}
70000	1409	1630.5	6.32×10^{-2}
77000	1852	---	---
Crack No. 4			
0000	00	11.5	4.60×10^{-3}
5000	23	25.5	9.99×10^{-4}
10000	28	31.5	1.40×10^{-3}
15000	35	38.0	1.20×10^{-3}
20000	41	52.0	4.40×10^{-3}
25000	63	79.5	6.60×10^{-3}
30000	96	97.5	5.99×10^{-4}
35000	99	122.5	9.39×10^{-3}
40000	146	169.0	9.19×10^{-3}
45000	192	234.0	1.68×10^{-2}
50000	276	313.0	1.48×10^{-2}
55000	350	397.5	1.90×10^{-2}
60000	445	493.0	1.92×10^{-2}
65000	541	641.0	4.00×10^{-2}
70000	741	891.0	4.28×10^{-2}
77000	1041	---	---

Corrosion fatigue crack growth data; Test No. : CF4;
$\Delta\tau$ = 900 MPa, $\Delta\gamma t$ = 1.20%, N_f = 77,000

No. of Cycles "N"	Crack Length "a" (μm)	Av. Crack Length "a_{av}" (μm)	Crack Growth Rate "da/dN" (μm/cycle)
	Crack No. 5		
0000	00	13.0	5.20×10^{-3}
5000	26	33.0	2.80×10^{-3}
10000	40	46.0	2.40×10^{-3}
15000	52	56.5	1.80×10^{-3}
20000	61	74.5	5.39×10^{-3}
25000	88.0	124.0	1.44×10^{-2}
30000	160	163.0	1.20×10^{-3}
35000	166	197.5	1.26×10^{-2}
40000	229	255.5	1.06×10^{-2}
45000	282	332.5	2.02×10^{-2}
50000	383	429.0	1.84×10^{-2}
55000	475	545.5	2.82×10^{-2}
60000	616	750.5	5.37×10^{-2}
65000	885	1008.0	4.92×10^{-2}
70000	1131	1296.0	4.71×10^{-2}
77000	1461	—	—
	Crack No. 6		
0000	00	17.5	6.99×10^{-3}
5000	35	40.5	2.20×10^{-3}
10000	46	55.5	3.80×10^{-3}
15000	65	71.5	2.60×10^{-3}
20000	78	83.5	2.20×10^{-3}
25000	89	98.0	3.60×10^{-3}
30000	107	128.5	8.59×10^{-3}
35000	150	180.5	1.22×10^{-2}
40000	211	245.0	1.36×10^{-2}
45000	279	322.0	1.72×10^{-2}
50000	365	419.0	2.16×10^{-2}
55000	473	534.5	2.46×10^{-2}
60000	596	654.0	2.32×10^{-2}
65000	712	818.0	4.24×10^{-2}
70000	924	1183.5	7.41×10^{-2}
77000	1443	—	—

Corrosion fatigue crack growth data; Test No. : CF4;
$\Delta\tau$ = 900 MPa, $\Delta\gamma t$ = 1.20%, N_f = 77,000

No. of Cycles "N"	Crack Length "a" (μm)	Av. Crack Length "a_{av}" (μm)	Crack Growth Rate "da/dN" (μm/cycle)
Crack No.7			
0000	00	27.5	1.10×10^{-2}
5000	55	60.0	2.00×10^{-3}
10000	65	85.5	8.19×10^{-3}
15000	106	131.5	1.02×10^{-2}
20000	157	176.5	7.80×10^{-3}
25000	196	249.0	2.12×10^{-2}
30000	302	373.5	2.86×10^{-2}
35000	445	529.0	3.36×10^{-2}
40000	613	702.5	3.58×10^{-2}
45000	792	918.5	5.06×10^{-2}
50000	1045	1177.5	5.30×10^{-2}
55000	1310	—	—
Crack No. 8			
0000	00	14.5	5.79×10^{-3}
5000	29	33.5	1.80×10^{-3}
10000	38	38.5	2.00×10^{-4}
15000	39	41.5	9.99×10^{-4}
20000	44	44.5	2.00×10^{-4}
25000	45	51.5	2.60×10^{-3}
30000	58	62.5	1.80×10^{-3}
35000	67	74.0	2.80×10^{-3}
40000	81	96.0	5.99×10^{-3}
45000	111	130.5	7.80×10^{-3}
50000	150	178.5	1.14×10^{-2}
55000	207	269.0	2.48×10^{-2}
60000	331	—	—

Corrosion fatigue crack growth data; Test No. : CF1;
$\Delta\tau$ = 817 MPa, $\Delta\gamma t$ = 1.03%, N_f = 107,000

No. of Cycles "N"	*Crack Length "a" (μm)*	*Av. Crack Length "a_{av}" (μm)*	*Crack Growth Rate "da/dN" (μm/cycle)*
	Crack No. 1		
0000	00	7.5	3.00×10^{-3}
5000	15	20.0	2.00×10^{-3}
10000	25	28.5	1.40×10^{-3}
15000	32	41.0	3.60×10^{-3}
20000	50	61.5	4.60×10^{-3}
25000	73	92.5	3.80×10^{-3}
30000	112	116.0	1.60×10^{-3}
35000	120	144.0	9.59×10^{-3}
40000	168	189.5	8.59×10^{-3}
45000	211	229.5	7.40×10^{-3}
50000	248	265.0	6.80×10^{-3}
55000	282	303.5	8.59×10^{-3}
60000	325	355.0	1.20×10^{-2}
65000	385	419.0	1.36×10^{-2}
70000	453	486.0	1.32×10^{-2}
75000	519	566.0	1.88×10^{-2}
80000	613	683.5	2.82×10^{-2}
85000	754	834.5	3.21×10^{-2}
90000	915	--	--
	Crack No. 2		
0000	00	26.0	1.04×10^{-2}
5000	52	65.5	5.39×10^{-3}
10000	79	97.5	7.40×10^{-3}
15000	116	124.0	3.20×10^{-3}
20000	132	140.5	3.40×10^{-3}
25000	149	159.5	4.19×10^{-3}
30000	170	186.5	6.60×10^{-3}
35000	203	223.5	8.19×10^{-3}
40000	244	271.0	1.08×10^{-2}
45000	298	321.5	9.39×10^{-3}
50000	345	362.0	6.80×10^{-3}
55000	379	404.5	1.02×10^{-2}
60000	430	470.0	1.60×10^{-2}
65000	510	546.5	1.46×10^{-2}
70000	583	623.0	1.60×10^{-2}
75000	663	717.5	2.18×10^{-2}
80000	772	844.0	2.88×10^{-2}
85000	916	1004.5	3.54×10^{-2}
90000	1093	--	--

Corrosion fatigue crack growth data; Test No. : CF1;
$\Delta\tau$ = 817 MPa, $\Delta\gamma t$ = 1.03%, N_f = 107,000

No. of Cycles "N"	Crack Length "a" (μm)	Av. Crack Length "a_{av}" (μm)	Crack Growth Rate "da/dN" (μm/cycle)
	Crack No. 3		
0000	00	30.5	1.22×10^{-2}
5000	61	81.5	8.19×10^{-3}
10000	102	104.0	7.99×10^{-4}
15000	106	109.0	1.20×10^{-3}
20000	112	121.5	3.80×10^{-3}
25000	131	151.0	7.99×10^{-3}
30000	171	191.0	7.99×10^{-3}
35000	211	241.0	1.20×10^{-2}
40000	271	300.0	1.16×10^{-2}
45000	329	362.0	1.32×10^{-2}
50000	395	421.5	1.06×10^{-2}
55000	448	489.5	1.66×10^{-2}
60000	531	581.5	1.02×10^{-2}
65000	632	729.0	3.87×10^{-2}
70000	826	930.0	4.16×10^{-2}
75000	1034	1141.5	4.30×10^{-2}
80000	1249	1381.0	5.28×10^{-2}
85000	1513		---
	Crack No. 4		
0000	00	10.0	4.00×10^{-3}
5000	20	21.0	4.00×10^{-4}
10000	22	24.5	9.99×10^{-4}
15000	27	34.0	2.80×10^{-3}
20000	41	51.0	4.00×10^{-3}
25000	61	68.5	3.00×10^{-3}
30000	76	89.5	5.39×10^{-3}
35000	103	119.5	6.60×10^{-3}
40000	136	161.5	1.02×10^{-2}
45000	187	202.5	6.20×10^{-3}
50000	218	244.0	1.04×10^{-2}
55000	270	294.0	9.59×10^{-3}
60000	318	358.0	1.60×10^{-2}
65000	398	451.0	2.12×10^{-2}
70000	504	544.5	1.62×10^{-2}
75000	585	691.5	4.26×10^{-2}
80000	798	902.5	4.18×10^{-2}
85000	1007	1085.5	3.14×10^{-2}
90000	1164	---	---

Corrosion fatigue crack growth data; Test No. : CF1;
$\Delta\tau$ = 817 MPa, $\Delta\gamma t$ = 1.03%, N_f = 107,000

No. of Cycles "N"	*Crack Length "a" (μm)*	*Av. Crack Length "a_{av}" (μm)*	*Crack Growth Rate "da/dN" (μm/cycle)*
	Crack No. 5		
0000	00	10.0	4.00×10^{-3}
5000	20	39.0	7.59×10^{-3}
10000	58	58.5	2.00×10^{-4}
15000	59	68.5	3.80×10^{-3}
20000	78	81.5	1.40×10^{-3}
25000	85	106.0	8.39×10^{-3}
30000	127	145.5	7.40×10^{-3}
35000	164	196.0	1.28×10^{-2}
40000	228	248.0	7.99×10^{-3}
45000	268	310.0	1.68×10^{-2}
50000	352	376.5	9.79×10^{-3}
55000	401	437.0	1.44×10^{-2}
60000	473	523.0	2.00×10^{-2}
65000	573	615.5	1.70×10^{-2}
70000	658	701.5	1.74×10^{-2}
75000	745	876.5	5.26×10^{-2}
80000	1008	1090.5	3.30×10^{-2}
85000	1173	1291.0	4.71×10^{-2}
90000	1409	---	---
	Crack No. 6		
0000	00	11.5	4.60×10^{-3}
5000	23	39.5	6.60×10^{-3}
10000	56	66.5	4.19×10^{-3}
15000	77	77.5	2.00×10^{-4}
20000	78	90.0	4.79×10^{-3}
25000	102	141.0	1.56×10^{-2}
30000	180	205.5	1.02×10^{-2}
35000	231	251.0	7.99×10^{-3}
40000	271	299.0	1.12×10^{-2}
45000	327	363.0	1.44×10^{-2}
50000	399	419.5	8.19×10^{-3}
55000	440	474.0	1.36×10^{-2}
60000	508	546.5	1.54×10^{-2}
65000	585	---	---

Corrosion fatigue crack growth data; Test No. : CF5;
$\Delta\tau$ = 601 MPa, $\Delta\gamma_t$ = 0.73%, N_f = 226,000

No. of Cycles "N"	Crack Length "a" (μm)	Av. Crack Length "a_{av}" (μm)	Crack Growth Rate "da/dN" (μm/cycle)
Crack No. 1			
0000	00	6.0	2.40×10^{-3}
5000	12	12.5	2.00×10^{-4}
10000	13	13.5	2.00×10^{-4}
15000	14	15.0	4.00×10^{-4}
20000	16	17.0	4.00×10^{-4}
25000	18	18.5	2.00×10^{-4}
30000	19	19.5	2.00×10^{-4}
35000	20	20.5	2.00×10^{-4}
40000	21	30.5	1.90×10^{-3}
50000	40	57.5	6.99×10^{-3}
55000	75	83.5	3.40×10^{-3}
60000	92	100.0	3.20×10^{-3}
65000	108	126.2	7.35×10^{-3}
70000	144	144.5	2.00×10^{-4}
75000	145	170.5	1.02×10^{-2}
80000	196	203.5	3.00×10^{-3}
85000	211	227.0	6.39×10^{-3}
90000	243	259.0	6.39×10^{-3}
95000	275	301.0	1.04×10^{-2}
100000	327	358.0	1.24×10^{-2}
105000	389	408.5	7.80×10^{-3}
110000	428	466.5	1.54×10^{-2}
115000	505	532.0	1.08×10^{-2}
120000	559	598.5	1.58×10^{-2}
125000	638	659.5	8.59×10^{-3}
130000	681	724.0	1.72×10^{-2}
135000	767	816.0	1.96×10^{-2}
140000	865	920.0	2.20×10^{-2}
145000	975	1069.5	3.78×10^{-2}
150000	1164	1322.5	3.16×10^{-2}
160000	1481	1721.0	4.79×10^{-2}
170000	1961	2238.0	5.54×10^{-2}
180000	2515	2964.5	8.98×10^{-2}
190000	3414	4004.5	0.118100
200000	4595	4836.5	9.66×10^{-2}
205000	5078	5210.5	5.30×10^{-2}
210000	5343	5961.5	0.123700
220000	6580	—	—

Corrosion fatigue crack growth data; Test No. : CF5;
$\Delta\tau$ = 601 MPa, $\Delta\gamma_t$ = 0.73%, N_f = 226,000

No. of Cycles "N"	Crack Length "a" (μm)	Av. Crack Length "a_{av}" (μm)	Crack Growth Rate "da/dN" (μm/cycle)
	Crack No. 2		
0000	00	3.5	1.40×10^{-3}
5000	07	7.5	2.00×10^{-4}
10000	08	9.0	4.00×10^{-4}
15000	10	12.0	7.99×10^{-4}
20000	14	17.0	1.20×10^{-3}
25000	20	28.0	3.20×10^{-3}
30000	36	42.0	2.40×10^{-3}
35000	48	67.0	7.59×10^{-3}
40000	86	108.5	4.55×10^{-3}
50000	131	131.5	2.00×10^{-4}
55000	132	156.5	9.79×10^{-3}
60000	181	198.0	6.80×10^{-3}
65000	215	227.5	5.00×10^{-3}
70000	240	251.5	4.60×10^{-3}
75000	263	284.5	8.59×10^{-3}
80000	306	325.0	7.59×10^{-3}
85000	344	356.0	4.79×10^{-3}
90000	368	390.5	9.00×10^{-3}
95000	413	430.0	6.80×10^{-3}
100000	447	479.0	1.28×10^{-2}
105000	511	531.0	7.99×10^{-3}
110000	551	585.0	1.36×10^{-2}
115000	619	644.5	1.02×10^{-2}
120000	670	699.0	1.16×10^{-2}
125000	728	750.0	8.80×10^{-3}
130000	772	828.5	2.26×10^{-2}
135000	885	930.0	1.80×10^{-2}
140000	975	1008.5	1.34×10^{-2}
145000	1042	1086.0	1.76×10^{-2}
150000	1130	1269.0	2.78×10^{-2}
160000	1408	1599.5	3.82×10^{-2}
170000	1791	2001.5	4.21×10^{-2}
180000	2212	2554.5	6.85×10^{-2}
190000	2897	3379.0	9.63×10^{-2}
200000	3861	3988.5	5.10×10^{-2}
205000	4116	4293.5	7.09×10^{-2}
210000	4471	5064.0	0.118600
220000	5657	---	---

Corrosion fatigue crack growth data; Test No. : CF5;
$\Delta\tau$ = 601 MPa, $\Delta\gamma_t$ = 0.73%, N_f = 226,000

No. of Cycles "N"	Crack Length "a" (μm)	Av. Crack Length "a_{av}" (μm)	Crack Growth Rate "da/dN" (μm/cycle)
Crack No. 3			
0000	00	11.0	4.40×10^{-3}
5000	22	22.5	2.00×10^{-4}
10000	23	23.5	2.00×10^{-4}
15000	24	25.0	4.00×10^{-4}
20000	26	27.5	5.99×10^{-4}
25000	29	30.5	5.99×10^{-4}
30000	32	33.5	5.99×10^{-4}
35000	35	37.0	7.99×10^{-4}
40000	39	41.5	5.00×10^{-4}
50000	44	46.0	7.99×10^{-4}
55000	48	50.0	7.99×10^{-4}
60000	52	60.5	3.40×10^{-3}
65000	69	75.0	2.40×10^{-3}
70000	81	89.5	3.40×10^{-3}
75000	98	111.0	5.20×10^{-3}
80000	124	132.5	3.50×10^{-3}
85000	141	141.5	2.00×10^{-3}
90000	142	173.5	1.26×10^{-2}
95000	205	207.0	7.99×10^{-4}
100000	209	248.0	1.56×10^{-2}
105000	287	298.5	4.60×10^{-3}
110000	310	341.5	1.26×10^{-2}
115000	373	387.0	5.60×10^{-3}
120000	401	424.5	9.39×10^{-3}
125000	448	462.5	5.79×10^{-3}
130000	477	514.5	1.50×10^{-2}
135000	552	589.0	1.48×10^{-2}
140000	626	678.0	2.08×10^{-2}
145000	730	780.5	2.02×10^{-2}
150000	831	937.5	2.85×10^{-2}
160000	1116	1301.5	3.70×10^{-2}
170000	1487	1669.0	3.64×10^{-2}
180000	1851	2083.0	4.64×10^{-2}
190000	2315	2548.5	4.66×10^{-2}
200000	2782	2950.0	6.71×10^{-2}
205000	3118	---	---

Corrosion fatigue crack growth data; Test No. : CF5;
$\Delta\tau$ = 601 MPa, $\Delta\gamma t$ = 0.73%, N_f = 226,000

No. of Cycles "N"	Crack Length "a" (μm)	Av. Crack Length "a_{av}" (μm)	Crack Growth Rate "da/dN" (μm/cycle)
Crack No. 4			
0000	00	56.0	2.24×10^{-2}
5000	112	112.5	2.00×10^{-4}
10000	113	114.0	4.00×10^{-4}
15000	115	115.5	2.00×10^{-4}
20000	116	117.5	5.99×10^{-4}
25000	119	122.5	1.40×10^{-3}
30000	126	128.0	7.99×10^{-4}
35000	130	131.0	4.00×10^{-4}
40000	132	132.5	9.99×10^{-5}
50000	133	134.0	4.00×10^{-4}
55000	135	136.0	4.00×10^{-4}
60000	137	164.0	1.08×10^{-2}
65000	191	193.5	9.99×10^{-4}
70000	196	216.5	8.19×10^{-3}
75000	237	246.5	3.80×10^{-3}
80000	256	269.0	5.20×10^{-3}
85000	282	285.5	1.40×10^{-3}
90000	289	315.5	1.06×10^{-2}
95000	342	353.0	4.40×10^{-3}
100000	364	408.0	1.76×10^{-2}
105000	452	473.5	8.59×10^{-3}
110000	495	528.5	1.34×10^{-2}
115000	562	578.0	6.39×10^{-3}
120000	594	633.0	1.56×10^{-2}
125000	672	694.5	9.00×10^{-3}
130000	717	768.5	2.06×10^{-2}
135000	820	861.0	1.64×10^{-2}
140000	902	949.5	1.90×10^{-2}
145000	997	1039.0	1.68×10^{-2}
150000	1081	1272.0	3.82×10^{-2}
160000	1463	1655.0	3.83×10^{-2}
170000	1847	2028.5	3.63×10^{-2}
180000	2210	2471.0	5.22×10^{-2}
190000	2732	2975.5	4.87×10^{-2}
200000	3219	3337.0	4.71×10^{-2}
205000	3455	---	---

Corrosion fatigue crack growth data; Test No. : CF5;
$\Delta\tau$ = 601 MPa, $\Delta\gamma t$ = 0.73%, N_f = 226,000

No. of Cycles "N"	Crack Length "a" (μm)	Av. Crack Length "a_{av}" (μm)	Crack Growth Rate "da/dN" (μm/cycle)
Crack No. 5			
0000	00	12.0	4.79×10^{-3}
5000	24	25.0	4.00×10^{-4}
10000	26	28.0	7.99×10^{-4}
15000	30	33.0	1.20×10^{-3}
20000	36	39.0	1.20×10^{-3}
25000	42	45.5	1.40×10^{-3}
30000	49	52.0	1.20×10^{-3}
35000	55	61.0	2.40×10^{-3}
40000	67	72.5	1.10×10^{-3}
50000	78	81.0	1.20×10^{-3}
55000	84	91.5	3.00×10^{-3}
60000	99	109.5	4.19×10^{-3}
65000	120	120.5	2.00×10^{-4}
70000	121	124.0	1.20×10^{-3}
75000	127	134.0	2.80×10^{-3}
80000	141	158.5	6.99×10^{-3}
85000	176	179.0	1.20×10^{-3}
90000	182	207.0	1.00×10^{-2}
95000	232	246.5	5.79×10^{-3}
100000	261	281.5	8.19×10^{-3}
105000	302	322.0	7.99×10^{-3}
110000	342	360.0	7.20×10^{-3}
115000	378	396.0	7.20×10^{-3}
120000	414	445.0	1.24×10^{-2}
125000	476	491.5	6.20×10^{-3}
130000	507	531.0	9.59×10^{-3}
135000	555	588.0	1.32×10^{-2}
140000	621	645.5	9.79×10^{-3}
145000	670	721.5	2.06×10^{-2}
150000	773	867.5	1.89×10^{-2}
160000	962	1099.5	2.75×10^{-2}
170000	1237	1335.5	1.97×10^{-2}
180000	1434	1614.5	3.60×10^{-2}
190000	1795	1986.5	3.82×10^{-2}
200000	2178	2266.0	3.52×10^{-2}
205000	2354	—	—

Corrosion fatigue crack growth data; Test No. : CF6;
$\Delta\tau$ = 404 MPa, $\Delta\gamma t$ = 0.49%, N_f = 902,000

No. of Cycles "N"	*Crack Length "a" (μm)*	*Av. Crack Length "a_{av}" (μm)*	*Crack Growth Rate "da/dN" (μm/cycle)*
Crack No. 1			
0000	00	6.0	2.40×10^{-3}
5000	12	12.5	1.33×10^{-5}
80000	13	30.5	3.18×10^{-4}
190000	48	82.5	7.26×10^{-4}
285000	117	124.5	1.47×10^{-4}
390000	132	132.5	4.54×10^{-6}
500000	133	200.5	1.03×10^{-3}
630000	268	293.0	1.66×10^{-3}
660000	318	337.0	3.80×10^{-3}
670000	356	381.5	5.10×10^{-3}
680000	407	438.5	6.30×10^{-3}
690000	470	580.0	6.28×10^{-3}
725000	690	800.5	1.47×10^{-2}
740000	911	981.0	1.40×10^{-2}
750000	1051	1257.0	2.06×10^{-2}
770000	1463	1703.5	2.40×10^{-2}
790000	1944	2065.5	2.43×10^{-2}
800000	2187	2309.5	2.45×10^{-2}
810000	2432	2639.0	4.13×10^{-2}
820000	2846	3049.0	4.05×10^{-2}
830000	3252	3435.5	3.67×10^{-2}
840000	3619	3881.5	5.24×10^{-2}
850000	4144	---	---

Corrosion fatigue crack growth data; Test No. : CF6;
$\Delta\tau$ = 404 MPa, $\Delta\gamma_t$ = 0.49%, N_f = 902,000

No. of Cycles "N"	*Crack Length "a" (μm)*	*Av. Crack Length "a_{av}" (μm)*	*Crack Growth Rate "da/dN" (μm/cycle)*
Crack No. 2			
0000	00	7.0	2.80×10^{-3}
5000	14	15.5	2.40×10^{-5}
130000	17	24.0	2.33×10^{-4}
190000	31	52.0	4.42×10^{-4}
285000	73	84.0	2.09×10^{-4}
390000	95	95.5	4.54×10^{-6}
500000	96	119.0	3.57×10^{-4}
630000	142	152.5	7.00×10^{-4}
660000	163	166.5	7.00×10^{-4}
670000	170	183.0	2.60×10^{-3}
680000	196	212.5	3.30×10^{-3}
690000	229	358.5	7.40×10^{-3}
725000	488	502.5	1.93×10^{-3}
740000	517	577.5	1.21×10^{-2}
750000	638	758.0	1.20×10^{-3}
770000	878	1026.5	1.48×10^{-2}
790000	1175	1248.5	1.47×10^{-2}
800000	1322	1353.0	6.20×10^{-3}
810000	1384	1463.5	1.59×10^{-2}
820000	1543	1647.0	2.08×10^{-2}
830000	1751	1816.0	1.30×10^{-2}
840000	1881	2057.5	3.52×10^{-2}
850000	2234	2375.0	2.82×10^{-2}
860000	2516	3543.0	5.13×10^{-2}
900000	4570	---	---

Corrosion fatigue crack growth data; Test No. : CF6;
$\Delta\tau$ = 404 MPa, $\Delta\gamma_t$ = 0.49%, N_f = 902,000

No. of Cycles "N"	Crack Length "a" (μm)	Av. Crack Length "a_{av}" (μm)	Crack Growth Rate "da/dN" (μm/cycle)
Crack No. 3			
0000	00	10.0	4.00×10^{-3}
5000	20	21.5	7.79×10^{-6}
390000	23	28.5	9.99×10^{-5}
500000	34	50.0	2.46×10^{-4}
630000	66	74.0	5.33×10^{-4}
660000	82	82.5	9.99×10^{-5}
670000	83	89.0	1.20×10^{-3}
680000	95	95.5	2.00×10^{-6}
690000	96	155.0	3.39×10^{-3}
725000	214	248.0	4.53×10^{-3}
740000	282	309.0	5.39×10^{-3}
750000	336	411.5	7.54×10^{-3}
770000	487	589.0	1.02×10^{-2}
790000	691	748.0	1.14×10^{-2}
800000	805	831.0	5.20×10^{-3}
810000	857	891.5	6.89×10^{-3}
820000	926	991.5	1.31×10^{-2}
830000	1057	1109.5	1.05×10^{-2}
840000	1162	1229.5	1.35×10^{-2}
850000	1297	1390.5	1.87×10^{-2}
860000	1484	1735.5	1.25×10^{-2}
900000	1987	2058.5	1.78×10^{-2}
908000	2130	---	---

Appendix E

Intermittent Air Fatigue/Corrosion Fatigue Crack Growth Results

Intermittent air fatigue/corrosion fatigue crack growth data; Test No. : IF6;

$\Delta\tau$ = 900 MPa, $\Delta\gamma_t$ = 1.20%

No. of cycles N	Crack length a, μm		Av. crack length a_{av}, μm		Crack growth rate da/dN, μm/cycle	
	Crack 1	Crack 2	Crack 1	Crack 2	Crack 1	Crack 2
0000	00	00	48.0	13.0	6.39×10^{-3}	1.73×10^{-4}
5000	96	---	105.0	---	1.20×10^{-3}	---
30000	114	---	114.5	---	1.33×10^{-5}	---
105000	115	---	115.0	----	0.0	---
150000	115	26	116.5	48.0	6.38×10^{-6}	9.36×10^{-5}
620000	118	70	118.0	73.0	0.0	2.72×10^{-5}
840000	118	76	118.0	77.0	0.0	1.25×10^{-5}
1000000	118	78	118.0	78.5	0.0	4.65×10^{-6}
1215000	118	79	118.0	79.5	0.0	3.61×10^{-6}
1492000	118	80	118.0	80.0	0.0	0.0
1811000	118	80	118.5	80.5	8.77×10^{-6}	8.77×10^{-6}
1925000	119	81	119.5	81.0	1.00×10^{-5}	0.0
2025000	120	81	126.0	94.5	2.40×10^{-3}	5.39×10^{-3}
2030000 e	132	108	133.5	112.0	3.00×10^{-4}	7.99×10^{-4}
2040000	135	116	135.0	124.0	0.0	1.77×10^{-4}
2130000	135	132	135.5	135.5	8.33×10^{-6}	5.83×10^{-5}
2250000	136	139	136.0	140.0	0.0	8.51×10^{-6}
2485000	136	141	137.0	141.0	2.28×10^{-5}	0.0
2572500	138	141	139.5	142.0	9.99×10^{-5}	6.66×10^{-5}
2602500	141	143	---	---	---	---
2692500 l	---	322	---	335.0	---	2.59×10^{-4}
2792500	---	348	---	348.5	---	8.69×10^{-6}
2907500	---	349	---	350.0	---	6.66×10^{-5}
2937500	---	351	---	359.0	---	2.66×10^{-4}
2997500	---	367	---	372.0	---	2.50×10^{-4}
3037500	---	377	---	379.5	---	2.50×10^{-4}
3057500	---	382	---	382.5	---	2.50×10^{-5}
3097500	---	383	---	384.0	---	3.33×10^{-5}
3157500	---	385	---	385.5	---	7.40×10^{-6}
3292500	---	386	---	386.5	---	1.66×10^{-5}
3352500	---	387	---	387.5	---	1.66×10^{-5}
3412500	---	388	---	388.5	---	3.33×10^{-5}
3442500	---	389	---	390.0	---	3.33×10^{-5}
3502500	---	391	---	392.0	---	1.81×10^{-5}
3612500	---	393	---	393.5	---	1.66×10^{-5}
3672500	---	394	---	405.0	---	4.00×10^{-4}
3727500	---	416	---	440.0	---	1.06×10^{-3}
3772500	---	464	---	531.5	---	4.50×10^{-3}
3802500	---	599	---	678.5	---	1.59×10^{-2}
3812500	---	758	---	809.0	---	1.02×10^{-2}
3822500	---	860	---	2306.5	---	7.23×10^{-2}
3862500	---	3753	---	---	---	---

e = Corrosion fatigue cycling.
l = Crack 1 and crack 2 coalesced.

Intermittent air fatigue/corrosion fatigue crack growth data;
Test No. : IF7;
$\Delta\tau$ = 853 MPa, $\Delta\gamma t$ = 1.10%

No. of Cycles "N"	*Crack Length "a" (μm)*	*Av. Crack Length "a_{av}" (μm)*	*Crack Growth Rate "da/dN" (μm/cycle)*
0000	00	10.0	4.00×10^{-3}
5000	20	23.5	4.60×10^{-5}
157000	`27	28.0	7.99×10^{-6}
407000	29	29.5	9.52×10^{-7}
1457000	30	31.0	1.98×10^{-6}
2467000	32	33.0	1.66×10^{-6}
3670000	34	50.0	6.39×10^{-3}
3675000 e	66	66.0	2.00×10^{-4}
3680000	67	67.5	9.99×10^{-5}
3690000	68	68.5	9.09×10^{-6}
3800000	69	69.5	2.56×10^{-6}
4190000	70	70.5	1.45×10^{-6}
4875000	71	83.0	4.79×10^{-3}
4880000 e	95	95.5	2.00×10^{-4}
4885000	96	96.5	9.99×10^{-5}
4895000	97	99.5	1.36×10^{-5}
5260000	102	102.5	3.57×10^{-6}
5540000	103	115.5	5.00×10^{-3}
5545000 e	128	130.5	9.99×10^{-4}
555000	133	142.5	1.90×10^{-3}
5560000	152	161.5	9.49×10^{-4}
5580000	171	181.5	7.00×10^{-4}
5610000	192	202.0	9.99×10^{-4}
5630000	212	232.5	4.10×10^{-3}
5640000	253	307.0	5.39×10^{-3}
5660000	361	433.0	7.20×10^{-3}
5680000	505	614.0	1.09×10^{-2}
5700000	723	1036.5	3.13×10^{-2}
5720000	1350	2132.5	7.82×10^{-2}
5740000	2915	4724.5	0.2412670
5755000	6534	---	---

e = Corrosion fatigue cycling.

Intermittent air fatigue/corrosion fatigue crack growth data;
Test No. : IF4;
$\Delta\tau$ = 815 MPa, $\Delta\gamma_t$ = 1.03%

No. of Cycles "N"	*Crack Length "a" (μm)*	*Av. Crack Length "a_{av}" (μm)*	*Crack Growth Rate "da/dN" (μm/cycle)*
00000	00	12.5	2.89×10^{-4}
86500	25	25.5	4.00×10^{-5}
111500	26	35.5	3.80×10^{-4}
161500	45	51.0	1.26×10^{-4}
256500	57	69.5	4.16×10^{-4}
316500	82	82.5	3.70×10^{-6}
586500	83	83.5	1.55×10^{-6}
1231500	84	84.5	1.17×10^{-5}
1316500	85	106.5	8.59×10^{-3}
1321500 e	128	128.5	9.99×10^{-5}
1331500	129	129.5	5.00×10^{-5}
1351500	130	130.5	3.33×10^{-5}
1381500	131	149.0	7.20×10^{-3}
1386500 e	167	177.0	3.33×10^{-3}
1392500	187	191.0	8.88×10^{-4}
1401500	195	196.0	2.00×10^{-4}
1411500	197	198.0	2.00×10^{-4}
1421500	199	202.0	2.00×10^{-4}
1451500	205	221.5	6.59×10^{-4}
1501500	238	269.0	1.24×10^{-3}
1551500	300	334.0	1.36×10^{-3}
1601500	368	782.5	2.07×10^{-2}
1641500	1197	2713.0	7.57×10^{-2}
1681500	4229	---	---

e = Corrosion fatigue cycling.

Intermittent air fatigue/corrosion fatigue crack growth data; Test No. : IF12;

$\Delta\tau$ = 600 MPa, $\Delta\gamma_t$ = 0.73%

No. of cycles N	Crack length a, μm		Av. crack length a_{av}, μm		Crack growth rate da/dN, μm/cycle	
	Crack 1	Crack 2	Crack 1	Crack 2	Crack 1	Crack 2
0000	00	00	11.5	12.0	1.91×10^{-6}	2.00×10^{-6}
11990000	23	24	26.0	32.5	5.99×10^{-4}	1.70×10^{-3}
12000000 e	29	41	29.0	41.0	0.0	0.0
13950000	29	41	33.5	42.5	1.80×10^{-3}	5.99×10^{-4}
13955000 e	38	44	38.0	44.0	0.0	0.0
14050000	38	44	41.0	58.0	1.20×10^{-3}	5.60×10^{-3}
14055000 e	44	72	44.0	72.0	0.0	0.0
14410000	44	72	50.5	79.0	2.60×10^{-3}	2.80×10^{-3}
14415000 e	57	86	58.0	87.0	6.15×10^{-6}	6.15×10^{-6}
14740000	59	88	62.5	92.5	1.40×10^{-3}	1.80×10^{-3}
14745000 e	66	97	66.5	99.5	6.89×10^{-6}	3.44×10^{-5}
14890000	67	102	70.5	115.0	1.40×10^{-3}	5.20×10^{-3}
14895000 e	74	128	75.5	129.0	1.22×10^{-5}	8.16×10^{-6}
15140000	77	130	85.5	150.0	3.40×10^{-3}	7.99×10^{-3}
15145000 e	94	170	96.5	173.0	8.26×10^{-6}	9.91×10^{-6}
15750000	99	176	109.5	186.0	4.19×10^{-3}	4.00×10^{-3}
15755000 e	120	196	120.0	196.0	0.0	0.0
15980000	120	196	147.0	202.5	1.08×10^{-2}	2.6×10^{-3}
15985000 e	174	209	175.0	209.0	5.06×10^{-6}	0.0
16380000	176	209	181.5	209.0	2.20×10^{-3}	0.0
16385000 e	187	209	188.0	209.0	5.00×10^{-6}	0.0
16785000	189	209	190.5	210.5	5.99×10^{-4}	5.99×10^{-4}
16790000 e	192	212	202.0	212.0	2.22×10^{-4}	0.0
16880000	212	212	212.0	212.0	0.0	0.0
16890000	212	212	---	---	---	---
16900000 l	---	464	---	466.0	---	9.99×10^{-5}
16940000	---	468	---	2234.0	---	1.41×10^{-2}
17190000	---	4000	---	---	---	---

e = Corrosion fatigue cycling.
l = Crack 1 and Crack 2 coalesced.